CENTRO INTERNACIONAL DE ESTUDOS
DE DOUTORAMENTO E AVANZADOS
DA USC (CIEDUS)

PhD Dissertation

Assessing simplifying hypotheses in density estimation

Jose Ameijeiras Alonso

ESCOLA DE DOUTORAMENTO EN CIENCIAS

DOUTORADO EN ESTATÍSTICA E INVESTIGACIÓN OPERATIVA

SANTIAGO DE COMPOSTELA

2017

USC
UNIVERSIDADE
DE SANTIAGO
DE COMPOSTELA

DECLARACIÓN DO AUTOR DA TESE

D. Jose Ameijeiras Alonso

Alumno do Programa de Doutoramento en Estatística e Investigación Operativa

Como Autor da Tese de Doutoramento titulada

"Assessing Simplifying Hypotheses in Density Estimation"

Presento a miña tese, seguindo o procedemento adecuado ao Regulamento, e declaro que:

1. A tese abarca os resultados da elaboración do meu traballo.
2. No seu caso, na tese se fai referencia as colaboracións que tivo este traballo.
3. A tese é a versión definitiva presentada para a súa defensa e coincide ca versión enviada en formato electrónico.
4. Confirmo que a tese non incorre en ningún tipo de plaxio de outros autores nin de traballos presentados por min para a obtención de outros títulos.

Asdo. Jose Ameijeiras Alonso

USC
UNIVERSIDADE
DE SANTIAGO
DE COMPOSTELA

AUTORIZACIÓN DOS DIRECTORES DA TESE

Dna. Rosa M. Crujeiras Casais

Profesora do Departamento de Estatística, Análise Matemática e Optimización

D. Alberto Rodríguez Casal

Profesor do Departamento de Estatística, Análise Matemática e Optimización

Como Directores da Tese de Doutoramento titulada

"Assessing Simplifying Hypotheses in Density Estimation"

Presentada por D. Jose Ameijeiras Alonso

Alumno do Programa de Doutoramento en Estatística e Investigación Operativa

Autorizan a presentación da tese indicada, considerando que reúne os requisitos esixidos no artigo 34 do regulamento de Estudos de Doutoramento, e que como Directores da mesma non incurre nas causas de abstención establecidas na lei 40/2015.

Asdo. Rosa M. Crujeiras Casais

Asdo. Alberto Rodríguez Casal

USC
UNIVERSIDADE
DE SANTIAGO
DE COMPOSTELA

Agradecimientos

Estos agradecimientos van por todas esas personas que me han ayudado a llegar hasta aquí. En primer lugar, me gustaría mostrar mi profunda gratitud a Rosa M. Crujeiras y a Alberto Rodríguez Casal: sin su apoyo personal esta tesis nunca podría haber sido realizada. A ellos les debo la madurez investigadora que he adquirido a lo largo de estos años, la cual considero que es la parte más importante de haber realizado esta tesis. A Rosa le agradezco que siempre haya tenido un momento para mí y que me haya guiado de forma excelente durante estos años. A Alberto, el haber confiado en mí desde mis *primeros pinitos* en el mundo de la investigación, el ejercer de *psicólogo* cuando ha hecho falta y todas su críticas constructivas. I would like also to thank the collaborators that appear along the thesis, especially Christophe Ley and Francesco Lagona for hosting me in Ghent and Rome and for their wonderful guidance during my research stays. Como Christophe me dijo una vez: *lo bueno* que tiene este trabajo es que investigas con personas que se acaban convirtiendo en tus amigos.

Cuando se está realizando una tesis también es importante cuidar la parte emocional. En este sentido, tengo que dar las gracias a Helena, por haber estado siempre ahí, aunque estuviese lejos en distancia, durante todos estos años, siempre ha sabido cómo hacerme una compañía cercana en lo personal. A mis compañeros de comida, departamento, café, a los *itmatis* and to my colleagues in Ghent and Rome. En particular a María, que a pesar de estar siempre ocupada, nunca ha dudado en sacar un momento para ayudarme cuando lo he necesitado, a Arís, Ángel, Edu y Juan Carlos por la compañía y por aguantar todas mis quejas, en especial, en esta parte final de la tesis. A mis compañeros de promoción (María, Óscar y Xabi) y al resto de mis amigos de Vigo y de Santiago (Álex, Borjita, Dani, Jandros, Keko y Rubén) que me han ayudado a *desconectar* cuando era necesario.

Finalmente y ya que en esta tesis se trata el tema de la circularidad, en este caso, me gustaría cerrar el círculo de los agradecimientos con otra Rosa, mi madre, a la que le debo tanto. Sin ella nunca habría llegado tan lejos en la vida, muchas gracias por todos los esfuerzos que has realizado. Espero que esta tesis también sirva para rendir homenaje a los buenos momentos que he pasado con mis abuelos, Lola y Perfecto.

Santiago de Compostela, septiembre de 2017.
Jose Ameijeiras Alonso.

USC
UNIVERSIDADE
DE SANTIAGO
DE COMPOSTELA

Determinando Hipóteses Simplificadoras na Estimación da Densidade

Resumo

A análise estatística clásica de variables aleatorias unidimensionais soe enfocarse asumindo fenómenos distribuídos simetricamente arredor dun único punto. Sen embargo, estes modelos poden non resultar adecuados cando tratan de capturar estruturas subxacentes máis complexas, frecuentes na análise de datos reais. Para resolver este problema, nos últimos anos, deseñáronse varias distribucións de probabilidade que tratan de capturar aquelas situacións nas que os datos presentan asimetría e multimodalidade (cando os datos se concentran arredor de máis dun valor). Esta problemática pódese atopar tamén en estruturas máis complexas de datos continuos, como nos datos circulares, é dicir, mostras que se poden representar como puntos na circunferencia dun círculo unitario. Non obstante, antes de aplicar estes modelos máis flexibles, pero tamén máis complexos, é importante determinar cando estes valen a pena. Neste senso, esta tese persegue dous obxectivos. Primeiro, dende un punto de vista non paramétrico, contrastar o número de modas para datos lineares e circulares. Para iso, realízase unha revisión das diferentes propostas dispoñibles na literatura estatística e proponse un novo método que presenta un comportamento superior en escenarios tanto lineares como circulares. O segundo obxectivo, no contexto dos datos circulares, é determinar se a distribución subxacente da mostra é (reflexivamente) simétrica arredor dunha dirección central. Respecto deste obxectivo, preséntase un novo test e demóstrase que é óptimo para contrastar a simetría circular. O comportamento das diferentes propostas, presentadas nesta tese, tamén se analiza a través de estudos de simulación e son ilustradas empregando diferentes aplicacións a datos reais.

Palabras chave

contraste de hipóteses, estatística circular, estimación non paramétrica, multimodalidade, simetría reflexiva

Determinando Hipótesis Simplificadoras en la Estimación de la Densidad

Resumen

El análisis estadístico clásico de variables aleatorias unidimensionales está enfocado, normalmente, a fenómenos que están simétricamente distribuidos y concentrados alrededor de un solo punto. Sin embargo, estos modelos pueden fallar a la hora de capturar estructuras subyacentes más complejas, que se encuentran frecuentemente en los datos reales. Para resolver este problema, en los últimos años, se han diseñado varias distribuciones de probabilidad que tratan de capturar aquellas situaciones en las que los datos presentan asimetría y multimodalidad (cuando los datos están concentrados en torno a más de un valor). También se puede encontrar esta problemática para estructuras más complejas de datos continuos, tales como los datos circulares, es decir, muestras que se pueden representar como puntos en la circunferencia de un círculo unitario. Sin embargo, antes de aplicar estos modelos más flexibles, pero también más complejos, es importante determinar cuándo estos merecen la pena. En este sentido, son dos los objetivos de la tesis. En primer lugar, desde un punto de vista no paramétrico, contrastar el número de modas para datos lineales y circulares. Para ello, se realiza una revisión de las diferentes propuestas disponibles en la literatura estadística, diseñándose, además, un nuevo método que presenta un comportamiento superior en ambos escenarios, lineal y circular. El segundo objetivo, en el contexto de los datos circulares, es el de determinar si la distribución subyacente de los datos es (reflexivamente) simétrica alrededor de una dirección central. Con respecto a este objetivo, se presenta un nuevo test y se demuestra que es óptimo para contrastar simetría circular. El comportamiento de las distintas propuestas, presentadas en esta tesis, también se analiza a través de estudios de simulación y se ilustra utilizando diferentes aplicaciones a datos reales.

Palabras clave

contraste de hipótesis, estadística circular, estimación no paramétrica, multimodalidad, simetría reflexiva

Assessing Simplifying Hypotheses in Density Estimation

Abstract

In the classical statistical analysis of univariate random variables, most distribution approaches are focused on phenomena that are symmetrically distributed and concentrated around a single point. However, such models may fail to capture more complex underlying structures, usually present in real data. To solve this issue, in the last years, several distribution proposals were designed to catch and reveal situations with asymmetry and multimodality (data are concentrated around more than one value). For more complex structures of continuous data, such as circular data, that is, samples that can be represented as points on the circumference of a unit circle, this problem can be also found. However, before applying these more flexible but complicated models, it is important to determine whether it is worth it. In this sense, the goal of this thesis is twofold. First, from a nonparametric point of view, testing the number of modes for linear and circular data. A review of the different proposals available in the statistical literature is provided and a new method outperforming these previous proposals is presented for both settings, linear and circular. The second objective is determining if the underlying distribution of the data is (reflective) symmetric around a central direction in circular data. Regarding this goal, a new proposal is presented and it is proved that it is optimal for testing circular symmetry. The performance of all the developed tests, in the finite case, is also analysed through simulation studies and illustrated using different real data applications.

Keywords

circular statistics, multimodality, nonparametric estimation, reflective symmetry, testing procedure

USC
UNIVERSIDADE
DE SANTIAGO
DE COMPOSTELA

Contents

USC
UNIVERSIDADE
DE SANTIAGO
DE COMPOSTELA

Chapter 1

Introduction

The classical statistical analysis of univariate continuous data is usually focused on the study of phenomena that are symmetrically distributed and concentrated around a single point. However, such models may fail to capture more complex underlying structures when applied to real data. To solve this issue, several distributions were designed trying to catch the situations where the data change when it is reflected around a central value (asymmetry) or when it is concentrated around more than one value (multimodality). On more complex structures of continuous data, such as circular data, that is, samples that can be represented as points on the circumference of a unit circle, this problem can be also found. In fact, one of the first references for statisticians in this field (Mardia, 1972, Ch. 1, compiling the first real progress in circular data analysis made during the 1950s and 1960s) deals with these topics from the very beginning, as asymmetric and multimodal distributions occur frequently in practice. However, before applying these more complicated models, it is important to determine whether it is worth it. With this objective, this essay is focused on assessing simplifying hypothesis in density estimation for linear and circular data.

The goal of this thesis is twofold. First, testing the number of modes for linear and circular data and second determining if the underlying distribution of the data is (reflective) symmetric around a central direction in circular data. Section 1.1 is devoted to present the concept of mode and a brief overview on the nonparametric techniques for determining the number of modes is also given. Section 1.2 provides an introduction to the topic of circular data. The need of adapting the techniques for assessing the number of modes and some of the most widely used parametric distributions are revised in this section. In this section is also presented the circular (reflective) symmetry. A new testing procedure will be obtained using the Le Cam theory. In Section 1.3 some real datasets that motivate and illustrate the different

topics of this essay are described. Finally, in Section 1.4 the organization of this manuscript is provided and in Section 1.5 the principal contributions of this thesis are described.

Contents

1.1 Assessment of the number of modes

The first problem to tackle is the determination of the number of modes. The concept of mode, for a continuous random variable X, is defined as the value (or values) at which the probability density function reaches a local maximum. If there is just one mode, then the density (or the associated distribution) is unimodal. Otherwise, it will be said that the density is multimodal (bimodal, if it has two modes; trimodal, if it has three; etc.). It will be seen that the local minima of the probability functions, namely antimodes, also play its role when the number of modes is tested. The local maxima and minima of the probability density function will be denoted as x_i in this manuscript. Then, if f is a class–one function (i.e. it has a continuous first derivative) with j modes and $(j-1)$ antimodes, $x_1, \ldots, x_{2j-1}$ will denote the location

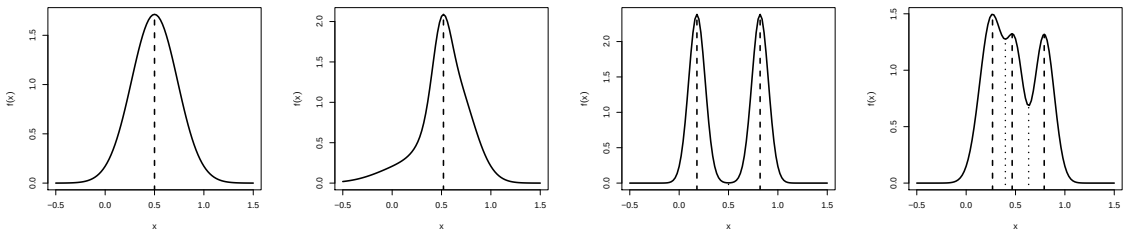

Figure 1.1: Examples of linear probability density functions. From left to right models (as described in Appendix A): M4, M7, M18 and M21. The dashed lines represent the mode and the dotted lines the antimode locations.

of these points. In Figure 1.1, some examples of unimodal and multimodal densities and their modes and antimodes are presented. The models considered for illustration are described in Appendix A and correspond to M4 (unimodal and symmetric), M7 (unimodal and assymetric), M18 (bimodal and symmetric) and M21 (trimodal and asymmetric).

The identification of the (unknown) number of modes is quite common in applied fields, such as, geology, neurology, economics, ecology or astronomy. Some examples include the study of the percentage of silica in chondrite meteors (Good and Gaskins, 1980), the analysis of the macaques neurons when performing an attention–demanding task (Mitchell et al., 2007), the distribution of household incomes of the United Kingdom (Marron and Schmitz, 1992), the study of the body–size in endangered fishes (Olden et al., 2007) or the analysis of the velocity at which galaxies are moving away from ours (Roeder, 1990). In all these examples, identifying the number (and location) of local maxima of the density function (i.e. modes) is important *per se*, or as a previous step for applying other procedures.

A first approach for determining the number of modes can be done in a parametric way, for example, using a mixture of distributions (a revision on this topic can be found in, for example, McLachlan and Peel, 2000). But, as it has been mentioned, the underlying structure of the data can be really complex, leading this parametric adjustment to a misspecification of the model. For that reason, a nonparametric perspective will be taken in this manuscript. Determining the number of modes can be done by estimating nonparametrically the probability density function f, as, in this case, it is not necessary to know anything about the real distribution of the sample. For doing that, the kernel density estimation can be used (see, for example, Wand and Jones, 1995, Ch. 2). Given a random sample $\mathcal{X} = (X_1, \ldots, X_n)$ of a random variable X with density function f, the kernel density estimation of f in a point x is

defined as:

$$\hat{f}_h(x) = \frac{1}{n}\sum_{i=1}^{n} K_h\left(x - X_i\right), \tag{1.1.1}$$

where K_h is the rescaled kernel function, that is, a unimodal and symmetric density function, centred at 0 and with bandwidth parameter h. An example of this estimator (and the one that it is going to be used later on) can be obtained using the Gaussian kernel:

$$\hat{f}_h(x) = \frac{1}{nh\sqrt{2\pi}}\sum_{i=1}^{n} \exp\left(-\frac{1}{2}\left(\frac{x - X_i}{h}\right)^2\right). \tag{1.1.2}$$

The bandwidth parameter plays a fundamental role in this estimation, as different number of modes can be obtained depending on the value of h. If the number of modes in $\hat{f}_h$ is equal to k, then the location of the estimated modes and antimodes will be denoted as $\widehat{x}_1, \ldots, \widehat{x}_{2k-1}$. In Figure 1.2 (left) the kernel density estimation with Gaussian kernel (1.1.2) obtained from a sample of size $n = 50$ from model M3 (see Appendix A) is represented, with bandwidths obtained from automatic rules, such us the rule of thumb and the Seather and Jones plug–in rule (see Wand and Jones, 1995, Ch.3). In this case, using the data–driven bandwidths, it is observed that the rule of thumb gives one mode and the plug–in rule shows four, while the real number of modes of f is $j = 1$. Although, in general, better results are achieved with the Seather and Jones plug–in bandwidth (for a discussion on this topic, see, for example, Wand and Jones, 1995, Ch.3), in this case it is the rule of thumb the one that detects correctly the underlying number of modes. The problem with these automatic bandwidths is that they are conceived to optimize the complete curve estimation (minimizing a global error criterion) and the problem here is focused only on the local maxima of f. Since the number of modes in $\hat{f}_h$ is a monotone decreasing function of h, when the Gaussian kernel is used (see Silverman, 1981), a simple exploratory solution, for determining the number of modes, is representing this density estimation for different values of h as it is done in Figure 1.2 (right). In fact, this is the idea of some graphical tools, such as the mode tree and forest (see Minnotte and Scott, 1993; Minnotte et al., 1998) or the SiZer (see Chaudhuri and Marron, 1999). The problems with these exploratory tools are that an "expert eye" is needed to determine the number of modes and they do not provide a formal way for determining the number of modes (in the sense that no "statistical significance" is attached to the output result). Moreover, they do not enable a systematic study when the aim is to determine the number of modes in a large number of samples. For these reasons, a testing perspective will be taken. The lack of a test on the number of modes providing a satisfactory performance in practice motivated the development of Chapters 2 and 3, for linear and circular data, respectively.

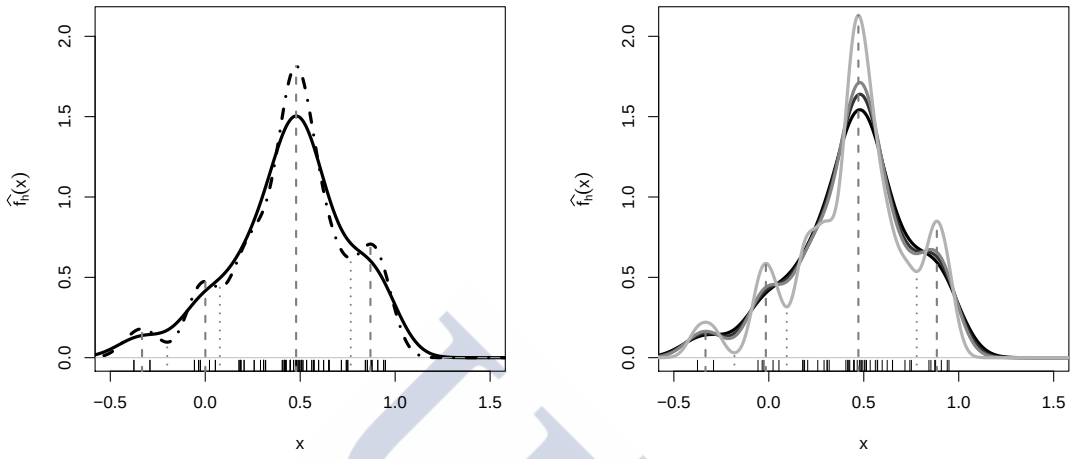

Figure 1.2: Kernel density estimation with Gaussian kernel (1.1.2) obtained from a sample of size $n = 50$ (from model M3) represented with ticks in the bottom of the plot. Left (black lines): $h = 0.116$ (continuous; rule of thumb) and $h = 0.0762$ (dot–dashed; plug–in). Right (continuous lines from dark to light grey): critical bandwidths for one ($h_1 = 0.110$), two ($h_2 = 0.096$), three ($h_3 = 0.087$) and four ($h_4 = 0.052$) modes. Grey discontinuous lines: (approximately) estimated location of the modes (dashed) and antimodes (dotted).

From a formal point of view, given a random variable with j modes, the testing problem was formulated in the statistical literature (see, for example, Silverman, 1981) as:

$$H_0 : j \leq k \quad \text{vs.} \quad H_a : j > k, \tag{1.1.3}$$

where k is the number of modes to be tested. It should be noted that the null hypothesis, in the new proposals presented in this essay, is restricted to $H_0 : j = k$, but this change will not present relevant practical consequences as it will be discussed. There have been quite a few proposals in the statistical literature for solving (1.1.3) in the linear case and the different techniques can be classified in two groups: a first group of tests based on or using a *critical bandwidth*, and a second group of tests based on the *excess mass*. A brief description of the underlying ideas of these two concepts are given below, and more details will be provided in Chapter 2.

The concept of critical bandwidth was introduced by Silverman (1981), using the aforementioned property of the number of modes being a monotone decreasing function of the density estimation (1.1.2). The critical bandwidth for k modes, denoted as

h_k is defined as the smallest bandwidth parameter for which $\hat{f}_h$ has k modes. In the example shown in Figure 1.2 (right), the kernel density estimation with bandwidth h_1 (the darkest line) is the last estimation having one mode (near 0.5), for smaller bandwidth parameters a second mode emerges (near location $x = -0.3$). In a similar way, $\hat{f}_{h_2}$ has these two estimated modes and for smaller bandwidth parameters a third mode appears (near $x = 0.9$). Silverman (1981) uses this parameter as the test statistic and the null hypothesis (1.1.3) will be rejected when h_k is too "large", since this means that it is necessary to oversmooth the kernel density estimation to obtain a k–modal structure. A calibration of this test statistic when the support (where the modes are located) is bounded and known was provided by Hall and York (2001) in the case of testing unimodality ($H_0 : j = 1$). The critical bandwidth is also used by Fisher and Marron (2001) to construct a Cramér–von Mises test statistic. In their paper, Fisher and Marron (2001) also provide a method for testing the number of modes when the random variable is circular using a U^2 of Watson (1961) test statistic. For the circular case, more details will be given in Chapter 3.

The second group of procedures use as a test statistic the excess mass introduced by Müller and Sawitzki (1991). For testing k modes, the underlying idea of this statistic is measure the difference in probability mass between considering that the density has $(k+1)$ or k modes. "Large" values of this test statistic will indicate that at least one more mode is present, i.e., that the null hypothesis is false. Although the first proposal in this group of tests, the one introduced by Hartigan and Hartigan (1985), does not use this test statistic, it will be presented in this block since the value of their test statistic (known as *dip*) is exactly a half of the value of the excess mass for the unimodal case. The dip statistic measures the maximum difference between the empirical distribution function and the integral of a "unimodal distribution function" (first convex, then with constant slope and in the final part concave) that minimizes that maximum difference. Both Hartigan and Hartigan (1985) and Müller and Sawitzki (1991) proposed the same way of calibrating the test statistic and although the dip and the excess mass are equivalent in the unimodal case, just the excess mass can be generalized for testing if the density is k–modal (with $k > 1$). The calibration of this test statistic for testing unimodality was provided by Cheng and Hall (1998). Finally, a comparative between the different methods is provided in Chapter 2. It will be seen that none of the existing proposals provides a satisfactory performance in practice. For that reason, a new procedure which combines the previous approaches (critical bandwidth and excess mass) is presented in Chapter 2 and compared with the existing methods, showing a superior behaviour (specially when testing $H_0 : j = k$, with $k > 1$).

1.2 Background on circular data

As it was already mentioned, the second focus of this essay will be set on the circular case. The need of circular statistics appears for one dimensional data when the periodicity must be taken into account and the sample can be represented on the circumference. Examples of circular data appears when the goal is to model orientations or a periodic phenomenon with known period. These examples are frequent in many applied fields, some of them related with orientations: the orientation of the red wood ants in reaction to different stimuli (Jander, 1957); the flight orientation in pigeons returning home (Schmidt-Koenig, 1963); the wind direction at Gorleston (England) during 1968 (Fisher, 1995, Ch. 5); or waves directions in the Adriatic sea (Jona-Lasinio et al., 2012; Lagona et al., 2015). Other examples are related with periodic phenomena: the number of soldiers deaths (along each year) during the Crimean War (originally introduced by Nightingale in 1858 and revisited in Brasseur, 2005); or the frosting and defrosting times (during the day) in glaciers Monte Alvear and Vinciguerra in Ushuaia, Argentina (Oliveira et al., 2013). Having in mind that the data is periodic, in order to provide their characterization, two choices must be done: an initial direction and sense of rotation; but the results cannot depend on these choices. It is for that reason that, from an inferential perspective, circular data require a different treatment to that given to linear data. An example of this issue can be found in the sample mean. For example, if one has two directions in radians $-\pi/6$ and $\pi/6$, using as initial direction $-\pi$, then the sample mean is equal to zero; meanwhile if the initial direction is zero, then $-\pi/6$ becomes to $11\pi/6$ and the sample mean is equal to π. For that reason, the sample mean direction must be defined taking into account the circular structure, given the circular sample in angles $\boldsymbol{\Theta} = (\Theta_1, ..., \Theta_n)$ from a circular random variable Θ, this mean can be defined as

$$\bar{\theta} = \arg\left\{ \frac{1}{n}\sum_{j=1}^{n} \cos\Theta_j + i\frac{1}{n}\sum_{j=1}^{n} \sin\Theta_j \right\} \tag{1.2.4}$$

where i is the imaginary unit and arg denotes the function which returns the argument of a complex number. As it was already mentioned, a complete introduction on this topic can be found in Mardia (1972). More modern references include Fisher (1995), Mardia and Jupp (2000), Jammalamadaka and Sengupta (2001) or Ley and Verdebout (2017).

A brief introduction to circular data is made in this essay to present notation and some special features of this kind of data. In this manuscript, the continuous and circular random variable Θ will be measured in radians an its support will be the interval $[0, 2\pi)$. To facilitate the explanation, an abuse of notation will be made denoting as f also to the circular density function, from now on and, also, in Chapters 3

and 4. Taking into account the aforementioned periodicity, the density function must satisfy the following conditions (Jammalamadaka and Sengupta, 2001, Ch. 2):

- $f(\theta) \geq 0, \forall \theta \in [0, 2\pi)$;
- $\int_0^{2\pi} f(\theta) d\theta = 1$;
- $f(\theta) = f(\theta + 2m\pi), \forall \theta \in [0, 2\pi)$ and $\forall m \in \mathbb{Z}$.

1.2.1 Some circular distribution models

Apart from the trivial case of the simple uniform distribution on $[0, 2\pi)$, some of the most well–known circular densities include the cardioid, the von Mises and the wrapped distributions such as the wrapped normal and the wrapped Cauchy (see, for example, Jammalamadaka and Sengupta, 2001). These four models (represented in Figure 1.3) are characterized by the concentration parameter, where "large" values of this parameter indicates when the distribution is more concentrated around zero. For simplicity, all the densities will be centred at 0, but a location parameter can be introduced to change the central direction, leading to densities of the form $f(\theta - \mu)$, with central direction $\mu \in [0, 2\pi)$.

Cardioid distribution. The cardioid distribution centred at 0 with parameter of concentration ρ, namely C_ρ, is a perturbation of the uniform circular density by a cosine function which has probability density function

$$f_{\mathrm{C}_\rho}(\theta) = (1/2\pi)(1 + 2\rho\cos\theta), \text{ with } \theta \in [0, 2\pi) \text{ and } 0 < \rho < 1/2.$$

Although in most of the references, introducing the circular topic, the concentration parameter is restricted to $|\rho| < 1/2$, both here and in the following distributions, the support of the concentration parameter is taken to guarantee that this distribution is going to be unimodal. Being the mode at 0 or μ, when the cardioid distribution with location parameter μ is considered, namely as $\mathrm{C}(\mu, \rho)$ and with density $f_{\mathrm{C}_\rho}(\theta - \mu)$.

Von Mises distribution. The von Mises distribution, $\mathrm{VM}(\mu, \kappa)$, was created to guarantee that the maximum likelihood estimator of μ is equal to the circular sample mean defined in (1.2.4). The von Mises centred at 0, VM_κ, has probability density function

$$f_{\mathrm{VM}_\kappa}(\theta) = \frac{1}{2\pi I_0(\kappa)} e^{\kappa\cos(\theta)}, \text{ with } \theta \in [0, 2\pi) \text{ and } \kappa > 0, \tag{1.2.5}$$

where the normalising constant contains I_0 which denotes the modified Bessel function of the first kind and order 0, $I_0 = (1/2\pi)\int_0^{2\pi} \exp(\kappa\cos(\theta))d\theta$.

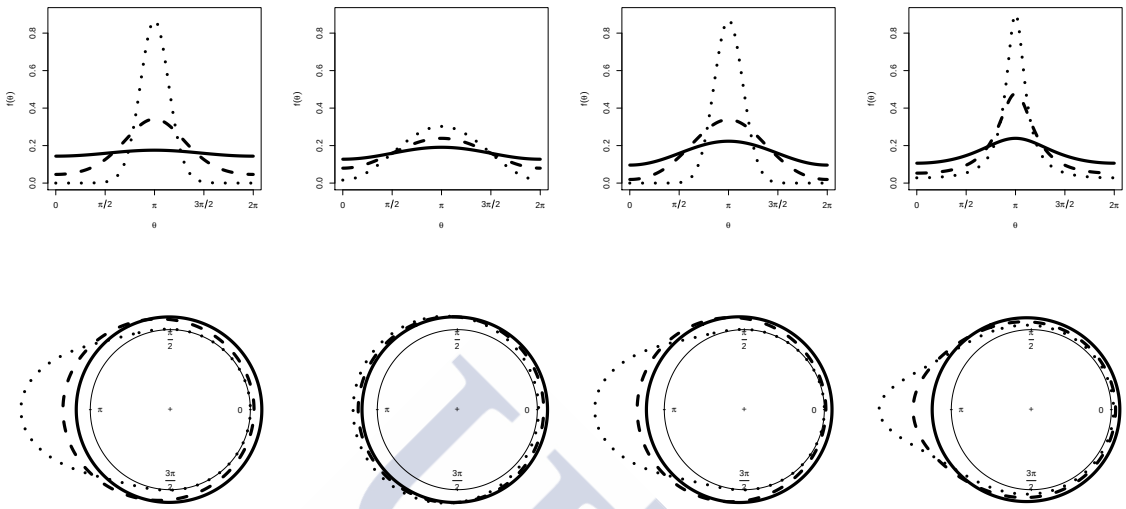

Figure 1.3: Examples of circular probability density functions. From left to right, linear (top) and circular (bottom) representation of the models centred on π with different concentration parameters: von Mises, with $\kappa = 0.1$ (solid line), 1 (dashed line) and 5 (dotted line); cardioid, with $\rho = 0.1$ (solid line), 0.25 (dashed line) and 0.45 (dotted line); wrapped normal, with $\rho = 0.2$ (solid line), 0.5 (dashed line) and 0.9 (dotted line); and wrapped Cauchy, with $\rho = 0.2$ (solid line), 0.5 (dashed line) and 0.7 (dotted line).

Wrapped distributions. Another way of obtaining circular distributions is wrapping around the circumference of unit radius a given linear distribution. That is, if X is a random variable on the real line, the corresponding circular random variable Θ is given by $\Theta = X \mod 2\pi$. Hence, if X has a linear density function f_L, then the corresponding circular density function f_C of Θ is

$$f_C(\theta) = \sum_{p=-\infty}^{\infty} f_L(\theta + 2p\pi).$$

Some of the most well–known distributions of this kind are the wrapped Cauchy and the wrapped normal distributions. As its name indicates, the wrapped Cauchy distribution, f_{WC_ρ}, is obtained wrapping the Cauchy distribution (see Johnson et al., 1995, Ch. 16), with location parameter 0 and scale parameter $-\log(\rho)$, where log is the natural logarithm. Its probability density function has the following expression

$$f_{\mathrm{WC}_\rho}(\theta) = \frac{1}{2\pi} \frac{1-\rho^2}{1+\rho^2-2\rho\cos\theta}, \text{ with } \theta \in [0, 2\pi) \text{ and } 0 < \rho < 1.$$

Meanwhile the wrapped normal distribution, f_{WN_ρ}, is constructed by wrapping the normal distribution centred in 0 and with variance $-2\log(\rho)$ onto the circle. The probability density function, in this case, is equal to

$$f_{\mathrm{WN}_\rho}(\theta) = \frac{1}{2\pi}\left(1 + 2\sum_{p=1}^{\infty}\rho^{p^2}\cos(p\theta)\right), \text{ with } \theta \in [0, 2\pi) \text{ and } 0 < \rho < 1. \quad (1.2.6)$$

1.2.2 Modes of circular data

The four previously introduced models represent examples of unimodal circular distributions. A value of Θ will be a mode if in this point, belonging to the interval $[0, 2\pi)$, the circular density function has a local maxima. Again, if there is one mode, the density (or the associated distribution) will be unimodal and if it has more than one mode, multimodal. If the class one density has a finite number of local extrema (with j modes), the modes and antimodes (local minima of f) will be denoted as $\theta_1, \ldots, \theta_{2j}$, since in this case there are the same amount of local minima and maxima, due to the periodicity. The models represented in Figure 1.3 are examples of unimodal circular densities (with a single mode at π).

The problem of testing if the circular random variable is k–modal will be treated again from a nonparametric point of view. Making again an abuse of notation, the circular kernel density estimation (see, for example, Oliveira et al., 2013) can be defined as follows

$$\hat{f}_\nu(x) = \frac{1}{n}\sum_{i=1}^{n} K_\nu\left(\theta - \Theta_i\right),$$

where K_ν is the circular kernel with concentration parameter ν. An example of circular kernel, and the one that is going to be used later on, is provided by the probability density function of the wrapped normal distribution (1.2.6) with concentration parameter $\nu \in (0, 1)$, that is,

$$\hat{f}_\nu(\theta) = \frac{1}{2\pi n}\sum_{i=1}^{n}\left(1 + 2\sum_{p=1}^{\infty}\nu^{p^2}\cos(p(\theta - \Theta_i))\right). \quad (1.2.7)$$

The role of the concentration parameter ν in the circular kernel density estimation is the opposite of the bandwidth parameter in the linear estimation, in the sense that, usually, small (large) values of ν leads to estimations with less (more) modes. The decision of considering the wrapped normal kernel instead of the usual von Mises is because with the first one the number of modes is always a nondecreasing function of ν, whereas with the von Mises kernel this property is not guaranteed (see Huckemann

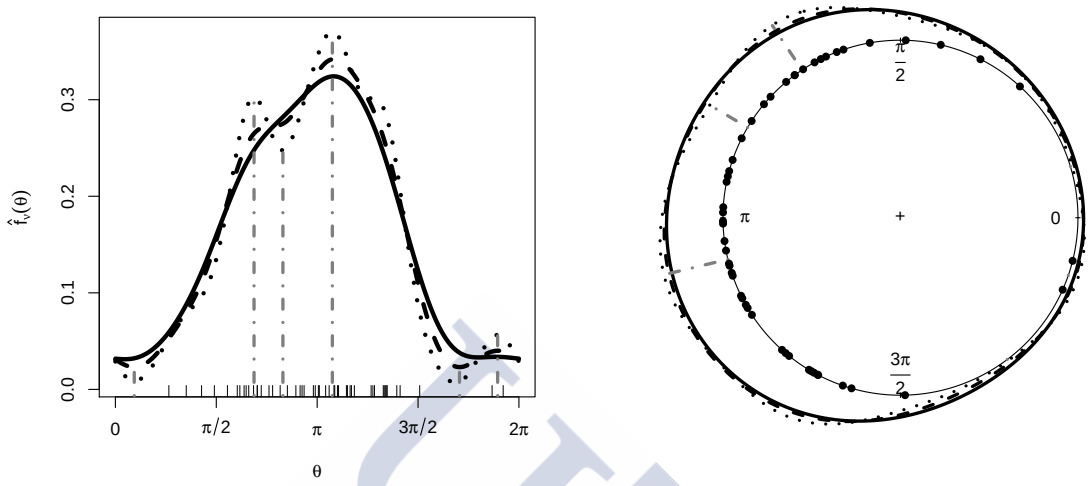

Figure 1.4: Kernel density estimation with wrapped normal kernel (1.2.7) obtained from the sample of size $n = 50$ (from model MC8). Using the critical concentration parameter for one ($\nu_1 = 0.873$; solid line), two ($\nu_2 = 0.925$; dashed line), three ($\nu_3 = 0.965$; dotted line) modes. Grey dot–dashed lines: (approximately) estimated location of the modes and antimodes. Left: linear plot with data represented with ticks in the bottom. Right: circular plot with data represented with points on the circle.

et al., 2016). In an analogous way to the critical bandwidth, one can define the critical concentration parameter ν_k, as the largest concentration parameter for which the kernel density estimation (1.2.7) has k modes. In Figure 1.4, employing a sample of size 50 generated from model MC8 (see Appendix A), the density estimation (1.2.7) with the critical concentration for one, two and three modes is represented. In this case, if $\hat{f}_\nu$ has k modes, the estimated modes and antimodes will be denoted as $\hat{\theta}_1, \ldots, \hat{\theta}_{2k}$.

1.2.3 Circular reflective symmetry

Also in the circular data context, the second problem that is going to be treated in this essay, in Chapter 4, is determining if the underlying density is symmetric. Since the circle symmetry is not uniquely defined (due to its compactness and the isometries of rotation and reflection), it is necessary to specify which one is going to be analysed. Apart from linear tests adapted to the circular settings (that can be

used when data are distributed over a reduced arc of the circle), in the literature three kinds of symmetry were studied. The first type of symmetry that can be tested is cyclic, or the l–fold, symmetry on the circle, if F is the circular distribution function of Θ, the testing problem is,

$$H_0 : F(\theta) - F(\vartheta) = F(\theta + 2\pi/m) - F(\vartheta + 2\pi/m) \tag{1.2.8}$$

with m a positive integer, so that F is invariant under rotation by $2\pi/m$. Testing (1.2.8) is interesting, for example, when one wants to know if the distribution is suitable for modelling axial data (taking $m = 2$), i.e., the circular probability density function also satisfies $f(\theta + \pi) = f(\theta)$. This problem was studied by Jupp and Spurr (1983) introducing rank–based procedures. One can also test reflective symmetry about a specified axis. A locally optimal rank test against rotational alternatives was constructed by Schach (1969) and it was also shown the asymptotic relative efficiency of the Wilcoxon test relative to the locally most powerful test for von Mises distributions. The last proposal is rather a location test and it can be applied when one wants to test for the circular median.

Finally, one can also test for reflective symmetry on the circle which is equivalent to the usual symmetry on the real line, i.e., test if the circular density f, with central direction μ, satisfies $f(\theta + \mu) = f(-\theta + \mu)$. The reflective symmetry is the one that is going to be tested and, for that reason, in this essay, it will be named simply as circular symmetry. The four circular models described (von Mises, cardioid, wrapped Cauchy and wrapped normal) are symmetric around zero and all belong to the family

$$\begin{aligned}\mathcal{F} \;=\; \Big\{ & f_0 : f_0(\theta) > 0 \,\text{almost everywhere (a.e.)},\ f_0(\theta + 2\pi m) = f_0(\theta),\ \forall m \in \mathbb{Z}, \\ & f_0(-\theta) = f_0(\theta), f_0 \text{ unimodal in } \theta \in [0, 2\pi) \text{ with mode at } 0, \int_0^{2\pi} f_0(\theta)\, d\theta = 1 \Big\}.\end{aligned}$$

Using the location parameter $\mu \in [0, 2\pi)$, if $f_0 \in \mathcal{F}$ then the density of the form $f_0(\theta - \mu)$ is symmetric around μ. In particular, the four models represented in Figure 1.3 are symmetric around π. In the last few years, several examples of (reflective) asymmetric circular models appear on the literature. Some of them can be found in Jones and Pewsey (2012) or in Kato and Jones (2015). In particular, a way of constructing asymmetric models is provided by Umbach and Jammalamadaka (2009), who inspired by the perturbation approach of Azzalini and Capitanio (2003) proposed circular densities of the form

$$2 f_0(\theta - \mu) G(\omega(\theta - \mu)),$$

where $f_0 \in \mathcal{F}$; G is the cumulative distribution function of some reflectively symmetric circular distribution and ω is a weighting function satisfying: (i) $\omega(-\theta) = -\omega(\theta)$; (ii) $\omega(\theta + 2\pi m) = \omega(\theta)\ \forall m \in \mathbb{Z}$; (iii) $|\omega(\theta)| \leq \pi$. Following the proposal of Umbach

and Jammalamadaka (2009), one can take $G(\theta) = (\pi + \theta)/(2\pi)$, the cumulative distribution function of the circular uniform distribution, $\omega(\theta) = \lambda\pi \sin(\mathtt{k}\theta)$, $\mathtt{k} \in \mathbb{N}_0 = \{1, 2, 3, \ldots\}$ and $\lambda \in [-1, 1]$. These choices yield the family of $\mathtt{k}$–*sine–skewed* distributions[1] with densities

$$f^{\mathtt{k}}_{\mu,\lambda}(\theta) = f_0(\theta - \mu)[1 + \lambda \sin(\mathtt{k}(\theta - \mu))], \tag{1.2.9}$$

where λ is the skewness parameter in the sense that for $\lambda = 0$ the density (1.2.9) is (reflectively) symmetric and when $\mathtt{k} = 1$, in general, the density is unimodal and it is skewed to the left if $\lambda > 0$ and to the right if $\lambda < 0$. For $\mathtt{k} \geq 2$ and $\lambda \neq 0$, the density (1.2.9) is generally multimodal, λ and $\mathtt{k}$ determine the number of modes as well as their heights and skewness (see Abe and Pewsey, 2011, for more information about the effect of these parameters). Some examples of $\mathtt{k}$–sine–skewed densities using as f_0 the von Mises density function (1.2.5) with $\mu = \pi$ are shown in Figure 1.5. Analysing the $\mathtt{k}$–sine–skewed densities, as aforementioned, just the densities with $\lambda = 0$ are symmetric. The number of modes of the $\mathtt{k}$–sine–skewed densities, on these particular cases, is one when $\mathtt{k} = 1$; also with concentration parameter $\kappa = 1$ (when $\lambda = 0.2$) and with $\kappa = 10$ the models are unimodal; the rest of the models (with $\lambda \neq 0$) are bimodal when $\mathtt{k} = 2$ and trimodal when $\mathtt{k} = 3$. Regarding their applications, the $\mathtt{k}$–sine–skewed distributions have been used as models for ant orientation data and the times of thunder storms, in Abe and Pewsey (2011), the CO_2 daily cycle at a rural site, in Pérez et al. (2012), and forest disturbance regimes, in Abe et al. (2012).

For testing reflective symmetry (or simply symmetry) in the linear case there are in the literature several proposals. The existing methods can be divided into two groups: when the central location is known and when it is unknown. Some references studying and comparing different proposals for testing the first group include McWilliams (1990), Modarres and Gastwirth (1996, 1998) or Ahmad and Li (1997, using kernel methods). Also, for this group, an optimal proposal for testing symmetry (against the general skewed distributions of Ferreira and Steel, 2006) can be found in Ley and Paindaveine (2009). The proposals of, for example, Romano et al. (1989) or Cabilio and Masaro (1996) can be used for testing linear symmetry when the central location is unknown (also, some references can be found on there of different parametric and nonparametric methods for testing symmetry). In this case, Cassart et al. (2008) have also proposed an optimal test for symmetry about an unknown centre (against Frechner–type alternatives). While testing for symmetry is a classical issue on the real line (and for that reason, it is not treated on this essay), the situation is very different in the circular case where there exist three principal proposals. For testing (reflective) circular symmetry when the central direction is known, there are two methods: the

[1] In order to make clearer the notation in the manuscript: k refers to the number of modes of being tested, $\mathtt{k}$ will be used for the $\mathtt{k}$–sine–skewed distributions and κ is the concentration parameter in a von Mises distribution.

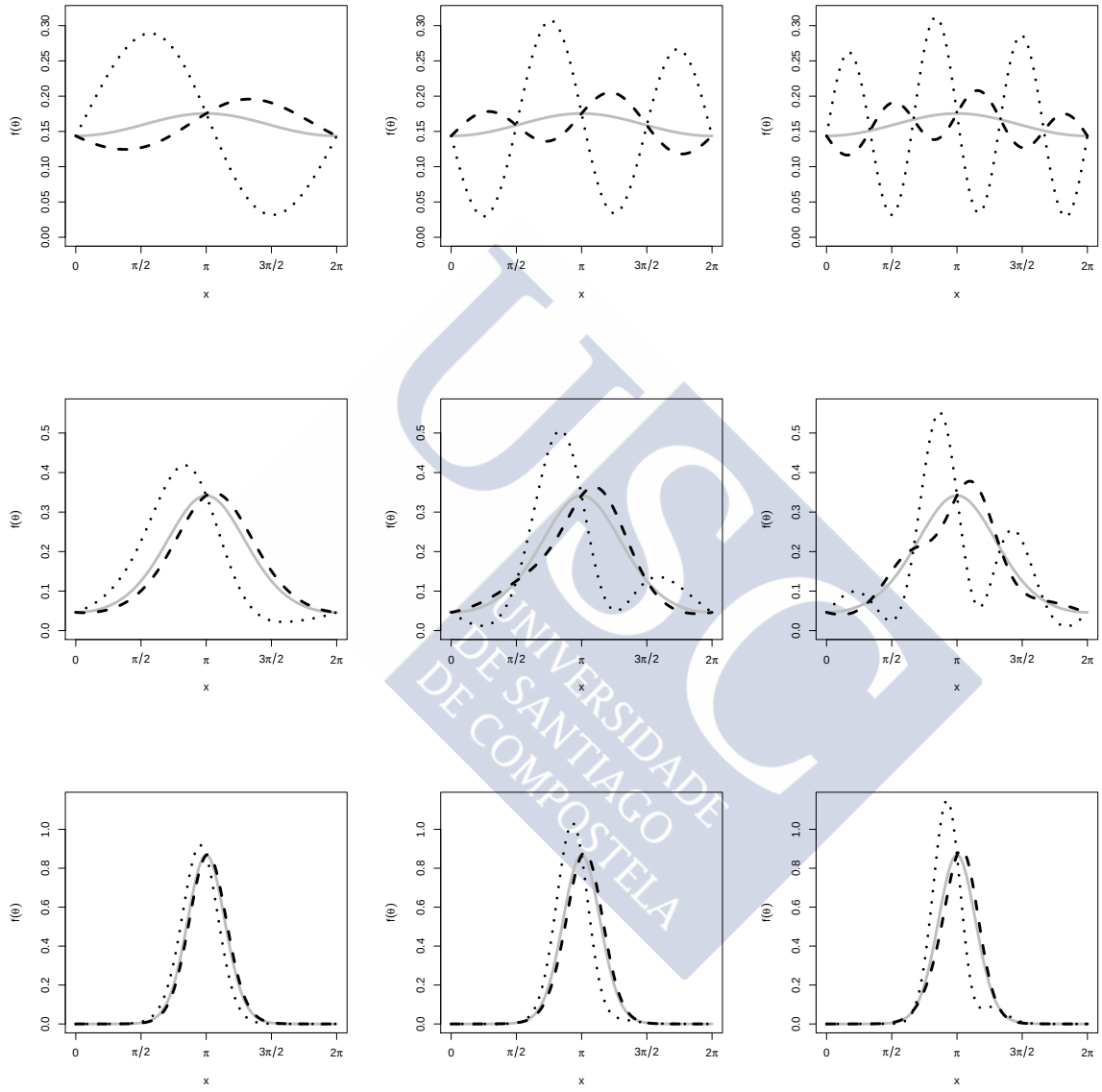

Figure 1.5: Examples of k–sine–skewed density functions using as f_0 the von Mises density function with $\mu = \pi$. From left to right: value of k equal to 1, 2 and 3. From top to bottom: parameter of concentration κ equal to 0.1, 1 and 5. With parameter of λ equal to 0 (solid grey line), 0.2 (dashed black line) and -0.8 (dotted black line).

b2–star test of Pewsey (2004, which can be seen as a non–parametric test), based on the second sine moment about the fixed central direction; and the optimal test (against k–sine–skewed alternatives) of Ley and Verdebout (2014). When the central direction is unknown, just the b2–bar proposal of Pewsey (2002) can be properly used for testing symmetry (and there is no notion of optimality in this test). The objective of the Chapter 4 is present a new optimal proposal (against the k–sine–skewed alternatives) for testing reflective symmetry when the central direction is unknown. A new test statistic and its asymptotic distribution under the null and under k–sine–skewed alternatives will be given. In Chapter 4, it will be also seen that the b2–bar test of Pewsey (2002), asymptotically, is a particular case of this new proposal. The proposal in the Chapter 4 will be test for reflective symmetry about an unknown central against the k–sine–skewed alternatives, i.e., it will be tested $H_0 : \lambda = 0$ vs. $H_1 : \lambda \neq 0$ in a parametric (when f_0 is determined) and in a semi–parametric way (when nothing about f_0 is known). The (optimal) tests will be obtained following the Le Cam methodology. For that reason, in this manuscript, the optimality will be understood in the *maximin* sense. A test ϕ^* is maximin in the class of test at level α, $\mathcal{C}_\alpha$, for the null hypothesis H_0 against the alternative H_1, if ϕ^* has level α and its power is such that $\inf_{P\in H_1} \mathbb{E}_P(\phi^*) \geq \sup_{\phi\in\mathcal{C}_\alpha} \inf_{P\in H_1} \mathbb{E}_P(\phi)$. A brief introduction on Le Cam Theory and the needed notation is given in Appendix D. A complete description can be found in, e. g., Le Cam (1986), van der Vaart (2002) or Ley and Verdebout (2017).

1.3 Real datasets

An introduction to the different datasets analysed and/or used for illustration in this essay is given below. The objective in the first two dataset will be to determine the number of modes in the linear case. The third one motivates a large part of this dissertation and it will be related with the problem of assessing the number of modes in the circular case. The goal the fourth dataset is to determine if they are reflective symmetric around the central direction.

1.3.1 The 1872 Hidalgo stamp issue of Mexico

A classical example which has been extensively considered in mode testing literature can be found in philately (the study of stamps and postal history and other related items). Research in this field has been motivated by the use of stamps for investment purposes. Before the 1940 decade, stamps images were printed on a variety of paper

types and, in general, with a lack of quality control in manufactured paper, which led to important fluctuations in paper thickness, being thin stamps more likely to be produced than thick ones. Given that the price of any stamp depends on its scarcity, the thickness of the paper is crucial for determining its value. Although the watermark of some stamps (a mark indicating were the stamp was produced; see Figure 1.6, right) can help to catalogue a stamp issue, there is not a standard rule for classifying stamps according to their thickness (not being available such a classification in catalogues), becoming this problem even harder in stamp issues printed on a mixture of paper types with possible differences in their thickness. A stamp issue with this problematic is the Hidalgo catalogue (an stamp of this issue can be seen in Figure 1.6, left), from the nineteenth century, and this particular example has been shown in several references in the literature as a paradigm of the problem of determining the number of modes/groups. From a nonparametric point of view, some examples of its utilization for mode testing have been shown by Efron and Tibshirani (1994, Ch. 16), Izenman and Sommer (1988) or Fisher and Marron (2001). It has been also analysed using nonparametric exploratory tools by Wilson (1983), Minnotte and Scott (1993) and by Chaudhuri and Marron (1999). This dataset was obtained from Table 2 in Izenman and Sommer (1988).

1.3.2 Seropositivity in malaria eradication

Malaria is a global health problem causing symptoms that typically include fever, fatigue, vomiting, headaches and, in the several cases, it can cause yellow skin, seizures, coma, or death. This disease, caused by *Plasmodium* parasites, is most commonly transmitted to humans by infected mosquitoes. Being two of the species of Plasmodium that can infect and be spread by humans, the *Plasmodium falciparum* (Pf) and the *Plasmodium vivax* (Pv). Due to the prevention measures in the last decades, in several countries are already targeting malaria elimination. A way of understanding the true malaria exposure in a given population is using the antibody data against different malaria antigens (see, for example, Corran et al., 2007, a test detecting the antigens is provided in Figure 1.7, left). The reason of using this data is that the antibody concentrations are directly correlated with the parasite exposure, thus, it provides information on current and recent infections. In seroepidemiological studies, one of the most popular antibodies is the *Merozoite Surface Protein–1* (PfMSP1 when referring to Pf and PvMSP1 when it is associated to Pv). Employing the antigen data, when no more information about the serological status (seropositive or seronegative) of the individuals is provided, a way to determine if malaria is still in a given population is try to determine if there are more than one latent subpopulation. With the objective of seeing if malaria is in an elimination phase, data from Aneityum island

Figure 1.6: Left: *doce centavos* stamp of the Hidalgo issue of Mexico printed on 1872 from Wikimedia Commons (2009b). Right: example of a watermark on the back of a Zululand (historical region of South Africa) stamp indicating that the stamp belongs to the *Crown CA* production, from Wikimedia Commons (2009a).

in Vanuatu archipelago and Chabahar in southeastern Iran are used. In this two regions, where Pf and Pv parasities co–exist, the antibodies PfMSP1 and PvMSP1 were quantified. The complete description of these two dataset is given in Cook et al. (2010) and Zakeri et al. (2016). More complete information about the malaria topics and some references can be found in, for example, Sepúlveda et al. (2015). These datasets were provided by Dr. Nuno Sepúlveda from the London School of Hygiene and Tropical Medicine, United Kingdom, for a joint work with other coauthors on this topic (see Section 1.5.1).

1.3.3 Date of the wildfires detected among the world

This dataset contains the location and date (in a daily resolution) of all the fires detected among the world by the *MODerate resolution Imaging Spectroradiometer* (MODIS), launched into Earth orbit by the *National Aeronautics and Space Administration* (NASA) on board the Terra (*EOS AM*) and the Aqua (*EOS PM*) satellites, from 10 July 2002 to 9 July 2012 (an example of some detected fires is included in Figure 1.8). Taking the date of all the fires detected in each cell of size 0.5° (latitude and longitude), the goal is to assess if there is one season of fires along the year or more than one. This study can help to understand where humans are altering the fire seasonality causing more peaks of fires than those ones expected due to climatolo-

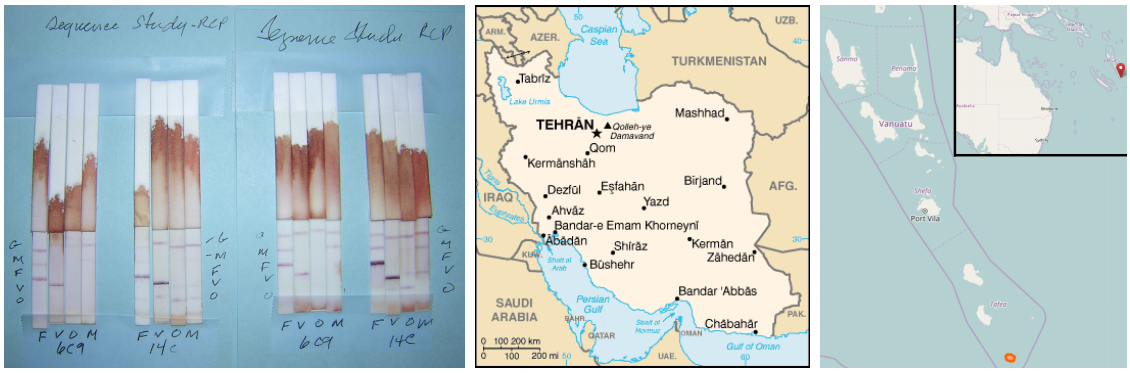

Figure 1.7: Left: example of a dipstick detecting some specific antigens produced by malaria parasites in the blood of infected individuals, from Wikimedia Commons (2004a). Center: map of Iran from Wikimedia Commons (2004b), Chabahar is located in the South–East of Iran. Right: map with the Vanuatu archipelago from OpenStreetMap contributors (2017), marking (in orange and with a pointer) the Aneityum island.

gical factors. In addition to the problem of testing the number of modes in the circle, another issue appears as the goal is to analyse the number of fire seasons globally. Then, due the territory division, the incorrect rejections of the null hypothesis caused the multiple testing must be controlled. In addition, the possible spatial correlation between the "closed" regions must be also taken into account. How to solve this problematic will be tackled in Chapter 3. This dataset was provided by Dr. José Miguel Cardoso Pereira and his research team from the Instituto Superior de Agronomia, Lisbon, Portugal, for a joint work with other coauthors on this topic (see Section 1.5.2).

1.3.4 Cracks in cemented femoral components

This dataset was collected during an in vitro fatigue study of total hip replacements described in Mann et al. (2003) and also analysed in Oliveira (2014) for illustrating the CircSiZer maps (see Figure 1.9 center and right). The data from the study consist of the directions, measured in angles relative to the centre of the stem, of fatigue cracks around the cemented femoral components in hip implants (how the angles are obtained is shown in Figure 1.9). After a substantial stress cycle had been applied, each femur was sectioned in 10 mm intervals from the level of the implant collar to the distal tip of the stem. Measurements at 60 and 70 mm were not made because of features in the experimental setup. As a result, two groups of measurements were

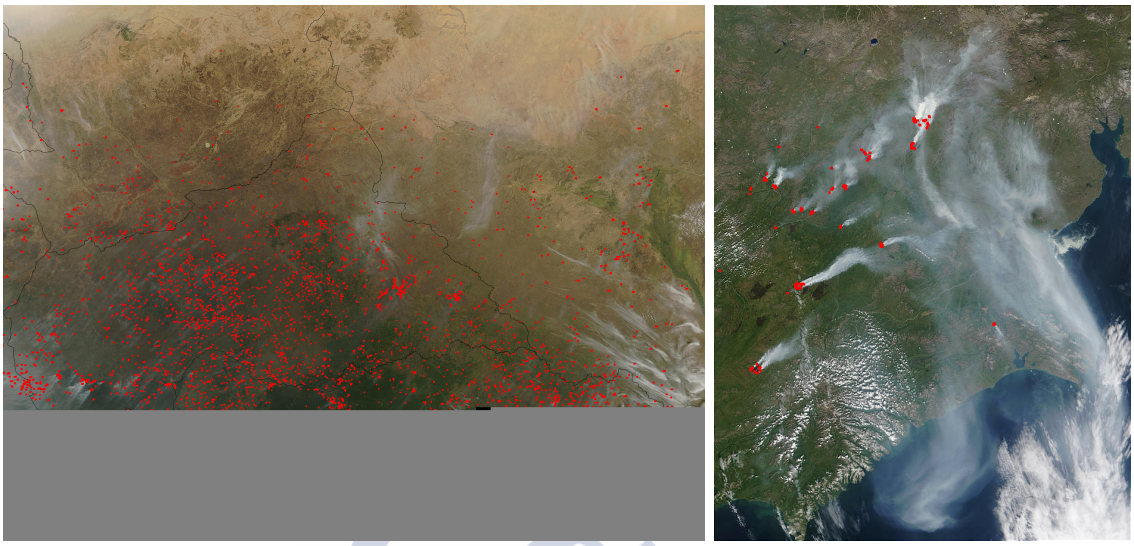

Figure 1.8: Fires detected (in red) by MODIS. Left: on board the Aqua satellite around Central African Republic on February 6, 2004, from NASA Visible Earth (2004). Right: on board the Terra satellite in the north–eastern part of Russia (near the Bering Sea) on July 18, 2003, from NASA Visible Earth (2003).

obtained: those in the proximal (10–50 mm) region and those in the distal (80–110 mm) region. Mann et al. (2003) showed that the directions of the fatigue cracks are not uniformly distributed and that their distributions in the two regions differ. The objective in this case is investigate whether the cracks in the two regions are symmetrically distributed about some unknown centre. This dataset was provided by Dr. Kenneth A. Mann from the Upstate Medical University, New York, United States of America.

1.4 Manuscript distribution

A brief summary of each chapter in this manuscript will be provided. The main topics will be highlighted, as well as the chapter distribution. In a subsequent section, the scientific contributions of this thesis will be presented.

Chapter 2 contains a review of the different proposals for testing the number of modes. This task has been approached in the statistical literature from two different perspectives: the critical bandwidth and the excess mass. Since none of the existing proposals provides a satisfactory performance in practice, a new procedure

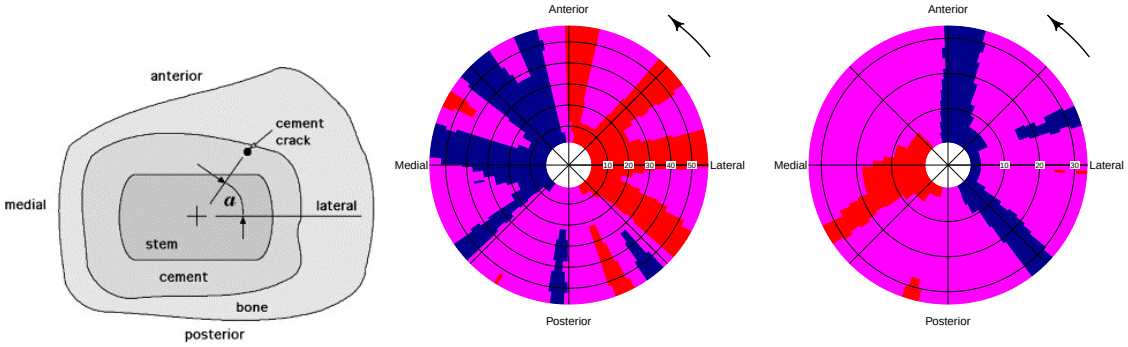

Figure 1.9: Left: the data is obtained from the angle of the crack with respect to the lateral direction, taking counterclockwise as the positive sense of rotation, from Mann et al. (2003). Center and right: CircSiZer maps for kernel density estimates in proximal (central panel) and distal (right panel) regions; given a concentration parameter (as indicated in the radius) and an angle, blue colour indicates locations where the curve is significantly increasing, red colour shows where it is significantly decreasing and purple indicates where it is not significantly different from zero; thus, for a given concentration, a blue–red pattern indicate where there is a significance peak.

which combines the previous approaches is presented and compared with the existing methods, showing a superior behaviour. The proposed technique is illustrated with the Hidalgo dataset and the example on the detection of seropositivity in malaria eradication.

In Chapter 3 a new method for assessing the number of modes in the circular case is given and it is provided its behaviour in the finite sample case. The proposed method is used in a real dataset of wildfires in a global scale. The issues related with the multiple testing problem and the spatial correlation between observations in the different locations are also solved in this chapter.

Chapter 4 is devoted to the development of a new procedure for testing circular reflective symmetry about an unknown central direction. The construction of the optimal (in the maximin sense) test will be done following the Le Cam theory. The asymptotic distribution of the test statistic under the null hypothesis of circular symmetry and under `k`–sine–skewed alternatives is provided. The behaviour of the test in the finite sample case is shown. Applications of the test in a dataset related with the cracks in cemented femoral components is also provided.

Finally, the manuscript includes some final comments and discussion in Chapter 5

and four appendices. In Appendix A, the circular and linear models used in the simulation studies in Chapters 2, 3, 4 and with illustration purposes along the manuscript are defined and represented. Appendix B collects the technical proofs of Chapters 2 and 4. Appendix C includes some numerical approaches made in Chapter 2. In Appendix C, the utilities of a new R package are presented. Package **multimode** includes different methods for testing and exploring the number of modes in a linear density function. In Appendix D, an introduction on Le Cam Theory is given.

1.5 Contributions of the thesis

The main goal of this thesis is to propose new tests for assessing simplifying hypothesis in linear and circular density modelling. As mentioned in the Introduction, the most relevant contributions can be summed up in three parts: multimodality tests in the linear setting, multimodality tests for circular data and symmetry tests for circular densities. In the following paragraphs, a summary of the main contributions is presented.

1.5.1 Contributions on multimodality tests for linear data

The objective is testing if a linear random variable has k modes against more than k using nonparametric methods, i.e, $H_0 : j = k$ vs. $H_0 : j > k$, where j denotes the unknown number of modes and $k \in \mathbb{Z}^+$.

State of the art

From a nonparametric perspective, the multimodality test were firstly introduced by Silverman (1981), Hartigan and Hartigan (1985), and Müller and Sawitzki (1991). Referring to the case when $k = 1$ (testing unimodality) just Cheng and Hall (1998) and Hall and York (2001, when the support of the random variable is known) provide asymptotically well calibrated procedures. In the more general case, when $k > 1$, just the proposals of Silverman (1981) and Fisher and Marron (2001) are available and none of them are well calibrated. A dataset in which analysing the number of modes is important is the known as the 1872 Hidalgo stamp issue of Mexico, introduced originally by Wilson (1983) and used as a motivational example since the analysis of Izenman and Sommer (1988), who employed the test proposed by Silverman (1981). Referring to the available software for testing the number of modes, up to the knowledge of the author, just the dip test of Hartigan and Hartigan (1985) and the critical bandwidth test of Silverman (1981) were implemented, see, for example, the **diptest**

package of R (Maechler, 2015) or the `silvtest` function in Stata (Salgado-Ugarte et al., 1998).

Contributions

A new test outperforming, in the unimodal case, the previous asymptotically well calibrated procedures and allowing the extension to the more general case (when $k > 1$) is presented in Ameijeiras-Alonso et al. (2016). A new procedure which combines the previous approaches (smoothing and excess mass) is presented and compared with the existing methods. For illustration purposes, it is also included the 1872 Hidalgo stamp issue of Mexico example for analysing the number of modes with a well calibrated test. Another application of the proposed test is done in the malaria field for identifying seropositive groups in the population in Sepúlveda et al. (2017). Finally, in Ameijeiras-Alonso et al. (2017a), the different methods, implemented in the **multimode** package of R, for testing and estimating the number and location of the modes are provided.

1.5.2 Contributions on multimodality tests for circular data

The objective is testing the number of modes in a circular sample. Then, apply the method for determining, in each region of the world, if there is one season of fires or more lead to a multiple testing problem, where a spatially–adapted *False Discovered Rate* (FDR) correction method must be applied.

State of the art

For testing if the circular sample has k modes nonparametrically, just the proposal of Fisher and Marron (2001) is available in the statistical literature and it seems to be not well calibrated. From a parametric point of view, determining the number of modes can be done using mixture models. In Benali et al. (2017), employing the mixture of two von Mises, the global map is catalogued in function of the number of modes.

It will be relevant also for our example how to handle the multiple testing problem with spatially correlated data. Benjamini and Heller (2007) proposed an algorithm with this purpose, relying on prior information on the locations which may be the driving force of the dependency structure.

Contributions

In Ameijeiras-Alonso et al. (2017b) a new proposal for testing the number of modes

in the circular setting is provided showing a correct calibration in the finite sample cases. Its performance is compared with the Fisher and Marron (2001) proposal and then applied for testing if there is one season of fires in each region of the world. Then, taking into account the spatial dependence between the different locations, the results are corrected using an adaptation of the Benjamini and Heller (2007) proposal.

1.5.3 Contributions on symmetry tests in the circular setting

The objective is testing circular reflective symmetry, i.e., if the density function of the data satisfies $f(\theta + \mu) = f(-\theta + \mu)$, when the central direction μ is unknown.

State of the art

For testing if the circular sample is reflective symmetric there are three proposals. The first one is the b2–bar test of Pewsey (2002), which allows to test the symmetry when the central direction is unknown, but there is no notion of optimality. When μ is previously given, both proposals of Pewsey (2004) and Ley and Verdebout (2014) can be used for testing circular symmetry, but just the second one is optimal (in the maximin sense) against the `k`–sine–skewed asymmetric models.

Contributions

In Ameijeiras-Alonso et al. (2017c) a new proposal for testing circular symmetry with unknown central location is given. The test is proved to be asymptotically well calibrated and optimal against `k`–sine–skewed alternatives. In addition, the asymptotic distributions of the test statistic under the null and, also, under these alternatives are given. The behaviour of this test for small sample sizes is analysed with an extensive simulation study. For illustration purposes, an example for studying if the cracks in the cemented femoral components of the hip implants are symmetrically distributed around a central direction is included.

1.6 Acknowledgements

This work has been supported by the PhD grant BES–2014–071006, the Project MTM2013–41383–P (both from the Spanish Ministry of Economy, Industry and Competitiveness), the Project MTM2016–76969–P (Spanish State Research Agency, AEI, being both projects co–funded by the European Regional Development Fund, ERDF) and IAP network P7/06 StUDyS (Developing crucial Statistical methods for Under-

standing major complex Dynamic Systems in natural, biomedical and social sciences) from the Belgian Science Policy. Part of the research done in Chapter 4 was carried out during a visit to Ghent University supported by the Grant EEBB–I–16–11503 (Spanish Ministry of Economy, Industry and Competitiveness). The support of the Mobility Grant EEBB–I-17–12716 (Spanish Ministry of Economy, Industry and Competitiveness) is also thanked. The Supercomputing Center of Galicia (CESGA) is acknowledged for providing the computational resources that allowed to run most of the simulations. Finally, Drs. Kenneth A. Mann, José M. C. Pereira and Nuno Sepúlveda and their research teams are thanked for providing some of the datasets employed in this manuscript.

Chapter 2

Mode testing for linear data

Several proposals were developed in the statistical literature for testing the number of modes of a random variable in the linear setting. This chapter is devoted to review different proposals for testing if the underlying distribution of the data is unimodal or multimodal from a nonparametric point of view. Some of these tests will be adaptable to the general case, when the objective is testing if the underlying distribution is k–modal. As mentioned in Chapter 1, the existing proposals can be divided in two groups: a first group of tests based on or using a critical bandwidth, introduced by Silverman (1981), further studied by Hall and York (2001) and also used by Fisher and Marron (2001); and a second group of tests based on the excess mass, such as those ones proposed by Hartigan and Hartigan (1985), Müller and Sawitzki (1991) and Cheng and Hall (1998). These methods are compared in this chapter, showing the behaviour of these procedures under different scenarios. The main contribution of this chapter is a new testing procedure combining the use of a critical bandwidth and an excess mass statistic, outperforming the existing procedures, in testing unimodality and more general hypotheses.

The illustration of the new technique for testing the number of modes will be done with two examples. The first one, in the philatelic field, introduced in Section 1.3.1, can be considered as a classical example for analysing the underlying number of modes. This real dataset, firstly studied by Wilson (1983), has become (since its use by Izenman and Sommer, 1988) a popular example, as determining the number of underlying groups, in this data, is not an easy task. This issue is shown in Figure 2.1, where observing the histograms or the kernel density estimations with different bandwidths (left panels) does not provide a clear answer about the number of modes. Not even the most well–known graphical tool for detecting significant features on a scale–space perspective, the SiZer map (Chaudhuri and Marron, 1999), provides a clear

answer. In this exploratory tool showed in Figure 2.1 (top right panel), and reading the map from left to right, a blue area followed by a red area indicates the presence of a mode for a certain range of values of the variable (horizontal axis) and a range of bandwidths (vertical axis). The lack of an automatic answer about the number of modes constitutes an argument for using testing procedures for solving this type of cases. This example will be discussed in detail in Section 2.3 and the results will be presented into the historical context of the 1872 Hidalgo issue production. The second example in this chapter, introduced in Section 1.3.2, in the context of malaria eradication, represents a novel solution for detecting populations with a group of people infected with the malaria disease.

This chapter is organized as follows. In Section 2.1, a review on mode testing methods is presented, considering the tests based on critical bandwidth and on excess mass, jointly with the new proposal. A simulation study comparing all the procedures, in terms of empirical size and power, is included in Section 2.2. Section 2.3 is devoted to the philatelic data analysis, revising the stamp dataset and presenting new results. In section 2.4 the new proposal is used as tool for detecting if the malaria is still in a population.

Contents

2.1 A review on multimodality tests

Different proposals for multimodality tests will be briefly revised in this section, according to the two aforementioned alternatives. Section 2.1.1 includes a review on the methods using the critical bandwidth (Silverman, 1981; Hall and York, 2001; Fisher and Marron, 2001). Excess mass approaches are detailed in Section 2.1.2 (Hartigan and Hartigan, 1985; Müller and Sawitzki, 1991; Cheng and Hall, 1998). The new proposal, borrowing strength from both alternatives, is presented in Section 2.1.3: an

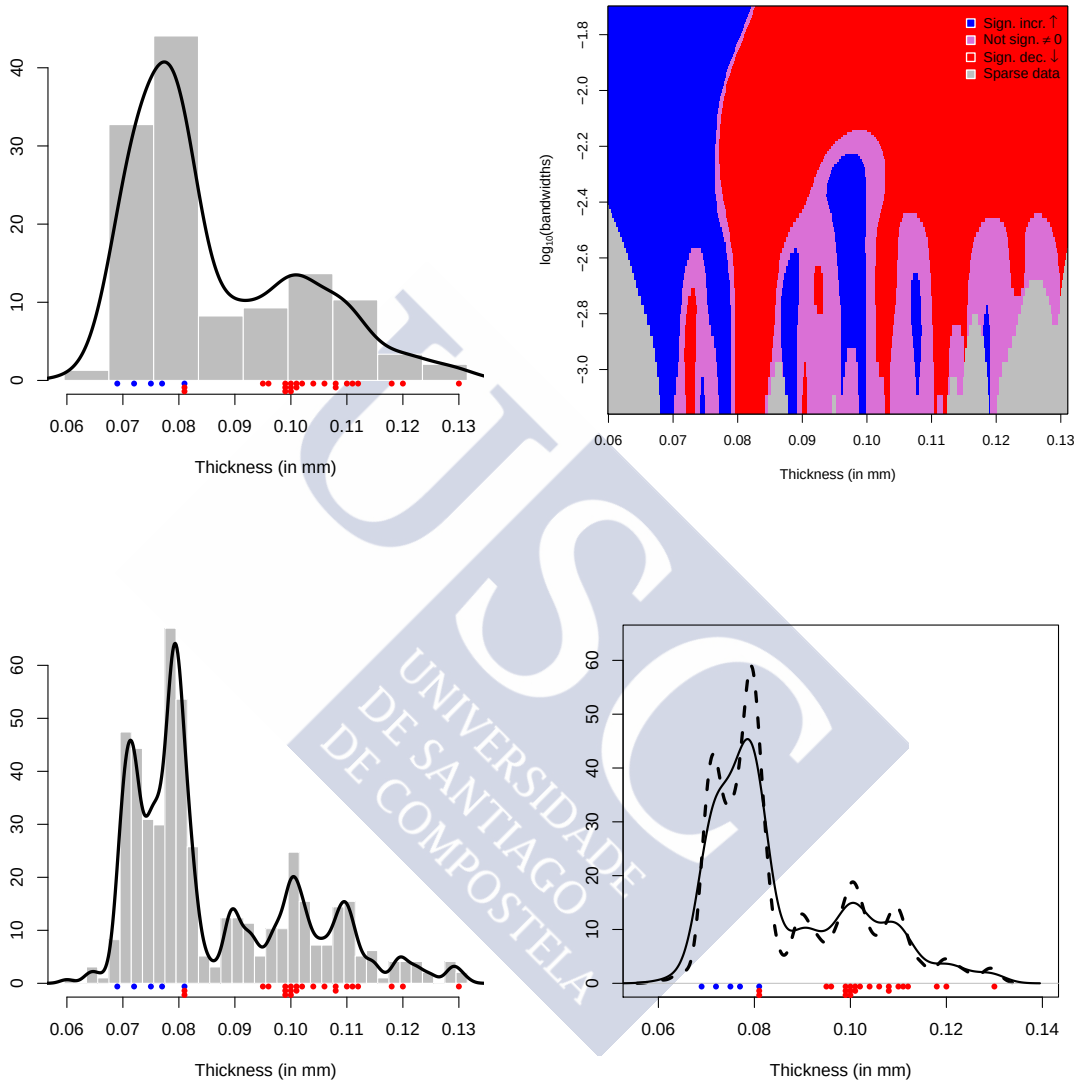

Figure 2.1: Sample of 485 stamps from the 1872 Hidalgo Issue of Mexico, distinguishing stamps watermarked with *LA+-F* (blue points) and stamps produced in *Papel sellado* (red points). Left column: histograms with different bin widths (0.002 -top- and 0.008 -bottom-) and kernel density estimators (Gaussian kernel; $h = 0.003910$ -rule of thumb- and $h = 0.001205$ -plug–in rule-, see Wand and Jones, 1995, Ch. 3). Right column: SiZer map (top) and kernel density estimators with two critical bandwidths (solid line: $h_4 = 0.002831$: dashed line: $h_7 = 0.001487$).

excess mass statistic will be calibrated from a modified nonparametric kernel density estimator using a critical bandwidth. Theoretical properties of the test supporting its correct behaviour can be derived under suitable conditions of a modified kernel estimator.

2.1.1 Tests based on the critical bandwidth

The cornerstone for these procedures is the critical bandwidth introduced by Silverman (1981). For a certain number of modes $k \in \mathbb{Z}^+$, the critical bandwidth is the smallest bandwidth such that the kernel density estimator has at most k modes:

$$h_k = \min\{h : \hat{f}_h \text{ has at most } k \text{ modes}\}, \tag{2.1.1}$$

where $\hat{f}_h$ denotes the kernel density estimator given in (1.1.1). Silverman (1981) proposed to use the critical bandwidth with the Gaussian kernel as a statistic to test $H_0 : j \leq k$ vs. $H_a : j > k$, being its use justified by the fact that, with a Gaussian kernel, the number of modes of $\hat{f}_h$ is a nonincreasing function of h. Hence, the null hypothesis is rejected for large values of h_k defined in (2.1.1), whose distribution is approximated using bootstrap procedures. Specifically, the proposed methodology consists in generating B samples $\mathcal{X}^{*b} = (X_1^{*b}, \cdots, X_n^{*b})$ with $b = 1, \cdots, B$, from $\hat{f}_{h_k}$ (the kernel density estimator (1.1.1) using the critical bandwidth for k modes, h_k and a Gaussian kernel). By computing the critical bandwidth, h_k^{*b}, from each sample $\mathcal{X}^{*b}$, given a significance level α, the null hypothesis is rejected if $\mathbb{P}(h_k^* \leq h_k | \mathcal{X}) \geq 1 - \alpha$. When $k = 1$, the testing problem tackled by Silverman (1981) coincides with (1.1.3). However, for a general k, the null hypothesis in (1.1.3) is more restrictive than the one considered by Silverman (1981), but asymptotic consistency of the test is only derived for $j = k$ (for a deeper insight see Hall and York, 2001).

Hall and York (2001) proved that the previous bootstrap algorithm does not provide a consistent approximation of the test statistic distribution under the null hypothesis and suggested a way for accurately calibrating the distribution of the test statistic when $k = 1$. Given a closed interval I where the null hypothesis is tested (f has a single mode in I), Hall and York (2001) showed that if both the support of f an the interval I are unbounded then properties of h_1 (critical bandwidth when $k = 1$) are generally determined by extreme values in the sample, not by the modes of f. To avoid this issue, the testing problem (1.1.3) is reformulated as follows:

$$H_0 : j = 1 \text{ in the interior of a given closed interval } I \text{ and no local minimum in } I, \tag{2.1.2}$$

and the critical bandwidth is redefined accordingly as:

$$h_{\text{HY}} = \min\{h : \hat{f}_h \text{ has exactly one mode in } I\}. \tag{2.1.3}$$

An issue that should be kept in mind in the computation of this critical bandwidth is that even if K is the Gaussian kernel in (1.1.1), the number of modes of $\hat{f}_h$ inside I is not necessarily a monotone function of h. But under relatively general conditions (see Hall and York, 2001), the probability that number of modes is monotone in h converges to 1 for a Gaussian kernel. Hall and York (2001) proposed using h_{HY} as a statistic to test (2.1.2). Similarly to Silverman (1981) the null distribution of h_{HY} is approximated by bootstrap, generating bootstrap samples from $\hat{f}_{\text{HY}}$.

Unfortunately, the critical bandwidths for the bootstrap samples h^*_{HY}, are smaller than h_{HY}, so for an α–level test, a correction factor λ_α to compute the p–value $\mathbb{P}(h^*_{\text{HY}} \leq \lambda_\alpha h_{\text{HY}}|\mathcal{X}) \geq 1-\alpha$ must be considered. Hall and York (2001) suggested two different methods to compute this factor λ_α, the first one based on a polynomial approximation and a second one using Monte Carlo techniques considering a simple unimodal distribution.

The previous proposal could be extended, as mentioned by Hall and York (2001), to test the null hypothesis that f has exactly k modes in I, against the alternative that it has $(k+1)$ or more modes there, with the following critical bandwidth:

$$h_{\text{HY},k} = \min\{h : \hat{f}_h \text{ has at most } k \text{ modes in } I\}.$$

Nevertheless, in this scenario, the bootstrap test cannot be directly calibrated under the hypothesis that f has k modes and $(k-1)$ antimodes, since the distribution of the test statistic depends on the $(2k-2)$ unknowns (c_i/c_1), where $c_i = f^{1/5}(t_i)/|f''(t_i)|^{2/5}$ (assuming $f''(t_i) \neq 0$ for all i), and t_i being the ordered turning points of f in I with $i = 1, \cdots, (2k-1)$. Therefore, if $j > 1$ the bootstrap test cannot be calibrated independently of the underlying density of the data.

Finally, it should be also commented that employing the critical bandwidth for testing (1.1.3) is not limited to its use as a test statistic. Consider a Cramér–von Mises test statistic:

$$T = n\int_{-\infty}^{\infty}[F_n(x) - F_0(x)]^2 dF_0(x) = \sum_{i=1}^{n}\left(F_0(X_{(i)}) - \frac{2i-1}{2n}\right)^2 + \frac{1}{12n}. \qquad (2.1.4)$$

where F_0 is a given continuous distribution function, $\{X_{(1)} \leq \cdots \leq X_{(n)}\}$ denotes the ordered sample and F_n is the empirical distribution function. Fisher and Marron (2001) proposed the use of (2.1.4) for solving the general problem of testing k modes $(H_0 : j \leq k)$ by taking $F_0(x) = \hat{F}_{h_k}(x) = \int_{-\infty}^{x}\hat{f}_{h_k}(t)dt$ and deriving the statistic:

$$T_k = \sum_{i=1}^{n}\left(\hat{F}_{h_k}(X_{(i)}) - \frac{2i-1}{2n}\right)^2 + \frac{1}{12n}, \qquad (2.1.5)$$

where the null hypothesis is rejected for large values of T_k. To approximate the distribution of the test statistic (2.1.5) under the null hypothesis, a bootstrap procedure is also proposed, drawing samples from $\hat{f}_{h_k}$. It will be seen in Section 2.2 that the behaviour of the Fisher and Marron (2001) proposal is far from satisfactory.

2.1.2 Tests based on excess mass

Müller and Sawitzki (1991) confront the testing problem (1.1.3), employing a different perspective, under the following premise: for $k \in \mathbb{Z}^+$, a mode is present where an excess of probability mass is concentrated. Specifically, given a continuous real density function f and a constant λ, the excess mass is defined as:

$$E(f,\lambda) = \int_{C_\lambda} f(x)dx - \lambda||C_\lambda||,$$

where $C_\lambda = \{x : f(x) \geq \lambda\}$ and $||C_\lambda||$ denotes the measure of C_λ. If f has at most k modes, the excess mass can be defined as:

$$E(f,\lambda) = \sup_{C_1,\ldots,C_k} \left\{ \sum_{m=1}^{k} \mathbb{P}(C_m) - \lambda||C_m|| \right\}, \tag{2.1.6}$$

where the supremum is taken over all families $\{C_m : m = 1, \cdots, k\}$ of pairwise disjoint connected sets over the support of f. As an example, for the density function and the value of λ shown in Figure 2.2, the excess mass is equal to the grey area and it is obtained when taking the union of intervals (a, b) and (c, d). Under the assumption that f has at most k modes, $E(f,\lambda)$ can be empirically estimated just replacing $\mathbb{P}(C_m)$ by $\mathbb{P}_n(C_m) = (1/n)\sum_{i=1}^{n} \mathcal{I}(X_i \in C_m)$, being $\mathcal{I}$ the indicator function. The difference $D_{n,k+1}(\lambda) = E_{n,k+1}(\mathbb{P}_n,\lambda) - E_{n,k}(\mathbb{P}_n,\lambda)$ measures the plausibility of the null hypothesis, that is, large values of $D_{n,k+1}(\lambda)$ would indicate that H_0 is false. Using these differences, Müller and Sawitzki (1991) proposed the following test statistic:

$$\Delta_{n,k+1} = \max_{\lambda}\{D_{n,k+1}(\lambda)\}, \tag{2.1.7}$$

rejecting the null hypothesis that f has at most k modes for large values of $\Delta_{n,k+1}$. Müller and Sawitzki (1991) showed that this statistic is an extension of the *dip* test introduced by Hartigan and Hartigan (1985), just valid for the unimodal case, since both quantities (dip and excess mass) coincide up to a factor, for the unimodality case. In addition, the proposal of Müller and Sawitzki (1991) for testing unimodality is the same as that one of Hartigan and Hartigan (1985) and considers a Monte Carlo calibration, generating resamples from the uniform distribution.

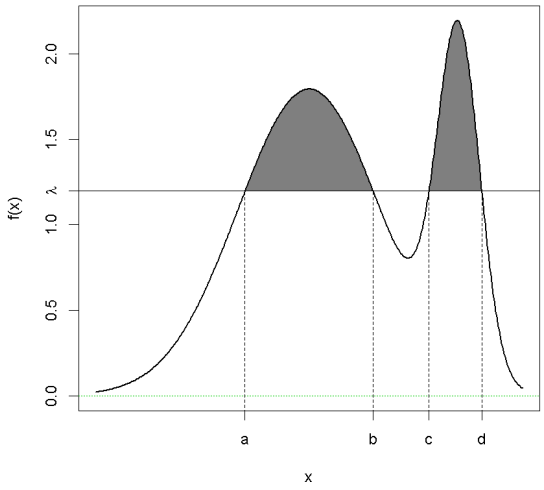

Figure 2.2: The excess mass is the probability mass exceeding a given level λ. In this case, it is equal to the grey area and it is obtained when taking the union of intervals (a, b) and (c, d).

In view of the extremely conservative behaviour of the calibration proposed by Hartigan and Hartigan (1985) and, later on, by Müller and Sawitzki (1991) (see Section 2.2 for details), Cheng and Hall (1998) proposed a calibration procedure to improve their level accuracy, based on the following result: for large samples and under the hypothesis that f is unimodal, the distribution of $\Delta_{n,2}$ is independent of unknowns except for a factor $c = \left(f^3(x_0)/|f''(x_0)|\right)^{1/5}$, where x_0 denotes the unique mode of f. Using this fact, for the case $k = 1$, Cheng and Hall (1998) approximated the distribution of $\Delta_{n,2}$ employing the values of $\Delta^*_{n,2}$ obtained from the samples generated from a parametric calibration distribution $\Psi(\cdot, \mathtt{b})$, being $\mathtt{b}$ a certain parameter. The authors suggested choosing this parametric distribution depending on the value of $d = c^{-5}$: if $d < 2\pi$, then a beta distribution is adviced; if $d = 2\pi$, any normal distribution can be used; if $d > 2\pi$, a rescaled Student t should be used. Given that d is unknown, it must be estimated from the sample, and this can be done by kernel methods. If $\widehat{x}_0$ denotes the largest mode of $\hat{f}_h$, the estimation of d is given by:

$$\hat{d} = |\hat{f}''_{h'}(\widehat{x}_0)|/\hat{f}_h{}^3(\widehat{x}_0),$$

were $\hat{f}''$ and $\hat{f}$ are taken as kernel estimators using a Gaussian kernel and h' and h are their respective asymptotically optimal global bandwidths, with unknown quantities depending on the density replaced by those for a normal $\mathrm{N}(0, \hat{\sigma}^2)$ distribution, being $\hat{\sigma}^2$ the sample variance.

The methodology proposed by Cheng and Hall (1998) consists in generating samples from $\Psi(\cdot, \hat{\mathtt{b}})$, where $\hat{\mathtt{b}}$ and the distribution family are chosen using $\hat{d}$. The excess mass statistic given in (2.1.7) when $k = 1$, $\Delta^*_{n,2}$, is computed from the resamples and, for a given significance level α, the null hypothesis is rejected if $\mathbb{P}(\Delta^*_{n,2} \leq \Delta_{n,2}|\mathcal{X}) \geq 1 - \alpha$.

2.1.3 A new proposal

The previous tests show some limitations: first, just the proposals of Silverman (1981) and Fisher and Marron (2001) allow to test (1.1.3) for $k > 1$. Despite the efforts of Cheng and Hall (1998) and Hall and York (2001) for providing good calibration algorithms, it will be shown in Section 2.2 that the behaviour of all the proposals is far from satisfactory. Specifically, the test presented by Silverman (1981) is very conservative in general (although sometimes can show the opposite behaviour) and the proposal of Fisher and Marron (2001) does not have a good level accuracy. The new proposal tries to overcome these drawbacks by considering an excess mass statistic, as the one proposed by Müller and Sawitzki (1991) with bootstrap calibration. Unlike the method presented by Cheng and Hall (1998), a completely data-driven and non-parametric procedure will be designed, using the critical bandwidth under the null hypothesis to test $H_0 : j = k$ vs. $H_a : j > k$, for a general $k \in \mathbb{Z}^+$.

The proposal, in a nutshell. Consider then the testing problem (1.1.3) and take the excess mass statistic given in (2.1.7), under the null hypothesis. Given a sample $\mathcal{X} = (X_1, ..., X_n)$, generate B samples $\mathcal{X}^{*b}$ $(b = 1, \ldots, B)$ of size n from (a modified version of) $\hat{f}_{h_k}$. For a significance level α, the null hypothesis will be rejected if $\mathbb{P}(\Delta^*_{n,k+1} \leq \Delta_{n,k+1}|\mathcal{X}) \geq 1 - \alpha$, where $\Delta^*_{n,k+1}$ is the excess mass statistic obtained from the generated samples. It should be also noted that the procedure can be easily adapted to handle Hall and York (2001) scenario: to test the null hypothesis that f has almost k modes in the interior of a given closed interval I, if I is known, use (a modified version of) $\hat{f}_{h_{\mathrm{HY},k}}$ to generate the samples. From this brief description, two questions arise: How is this *modified* version of $\hat{f}_{h_k}$ constructed? Does the procedure guarantee a correct calibration of the test? In fact, the construction of the modified kernel density estimator, namely the calibration function and subsequently denoted by g, is intended to ensure the correct calibration, under some regularity conditions.

Regularity conditions (RC1) The density function f has continuous derivative. (RC2) There exist t_1 and t_2, such that f is monotone in $(-\infty, t_1)$ and in (t_2, ∞). (RC3) The unique points satisfying $\{x : f'(x) = 0 \text{ and } f(x) \neq 0\}$ are the modes and

antimodes of f, denoted as x_i, with $i = 1, \ldots, (2j-1)$; and $f''(x_i) \neq 0$. (RC4) f'' exists and is Hölder continuous in a neighbourhood of each x_i.

Although these premises are quite general, it should be noted that they exclude some classical distributions, such us, those ones having an unbounded density function (e.g., the Beta distributions with parameters equal to 0.5, see Johnson et al., 1995) or the uniform distribution. Under the regularity conditions, Cheng and Hall (1998) indicated that the distribution of the test statistic (2.1.7) is independent from the underlying density f, except for the values in the modes and antimodes:

$$d_i = \frac{|f''(x_i)|}{f^3(x_i)} \text{ with } i = 1, \ldots, (2k-1). \tag{2.1.8}$$

Using the results of Cheng and Hall (1998), and assuming that f has k modes, the distribution of $\Delta_{n,k+1}$ can be approximated by $\Delta^*_{n,k+1}$, just with bootstrap values obtained from samples coming from a calibration distribution with k modes. This calibration distribution must satisfy that the estimated values $\widehat{d}_i$ converge in probability to d_i, as $n \to \infty$, for $i = 1, \ldots, (2k-1)$. As aforementioned, it is for that reason that Cheng and Hall (1998) proposed using a parametric family depending on the value of d_1 when $k = 1$. Two issues appear related with their calibration procedure. First, it is not an easy task to construct a parametric family having the desired values of d_i, for $i = 1, \ldots, (2k-1)$, when $k > 1$. Second, as Cheng and Hall (1998) pointed out the second–order limiting properties of the test depend on the form of the density function. Then, it is expected a better behaviour if the calibration function is "more similar" to the real density function. Our method deals with these two issues to get a test having a good behaviour in the finite–sample case and allowing solving the general problem of testing k modes.

In order to estimate the location of modes and antimodes, as well as the value of the density in these points under H_0, the kernel density estimator (1.1.1) with critical bandwidth $\hat{f}_{h_k}$ is a good candidate. In addition, if f is also a bounded density with bounded support $[a, b]$[1], twice–differentiable in (a, b) and $\lim_{x \to a^+} f'(x) > 0$, $\lim_{x \to b^-} f'(x) < 0$, the result in Mammen et al. (1992) holds and the critical bandwidth is of order $n^{-1/5}$, being then optimal for estimating f. Unfortunately, a suitable bandwidth for estimating f cannot be used for effectively estimating f''. In fact, the optimal bandwidth for estimating the second derivative of the density is of order $n^{-1/9}$. Therefore, a simple $\widehat{d}_i$ obtained as the ratio $|\widehat{f}''_{h_k}(\widehat{x}_i)|/\widehat{f}^3_{h_k}(\widehat{x}_i)$, where $\widehat{x}_i$ is the estimated location of the mode (antimode), will not estimate correctly d_i.

For this reason, the kernel density estimator with critical bandwidth h_k cannot be used as calibration function g, which needs to provide a good estimator of d_i. Under

[1]When $[a, b]$ is known, the critical bandwidth proposed by Hall and York (2001) can be used.

the conditions of Mammen et al. (1992), such an estimator can be calculated using the ratio $\widehat{d}_i = |\widehat{f}''_{h_{\mathrm{PI}}}(\widehat{x}_i)|/\widehat{f}^3_{h_k}(\widehat{x}_i)$, where h_{PI} is a plug–in bandwidth. In this thesis, the plug–in rule for the second derivative will be obtained deriving the *Asymptotic Mean Integrated Squared Error* (AMISE) and replacing f in its expression using a two–step procedure (see, for example, Wand and Jones, 1995, Ch. 3).

The calibration function g will be obtained by modifying $\widehat{f}_{h_k}$ in a neighbourhood of $\{x : \widehat{f}'_{h_k}(x) = 0\}$, being such values a finite collection (see Silverman, 1981), having estimated density positive. The form of this calibration function g is given in (2.1.9) and explained below. Depending on the nature of these points, two modifications in their neighbourhood will be done. If the point $\widehat{x}_i$ is a mode or an antimode of $\widehat{f}_{h_k}$ then the modification will preserve its location and its estimated density value, and its second derivative will satisfy $g''(\widehat{x}_i) = \widehat{f}''_{h_{\mathrm{PI}}}(\widehat{x}_i)$[2]. For $i = 1, \ldots, (2k-1)$, this will be the role of the function J, in the neighbourhood $(\mathfrak{r}_i, \mathfrak{s}_i)$ of $\widehat{x}_i$ for guaranteeing $|g''(\widehat{x}_i)|/g^3(\widehat{x}_i) = \widehat{d}_i$ and satisfying (RC4). The second modification will remove the t saddle points of $\widehat{f}_{h_k}$, denoted as ζ_p, with $p = \{1, \ldots, t\}$. In order to ensure that g satisfies (RC3), in a neighbourhood $(z_{(2p-1)}, z_{(2p)})$ of ζ_p a function L will be introduced. Finally, as $\widehat{f}_{h_k}$ verifies (RC1) and (RC2), and the modifications of the functions J and L will be done in bounded neighbourhoods and preserving condition (RC1), g will satisfy also these two conditions. Then, the calibration function g will be constructed as follows:

$$g(x; h_k, h_{\mathrm{PI}}, \boldsymbol{\varsigma}) = \begin{cases} J(x; \widehat{x}_i, h_k, h_{\mathrm{PI}}, \varsigma_i) & \text{if } x \in (\mathfrak{r}_i, \mathfrak{s}_i) \text{ for some } i \in \{1, \ldots, (2k-1)\}, \\ L(x; z_{(2p-1)}, z_{(2p)}, h_k) & \text{if } x \in (z_{(2p-1)}, z_{(2p)}) \text{ for some } p \in \{1, \ldots, t\}, \\ & \text{and } \zeta_p \notin (\mathfrak{r}_i, \mathfrak{s}_i) \text{ for any } i \in \{1, \ldots, (2k-1)\}, \\ \widehat{f}_{h_k}(x) & \text{otherwise,} \end{cases} \tag{2.1.9}$$

where $\boldsymbol{\varsigma}$ has k components $\varsigma_i \in (0, 1/2)$, with $i = 1, \ldots, k$, determining at which height of the kernel density estimation the modification in the neighbourhood of the modes or antimodes will be done. Values of ς_i close to 0 imply a modification in an "small" neighbourhood around the mode or antimode. Note that a little abuse of notation was made as g will depend on the function $\widehat{f}_{h_k}$ (not only on h_k) and on the values $\widehat{f}''_{h_{\mathrm{PI}}}(\widehat{x}_i)$, for $i \in \{1, \ldots, (2k-1)\}$. An example of the effect of g can be seen in Figure 2.3 and it will be further described later on. Before defining function J (and also function L), to ensure that g has continuous derivative, a link function l must

[2]Note that, although asymptotically the sign of $\widehat{f}''_{h_{\mathrm{PI}}}(\widehat{x}_i)$ is always correct, in the finite–sample case, it may not be negative in the modes or positive in the antimodes. In that case, an abuse of notation will be done, denoting as h_{PI} to the critical or other plug–in bandwidth in order to guarantee that the sign of this second derivative remains correct.

be introduced:

$$\begin{aligned} l(x;u,v,a_0,a_1,b_0,b_1) &= \frac{a_0-a_1}{2}\left(1+2\left(\frac{x-u}{v-u}\right)^3-3\left(\frac{x-u}{v-u}\right)^2\right)\exp\left(\frac{2(x-u)b_0}{a_0-a_1}\right)+ \\ &+ \frac{a_0-a_1}{2}\left(2\left(\frac{x-u}{v-u}\right)^3-3\left(\frac{x-u}{v-u}\right)^2\right)\exp\left(\frac{2(v-x)b_1}{a_0-a_1}\right)+\frac{a_0+a_1}{2}, \end{aligned} \tag{2.1.10}$$

where $a_0 \neq a_1$ and $v > u$. Two issues must be noticed in this function. First, it will allow for a smooth connection between other two functions, being u and v the starting and the ending points where the link function is used, a_0 and a_1 the values of the connected functions on these points and b_0 and b_1 their first derivative values. Second, if the sign of b_0, b_1 and $(a_1 - a_2)$ is the same, then the first derivative of l will not be equal to 0 for any point inside the interval $[u, v]$.

The form of the function J is given in equation (2.1.11) and its construction guarantees that $\widehat{x}_i$ is the unique point in which the derivative is equal to 0 in the neighbourhood where it is defined. The construction of J is achieved with the $\mathcal{K}$ function defined below and properly linked with the link function (2.1.10) to preserve (RC1). The $\mathcal{K}$ function is defined as follows

$$\mathcal{K}(x;\widehat{x}_i,\mathfrak{p}_i,\mathfrak{q}_i,\eta_i) = \mathfrak{p}_i\left(1+\delta_i\left(\frac{x-\widehat{x}_i}{\eta_i}\right)^2\right)^{\eta_i^2\frac{\delta_i\cdot\mathfrak{q}_i}{2\mathfrak{p}_i}},$$

being δ_i a value indicating if $\widehat{x}_i$ is a mode ($\delta_i = -1$) or an antimode ($\delta_i = 1$). The value η_i will be defined later and it will depend on ς_i. The second derivative of this function exists and is Hölder continuous in $(\widehat{x}_i - \eta_i/2, \widehat{x}_i + \eta_i/2)$. The following equalities are also satisfied: $\mathcal{K}(\widehat{x}_i;\widehat{x}_i,\mathfrak{p}_i,\mathfrak{q}_i,\eta_i) = \mathfrak{p}_i$ and $\mathcal{K}''(\widehat{x}_i;\widehat{x}_i,\mathfrak{p}_i,\mathfrak{q}_i,\eta_i) = \mathfrak{q}_i$. Then, denoting as $\boldsymbol{\rho}_i = (\widehat{x}_i, \widehat{f}_{h_k}(\widehat{x}_i), \widehat{f}''_{h_{\mathrm{PI}}}(\widehat{x}_i))$, the J function can be defined as follows

$$J(x;\widehat{x}_i,h_k,h_{\mathrm{PI}},\varsigma_i) = \begin{cases} l\left(x;\mathfrak{r}_i,\mathfrak{v}_i,\widehat{f}_{h_k}(\mathfrak{r}_i),\mathcal{K}(\mathfrak{v}_i;\boldsymbol{\rho}_i,\eta_i),\widehat{f}'_{h_k}(\mathfrak{r}_i),\mathcal{K}'(\mathfrak{v}_i;\boldsymbol{\rho}_i,\eta_i)\right) & \text{if } x\in(\mathfrak{r}_i,\mathfrak{v}_i), \\ \mathcal{K}(x;\boldsymbol{\rho}_i,\eta_i) & \text{if } x\in[\mathfrak{v}_i,\mathfrak{w}_i], \\ l\left(x;\mathfrak{w}_i,\mathfrak{s}_i,\mathcal{K}(\mathfrak{w}_i;\boldsymbol{\rho}_i,\eta_i),\widehat{f}_{h_k}(\mathfrak{s}_i),\mathcal{K}'(\mathfrak{w}_i;\boldsymbol{\rho}_i,\eta_i),\widehat{f}'_{h_k}(\mathfrak{s}_i)\right) & \text{if } x\in(\mathfrak{w}_i,\mathfrak{s}_i), \end{cases} \tag{2.1.11}$$

being $\mathfrak{v}_i = \widehat{x}_i - \eta_i/2$ and $\mathfrak{w}_i = \widehat{x}_i + \eta_i/2$. As it was mentioned, the function J described in (2.1.11) (and hence also the calibration function g) depends on the constant $\varsigma_i \in (0, 1/2)$. Ordering the modes and denoting as $\widehat{x}_0 = -\infty$ and $\widehat{x}_{(2k)} = \infty$, that is $-\infty = \widehat{x}_0 < \widehat{x}_1 < \ldots < \widehat{x}_{2k-1} < \widehat{x}_{2k} = \infty$, the remaining unknowns values in (2.1.11) will be obtained as follows. First, it is necessary to decide at which height ϑ_i the modification in $\widehat{f}_{h_k}$ is done. For values of ς_i close to 0, ϑ_i will be close to $\widehat{f}_{h_k}(\widehat{x}_i)$; while for values close to 0.5, ϑ_i will be in the middle point between $\widehat{f}_{h_k}(\widehat{x}_i)$

and the highest (or lowest if $\widehat{x}_i$ is an antimode) value of $\widehat{f}_{h_k}$ in the two closest modes or antimodes ($\widehat{x}_{i-1}$ and $\widehat{x}_{i+1}$). Second, once the height is decided, $\mathfrak{r}_i$ and $\mathfrak{s}_i$ will be the left and the right closest points to $\widehat{x}_i$ at which the density estimation is equal to ϑ_i. Third, in order to link correctly the $\mathcal{K}$ function, it is necessary to define η_i ensuring that $\mathcal{K}(\widehat{x}_i \pm \eta_i/2; \boldsymbol{\rho}_i, \eta_i)$ will be higher (lower in the antimodes) than ϑ_i. With this objective, η_i is chosen in such a way that $\mathcal{K}(\widehat{x}_i \pm \eta_i/2; \boldsymbol{\rho}_i, \eta_i)$ is near $\widehat{f}_{h_k}(\widehat{x}_i)$ and as close as possible to the middle point between ϑ_i and $\widehat{f}_{h_k}(\widehat{x}_i)$. Also, the value η_i will ensure that the neighbourhood $[\mathfrak{v}_i, \mathfrak{w}_i]$ in which $\mathcal{K}$ is defined is inside $(\mathfrak{r}_i, \mathfrak{s}_i)$. Finally, $\widehat{f}'_{h_k}$ must be different to 0 in the four points ($\mathfrak{r}_i$, $\mathfrak{v}_i$, $\mathfrak{w}_i$ and $\mathfrak{s}_i$) where the two link functions are employed. An example of the modifications achieved by the J function in the modes and antimodes of $\widehat{f}_{h_k}$ is shown in Figure 2.3 and the complete characterization is provided below

$$\begin{aligned}
\vartheta_i &= \widehat{f}_{h_k}(\widehat{x}_i) + \delta_i \cdot \varsigma_i \cdot \min\left(|\widehat{f}_{h_k}(\widehat{x}_i) - \widehat{f}_{h_k}(\widehat{x}_{i-1})|, |\widehat{f}_{h_k}(\widehat{x}_i) - \widehat{f}_{h_k}(\widehat{x}_{i+1})|\right), \\
\mathfrak{r}_i &= \inf\{x : x > \widehat{x}_{i-1}, \delta_i \cdot \widehat{f}_{h_k}(x) \leq \delta_i \cdot \vartheta_i \text{ and } \widehat{f}'_{h_k}(x) \neq 0\}, \\
\mathfrak{s}_i &= \sup\{x : x < \widehat{x}_{i+1}, \delta_i \cdot \widehat{f}_{h_k}(x) \leq \delta_i \cdot \vartheta_i \text{ and } \widehat{f}'_{h_k}(x) \neq 0\}, \\
\eta_i &= \sup\{\gamma : \gamma \in (0, \min(\widehat{x}_i - \mathfrak{r}_i, \mathfrak{s}_i - \widehat{x}_i)), \delta_i \mathcal{K}(\widehat{x}_i + \gamma/2; \boldsymbol{\rho}_i, \gamma) \leq \delta_i(\widehat{f}_{h_k}(\widehat{x}_i) + \vartheta_i)/2 \\
&\qquad \text{and } \widehat{f}'_{h_k}(\widehat{x}_i \pm \gamma/2) \neq 0\}.
\end{aligned} \tag{2.1.12}$$

In order to proceed with the modification achieved with the L function, assume that this estimator has t saddle points ζ_p, with $p = 1, \ldots, t$. Define as $\xi = \min\{|x-y| : x, y \in (\zeta_1, \ldots, \zeta_t) \cup (\mathfrak{r}_1, \mathfrak{s}_1, \ldots, \mathfrak{r}_{2k-1}, \mathfrak{s}_{2k-1})\}$. Then, if ζ_p is not inside the interval where the J funtions are defined, the neighbourhood used to remove the stationary and turning points will be delimited by $z_{(2p-1)} = \zeta_p - \varpi\xi$ and $z_{(2p)} = \zeta_p + \varpi\xi$, with $\varpi \in (0, 1/4)$. In the simulation study, the value of ϖ will be taken close enough to 0 to avoid an impact in the value of the integral associated to g. Once these points are calculated, the saddle points can be removed from g with the link function by taking L equal to

$$L(x; z_{(2p-1)}, z_{(2p)}, h_k) = l(x; z_{(2p-1)}, z_{(2p)}, \widehat{f}_{h_k}(z_{(2p-1)}), \widehat{f}_{h_k}(z_{(2p)}), \widehat{f}'_{h_k}(z_{(2p-1)}), \widehat{f}'_{h_k}(z_{(2p)})). \tag{2.1.13}$$

To construct the calibration function, values of $\varsigma_i \in (0, 1/2)$, for $i \in \{1, \ldots, (2k-1)\}$ must be fixed. Then, using the J function (2.1.11) with the values given in (2.1.12) and the L function (2.1.13), the function g defined in (2.1.9) satisfies the specified regularity conditions and $|g''(\widehat{x}_i; h_k, h_{\text{PI}}, \boldsymbol{\varsigma})|/g^3(\widehat{x}_i; h_k, h_{\text{PI}}, \boldsymbol{\varsigma})$ converges in probability to d_i. With this modification the calibration function also preserves the structure of

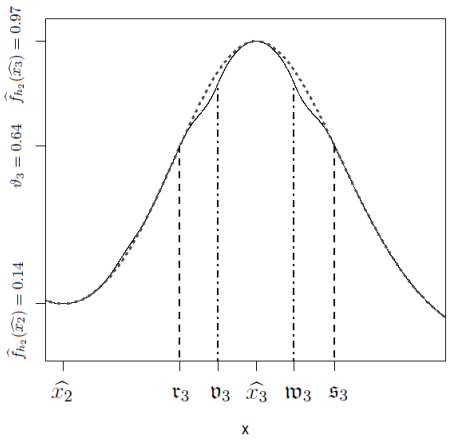

Figure 2.3: Sample of $n = 1000$ observations from model M16 (Appendix A). Dotted grey line: $\widehat{f}_{h_2}$. Solid line: g function. Dashed line: support of $J(\cdot; \widehat{x}_i, h_2, h_{\text{PI}}, 0.4)$, with $i = 1, 2, 3$, Dot–dashed line: support of $\mathcal{K}(\cdot; \boldsymbol{\rho}_3, \eta_3)$. Left: in the support $(-0.2, 1.1)$. Right: in a neighbourhood of the mode $\widehat{x}_3$.

the data under the hypothesis that f has k modes, which will help to have better results in the practice. However, this calibration function g may not be a density function since

$$q(\boldsymbol{\varsigma}) = \int_{-\infty}^{\infty} g(x; h_k, h_{\text{PI}}, \boldsymbol{\varsigma}) dx \tag{2.1.14}$$

may not be equal to 1. To guarantee that g is indeed a density, a possible approach consists in proceeding with a search of values for $\boldsymbol{\varsigma}$ such that $q(\boldsymbol{\varsigma})$ is equal to 1, which is guaranteed since

$$\lim_{\varsigma_i \to 0^+; \forall i \in (1,\ldots,2k-1)} q(\boldsymbol{\varsigma}) = \int_{-\infty}^{\infty} \widehat{f}_{h_k}(x) dx = 1.$$

For convenience, in the simulation study, the employed approach will be followed using ς_i close enough to 0 ($\forall i \in \{1, \ldots, 2k-1\}$) in order to avoid an impact on the integral value.

To conclude this section it is important to mention the necessary condition of the bounded support in order to ensure the results of Mammen et al. (1992). Although, in general, it will not have an important effect, as shown in Section 2.2, in case of a known support, $h_{\text{HY},k}$ can be used to create the calibration function. An alternative approach for known support is given below in Section 2.1.3.1. Once a conclusion

about the number of modes is made, when both the estimation of the modes and antimodes is needed, this known support plays an special role. In Section B.1 of the Appendix, it is shown that $\hat{f}_{h_{\mathrm{HY},k}}$ provides a good estimation of their localization.

It should be also reminded that the methods proposed by Silverman (1981) and Fisher and Marron (2001) can be extended from unimodality to test a general null hypothesis as $H_0 : j \leq k$. Nevertheless, the proposal presented in this work just allows to test $H_0 : j = k$ vs. $H_0 : j > k$. The reason why the k–modal test should not be used when the true underlying density has less than k modes is that the test statistic in the bootstrap resamples converge in distribution to a random variable, depending only on the values $\widehat{d}_i$ with $i = 1, \ldots, (2k-1)$ (see Cheng and Hall, 1998). When $j < k$, in the calibration function g, there exist $(2k - 2j)$ turning points that they will not converge to any fixed value depending on the real density function. As the (asymptotic) distribution of the test statistic in the bootstrap resamples depends also on this $(2k - 2j)$ values, one would expect that the sample distribution of the test statistic will not be correctly approximated with the bootstrap resamples.

Testing $H_0 : j = k$ instead of $H_0 : j \leq k$ is not, in general, an important limitation for practical purposes. As it will be seen in the stamp example in Section 2.3, the usual procedure is to perform a stepwise algorithm starting with one mode and, if the null hypothesis is rejected, increasing the number of modes in the null hypothesis by one until there is no evidences for rejection. Despite this note of caution, in Section 2.2, it is showed that, generally, testing $H_0 : j = k$, when $j < k$, reports also good calibration results.

2.1.3.1 New proposal when the support is known

When the bounded support is known, an alternative approach for the new proposal can be used in order to get better results in practice. This new proposal consists in replacing the critical bandwidth of Silverman (1981) for the one of Hall and York (2001) in the definition of the calibration function g. If the number of modes of g in the entire support is equal to k when testing $H_0 : j = k$ (with $(k-1)$ antimodes) in $[a, b]$, then no more changes are needed. If modes appear outside $[a, b]$, then the link function (2.1.10) can be used in order to preserve the required regularity conditions. Denoting as $a < \widehat{x}_1 < \ldots < \widehat{x}_{2k-1} < b$, being $\widehat{x}_1$ and $\widehat{x}_{2k-1}$ modes, the points $\widehat{x}_0$ and $\widehat{x}_{2k}$, needed to obtain the values in (2.1.12), will be redefined to remove the modes outside $[a, b]$. If there are modes lower than $\widehat{x}_1$, then $\widehat{x}_0 = \min\{x : x \geq a \text{ and } \widehat{f}'_{h_{\mathrm{HY},k}}(x) > 0\}$ and if there are modes greater than $\widehat{x}_{2k-1}$, then $\widehat{x}_{2k} = \max\{x : x \leq b \text{ and } \widehat{f}'_{h_{\mathrm{HY},k}}(x) < 0\}$. Once this change is done, two extra values, $\mathfrak{a} < \widehat{x}_0$ and $\mathfrak{b} > \widehat{x}_{2k}$, are needed in order to use the link function. The steps to obtain these two values will be defined later and,

from them, the calibration function in (2.1.9) can be modified in its tails to define $g(x; h_{\mathrm{HY},k}, h_{\mathrm{PI}}, \varsigma, \mathfrak{a}, \mathfrak{b})$ as follows

$$\begin{cases} 0 & \text{if } x \leq \mathfrak{a} \text{ and } \widehat{f}_{h_{\mathrm{HY},k}} \text{has modes lower than } a, \\ l(x; \mathfrak{a}, \widehat{x}_0, 0, \widehat{f}_{h_{\mathrm{HY},k}}(\widehat{x}_0), 0, \widehat{f}'_{h_{\mathrm{HY},k}}(\widehat{x}_0)) & \text{if } x \in (\mathfrak{a}, \widehat{x}_0) \text{ and } \widehat{f}_{h_{\mathrm{HY},k}} \text{has modes lower than } a, \\ J(x; \widehat{x}_i, h_{\mathrm{HY},k}, h_{\mathrm{PI}}, \varsigma_i) & \text{if } x \in (\mathfrak{r}_i, \mathfrak{s}_i) \text{ for some } i \in \{1, \ldots, (2k-1)\}, \\ L(x; \zeta_p, h_{\mathrm{HY},k}) & \text{if } x \in (z_{(2p-1)}, z_{(2p)}) \text{ for some } p \in \{1, \ldots, t\}, \\ & \text{and } \zeta_p \notin (\mathfrak{r}_i, \mathfrak{s}_i) \text{ for any } i \in \{1, \ldots, (2k-1)\}, \\ l(x; \widehat{x}_{2k}, \mathfrak{b}, \widehat{f}_{h_{\mathrm{HY},k}}(\widehat{x}_{2k}), 0, \widehat{f}'_{h_{\mathrm{HY},k}}(\widehat{x}_{2k}), 0) & \text{if } x \in (\widehat{x}_{2k}, \mathfrak{b}) \text{ and } \widehat{f}_{h_{\mathrm{HY},k}} \text{has modes greater than } b, \\ 0 & \text{if } x \geq \mathfrak{b} \text{ and } \widehat{f}_{h_{\mathrm{HY},k}} \text{has modes greater than } b, \\ \widehat{f}_{h_{\mathrm{HY},k}}(x) & \text{otherwise,} \end{cases}$$

the functions J and L are defined as in Section 2.1.3, replacing the kernel density estimator $\widehat{f}_{h_k}$ by $\widehat{f}_{h_{\mathrm{HY},k}}$ and changing the values of $\widehat{x}_0$ and $\widehat{x}_{2k}$ as it was pointed out. The neighborhood in which the J functions are defined is chosen by the same method as in the approach described in the main text. To guarantee that the calibration function is a density, it is also necessary to select correctly the values of $\mathfrak{a}$ (if $\widehat{f}_{h_{\mathrm{HY},k}}$ has modes lower than a) and $\mathfrak{b}$ (if it has modes greater than b) to obtain an integral equal to one. An option is to employ $\mathfrak{a}$ and $\mathfrak{b}$ satisfying

$$\begin{aligned} &\int_{-\infty}^{\widehat{x}_0} g(x; h_{\mathrm{HY},k}, h_{\mathrm{PI}}, \varsigma, \mathfrak{a}, \mathfrak{b}) dx + \int_{\widehat{x}_{2k}}^{\infty} g(x; h_{\mathrm{HY},k}, h_{\mathrm{PI}}, \varsigma, \mathfrak{a}, \mathfrak{b}) dx = \\ &\int_{-\infty}^{\widehat{x}_0} \widehat{f}_{h_k}(x) dx + \int_{\widehat{x}_{2k}}^{\infty} \widehat{f}_{h_k}(x) dx. \end{aligned} \tag{2.1.15}$$

It may happen that the equality (2.1.15) is not satisfied for any pair $(\mathfrak{a}, \mathfrak{b})$, being $\mathfrak{a} \in (-\infty, \widehat{x}_0)$ and $\mathfrak{b} \in (\widehat{x}_{2k}, \infty)$. In this case, the calibration function can be divided by the normalizing constant to correct the value of the integral. Another alternative can be to take other values of $\widehat{x}_0 < \widehat{x}_1$ and $\widehat{x}_{2k} > \widehat{x}_{2k-1}$, such as $\widehat{f}'_{h_{\mathrm{HY},k}}(x) > 0$, for all $x \in [\widehat{x}_0, \widehat{x}_1)$, and $\widehat{f}'_{h_{\mathrm{HY},k}}(x) < 0$, for all $x \in (\widehat{x}_{2k-1}, \widehat{x}_{2k}]$.

The approach considered in the simulation study (when the support is known) is search the value of $\mathfrak{a}$ in the interval $[\widehat{x}_0 - b + a, \widehat{x}_0)$ and the value of $\mathfrak{b}$ in $(\widehat{x}_{2k}, \widehat{x}_{2k} + b - a]$. If for all the possible values of $\mathfrak{a}$ and $\mathfrak{b}$ the integral

$$q_2 = \int_{-\infty}^{\infty} g(x; h_{\mathrm{HY},k}, h_{\mathrm{PI}}, \varsigma, \mathfrak{a}, \mathfrak{b}) dx,$$

is not equal to 1, then the solution is take $\mathfrak{a}$ and $\mathfrak{b}$ in such a way that q_2 is as close as possible to one and, then, employ the quotient $g(\cdot; h_{\mathrm{HY},k}, h_{\mathrm{PI}}, \varsigma, \mathfrak{a}, \mathfrak{b})/q_2$ as the calibration function.

2.2 Simulation study

The aim of the following simulation study is to compare the level accuracy and power of the different proposals presented in Section 2.1. With this goal, samples of size $n = 50$, $n = 200$ and $n = 1000$ ($n = 100$ instead of $n = 1000$ in power studies) were drawn from twenty six different distributions, eleven of them unimodal (models M1–M10 and M26), ten bimodal (models M11–M20) and five trimodal (models M21–M25), see Appendix A. For each choice of sampling distribution and sample size, 500 realizations of the sample were generated. Conditionally on each of those samples, for testing purposes, 500 resamples of size n were drawn from the population. Tables 2.1–2.7 report the percentages of rejections for significance levels $\alpha = 0.01$, $\alpha = 0.05$ and $\alpha = 0.10$ under different scenarios: testing unimodality vs. multimodality (Table 2.1 and 2.2); testing bimodality against more than two modes when the true distribution has two modes (Table 2.4) or one (Table 2.5) mode and their power analysis (respectively Tables 2.3 and 2.6). The procedures considered include the proposals by Silverman (1981) (SI), Fisher and Marron (2001) (FM), Hall and York (2001) (HY), Hartigan and Hartigan (1985) (HH), Cheng and Hall (1998) (CH) and the new proposal (NP) in this manuscript. Note that for testing $H_0 : j = 2$, only SI, FM and NP can be compared. For the critical bandwidth test HY, the two proposed methods for computing λ_α have been tried, with very similar results. The ones reported in this section correspond to a polynomial approximation for λ_α. $I = [0, 1]$ is used both for HY and for NP, when the interval containing the modes is assumed to be known (Tables 2.8 and 2.7). Further computational details are included in Appendix C.2.

Testing unimodality vs. multimodality. From the results in Tables 2.1 and 2.2, it is concluded that SI is quite conservative, since even for high sample sizes, the percentage of rejections is below the significance level, being quite close to 0 even for $\alpha = 0.10$. An exception to this conservative behaviour can be found in models M5 (with outliers in tails) and M6 (with a *flat tail*), finding percentages of rejections between 0.03 and 0.052 for $n = 200$ or $n = 1000$, when $\alpha = 0.10$. Regarding FM, a systematic behaviour cannot be concluded: the percentage of rejections is above the significance level for models M1, M5, M7, M9 or M10, but it can be also below the true level for M2, M4 or M8.

The behaviour of HY is quite good when using $I = [0, 1]$ for the different distributions and large sample sizes. For $n = 1000$, the percentage of rejections is quite close to α, except for model M5 (for $\alpha = 0.05$, below level) and for models M6 and M7 (for $\alpha = 0.10$, above level). However, the percentage of rejections is usually below the significance level for small sample sizes. Exceptions to this general pattern are found for model M1 ($n = 200$), M3 ($n = 50$) and M10 ($n = 200$), where percentage of rejections is close to α and models M3 ($n = 200$), M6 ($n = 200$) and M7 with percentages

above α. Nevertheless, it should be kept in mind that the support where unimodality is tested must be known. Similarly to SI, the results obtained with HH are quite conservative. For instance, for $n = 1000$, even taking $\alpha = 0.10$, the percentage of rejections is always below 0.002.

In simple models, the CH proposal has a correct calibration, although slightly conservative in some cases, such as for model M4 ($n = 1000$), M5 ($n = 200$) and M8 ($n = 200$). As expected by Cheng and Hall (1998), the parametric calibration distributions do not capture, for example, the skewness and this affects the second–order properties in more complex models. This effect is reflected in the asymmetric M3, M7 and M10 ($n = 1000$), or model M9, where the percentage of rejections is below α, and for model M6 where is considerably higher than the significance level.

Finally, regarding the new proposal NP, it seems that the calibration is quite satisfactory, even for complicated models, with a slightly conservative performance for M3 ($n = 200$), M4 ($n = 1000$) or M7 ($n = 200$), being this effect more clear for model M9. The unique scenario where the percentage of rejections is above α is for M6 with $n = 200$, but this behaviour is corrected when increasing the sample size. Although the performance is better for higher sample sizes ($n = 200$ or $n = 1000$), in some cases, such as M9 or M16 (in the bimodal case), even for $n = 1000$, a percentage of rejections close to α is hard to get. In this difficult cases, the knowledge of the support can be used for obtaining better results as it was reported in Table 2.8, where the percentage of rejections is close to α for the sample sizes $n = 200$ and $n = 1000$.

Regarding power behaviour (and just commenting on the three methods which exhibit a correct calibration: HY, CH and NP), results are reported in Table 2.3: none of the proposals is clearly more powerful. For instance, for model M13, HY clearly detects (even for $n = 50$) the appearance of the second small mode, whereas the other approaches do not succeed in doing so. For models M11, M12, M14 and M15 ($n = 50$), CH presents the highest empirical power and HY shows the lowest one.

Assessing bimodality. For testing $H_0 : j = 2$, Hall and York (2001) prove that, even knowing the density support, SI cannot be consistently calibrated by a bootstrap procedure, similar to the one used for the unimodality vs. multimodality test. Hence, in some models such as M15 or M16 ($n = 50$), the percentage of rejections is close to α, whereas the conservative behaviour observed in the unimodality test, is just perceived in M14 and M19, for large sample sizes. Also, in this case, there is a model where the percentage of rejections is considerably higher than the significance level, M20 ($n = 200$ and $n = 1000$), being this bimodal model similar to the conservative M19, just generating some atypical data in the tails. FM presents again an erratic behaviour: for M17 (except for $n = 200$), M18 or M19, the percentage of rejections

is below α, whereas the opposite happens for M11, M12, M15, M16 or M20 (except for $n = 50$).

For testing bimodality, NP presents good results. The percentage of rejections is close to the significance level, except for M12 ($n = 200$) and M13 ($n = 200$), slightly below α, and M11 ($n = 50$), M15 ($n = 50$, $n = 200$), M16 and M19 ($n = 50$), slightly above α. For $n = 1000$, all the results are good except for M16, but the calibration problem is corrected (as seen in Table 2.8) applying NP with known support, taking for that purpose $I = [0, 1]$. So, just the new proposal presents a correct calibration. Hence, power results reported in Table 2.6 are only judged for the new proposal: power increases with sample size, detecting that all the alternative distributions do not satisfy the null hypothesis, except for M21 ($n = 50$) and M24 ($n = 50$).

Assessing bimodality in the unimodal cases. The conclusions from the results reported in Table 2.5 are quite similar to those given previously when $H_0 : j = 1$ was tested. First, although SI still reports a percentage of rejections below the significance level, it is less conservative than for the initial results (testing $H_0 : j = 1$). For all the available models and all sample sizes and significance levels, the percentage of rejections employing the bimodality test is greater or equal than the one obtained when the unimodality test was applied but lower than the significance level. In fact, taking into account the two largest sample sizes ($n = 200$ and $n = 1000$), the percentage of rejections is always strictly greater in the bimodal test with the exceptions of the models M3 ($n = 50$ and $\alpha = 0.05$), M6 ($n = 200$ and $\alpha = 0.10$) and M10 ($n = 50$ and $\alpha = 0.05$). Regarding FM, again a systematic behaviour cannot be concluded, being the results similar to those ones reported previously when unimodality was tested on the same models. Finally, the results for the new proposal seem to be again quite satisfactory, with a slightly conservative performance in some models, such as M2, M3 ($n = 1000$ and $\alpha = 0.10$), M4, M5 ($n = 200$), M7, M9 and M10 ($n = 50$). Observing these results, it seems that, in practice, NP can be used for testing $H_0 : j \leq k$, but it should be kept in mind that a correct calibration is not guaranteed. An example of poor behaviour can be observed for (unimodal) model M26. Analysing the results reported in Table 2.7 for NP, when testing $H_0 : j = 1$ and $n = 1000$, the percentage of rejections is close to the significance level, whereas when testing $H_0 : j = 2$, the percentage of rejections is below α, even employing the correction provided when the support is known.

		α	0.01	0.05	0.10	0.01	0.05	0.10	0.01	0.05	0.10
M1	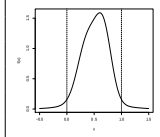			SI			FM			HY	
		$n = 50$	0(0)	0(0)	0.002(0.004)	0.010(0.009)	0.076(0.023)	0.178(0.034)	0(0)	0.022(0.013)	0.050(0.019)
		$n = 200$	0(0)	0.002(0.004)	0.020(0.012)	0.056(0.020)	0.162(0.032)	0.262(0.039)	0.002(0.004)	0.046(0.018)	0.090(0.025)
		$n = 1000$	0(0)	0(0)	0.020(0.012)	0.036(0.016)	0.126(0.029)	0.210(0.036)	0.002(0.004)	0.052(0.019)	0.096(0.026)
				HH			CH			NP	
		$n = 50$	0(0)	0.006(0.007)	0.022(0.013)	0.022(0.013)	0.072(0.023)	0.140(0.030)	0.010(0.009)	0.064(0.021)	0.120(0.028)
		$n = 200$	0(0)	0.002(0.004)	0.002(0.004)	0.014(0.010)	0.058(0.020)	0.122(0.029)	0.010(0.009)	0.044(0.018)	0.120(0.028)
		$n = 1000$	0(0)	0(0)	0(0)	0.006(0.007)	0.048(0.019)	0.104(0.027)	0.008(0.008)	0.052(0.019)	0.108(0.027)
M2	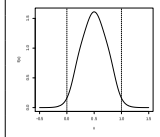			SI			FM			HY	
		$n = 50$	0(0)	0(0)	0.012(0.010)	0.004(0.006)	0.040(0.017)	0.076(0.023)	0(0)	0.024(0.013)	0.068(0.022)
		$n = 200$	0(0)	0(0)	0.006(0.007)	0(0)	0.006(0.007)	0.056(0.020)	0(0)	0.030(0.015)	0.082(0.024)
		$n = 1000$	0(0)	0(0)	0.014(0.010)	0(0)	0.014(0.010)	0.040(0.017)	0.004(0.006)	0.038(0.017)	0.080(0.024)
				HH			CH			NP	
		$n = 50$	0(0)	0.012(0.010)	0.028(0.014)	0.046(0.018)	0.100(0.026)	0.140(0.030)	0.016(0.011)	0.070(0.022)	0.122(0.029)
		$n = 200$	0(0)	0.002(0.004)	0.004(0.006)	0.020(0.012)	0.074(0.023)	0.164(0.032)	0.004(0.006)	0.050(0.019)	0.114(0.028)
		$n = 1000$	0(0)	0(0)	0(0)	0.008(0.008)	0.032(0.015)	0.092(0.025)	0.006(0.007)	0.030(0.015)	0.082(0.024)
M3	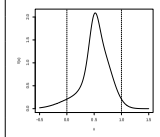			SI			FM			HY	
		$n = 50$	0(0)	0(0)	0.002(0.004)	0.026(0.014)	0.112(0.028)	0.222(0.036)	0.008(0.008)	0.066(0.022)	0.108(0.027)
		$n = 200$	0(0)	0(0)	0.004(0.006)	0.014(0.010)	0.072(0.023)	0.146(0.031)	0.030(0.015)	0.088(0.025)	0.146(0.031)
		$n = 1000$	0(0)	0(0)	0.006(0.007)	0.002(0.004)	0.050(0.019)	0.128(0.029)	0.018(0.012)	0.070(0.022)	0.120(0.028)
				HH			CH			NP	
		$n = 50$	0(0)	0(0)	0.004(0.006)	0.002(0.004)	0.032(0.015)	0.056(0.020)	0.004(0.006)	0.042(0.018)	0.078(0.024)
		$n = 200$	0(0)	0(0)	0.002(0.004)	0.002(0.004)	0.004(0.006)	0.030(0.015)	0.002(0.004)	0.022(0.013)	0.054(0.020)
		$n = 1000$	0(0)	0(0)	0(0)	0.002(0.004)	0.012(0.010)	0.032(0.015)	0.006(0.007)	0.032(0.015)	0.082(0.024)
M4	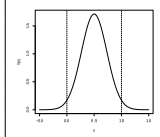			SI			FM			HY	
		$n = 50$	0(0)	0(0)	0.002(0.004)	0.002(0.004)	0.018(0.012)	0.060(0.021)	0(0)	0.020(0.012)	0.050(0.019)
		$n = 200$	0(0)	0(0)	0.004(0.006)	0(0)	0.012(0.010)	0.044(0.018)	0.004(0.006)	0.026(0.014)	0.074(0.023)
		$n = 1000$	0(0)	0.004(0.006)	0.014(0.010)	0(0)	0.010(0.009)	0.046(0.018)	0.008(0.008)	0.052(0.019)	0.090(0.025)
				HH			CH			NP	
		$n = 50$	0(0)	0.004(0.006)	0.018(0.012)	0.016(0.011)	0.064(0.021)	0.118(0.028)	0.014(0.010)	0.050(0.019)	0.102(0.027)
		$n = 200$	0(0)	0(0)	0(0)	0.008(0.008)	0.032(0.015)	0.082(0.024)	0.004(0.006)	0.030(0.015)	0.080(0.024)
		$n = 1000$	0(0)	0(0)	0(0)	0.004(0.006)	0.034(0.016)	0.066(0.022)	0(0)	0.028(0.014)	0.066(0.022)
M5	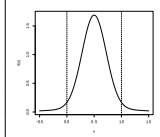			SI			FM			HY	
		$n = 50$	0(0)	0(0)	0.004(0.006)	0.186(0.034)	0.366(0.042)	0.494(0.044)	0(0)	0.006(0.007)	0.038(0.017)
		$n = 200$	0(0)	0(0)	0.032(0.015)	0.268(0.039)	0.500(0.044)	0.612(0.043)	0.002(0.004)	0.030(0.015)	0.074(0.023)
		$n = 1000$	0(0)	0.004(0.006)	0.030(0.015)	0.210(0.036)	0.380(0.043)	0.504(0.044)	0.006(0.007)	0.028(0.014)	0.080(0.024)
				HH			CH			NP	
		$n = 50$	0(0)	0(0)	0.006(0.007)	0.004(0.006)	0.052(0.019)	0.084(0.024)	0.006(0.007)	0.062(0.021)	0.106(0.027)
		$n = 200$	0(0)	0(0)	0(0)	0.010(0.009)	0.034(0.016)	0.064(0.021)	0.012(0.010)	0.050(0.019)	0.092(0.025)
		$n = 1000$	0(0)	0(0)	0(0)	0.006(0.007)	0.022(0.013)	0.082(0.024)	0.006(0.007)	0.052(0.019)	0.106(0.027)

Table 2.1: Percentages of rejections for testing unimodality, with 500 simulations (1.96 times their estimated standard deviation in parenthesis) and $B = 500$ bootstrap samples.

		α	0.01	0.05	0.10	0.01	0.05	0.10	0.01	0.05	0.10
M6	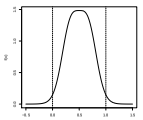		SI			FM			HY		
		$n = 50$	0(0)	0(0)	0.012(0.010)	0.004(0.006)	0.040(0.017)	0.082(0.024)	0.002(0.004)	0.022(0.013)	0.074(0.023)
		$n = 200$	0(0)	0.012(0.010)	0.052(0.019)	0.010(0.009)	0.064(0.021)	0.122(0.029)	0.012(0.010)	0.110(0.027)	0.196(0.035)
		$n = 1000$	0.002(0.004)	0.020(0.012)	0.048(0.019)	0.008(0.008)	0.042(0.018)	0.100(0.026)	0.048(0.019)	0.118(0.028)	0.216(0.036)
			HH			CH			NP		
		$n = 50$	0(0)	0.006(0.007)	0.012(0.010)	0.028(0.014)	0.092(0.025)	0.168(0.033)	0.008(0.008)	0.050(0.019)	0.112(0.028)
		$n = 200$	0(0)	0.008(0.008)	0.012(0.010)	0.050(0.019)	0.136(0.030)	0.236(0.037)	0.018(0.012)	0.088(0.025)	0.160(0.032)
		$n = 1000$	0(0)	0.002(0.004)	0.002(0.004)	0.038(0.017)	0.112(0.028)	0.202(0.035)	0.016(0.011)	0.046(0.018)	0.116(0.028)
M7	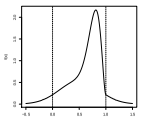		SI			FM			HY		
		$n = 50$	0(0)	0(0)	0(0)	0.072(0.023)	0.246(0.038)	0.378(0.043)	0.012(0.010)	0.072(0.023)	0.146(0.031)
		$n = 200$	0(0)	0.002(0.004)	0.006(0.007)	0.064(0.021)	0.210(0.036)	0.368(0.042)	0.016(0.011)	0.078(0.024)	0.144(0.031)
		$n = 1000$	0(0)	0(0)	0(0)	0.060(0.021)	0.214(0.036)	0.346(0.042)	0.004(0.006)	0.072(0.023)	0.134(0.030)
			HH			CH			NP		
		$n = 50$	0(0)	0(0)	0.010(0.009)	0.008(0.008)	0.026(0.014)	0.082(0.024)	0.006(0.007)	0.032(0.015)	0.084(0.024)
		$n = 200$	0(0)	0(0)	0(0)	0(0)	0.014(0.010)	0.042(0.018)	0.002(0.004)	0.028(0.014)	0.070(0.022)
		$n = 1000$	0(0)	0(0)	0(0)	0(0)	0.012(0.010)	0.036(0.016)	0.004(0.006)	0.042(0.018)	0.094(0.026)
M8	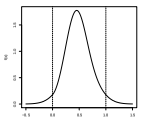		SI			FM			HY		
		$n = 50$	0(0)	0(0)	0(0)	0.006(0.007)	0.024(0.013)	0.062(0.021)	0(0)	0.012(0.010)	0.046(0.018)
		$n = 200$	0(0)	0(0)	0.002(0.004)	0.002(0.004)	0.022(0.013)	0.064(0.021)	0(0)	0.024(0.013)	0.054(0.020)
		$n = 1000$	0(0)	0(0)	0(0)	0.002(0.004)	0.018(0.012)	0.048(0.019)	0.010(0.009)	0.054(0.020)	0.092(0.025)
			HH			CH			NP		
		$n = 50$	0(0)	0(0)	0.006(0.007)	0.006(0.007)	0.034(0.016)	0.078(0.024)	0.006(0.007)	0.032(0.015)	0.076(0.023)
		$n = 200$	0(0)	0(0)	0(0)	0.004(0.006)	0.026(0.014)	0.066(0.022)	0.006(0.007)	0.028(0.014)	0.088(0.025)
		$n = 1000$	0(0)	0(0)	0.002(0.004)	0.016(0.011)	0.038(0.017)	0.082(0.024)	0.014(0.010)	0.044(0.018)	0.088(0.025)
M9	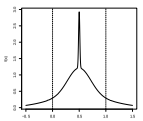		SI			FM			HY		
		$n = 50$	0(0)	0(0)	0(0)	0.018(0.012)	0.084(0.024)	0.198(0.035)	0(0)	0.006(0.007)	0.014(0.010)
		$n = 200$	0(0)	0(0)	0(0)	0.048(0.019)	0.182(0.034)	0.328(0.041)	0.002(0.004)	0.022(0.013)	0.060(0.021)
		$n = 1000$	0(0)	0(0)	0(0)	0.014(0.010)	0.160(0.032)	0.318(0.041)	0.012(0.010)	0.048(0.019)	0.086(0.025)
			HH			CH			NP		
		$n = 50$	0(0)	0(0)	0(0)	0.002(0.004)	0.016(0.011)	0.032(0.015)	0.004(0.006)	0.026(0.014)	0.068(0.022)
		$n = 200$	0(0)	0(0)	0(0)	0.002(0.004)	0.018(0.012)	0.042(0.018)	0.010(0.009)	0.046(0.018)	0.084(0.024)
		$n = 1000$	0(0)	0(0)	0(0)	0.002(0.004)	0.010(0.009)	0.014(0.010)	0.004(0.006)	0.020(0.012)	0.062(0.021)
M10	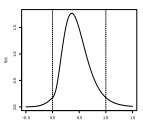		SI			FM			HY		
		$n = 50$	0(0)	0(0)	0(0)	0.016(0.011)	0.054(0.020)	0.116(0.028)	0(0)	0.014(0.010)	0.050(0.019)
		$n = 200$	0(0)	0(0)	0.006(0.007)	0.018(0.012)	0.092(0.025)	0.182(0.034)	0.006(0.007)	0.038(0.017)	0.086(0.025)
		$n = 1000$	0(0)	0(0)	0.008(0.008)	0.022(0.013)	0.094(0.026)	0.168(0.033)	0.010(0.009)	0.050(0.019)	0.096(0.026)
			HH			CH			NP		
		$n = 50$	0(0)	0.002(0.004)	0.008(0.008)	0.004(0.006)	0.046(0.018)	0.086(0.025)	0.012(0.010)	0.044(0.018)	0.094(0.026)
		$n = 200$	0(0)	0(0)	0(0)	0.014(0.010)	0.042(0.018)	0.078(0.024)	0.010(0.009)	0.062(0.021)	0.094(0.026)
		$n = 1000$	0(0)	0(0)	0(0)	0.008(0.008)	0.028(0.014)	0.074(0.023)	0.008(0.008)	0.040(0.017)	0.104(0.027)

Table 2.2: Percentages of rejections for testing unimodality, with 500 simulations (1.96 times their estimated standard deviation in parenthesis) and $B = 500$ bootstrap samples.

		α	0.01	0.05	0.10	0.01	0.05	0.10	0.01	0.05	0.10
M11	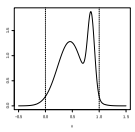		SI			FM			HY		
		$n = 50$	0(0)	0.008(0.008)	0.100(0.026)	0.084(0.024)	0.250(0.038)	0.394(0.043)	0.008(0.008)	0.168(0.033)	0.330(0.041)
		$n = 100$	0.002(0.004)	0.154(0.032)	0.368(0.042)	0.374(0.042)	0.640(0.042)	0.738(0.039)	0.168(0.033)	0.502(0.044)	0.630(0.042)
		$n = 200$	0.094(0.026)	0.304(0.040)	0.500(0.044)	0.600(0.043)	0.788(0.036)	0.860(0.030)	0.378(0.043)	0.604(0.043)	0.714(0.040)
			HH			CH			NP		
		$n = 50$	0.012(0.010)	0.088(0.025)	0.156(0.032)	0.196(0.035)	0.370(0.042)	0.494(0.044)	0.090(0.025)	0.238(0.037)	0.376(0.042)
		$n = 100$	0.060(0.021)	0.182(0.034)	0.274(0.039)	0.442(0.044)	0.630(0.042)	0.722(0.039)	0.228(0.037)	0.418(0.043)	0.542(0.044)
		$n = 200$	0.106(0.027)	0.238(0.037)	0.356(0.042)	0.584(0.043)	0.768(0.037)	0.824(0.033)	0.328(0.041)	0.506(0.044)	0.600(0.043)
M12	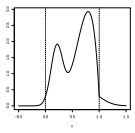		SI			FM			HY		
		$n = 50$	0(0)	0.006(0.007)	0.058(0.020)	0.332(0.041)	0.584(0.043)	0.716(0.040)	0(0)	0.174(0.033)	0.422(0.043)
		$n = 100$	0.006(0.007)	0.186(0.034)	0.496(0.044)	0.662(0.041)	0.838(0.032)	0.896(0.027)	0.224(0.037)	0.642(0.042)	0.802(0.035)
		$n = 200$	0.026(0.014)	0.486(0.044)	0.804(0.035)	0.914(0.025)	0.966(0.016)	0.986(0.010)	0.584(0.043)	0.912(0.025)	0.950(0.019)
			HH			CH			NP		
		$n = 50$	0.042(0.018)	0.118(0.028)	0.202(0.035)	0.268(0.039)	0.480(0.044)	0.594(0.043)	0.100(0.026)	0.266(0.039)	0.400(0.043)
		$n = 100$	0.158(0.032)	0.346(0.042)	0.460(0.044)	0.636(0.042)	0.788(0.036)	0.844(0.032)	0.346(0.042)	0.578(0.043)	0.680(0.041)
		$n = 200$	0.262(0.039)	0.490(0.044)	0.622(0.043)	0.818(0.034)	0.926(0.023)	0.956(0.018)	0.524(0.044)	0.752(0.038)	0.844(0.032)
M13	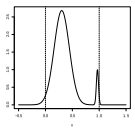		SI			FM			HY		
		$n = 50$	0(0)	0(0)	0(0)	0.064(0.021)	0.492(0.044)	0.776(0.037)	0.634(0.042)	0.858(0.031)	0.892(0.027)
		$n = 100$	0(0)	0.272(0.039)	0.956(0.018)	0.914(0.025)	0.998(0.004)	1(0)	0.994(0.007)	1(0)	1(0)
		$n = 200$	0.898(0.027)	1(0)	1(0)	1(0)	1(0)	1(0)	1(0)	1(0)	1(0)
			HH			CH			NP		
		$n = 50$	0(0)	0.004(0.006)	0.014(0.010)	0.014(0.010)	0.052(0.019)	0.096(0.026)	0.016(0.011)	0.058(0.020)	0.112(0.028)
		$n = 100$	0(0)	0(0)	0(0)	0(0)	0.032(0.015)	0.062(0.021)	0.008(0.008)	0.050(0.019)	0.102(0.027)
		$n = 200$	0(0)	0(0)	0.002(0.004)	0.006(0.007)	0.048(0.019)	0.366(0.042)	0.016(0.011)	0.276(0.039)	0.758(0.038)
M14	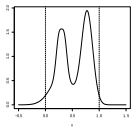		SI			FM			HY		
		$n = 50$	0.002(0.004)	0.044(0.018)	0.352(0.042)	0.662(0.041)	0.864(0.030)	0.922(0.024)	0.050(0.019)	0.576(0.043)	0.830(0.033)
		$n = 100$	0.234(0.037)	0.922(0.024)	0.990(0.009)	0.990(0.009)	1(0)	1(0)	0.920(0.024)	1(0)	1(0)
		$n = 200$	0.866(0.030)	1(0)	1(0)	1(0)	1(0)	1(0)	1(0)	1(0)	1(0)
			HH			CH			NP		
		$n = 50$	0.226(0.037)	0.514(0.044)	0.646(0.042)	0.718(0.039)	0.860(0.030)	0.924(0.023)	0.460(0.044)	0.716(0.040)	0.806(0.035)
		$n = 100$	0.784(0.036)	0.946(0.020)	0.978(0.013)	0.994(0.007)	0.996(0.006)	1(0)	0.950(0.019)	0.992(0.008)	0.994(0.007)
		$n = 200$	1(0)	1(0)	1(0)	1(0)	1(0)	1(0)	1(0)	1(0)	1(0)
M15	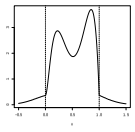		SI			FM			HY		
		$n = 50$	0(0)	0.004(0.006)	0.038(0.017)	0.042(0.018)	0.118(0.028)	0.228(0.037)	0.014(0.010)	0.128(0.029)	0.268(0.039)
		$n = 100$	0(0)	0.034(0.016)	0.136(0.030)	0.118(0.028)	0.334(0.041)	0.472(0.044)	0.066(0.022)	0.342(0.042)	0.500(0.044)
		$n = 200$	0.008(0.008)	0.176(0.033)	0.370(0.042)	0.266(0.039)	0.524(0.044)	0.636(0.042)	0.298(0.040)	0.576(0.043)	0.736(0.039)
			HH			CH			NP		
		$n = 50$	0.010(0.009)	0.046(0.018)	0.072(0.023)	0.098(0.026)	0.242(0.038)	0.374(0.042)	0.054(0.020)	0.156(0.032)	0.274(0.039)
		$n = 100$	0.014(0.010)	0.070(0.022)	0.150(0.031)	0.232(0.037)	0.424(0.043)	0.542(0.044)	0.124(0.029)	0.288(0.040)	0.400(0.043)
		$n = 200$	0.026(0.014)	0.104(0.027)	0.194(0.035)	0.364(0.042)	0.582(0.043)	0.690(0.041)	0.192(0.035)	0.400(0.043)	0.548(0.044)

Table 2.3: Percentages of rejections for testing unimodality, with 500 simulations (1.96 times their estimated standard deviation in parenthesis) and $B = 500$ bootstrap samples.

		α	0.01	0.05	0.10	0.01	0.05	0.10	0.01	0.05	0.10
			SI			FM			NP		
M11		$n = 50$	0(0)	0.012(0.010)	0.058(0.020)	0.016(0.011)	0.076(0.023)	0.152(0.031)	0.028(0.014)	0.088(0.025)	0.178(0.034)
		$n = 200$	0.006(0.007)	0.026(0.014)	0.062(0.021)	0.092(0.025)	0.276(0.039)	0.392(0.043)	0.014(0.010)	0.056(0.020)	0.108(0.027)
		$n = 1000$	0.010(0.009)	0.028(0.014)	0.066(0.022)	0.080(0.024)	0.218(0.036)	0.316(0.041)	0.006(0.007)	0.046(0.018)	0.084(0.024)
			SI			FM			NP		
M12		$n = 50$	0(0)	0.004(0.006)	0.034(0.016)	0.030(0.015)	0.100(0.026)	0.178(0.034)	0.004(0.006)	0.034(0.016)	0.074(0.023)
		$n = 200$	0.006(0.007)	0.022(0.013)	0.038(0.017)	0.038(0.017)	0.134(0.030)	0.184(0.034)	0.002(0.004)	0.030(0.015)	0.076(0.023)
		$n = 1000$	0.014(0.010)	0.022(0.013)	0.030(0.015)	0.052(0.019)	0.094(0.026)	0.168(0.033)	0.008(0.008)	0.046(0.018)	0.082(0.024)
			SI			FM			NP		
M13		$n = 50$	0(0)	0.002(0.004)	0.026(0.014)	0.006(0.007)	0.044(0.018)	0.102(0.027)	0.006(0.007)	0.052(0.019)	0.118(0.028)
		$n = 200$	0(0)	0.004(0.006)	0.022(0.013)	0(0)	0.024(0.013)	0.056(0.020)	0.006(0.007)	0.028(0.014)	0.070(0.022)
		$n = 1000$	0.002(0.004)	0.012(0.010)	0.044(0.018)	0.004(0.006)	0.036(0.016)	0.072(0.023)	0.010(0.009)	0.044(0.018)	0.088(0.025)
			SI			FM			NP		
M14		$n = 50$	0(0)	0.010(0.009)	0.022(0.013)	0.020(0.012)	0.072(0.023)	0.132(0.030)	0.008(0.008)	0.034(0.016)	0.074(0.023)
		$n = 200$	0(0)	0(0)	0.006(0.007)	0.018(0.012)	0.088(0.025)	0.152(0.031)	0.004(0.006)	0.034(0.016)	0.088(0.025)
		$n = 1000$	0.002(0.004)	0.006(0.007)	0.008(0.008)	0.024(0.013)	0.058(0.020)	0.114(0.028)	0.008(0.008)	0.056(0.020)	0.092(0.025)
			SI			FM			NP		
M15		$n = 50$	0(0)	0.014(0.010)	0.048(0.019)	0.008(0.008)	0.072(0.023)	0.136(0.030)	0.012(0.010)	0.078(0.024)	0.158(0.032)
		$n = 200$	0.004(0.006)	0.040(0.017)	0.090(0.025)	0.032(0.015)	0.128(0.029)	0.214(0.036)	0.024(0.013)	0.106(0.027)	0.200(0.035)
		$n = 1000$	0.004(0.006)	0.040(0.017)	0.088(0.025)	0.062(0.021)	0.154(0.032)	0.224(0.037)	0.014(0.010)	0.048(0.019)	0.104(0.027)
			SI			FM			NP		
M16		$n = 50$	0.008(0.008)	0.048(0.019)	0.080(0.024)	0.092(0.025)	0.210(0.036)	0.284(0.040)	0.006(0.007)	0.064(0.021)	0.112(0.028)
		$n = 200$	0.014(0.010)	0.032(0.015)	0.036(0.016)	0.058(0.020)	0.128(0.029)	0.186(0.034)	0.016(0.011)	0.098(0.026)	0.200(0.035)
		$n = 1000$	0.006(0.007)	0.012(0.010)	0.014(0.010)	0.038(0.017)	0.082(0.024)	0.156(0.032)	0.010(0.009)	0.074(0.023)	0.150(0.031)
			SI			FM			NP		
M17		$n = 50$	0(0)	0.014(0.010)	0.036(0.016)	0.002(0.004)	0.028(0.014)	0.060(0.021)	0.012(0.010)	0.060(0.021)	0.136(0.030)
		$n = 200$	0(0)	0.028(0.014)	0.068(0.022)	0.008(0.008)	0.046(0.018)	0.096(0.026)	0.008(0.008)	0.070(0.022)	0.106(0.027)
		$n = 1000$	0.002(0.004)	0.004(0.006)	0.026(0.014)	0.002(0.004)	0.026(0.014)	0.048(0.019)	0.008(0.008)	0.038(0.017)	0.074(0.023)
			SI			FM			NP		
M18		$n = 50$	0(0)	0(0)	0.002(0.004)	0(0)	0.008(0.008)	0.038(0.017)	0.004(0.006)	0.054(0.020)	0.108(0.027)
		$n = 200$	0(0)	0.008(0.008)	0.020(0.012)	0.004(0.006)	0.032(0.015)	0.050(0.019)	0.006(0.007)	0.048(0.019)	0.108(0.027)
		$n = 1000$	0(0)	0.008(0.008)	0.028(0.014)	0.004(0.006)	0.028(0.014)	0.066(0.022)	0.002(0.004)	0.034(0.016)	0.080(0.024)
			SI			FM			NP		
M19		$n = 50$	0(0)	0(0)	0(0)	0(0)	0.004(0.006)	0.034(0.016)	0.024(0.013)	0.070(0.022)	0.132(0.030)
		$n = 200$	0(0)	0(0)	0(0)	0(0)	0.008(0.008)	0.030(0.015)	0.012(0.010)	0.066(0.022)	0.118(0.028)
		$n = 1000$	0(0)	0.004(0.006)	0.008(0.008)	0(0)	0.022(0.013)	0.044(0.018)	0.008(0.008)	0.040(0.017)	0.100(0.026)
			SI			FM			NP		
M20		$n = 50$	0(0)	0(0)	0(0)	0.002(0.004)	0.004(0.006)	0.022(0.013)	0.010(0.009)	0.068(0.022)	0.112(0.028)
		$n = 200$	0.250(0.038)	0.420(0.043)	0.542(0.044)	0.958(0.018)	0.974(0.014)	0.982(0.012)	0.016(0.011)	0.060(0.021)	0.128(0.029)
		$n = 1000$	0.334(0.041)	0.466(0.044)	0.570(0.043)	0.976(0.013)	0.990(0.009)	0.998(0.004)	0.004(0.006)	0.038(0.017)	0.096(0.026)

Table 2.4: Percentages of rejections for testing bimodality, with 500 simulations (1.96 times their estimated standard deviation in parenthesis) and $B = 500$ bootstrap samples.

		α	0.01	0.05	0.10	0.01	0.05	0.10	0.01	0.05	0.10
			SI			FM			NP		
M1		$n = 50$	0(0)	0.004(0.006)	0.042(0.018)	0.004(0.006)	0.040(0.017)	0.120(0.028)	0.014(0.010)	0.054(0.020)	0.120(0.028)
		$n = 200$	0(0)	0.010(0.009)	0.086(0.025)	0.008(0.008)	0.094(0.026)	0.180(0.034)	0.010(0.009)	0.042(0.018)	0.096(0.026)
		$n = 1000$	0(0)	0.012(0.010)	0.045(0.018)	0.010(0.009)	0.052(0.020)	0.138(0.030)	0.018(0.011)	0.052(0.020)	0.092(0.025)
			SI			FM			NP		
M2		$n = 50$	0(0)	0.002(0.004)	0.018(0.012)	0.002(0.004)	0.020(0.012)	0.046(0.018)	0.006(0.007)	0.060(0.021)	0.126(0.029)
		$n = 200$	0(0)	0.004(0.006)	0.032(0.015)	0(0)	0.014(0.010)	0.060(0.021)	0.008(0.008)	0.032(0.015)	0.088(0.025)
		$n = 1000$	0(0)	0.010(0.009)	0.020(0.012)	0(0)	0.016(0.011)	0.038(0.017)	0.010(0.009)	0.042(0.018)	0.072(0.023)
			SI			FM			NP		
M3		$n = 50$	0(0)	0(0)	0.020(0.012)	0.010(0.009)	0.054(0.020)	0.146(0.031)	0.004(0.006)	0.032(0.015)	0.064(0.021)
		$n = 200$	0(0)	0.012(0.010)	0.030(0.015)	0.008(0.008)	0.064(0.021)	0.150(0.031)	0.004(0.006)	0.028(0.014)	0.066(0.022)
		$n = 1000$	0(0)	0.002(0.004)	0.020(0.012)	0.002(0.004)	0.042(0.018)	0.110(0.027)	0.006(0.007)	0.034(0.016)	0.062(0.021)
			SI			FM			NP		
M4		$n = 50$	0(0)	0.002(0.004)	0.016(0.011)	0.004(0.006)	0.020(0.012)	0.052(0.019)	0.010(0.009)	0.066(0.022)	0.112(0.028)
		$n = 200$	0(0)	0.002(0.004)	0.012(0.010)	0.002(0.004)	0.008(0.008)	0.026(0.014)	0.012(0.010)	0.028(0.014)	0.050(0.019)
		$n = 1000$	0(0)	0.012(0.010)	0.032(0.015)	0(0)	0.014(0.010)	0.048(0.019)	0.006(0.007)	0.046(0.018)	0.102(0.027)
			SI			FM			NP		
M5		$n = 50$	0(0)	0.034(0.016)	0.100(0.026)	0.056(0.020)	0.168(0.033)	0.244(0.038)	0.008(0.008)	0.044(0.018)	0.094(0.026)
		$n = 200$	0.002(0.004)	0.032(0.015)	0.114(0.028)	0.130(0.029)	0.298(0.040)	0.414(0.043)	0.002(0.004)	0.026(0.014)	0.084(0.024)
		$n = 1000$	0.004(0.006)	0.008(0.008)	0.048(0.019)	0.072(0.023)	0.228(0.037)	0.364(0.042)	0.010(0.009)	0.046(0.018)	0.094(0.026)
			SI			FM			NP		
M6		$n = 50$	0(0)	0.002(0.004)	0.014(0.010)	0(0)	0.012(0.010)	0.036(0.016)	0.010(0.009)	0.048(0.019)	0.110(0.027)
		$n = 200$	0(0)	0.018(0.012)	0.052(0.019)	0.010(0.009)	0.042(0.018)	0.072(0.023)	0.008(0.008)	0.058(0.020)	0.108(0.027)
		$n = 1000$	0.002(0.004)	0.024(0.013)	0.074(0.023)	0.002(0.004)	0.030(0.015)	0.082(0.024)	0.014(0.010)	0.052(0.019)	0.098(0.026)
			SI			FM			NP		
M7		$n = 50$	0(0)	0.014(0.010)	0.052(0.019)	0.070(0.022)	0.186(0.034)	0.338(0.041)	0.002(0.004)	0.016(0.011)	0.042(0.018)
		$n = 200$	0(0)	0.010(0.009)	0.044(0.018)	0.064(0.021)	0.188(0.034)	0.320(0.041)	0.004(0.006)	0.034(0.016)	0.078(0.024)
		$n = 1000$	0(0)	0.002(0.004)	0.028(0.014)	0.038(0.017)	0.160(0.032)	0.262(0.039)	0.008(0.008)	0.042(0.018)	0.092(0.025)
			SI			FM			NP		
M8		$n = 50$	0(0)	0.004(0.006)	0.024(0.013)	0.002(0.004)	0.024(0.013)	0.050(0.019)	0.008(0.008)	0.034(0.016)	0.084(0.024)
		$n = 200$	0(0)	0.008(0.008)	0.034(0.016)	0(0)	0.024(0.013)	0.064(0.021)	0.006(0.007)	0.040(0.017)	0.076(0.023)
		$n = 1000$	0(0)	0.008(0.008)	0.028(0.014)	0(0)	0.020(0.012)	0.058(0.020)	0.008(0.008)	0.044(0.018)	0.102(0.027)
			SI			FM			NP		
M9		$n = 50$	0(0)	0.010(0.009)	0.038(0.017)	0.014(0.010)	0.064(0.021)	0.132(0.030)	0.004(0.006)	0.024(0.013)	0.066(0.022)
		$n = 200$	0(0)	0.010(0.009)	0.030(0.015)	0.036(0.016)	0.222(0.036)	0.376(0.042)	0.010(0.009)	0.044(0.018)	0.092(0.025)
		$n = 1000$	0(0)	0.006(0.007)	0.022(0.013)	0.032(0.015)	0.188(0.034)	0.334(0.041)	0.010(0.009)	0.048(0.019)	0.110(0.027)
			SI			FM			NP		
M10		$n = 50$	0(0)	0(0)	0.014(0.010)	0(0)	0.026(0.014)	0.066(0.022)	0.002(0.004)	0.026(0.014)	0.072(0.023)
		$n = 200$	0(0)	0.014(0.010)	0.034(0.016)	0.004(0.006)	0.034(0.016)	0.082(0.024)	0.008(0.008)	0.042(0.018)	0.098(0.026)
		$n = 1000$	0(0)	0.008(0.008)	0.056(0.020)	0.006(0.007)	0.048(0.019)	0.096(0.026)	0.002(0.004)	0.042(0.018)	0.088(0.025)

Table 2.5: Percentages of rejections for testing bimodality when the true distribution is unimodal, with 500 simulations (1.96 times their estimated standard deviation in parenthesis) and $B = 500$ bootstrap samples.

		α	0.01	0.05	0.10	0.01	0.05	0.10	0.01	0.05	0.10
			SI			FM			NP		
M21		$n = 50$	0(0)	0.026(0.014)	0.058(0.020)	0.010(0.009)	0.052(0.019)	0.112(0.028)	0.014(0.010)	0.054(0.020)	0.112(0.028)
		$n = 100$	0.002(0.004)	0.056(0.020)	0.154(0.032)	0.044(0.018)	0.148(0.031)	0.228(0.037)	0.020(0.012)	0.092(0.025)	0.168(0.033)
		$n = 200$	0.024(0.013)	0.104(0.027)	0.208(0.036)	0.076(0.023)	0.202(0.035)	0.278(0.039)	0.050(0.019)	0.134(0.030)	0.194(0.035)
			SI			FM			NP		
M22		$n = 50$	0.002(0.004)	0.006(0.007)	0.022(0.013)	0.036(0.016)	0.142(0.031)	0.300(0.040)	0.080(0.024)	0.256(0.038)	0.402(0.043)
		$n = 100$	0(0)	0.026(0.014)	0.180(0.034)	0.248(0.038)	0.610(0.043)	0.804(0.035)	0.266(0.039)	0.542(0.044)	0.706(0.040)
		$n = 200$	0.052(0.019)	0.500(0.044)	0.806(0.035)	0.740(0.038)	0.960(0.017)	0.982(0.012)	0.890(0.027)	0.956(0.018)	0.980(0.012)
			SI			FM			NP		
M23		$n = 50$	0(0)	0.068(0.022)	0.206(0.035)	0.054(0.020)	0.196(0.035)	0.338(0.041)	0.050(0.019)	0.204(0.035)	0.336(0.041)
		$n = 100$	0.082(0.024)	0.486(0.044)	0.684(0.041)	0.334(0.041)	0.658(0.042)	0.780(0.036)	0.326(0.041)	0.624(0.042)	0.746(0.038)
		$n = 200$	0.570(0.043)	0.780(0.036)	0.840(0.032)	0.832(0.033)	0.906(0.026)	0.938(0.021)	0.722(0.039)	0.878(0.029)	0.934(0.022)
			SI			FM			NP		
M24		$n = 50$	0(0)	0.008(0.008)	0.038(0.017)	0.004(0.006)	0.030(0.015)	0.082(0.024)	0.008(0.008)	0.060(0.021)	0.134(0.030)
		$n = 100$	0(0)	0.006(0.007)	0.026(0.014)	0.012(0.010)	0.052(0.019)	0.108(0.027)	0.034(0.016)	0.110(0.027)	0.176(0.033)
		$n = 200$	0.006(0.007)	0.040(0.017)	0.108(0.027)	0.050(0.019)	0.160(0.032)	0.288(0.040)	0.096(0.026)	0.232(0.037)	0.334(0.041)
			SI			FM			NP		
M25		$n = 50$	0.002(0.004)	0.046(0.018)	0.138(0.030)	0.068(0.022)	0.200(0.035)	0.312(0.041)	0.018(0.012)	0.098(0.026)	0.148(0.031)
		$n = 100$	0.004(0.006)	0.064(0.021)	0.176(0.033)	0.170(0.033)	0.344(0.042)	0.462(0.044)	0.098(0.026)	0.232(0.037)	0.320(0.041)
		$n = 200$	0.008(0.008)	0.084(0.024)	0.198(0.035)	0.190(0.034)	0.404(0.043)	0.552(0.044)	0.106(0.027)	0.248(0.038)	0.356(0.042)

Table 2.6: Percentages of rejections for testing bimodality, with 500 simulations (1.96 times their estimated standard deviation in parenthesis) and $B = 500$ bootstrap samples.

		α	0.01	0.05	0.10	0.01	0.05	0.10	0.01	0.05	0.10
			NP (unknown support)			NP (unknown support)			NP (known support)		
M26		$n = 50$	0.008(0.008)	0.032(0.015)	0.066(0.022)	0.004(0.006)	0.028(0.014)	0.048(0.019)	0.002(0.004)	0.022(0.013)	0.076(0.023)
		$n = 200$	0(0)	0.022(0.013)	0.068(0.022)	0.006(0.007)	0.030(0.015)	0.074(0.023)	0.004(0.006)	0.034(0.016)	0.062(0.021)
		$n = 1000$	0.004(0.006)	0.040(0.017)	0.080(0.024)	0(0)	0.020(0.012)	0.054(0.020)	0(0)	0.026(0.014)	0.052(0.019)

Table 2.7: Percentages of rejections for testing unimodality (first column) and bimodality (second and third column), with 500 simulations (1.96 times their estimated standard deviation in parenthesis) and $B = 500$ bootstrap samples.

		α	0.01	0.05	0.10
			NP (known support)		
$n = 50$	M9	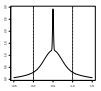	0(0)	0.014(0.010)	0.034(0.016)
$n = 200$			0.012(0.010)	0.052(0.019)	0.090(0.025)
$n = 1000$			0.010(0.009)	0.040(0.017)	0.092(0.025)
$n = 50$	M16	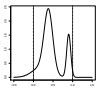	0.002(0.004)	0.024(0.013)	0.076(0.023)
$n = 200$			0.008(0.008)	0.058(0.020)	0.126(0.029)
$n = 1000$			0.016(0.011)	0.038(0.017)	0.080(0.024)

Table 2.8: Percentages of rejections for testing unimodality (in model M9) and bimodality (in model M16), with 500 simulations (1.96 times their estimated standard deviation in parenthesis) and $B = 500$ bootstrap samples.

2.3 The 1872 Hidalgo stamp issue of Mexico

As explained in Section 1.3.1, the value of stamps depends on its scarcity, and thickness is determinant in this sense. However, in general, the designation of thick, medium or thin stamps is relative and can only refer to a particular stamp issue. Otherwise, making uniform categories for all stamp issues may lead to inaccurate classifications. In addition, there is not such a differentiation between groups available in stamps catalogues, leaving this classification to a personal subjective judgement. The importance of establishing an objective criterion specially appears in stamp issues printed on a mixture of paper types, with possible differences in their thickness.

A stamp issue where the problem of determining the number of different groups of stamps appears is in the 1872 Hidalgo issue. First, for this particular issue, and in general in the Mexican ones, it is known that the handmade paper presents a lot of variability in the thickness of the paper. Second, since of scarcity of ordinary white wove paper, other types of paper were used to produce the Hidalgo issue. A small quantity of "vertically laid" paper, a fiscal type of white wove paper denominated *Papel Sellado* (some of them were watermarked vertically), other type of white wove, the *La Croix–Freres* of France (some of them with a watermark of *LA+-F*) and also another unwatermarked white wove paper might also have been used. It is estimated than the watermark of *Papel Sellado* can appear in between 6 and 18 stamps in each sheet of 100. For the *La Croix–Freres* watermark, it is estimated that the symbol appears in between 4 and 10 stamps if the sheet was watermarked, and some authors suggested that this watermark appears only once of every 4 sheets. In order to get more information about this particular problem and to obtain some further references, see Izenman and Sommer (1988).

This particular example has been explored in several references in the literature for determining the number of different groups of stamps. From a nonparametric point of view, some examples of its utilization for mode testing can be shown in Efron and Tibshirani (1994, Ch. 16), Izenman and Sommer (1988) or in Fisher and Marron (2001). Also it was analysed using nonparametric exploratory tools in Wilson (1983), Minnotte and Scott (1993) and in Chaudhuri and Marron (1999). Some parametric studies of the 1872 Hidalgo issue can be found in Basford et al. (1997) or in McLachlan and Peel (2000, Ch. 6).

Taking a subsample of 437 stamps on white wove, Wilson (1983) represented a histogram and the conclusion was that only two kinds of paper were used, the *Papel Sellado* and the *La Croix–Freres*, and that there was not a third kind of paper. Izenman and Sommer (1988) revisited the example considering a more complete collection, with 485 stamps. A histogram with the same parameters as those used by Wilson (1983) (same starting point and bin width) is shown in Figure 2.1 (top–left panel), revealing the same features as those noticed in the original reference. Two groups are also shown by a kernel density estimator, shown in the same plot, considering a Gaussian kernel and a rule of thumb bandwidth (see Wand and Jones, 1995, Section 3.2). However, both approximations (histogram and kernel density estimator) depend heavily on the bin width and bandwidth, respectively. Specifically, the use of an automatic rule for selecting the bandwidth value (focused on the global estimation of the entire density function) does not guarantee an appropriate recovery of the modes. In fact, using another automatic rule as the plug–in bandwidth (Figure 2.1, bottom–left panel), nine modes are observed. A histogram with a smaller bin width is also included in this plot, exhibiting apparently more modes than the initial one.

Given that the exploratory tools did not provide a formal way of determining if there are more than two groups, *Papel Sellado* and *La Croix–Freres*, Izenman and Sommer (1988) decided to employ the multimodality test of Silverman (1981). Note that for this purpose, just FM, SI and the new proposal NP can be employed, and the first two proposals present a poor calibration, as shown in the simulation study. Results from Izenman and Sommer (1988), applying SI with $B = 100$, are shown in Table 2.9 (note that with $B = 500$, different p–values are obtained). For $\alpha = 0.05$, the conclusions are the same, except in the crucial case of testing $H_0 : j \leq 2$, where for $B = 500$, there are no evidences to reject the null hypothesis. These differences may be caused by the approximations implemented by Izenman and Sommer (1988) to obtain the critical bandwidth. Both Efron and Tibshirani (1994, Ch. 16) (using $B = 500$ bootstrap replicates) and Salgado-Ugarte et al. (1998) (employing $B = 600$) obtained similar results to ours. Hence, the null hypothesis must not be rejected when the hypothesis is that the distribution has at most two modes, but it has to be rejected when H_0 is that the distribution has at most six modes. This strange behaviour also

	k	1	2	3	4	5	6	7	8	9
SI	$B = 100$	0	0.04	0.06	0.01	0	0	0.44	0.31	0.82
	$B = 500$	0.006	0.348	0.092	0.016	0.006	0.002	0.494	0.308	0.616
FM		0	0.04	0	0	0	0	0.06	0.01	0.06
NP		0	0.022	0.004	0.506	0.574	0.566	0.376	0.886	0.808

Table 2.9: P–values obtained using different proposals for testing k–modality, with k between 1 and 9. Methods: SI, FM and NP. For SI method, $B = 100$ (first row; Izenman and Sommer, 1988) and $B = 500$.

happens in Izenman and Sommer (1988) analysis, when testing $H_0 : j \leq 3$ and $H_0 : j \leq 6$.

Izenman and Sommer (1988) suggested non–rejecting the null hypothesis the first time that the p–value is higher than 0.4. The consideration of a *flexible* rule for rejecting the null hypothesis is justified by the fluctuations in the p–values of SI and, as Izenman and Sommer (1988) mentioned, by the "conservative" nature of this test. Under this premise, the result when applying SI would be that the null hypothesis is rejected until it is tested $H_0 : j \leq 7$. Hence, Izenman and Sommer (1988) conclude that the number of groups in the 1872 Hidalgo Issue is seven.

As shown in Section 2.2, SI does not present a good calibration and sometimes it can be also anticonservative. It is not surprising that SI behaves differently when testing $H_0 : j \leq k$ for $k = 2, 3$, with respect to the rest of cases until $k = 7$. Since NP has a good calibration behaviour, even with "small" sample sizes, this method is going to be used, first for testing the important case $H_0 : j = 2$ vs. $H_a : j > 2$ and then to figure out how many groups are there in the 1872 Hidalgo Issue.

The computation of the excess mass statistic requires a non–discrete sample and the original data (denoted as $\mathcal{X}$) contained repeated values, the artificial sample $\mathcal{Y} = \mathcal{X} + \mathcal{E}$ will be employed for testing the number of modes, where $\mathcal{E}$ is a sample of size 485 from the $U(-5 \cdot 10^{-4}, 5 \cdot 10^{-4})$ distribution. This modification of the data was also considered by Fisher and Marron (2001). The p–values obtained in their studio (using $B = 200$ bootstrap replicates) are shown in Table 2.9: it is not clear which conclusion has to be made. They mentioned that their results are consistent with the previous studies, detecting 7 modes. But it should be noticed that, as shown in the simulation, FM does not present a good calibration behaviour.

Finally, the p–values obtained with NP are also shown in Table 2.9, with $B = 500$. Similar results can be obtained employing the interval $I = [0.04, 0.15]$ in NP with

known support, as Izenman and Sommer (1988) notice that the thickness of the stamps is always in this interval I. Employing a significance level $\alpha = 0.05$ for testing $H_0 : j = 2$, the null hypothesis is rejected. This null hypothesis is rejected until $k = 4$, and then there is no evidences to reject H_0 employing greater values of k. Then, applying our new procedure, the conclusion is that the number of groups in the 1872 Hidalgo Issue is four.

In order to compare the results obtained by Izenman and Sommer (1988) and the ones derived applying the new proposal, two kernel density estimators, with Gaussian kernel and critical bandwidths h_4 and h_7 are depicted in Figure 2.1 (bottom–right panel). Izenman and Sommer (1988) conclude that seven modes were present, and argued that the stamps could be divided in, first, three groups (pelure paper with mode at 0.072 mm, related with the forged stamps; the medium paper in the point 0.080 mm; and the thick paper at 0.090 mm). Given the efforts made in the new issue in 1872 to avoid forged stamps, it seems quite reasonable to assume that the group associated with the pelure paper had disappeared in this new issue. In that case, the asymmetry in the first mode using h_4 can be attributed to the modifications in the paper made by the manufacturers. Also, this first and asymmetric group, justifies the application of nonparametric techniques to determine the number of groups. In the Section 7 of Izenman and Sommer (1988) and in other references using mixtures of Gaussian densities to model this data (see, for example, McLachlan and Peel, 2000, Ch. 6), it is shown that these parametric techniques have problems in capturing this asymmetry, and they always determine that there are two modes in this first part of the density, one near the point 0.07 mm and another one near 0.08 mm. For the two modes near the points 0.10 and 0.11 mm, both corresponding to stamps produced in 1872. As Izenman and Sommer (1988) noticed, it seems that the stamps of 1872 were printed on two different paper types, one with the same characteristics as the unwatermarked white wove paper used in the 1868 issue, and a second much thicker paper that disappeared completely by the end of 1872. Using this explanation, it seems quite reasonable to think that the two final modes using h_4, corresponds with the medium paper and the thick paper in this second block of stamps produced in 1872. Finally, for the two minor modes appearing near 0.12 and 0.13 mm, when h_7 is used, Izenman and Sommer (1988) do not find an explanation and they mention that probably they could be artefacts of the estimation procedure. This seems to confirm the conclusions obtained with our new procedure. The reason of determining more groups than the four obtained with our proposal, seems to be quite similar to that of the model M20 in the simulation study (Section 2.2). This possible explanation is that the spurious data in the right tail of the last mode are causing the rejection of H_0, when SI is used.

2.4 Seropositivity in malaria eradication

As mentioned in the Introduction, multimodality tests are not only important *per se*, but also as a previous step for applying other procedures. An example where this happens is found when one wants to model and determine a threshold dividing the healthy people and those ones infected with a malaria disease (see Section 1.3.2).

Classical methods to understand the degree of malaria exposure in a population (as, for example, catch the mosquitoes when they attempt to land on the exposed limbs of field workers), can be quite laborious, specially in low transmission populations. For that reason, in the last few years, alternative indicators such as those ones based on antibodies against the malaria antigens are being used. The problem of using such data is that there is not a fixed rule determining from which quantity on an individual is infected (seropositive) or not (seronegative). Even more, in a given infected population, there can be different kinds of seropositive subpopulations. For that reason, in each population it is necessary to analyse each antigen in order to understand the true malaria exposure.

Identifying seropositivity is simplified in studies where there is a training set of individuals with known serological status. In such settings, one can use this information to define a cutoff for seropositivity, e.g., using the sample mean plus three times the estimated standard deviation of the seronegative population (Drakeley et al., 2005) or constructing a mixture model from this prior information (Vounatsou et al., 1998). The problem is that, in general, such training set is not easily available in endemic areas and, therefore, the serological classification of the individuals collected from those areas is more ambiguous. When nothing about the serological status of the individuals is known, a first step, to understand the degree of malaria exposure in a given population, is analyse if there are at least two subpopulations (one seropositive and at least another seronegative). For seeing that, one can test if the number of modes in an antibody sample is equal or greater than one. If the number of modes is equal to one, two things may be happen, that the antibodies against the malaria antigens are similar in both subpopulations or that the malaria is (almost) eliminated from the population. If more than one mode appears, it means that at least one seropositive group is still in the population, as it is expected that the antigens of the seronegative individuals behave in a similar way and show just one peak. In this example, the multimodality tests can be employed to analyse if the malaria disease is still in the population. Then, these tools can be used as a preliminary step to adjust more complicated parametric models in order to catch the (at least) two subpopulation. Also, when the support of the antibody data is known, and a conclusion about the number of modes is obtained, due the results reported in Section B.1, one can use the kernel density estimator (1.1.2), with the critical bandwidth, to estimate the

cutoff between the seronegative and the seropositive subpopulations. A simple approach for doing so is taking the antimode in this density estimation. In that case, the first and principal group is expected to be related with the seronegative individuals and the following groups with the seropositive ones.

With illustrative purposes, the new method for testing multimodality will be applied to two case studies from malaria elimination settings: Aneityum island in Vanuatu archipelago and Chabahar in southeastern Iran. In these two regions, it is known that the Plasmodium falciparum (Pf) and Plasmodium vivax (Pv) parasites, which cause malaria diesase, co–exist. The Aneityum dataset ($n = 517$) is part of a larger cross–sectional survey conducted in 2009 in Tafea province, Vanuatu (Cook et al., 2010). This small island has approximately 800 permanent residents and has been under strong malaria control since 1991 (Chan et al., 2017). According to annual surveillance surveys routinely conducted in the island, there are no reports of malaria infections between 1992 and 2009 with the exception of an Plasmodium vivax occurred in the year of 2002. The Iran dataset comprises a total number of 1479 people of all ages collected from the Chabahar city and surrounding villages in the southeastern part of the country (Zakeri et al., 2016). In both datasets, antibody titers against the antibody Merozoite Surface Protein–1 for Pf or Pv were analysed.

After applying the new procedure for testing unimodality (with $B = 1000$ bootstrap resamples), for the two antigens (PfMSP1 and PvMSP1) and in the two populations (Aneityum and Chabahar), there are no evidences (using a significance level of $\alpha = 0.10$) for rejecting the null hypothesis. The obtained p–values are provided in Table 2.10. Since the null hypothesis of unimodality is not rejected in any case, in Figure 2.4, the kernel density estimation with the Silverman (1981) critical bandwidth for one mode is shown. Observing the smoothed density estimation in the four cases, one may ask if the outlier data far from the zero are altering the results of the test. For that reason, the data study was repeated assuming that the compact support was known. As expected with the results reported in Section 2.2, analysing Table 2.10 is clear that the non–rejection of the null hypothesis is not caused by this factor. Taking this compact support, the kernel density estimation with the critical bandwidth of Hall and York (2001) seems more accurate. The non–rejection of unimodality seems to be caused by the almost complete elimination of the malaria disease in both datasets and in case that it remains seropositive individuals, they are atypical data in the population. Also, observing the shape of the data, one can think about applying a transformation of the data, such us the Box–Cox method. Although in that case, one should be careful with the extracted conclusions, as there is no guarantee that more than one mode in the transformed data imply one than more group in the original data. In any case, applying this transformation, the results are consistent, as the null hypothesis is still not rejected for a significance level of $\alpha = 0.10$ in all the datasets.

Finally, for future analysis in other datasets, if one knows that there are still two groups in the population, a natural question is: where is the threshold dividing the two subpopulations (seronegative and seropositive)? As aforementioned, in that case, the critical bandwidth can be used for that purpose, but one must be careful with the derived conclusions as the bounded support is unknown. Thus, observing Table 2.11, in the case that the critical bandwidth of Silverman (1981) is used, in the four cases, just the highest observation is detected as seropositive. If previous information about the typical values of an antigen in the population are provided, then they can be used for a more accurate study determining the cutoff point and therefore which individuals can be seropositive, as shown in Table 2.11.

Aneityum	PfMSP1	Support	$\mathbb{R}$	$[0, 100]$	$[0, 200]$
		P–value	0.914	0.874	0.881
	PvMSP1	Support	$\mathbb{R}$	$[0, 100]$	$[0, 200]$
		P–value	0.902	0.831	0.871
Chabahar	PfMSP1	Support	$\mathbb{R}$	$[0, 200]$	$[0, 500]$
		P–value	0.884	0.866	0.865
	PvMSP1	Support	$\mathbb{R}$	$[0, 200]$	$[0, 300]$
		P–value	0.504	0.394	0.407

Table 2.10: P–values obtained using the new proposal for testing unimodality in the antigens data ($B = 1000$). In the two last columns, since the support is given, the proposal provided in Section 2.1.3.1 is employed.

			Unimodality			Bimodality								
			Mode			Mode 1			Antimode			Mode 2		
Aneityum	PfMSP1	Support	$\mathbb{R}$	$[0, 100]$	$[0, 200]$	$\mathbb{R}$	$[0, 100]$	$[0, 200]$	$\mathbb{R}$	$[0, 100]$	$[0, 200]$	$\mathbb{R}$	$[0, 100]$	$[0, 200]$
		Location	28.93	21.42	24.46	24.46	20.90	23.86	225.48	90.10	134.95	283.08	99.32	147.29
	PvMSP1	Support	$\mathbb{R}$	$[0, 100]$	$[0, 200]$	$\mathbb{R}$	$[0, 100]$	$[0, 200]$	$\mathbb{R}$	$[0, 100]$	$[0, 200]$	$\mathbb{R}$	$[0, 100]$	$[0, 200]$
		Location	32.01	23.46	27.33	31.64	22.45	24.85	401.40	83.94	136.49	443.75	89.18	158.86
Chabahar	PfMSP1	Support	$\mathbb{R}$	$[0, 200]$	$[0, 500]$	$\mathbb{R}$	$[0, 200]$	$[0, 500]$	$\mathbb{R}$	$[0, 200]$	$[0, 500]$	$\mathbb{R}$	$[0, 200]$	$[0, 500]$
		Location	47.20	31.84	29.76	45.91	29.91	34.46	1505.30	168.18	218.52	2488.26	173.18	277.27
	PvMSP1	Support	$\mathbb{R}$	$[0, 200]$	$[0, 300]$	$\mathbb{R}$	$[0, 200]$	$[0, 300]$	$\mathbb{R}$	$[0, 200]$	$[0, 300]$	$\mathbb{R}$	$[0, 200]$	$[0, 300]$
		Location	38.27	31.13	31.15	34.83	30.93	31.15	673.50	182.20	221.38	797.74	192.72	262.77

Table 2.11: Estimated location of the modes and antimodes in the antigens data.

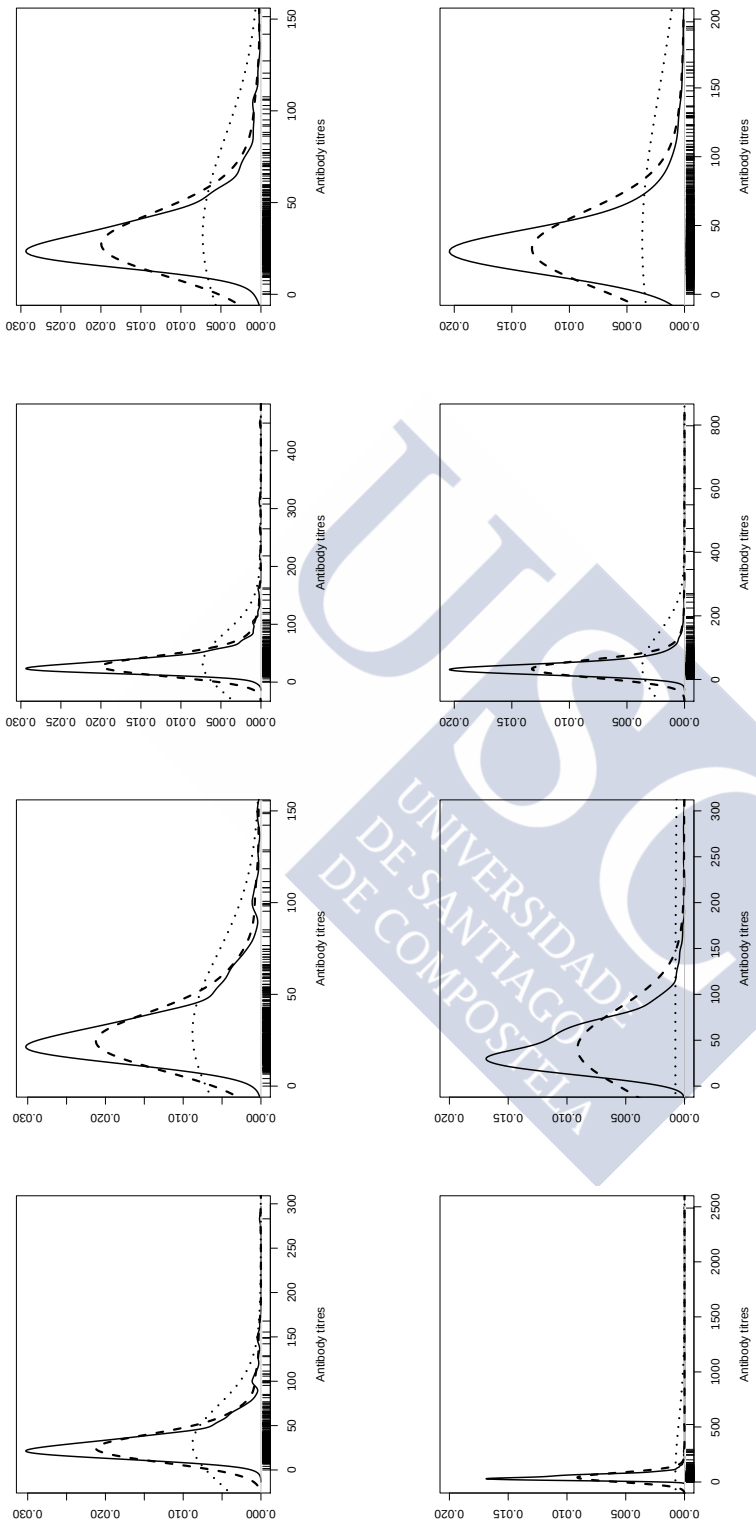

Figure 2.4: Kernel density estimation with Gaussian kernel and critical bandwidth for one mode. Top: Aneityum dataset. Bottom: Chabalar observations. Left: antigen PfMSP1 (first column: in the entire range, second column: in a subinterval). Right: antigen PvMSP1 (third column: in the entire range, forth column: in a subinterval). Dotted lines: Silverman (1981) critical bandwidth. Dashed and solid lines: Hall and York (2001) critical bandwidth. Dashed lines: in the support $[0, 200]$, Aneityum datasets; $[0, 500]$, PfMSP1 in the Chabalar case; $[0, 300]$, PvMSP1 in Chabalar. solid lines: in the support $[0, 100]$, Aneityum datasets; $[0, 200]$, Chabalar samples. The different samples are represented at the bottom of the graphics with ticks.

USC
UNIVERSIDADE
DE SANTIAGO
DE COMPOSTELA

Chapter 3

Mode testing in circular data

One of the principal motivations of this thesis was to asses if there is one season of fires or more than one in each region on the globe (see Section 1.3.3). For that reason, this chapter will be presented just as this problem was tackled step by step. The entire motivation that originated this study is presented in Section 3.1. Given a particular region (cell of size of size 0.5°) on the globe, the first objective will be to test the null hypothesis that there is one season of fires. In the circular case, just Fisher and Marron (2001) provide an approach for testing modality, using the U^2 of Watson as a test statistic, but it seems to be poorly calibrated in practice even for "large" sample sizes. This fact motivates, again, the need of introducing a new method for testing modality in this context. For this purpose, it is employed an analogous version of the excess mass statistic for circular data and the calibration of this test statistic is done adapting the ideas presented in Section 2.1.3 to the circular setting, which is detailed in Section 3.2. To analyse the performance of the new procedure and to compare this method with that one by Fisher and Marron (2001), in terms of empirical size and power, in Section 3.3 a simulation study is provided. As pointed out in Section 3.1, since the objective is to analyse the entire world, not just a 0.5° cell, two new issues appear related with the multiple testing and the spatial relation (in terms of the behaviour of the fires) between the cells. How to address this problematic and the analysis of the number of fire seasons in the entire world is done in Section 3.4.

Contents

3.1 Motivation of the wildfires problem

Vegetation fires are caused by several factors, being their occurrence strongly influenced by climate. In general, in the different parts of the world, the climatological conditions favour the occurrence of fires concentrated around one specific season. Attending to the climatological reasons, in most of the regions over the Tropic of Cancer (approximately 23.5° north latitude) the fires should be produced from May to September, when dry conditions are predominant. In the North Tropic (from 0 to 23.5° north latitude), the fire season should occur from November to March and in the South Tropic (from 23.5 to 0° south latitude), from June to October. In the temperate (under 23.5° south latitude) and in the Mediterranean–like regions of Australia, Africa and South America the season of fires should be produced from October to March (Le Page et al., 2010). Besides the climatic tendency, human activity also influences the wildfire regimes, altering the fire seasonality. Fires are employed for many purposes related to land use practices, with preferential timings. Human fires are used, e.g., for hunting, pasture management, clearing fields for agriculture, eliminating crop and forest harvest residues, manage fuels and reduce wildfire risk or clear brush and drive away wild animals. Analysing in which regions the seasonality due to human burning activities can be separated from fires occurring during climatological seasons helps to explain where fire is used as a land management tool (Magi et al., 2012). As mentioned before, in the fires occurrence a strong seasonal pattern appears causing the fires always in a similar period of the year. This periodicity will motivate to use circular statistics to analyse this kind of data.

The objective of this chapter will be to provide new tools for analysing how many fire seasons can be identified and its application will be seen in each grid cell of size 0.5° in the entire globe. The analysis of the number of seasons, in the different areas

of the world, can be used as an indicator of human activity, studying in which regions more seasons of fires appear than those expected under the appropriate climate. In the forest science literature, several references can be found trying to determine where the fire seasonality have been altered by humans (see, e.g., Korontzi et al., 2006; Le Page et al., 2010; Magi et al., 2012; Benali et al., 2017). These altered seasons present complicate features and they are not easily characterizable. As an example, in the southern part of Africa, where the climatological season of fires is produced around their (southern–hemisphere) winter, the human fires alter the seasonality depending on the activity of each region. Broadly speaking, in the south–western part of this region the peak of human fires is produced during the months of March and April and they are related with the burning of winter wheat crop residues before the new planting season; in the south–western and south–central Africa, the peak of human fires is produced immediately after the climatological season (during the late winter or spring) and it is associated with sugar cane burning prior to harvesting (in the western part) or with the burn of maize residues after harvesting (central part); also since most agricultural land is pasture, it is expected that some fires can be produced to manage these fields and for clearing the fields in order to avoid the burning of trees before the climatological season of fires.

The issue of determining the number of fire seasons can be translated in the statistical problem of testing the number of modes. Taking a parametric perspective, there is a first approach tackling this problem, employing a mixture of two von Mises in Benali et al. (2017). However, the human–altered seasons of fires can be caused by several factors and as the shapes counting the number of human fires show (Korontzi et al., 2006, Figure 5), the underlying structure of the wildfires can be very complex (presenting, e.g., asymmetry), leading this parametric adjustment to a misspecification of the model. This last fact motivates the use of nonparametric techniques for solving this problem. As most of the regions are expected to have only one season of fires related with climatological reasons, in each cell it was tested $H_0 : j = 1$. Then, in general, rejecting H_0 will represent evidence of strong human control over fire seasonality in the region. Nevertheless, as some areas may present more than one peak of fires related with climatological regimes, in a deeper analysis, it should be studied region by region the number of expected climatological seasons. Once this is done, the developed techniques allow the extension for testing $H_0 : j = k$ against $H_1 : j > k$ in these regions (with $k > 1$).

Another issue that will be treated in this chapter arises by the spatial area division. The world map is separated in cells of size $0.5°$ and the nonparametric test must be applied systematically in the different cells. In this context, a FDR procedure is required in order to control the incorrect rejections of the null hypothesis, that is, the identification of unimodal fire regimes as multimodal. It must be also taken

into account that the temporal pattern of fires can be spatially correlated with the neighbouring cells. For seeing in which regions the fires occurrence is expected to be similar, as pointed out in the example of the southern part of Africa, the land use can be employed to somehow reflect the spatial relation between the cells. Then, using this information, an adaptation of the Benjamini and Heller (2007) proposal will be applied in order to correct the FDR accounting for the spatial dependence of the data.

3.2 A new test for circular multimodality

The objective of this section, given a circular random variable Θ, with probability density function f, will be to test if the number of modes of f, namely j, is equal to a given value of $k \in \mathbb{Z}^+$, against if it is greater than k. That is, the statistical problem given in (1.1.3) but referring to the circular setting. For testing H_0, an adaptation of the excess mass can be used again as a test statistic. Being the difference in the circular case, that the sumpremum of the empirical excess mass function (2.1.6) is taken over all families $\{C_m : m = 1, \cdots, k\}$ of disjoint closed arcs, instead of closed intervals, due the periodicity of the circular data.

To calibrate this test statistic, a similar approach to that one given in Section 2.1.3 will be used, assuming that the results of Cheng and Hall (1998) are still valid in the circular setting. In that case, in the regularity conditions, two modifications are needed: first, in (RC3) there are $2k$ turning points; second, since in the circular case there are no tails, the part referring to them in (RC2) can be removed. Then, to construct the circular calibration function, one can start from the kernel density estimation, adapted to the circular case (1.2.7), under the assumption that f has k modes. In that case, since with the wrapped normal kernel, the number of modes of $\hat{f}_\nu$ is always a nondecreasing function of ν (Huckemann et al., 2016), the critical concentration, defined as

$$\nu_k = \max\{\nu : \hat{f}_\nu \text{ has at most } k \text{ modes}\}, \tag{3.2.1}$$

can be used as the concentration parameter for the density estimation (1.2.7). Then, one can follow the steps given in Section 2.1.3, in order to modify the kernel density estimation in its stationary points. In that case, to construct the calibration function g it is necessary to obtain a good estimator of f'' in the turning points of f. This can be done taken the ν minimizing the AMISE expression of $\hat{f}''_\nu$, replacing f for a mixture of M von Mises, in a similar way to the procedure in Oliveira et al. (2012), where this plug–in rule was used for obtaining an estimator of f employing a von

Mises kernel. If ν_{PI} denotes this parameter and $\widehat{\theta}_i$ the modes and antimodes of $\hat{f}_{\nu_k}$, then, in the circular case, d_i is going to be estimated from the sample with

$$\hat{d}_i = \frac{|\hat{f}''_{\nu_{\mathrm{PI}}}(\widehat{\theta}_i)|}{(\hat{f}_{\nu_k}(\widehat{\theta}_i))^3}, \text{ with } i = 1\ldots, 2k. \tag{3.2.2}$$

To construct the circular calibration function again two modifications are needed. First, the density estimator will be modified in a neighbourhood of the estimated modes and antimodes with the J function (2.1.11) using the estimated value of $\hat{d}_i$, obtained in (3.2.2). Second the t saddle points denoted as ζ_p, for $p \in \{1, \ldots, t\}$ will be removed with the L function (2.1.13). In the circular case, the periodicity must be taken into account for both functions. In the definition of the J functions, to provide the constants given in (2.1.12), the modes and antimodes must be sorted, as it was a real sequence, $(0 \leq \widehat{\theta}_1 < \ldots < \widehat{\theta}_{2k} < 2\pi)$ and it is also needed to modify the values $\widehat{\theta}_0 = \widehat{\theta}_{2k} - 2\pi$ and $\widehat{\theta}_{2k+1} = \widehat{\theta}_1 + 2\pi$, then the linear $\widehat{f}_{h_k}$ is replaced by the circular $\widehat{f}_{\nu_k}$ taking into account its periodicity where $\widehat{f}_{\nu_k}(\theta) = \widehat{f}_{\nu_k}(\theta + 2m\pi)$, with $\theta \in [0, 2\pi)$ and $\forall m \in \mathbb{Z}$. A representation of the modification achieved with the J function in the circular case, can be seen in Figure 3.1. Regarding the saddle points, they must be ordered $(0 \leq \zeta_1 < \ldots < \zeta_t < 2\pi)$ and in the definition of the L function (2.1.13), in the circular setting, ξ must be redefined as $\xi = \min\{d(\dot{\theta}, \ddot{\theta}) : \dot{\theta}, \ddot{\theta} \in (\zeta_1, \ldots, \zeta_t) \cup (\mathfrak{r}_1, \mathfrak{s}_1, \ldots, \mathfrak{r}_{2k-1}, \mathfrak{s}_{2k-1})\}$, where d is the circular distance. Once these modifications are done, taking into account the circular structure, given the vector $\boldsymbol{\varsigma} = (\varsigma_1, \ldots, \varsigma_{2k})$, the circular calibration function g for testing $H_0 : j = k$ for a value $\theta \in [0, 2\pi)$, that is $g(\theta; \nu_k, \nu_{\mathrm{PI}}, \boldsymbol{\varsigma})$, is defined as follows

$$\begin{cases} J(\theta; \widehat{\theta}_i, \nu_k, \nu_{\mathrm{PI}}, \varsigma_i) & \text{if } \theta \in [\widehat{\theta}_1, \widehat{\theta}_{2k}] \text{ and } \theta \in (\mathfrak{r}_i, \mathfrak{s}_i) \text{for some } i \in \{1, \ldots, 2k\}, \\ J(\theta; \widehat{\theta}_1, \nu_k, \nu_{\mathrm{PI}}, \varsigma_1) & \text{if } \mathfrak{r}_1 \geq 0 \text{ and } \theta \in (\mathfrak{r}_1, \widehat{\theta}_1) \text{ or if } \mathfrak{r}_1 < 0 \text{ and } \theta \in [0, \widehat{\theta}_1), \\ J(\theta - 2\pi; \widehat{\theta}_1, \nu_k, \nu_{\mathrm{PI}}, \varsigma_1) & \text{if } \mathfrak{r}_1 < 0 \text{ and } \theta \in (\mathfrak{r}_1, 2\pi), \\ J(\theta; \widehat{\theta_{2k}}, \nu_k, \nu_{\mathrm{PI}}, \varsigma_{2k}) & \text{if } \mathfrak{s}_{2k} < 2\pi \text{ and } \theta \in (\widehat{\theta}_{2k}, \mathfrak{s}_{2k}) \text{ or if } \mathfrak{s}_{2k} \geq 2\pi \text{ and } \theta \in (\widehat{\theta}_{2k}, 2\pi), \\ J(\theta + 2\pi; \widehat{\theta_{2k}}, \nu_k, \nu_{\mathrm{PI}}, \varsigma_{2k}) & \text{if } \mathfrak{s}_{2k} \geq 2\pi \text{ and } \theta \in [0, \mathfrak{s}_{2k} - 2\pi), \\ L\left(\theta; z_{(2p-1)}, z_{(2p)}, \nu_k\right) & \text{if } \theta \in [\zeta_1, \zeta_t] \text{ and } \theta \in (z_{(2p-1)}, z_{(2p)}) \text{for some } p \in \{1, \ldots, t\}, \\ L\left(\theta; z_{(1)}, z_{(2)}, \nu_k\right) & \text{if } z_1 \geq 0 \text{ and } \theta \in (z_1, \zeta_1) \text{ or if } z_1 < 0 \text{ and } \theta \in [0, \zeta_1), \\ L\left(\theta - 2\pi; z_{(1)}, z_{(2)}, \nu_k\right) & \text{if } z_1 < 0 \text{ and } \theta \in (z_1, 2\pi), \\ L\left(\theta; z_{(2t-1)}, z_{(2t)}, \nu_k\right) & \text{if } z_{2t} < 2\pi \text{ and } \theta \in (\zeta_t, z_{2t}) \text{ or if } z_{2t} \geq 2\pi \text{ and } \theta \in (\zeta_{2k}, 2\pi), \\ L\left(\theta + 2\pi; z_{(2t-1)}, z_{(2t)}, \nu_k\right) & \text{if } z_{2t} \geq 2\pi \text{ and } \theta \in [0, z_{2t} - 2\pi), \\ \hat{f}_{\nu_k}(\theta) & \text{in other case.} \end{cases} \tag{3.2.3}$$

The same approach with $\boldsymbol{\varsigma}$ as in the Section 2.1.3 is taken to obtain the circular calibration function g. For calibrating the circular excess mass statistic when testing $H_0 : j = k$, a bootstrap procedure is employed. Given the sample $\boldsymbol{\Theta} = (\Theta_1, \ldots, \Theta_n)$, for doing that, B samples $\boldsymbol{\Theta}^{*b}$ $(b = 1, \ldots, B)$ of size n are generated from the distribution associated to $g(\cdot; k)$. Then, if $\Delta^*_{n,k+1}$ is the excess mass statistic obtained from

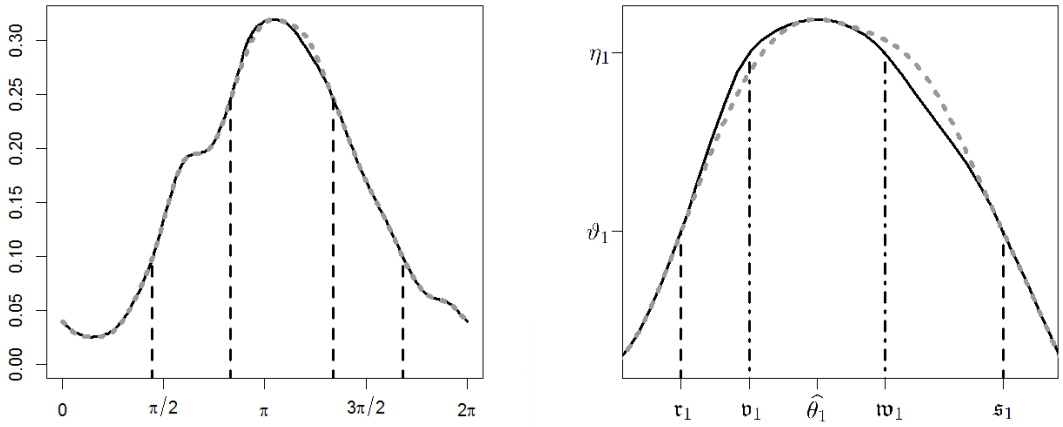

Figure 3.1: Sample of $n = 200$ observations obtained from model MC7 (described in Appendix A). Dotted grey line: $\hat{f}_{\nu_1}$. Solid line: g function. Dashed line: neighbourhood where the functions $J(\cdot; \widehat{\theta}_i, \nu_1, \nu_{\text{PI}}, 0.25)$ are defined, with $i = 1, 2$. Dot–dashed line: neighbourhood where $\mathcal{K}(\cdot; \boldsymbol{\rho}_1, \eta_1)$ is defined. Left: in the support $[0, 2\pi)$. Right: in a neighbourhood of the mode $\widehat{\theta}_1$.

the generated samples, for a significance level α, the null hypothesis will be rejected if $\mathbb{P}(\Delta^*_{n,k+1} \leq \Delta_{n,k+1} | \mathcal{X}) \geq 1 - \alpha$.

Since, in the circular case, an analogous of the critical bandwidth in the bounded support $[0, 2\pi)$ is obtained, the critical concentration defined in (3.2.1), one can think in adapting the ideas of Hall and York (2001) for testing unimodality. In this case, even for the most simple case, $H_0 : j = 1$, observing the simulation results it seems that the calibration of the test statistic is not independent of the underlying distribution of the data, which make sense as in this case the number of turning points of f in $[0, 2\pi)$ is always greater than one and, in this situation, even in the linear case (see Section 2.1.1), the test statistic cannot be directly calibrated.

3.3 Simulation study

The aim of the following simulation study is to analize the performance of the bootstrap procedure to calibrate the circular excess mass statistic using the calibration

function g described in (3.2.3) for obtaining the bootstrap resamples. In this simulation study, it is also compared the level accuracy and power of our new method with the other proposal for testing multimodality for circular data, the one introduced by Fisher and Marron (2001). They propose using the U^2 statistic of Watson (1961) as a test statistic, that is

$$U^2 = n \int_0^{2\pi} \left[F_n(x) - F_0(x) - \int_0^{2\pi} (F_n(y) - F_0(y)) dF_0(y) \right]^2 dF_0(x),$$

estimating F_0 (circular distribution function) employing a kernel distribution estimation with k modes, when the problem of interest is testing $H_0 : j \leq k$. In this simulation study, to estimate F_0, it is used the distribution function associated to $\hat{f}_{\nu_k}$ and its associated distribution is used to generate the bootstrap resamples to calibrate the test statistic.

With these objectives, samples of size $n = 50$, $n = 200$ and $n = 1000$ ($n = 100$ instead of $n = 1000$ in power studies) were drawn from 25 different distribution, ten of them unimodal (MC1–MC10), ten bimodal (MC11–MC20) and five trimodal (MC21–MC25), including unimodal symmetric models, mixtures of them and reflective asymmetric models. Those distributions are described in Appendix A. For each model (MC1–MC25) and sample size, 500 sample realizations were generated. Conditionally on each sample, for each test, 500 resamples of size n were drawn using the calibration function of that specific test. Tables 3.1–3.6 report estimates of the nominal levels $\alpha = 0.01$, $\alpha = 0.05$ and $\alpha = 0.10$.

Tables 3.1 and 3.2 will be used to study the calibration of these tests when the problem of interest is testing $H_0 : j = 1$. Table 3.3 will be employed to analyse the power of the proposals for testing unimodality. Tables 3.4 and 3.5 will be used to study the calibration of these tests when the problem of interest is $H_0 : j = 2$. Table 3.6 will be employed to analyse the power of the proposals for testing bimodality.

Analysing Tables 3.1, 3.2, 3.4 and 3.5, the poor calibration of the Fisher and Marron (2001) proposal can be observed. Even for sample size equal to 1000, sometimes, the percentage of rejections is under the significance level, as in the distributions where unimodality is tested: MC1, MC2, MC4, MC8, MC9 or MC10; or the models in which bimodality is tested: MC12, MC14, MC16 or MC17. It should be also noticed that for models MC3 and MC5 (unimodality) and MC11 and MC20 (bimodality), the percentage of rejections is above α.

Studying the calibration of our new proposal (Tables 3.1, 3.2, 3.4 and 3.5), it provides, in general, a good level accuracy, except for model MC3. Even for small sample sizes ($n = 50$), when the null hypothesis of unimodality is tested, the percentage of rejections is close to the significance level α, except in the commented case

MC3, and also on models: MC1 ($n = 50$), MC4 ($n = 200$), MC8 ($n = 50$), MC9 ($n = 200$) and MC10 ($n = 50$), where the percentage of rejections is slightly below the significance level. In the case of testing bimodality, taking a sample size equal at least to $n = 200$, our proposal seems to calibrate correctly, except for model MC11 where, the percentage of rejections is slightly below α. In the case of the model MC3, the conservative behaviour observed, even for sample size equal to 1000, is corrected when considering a larger sample size ($n = 2000$).

In Tables 3.3 and 3.6, power results are presented. Our new proposal, which seems to be the only one which is well calibrated, appears to have also good power, in terms that the percentage of rejections increases with the sample size. This method detects the clearly rejection of the null hypothesis on the bimodal model MC11 and on the trimodal models MC21 and MC22. This new proposal, also detects the small blips, for example on models MC14, MC15 (bimodal) and MC25 (trimodal), although, in other distributions, it has some troubles, when this small blips represents a low percentage of the data and also the sample size is small, like, for example, in model MC10. In the difficult cases, with almost overlapping peaks, such as on models MC13 (bimodal), MC23 (trimodal) and MC24 (trimodal), when the sample size is small, our method has some difficulties to detect the rejection of unimodality (with $n = 50$ in MC13) and the rejection of bimodality (with $n = 100$ in MC23 and with $n = 50$ in MC24), but the percentage of rejections increases with n.

3.4 Data analysis: detection of fire seasonality

As explained in Section 3.1, determining the number of fire seasons in the different regions of the world has a special importance when the relationships between the climate and the land managment are studied. Using the data described in Section 3.4.1, the goal is to assess, in the study area, if there is one ore more fire seasons. If just one cell is considered, this problem can be tackled employing the new procedure introduced in Section 3.2, as the simulation study in Section 3.3 supports, in the finite–sample case, that the proposal presents a correct behaviour in terms of calibration and power. Since the goal is to analyse the number of fire seasons all across the world, the globe can be divided in a grid and then the proposed procedure can be applied systematically in each cell. As mentioned before, a FDR procedure is required in order to control the incorrect rejections of the null hypothesis. For performing such a correction, the spatial correlation between the p–values computed at different cells must be considered. These two issues will be solved in Section 3.4.2 and the obtained results are provided in Section 3.4.3.

			α	0.01	0.05	0.10
MC1	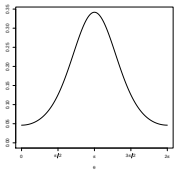	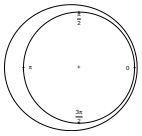			U^2 statistic	
			$n = 50$	0.008(0.008)	0.028(0.014)	0.064(0.021)
			$n = 200$	0.006(0.007)	0.030(0.015)	0.064(0.021)
			$n = 1000$	0.004(0.006)	0.032(0.015)	0.058(0.020)
					Excess mass	
			$n = 50$	0.002(0.004)	0.022(0.013)	0.070(0.022)
			$n = 200$	0.004(0.006)	0.034(0.016)	0.074(0.023)
			$n = 1000$	0.006(0.007)	0.052(0.019)	0.088(0.025)
MC2	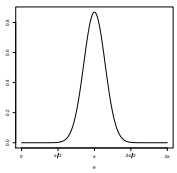	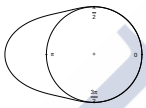			U^2 statistic	
			$n = 50$	0(0)	0.022(0.013)	0.068(0.022)
			$n = 200$	0(0)	0.012(0.010)	0.058(0.020)
			$n = 1000$	0.004(0.006)	0.008(0.008)	0.032(0.015)
					Excess mass	
			$n = 50$	0.012(0.010)	0.054(0.020)	0.094(0.026)
			$n = 200$	0.008(0.008)	0.038(0.017)	0.092(0.025)
			$n = 1000$	0.006(0.007)	0.040(0.017)	0.086(0.025)
MC3	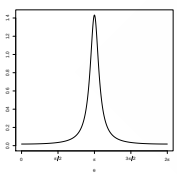	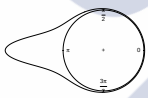			U^2 statistic	
			$n = 50$	0.654(0.042)	0.828(0.033)	0.886(0.028)
			$n = 200$	0.708(0.040)	0.822(0.034)	0.884(0.028)
			$n = 1000$	0.574(0.043)	0.718(0.039)	0.770(0.037)
					Excess mass	
			$n = 50$	0(0)	0.018(0.012)	0.038(0.017)
			$n = 200$	0.002(0.004)	0.012(0.010)	0.024(0.013)
			$n = 1000$	0(0)	0.014(0.010)	0.022(0.013)
MC4	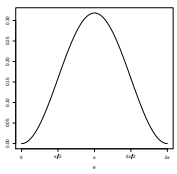	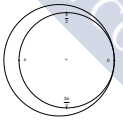			U^2 statistic	
			$n = 50$	0(0)	0.024(0.013)	0.066(0.022)
			$n = 200$	0(0)	0.020(0.012)	0.042(0.018)
			$n = 1000$	0.004(0.006)	0.024(0.013)	0.058(0.020)
					Excess mass	
			$n = 50$	0.006(0.007)	0.044(0.018)	0.114(0.028)
			$n = 200$	0.008(0.008)	0.026(0.014)	0.068(0.022)
			$n = 1000$	0.01(0.008)	0.046(0.018)	0.082(0.024)
MC5	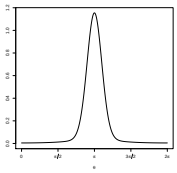	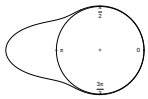			U^2 statistic	
			$n = 50$	0.370(0.042)	0.520(0.044)	0.598(0.043)
			$n = 200$	0.648(0.042)	0.776(0.037)	0.848(0.031)
			$n = 1000$	0.498(0.044)	0.648(0.042)	0.728(0.039)
					Excess mass	
			$n = 50$	0.008(0.008)	0.044(0.018)	0.104(0.027)
			$n = 200$	0.014(0.010)	0.036(0.016)	0.076(0.023)
			$n = 1000$	0.012(0.010)	0.040(0.017)	0.074(0.023)

Table 3.1: Percentages of rejections for testing unimodality, with 500 simulations (1.96 times their estimated standard deviation in parenthesis) and $B = 500$ bootstrap samples.

			α	0.01	0.05	0.10
MC6	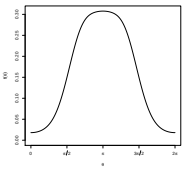	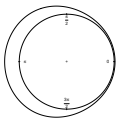			U^2 statistic	
			$n = 50$	0.006(0.007)	0.040(0.017)	0.064(0.021)
			$n = 200$	0.004(0.006)	0.044(0.018)	0.108(0.027)
			$n = 1000$	0.016(0.011)	0.070(0.022)	0.132(0.030)
					Excess mass	
			$n = 50$	0.002(0.004)	0.046(0.018)	0.094(0.026)
			$n = 200$	0.020(0.012)	0.058(0.020)	0.118(0.028)
			$n = 1000$	0.006(0.007)	0.048(0.019)	0.098(0.026)
MC7	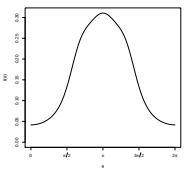	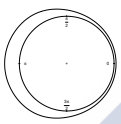			U^2 statistic	
			$n = 50$	0.002(0.004)	0.020(0.012)	0.052(0.019)
			$n = 200$	0.012(0.010)	0.048(0.019)	0.096(0.026)
			$n = 1000$	0.010(0.009)	0.050(0.019)	0.092(0.025)
					Excess mass	
			$n = 50$	0.008(0.008)	0.034(0.016)	0.086(0.025)
			$n = 200$	0.012(0.010)	0.064(0.021)	0.114(0.028)
			$n = 1000$	0.004(0.006)	0.040(0.017)	0.094(0.026)
MC8	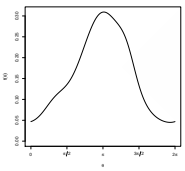	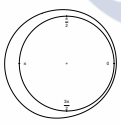			U^2 statistic	
			$n = 50$	0.004(0.006)	0.030(0.015)	0.062(0.021)
			$n = 200$	0.004(0.006)	0.032(0.015)	0.052(0.019)
			$n = 1000$	0.002(0.004)	0.018(0.012)	0.048(0.019)
					Excess mass	
			$n = 50$	0(0)	0.024(0.013)	0.044(0.018)
			$n = 200$	0.006(0.007)	0.044(0.018)	0.100(0.026)
			$n = 1000$	0.010(0.009)	0.048(0.019)	0.100(0.026)
MC9	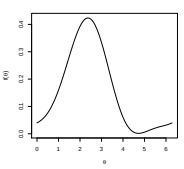	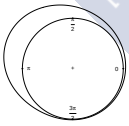			U^2 statistic	
			$n = 50$	0.010(0.009)	0.054(0.020)	0.114(0.028)
			$n = 200$	0.008(0.008)	0.020(0.012)	0.076(0.023)
			$n = 1000$	0(0)	0.010(0.009)	0.044(0.018)
					Excess mass	
			$n = 50$	0.004(0.006)	0.038(0.017)	0.064(0.021)
			$n = 200$	0.008(0.008)	0.030(0.015)	0.062(0.021)
			$n = 1000$	0.004(0.006)	0.036(0.016)	0.084(0.024)
MC10	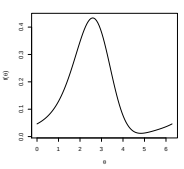	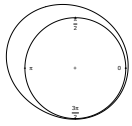			U^2 statistic	
			$n = 50$	0.014(0.010)	0.056(0.020)	0.106(0.027)
			$n = 200$	0.012(0.010)	0.064(0.021)	0.122(0.029)
			$n = 1000$	0.004(0.006)	0.026(0.014)	0.064(0.021)
					Excess mass	
			$n = 50$	0(0)	0.030(0.015)	0.070(0.022)
			$n = 200$	0.012(0.010)	0.038(0.017)	0.082(0.024)
			$n = 1000$	0.002(0.004)	0.038(0.017)	0.086(0.024)

Table 3.2: Percentages of rejections for testing unimodality, with 500 simulations (1.96 times their estimated standard deviation in parenthesis) and $B = 500$ bootstrap samples.

			α	0.01	0.05	0.10
MC11	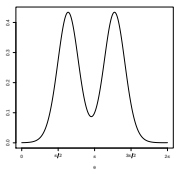	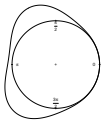			U^2 statistic	
			$n = 50$	0.782(0.036)	0.920(0.024)	0.958(0.018)
			$n = 100$	0.978(0.013)	0.996(0.006)	0.998(0.004)
			$n = 200$	1(0)	1(0)	1(0)
					Excess mass	
			$n = 50$	0.534(0.044)	0.758(0.038)	0.854(0.031)
			$n = 100$	0.914(0.025)	0.968(0.015)	0.984(0.011)
			$n = 200$	0.996(0.006)	1(0)	1(0)
MC12	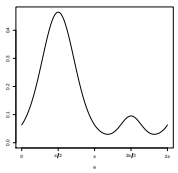	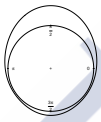			U^2 statistic	
			$n = 50$	0.338(0.041)	0.548(0.044)	0.654(0.042)
			$n = 100$	0.594(0.043)	0.758(0.038)	0.830(0.033)
			$n = 200$	0.880(0.028)	0.940(0.021)	0.956(0.018)
					Excess mass	
			$n = 50$	0.002(0.004)	0.040(0.017)	0.076(0.023)
			$n = 100$	0.010(0.009)	0.058(0.020)	0.112(0.028)
			$n = 200$	0.040(0.017)	0.116(0.028)	0.238(0.037)
MC13	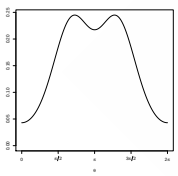	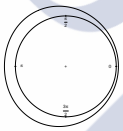			U^2 statistic	
			$n = 50$	0.014(0.010)	0.070(0.022)	0.130(0.029)
			$n = 100$	0.038(0.017)	0.124(0.029)	0.196(0.035)
			$n = 200$	0.066(0.022)	0.170(0.033)	0.246(0.038)
					Excess mass	
			$n = 50$	0.022(0.013)	0.072(0.023)	0.140(0.030)
			$n = 100$	0.032(0.015)	0.084(0.024)	0.156(0.032)
			$n = 200$	0.044(0.018)	0.102(0.027)	0.204(0.035)
MC14	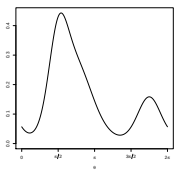	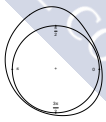			U^2 statistic	
			$n = 50$	0.476(0.044)	0.730(0.039)	0.840(0.032)
			$n = 100$	0.828(0.033)	0.952(0.019)	0.976(0.013)
			$n = 200$	0.990(0.009)	0.998(0.004)	1(0)
					Excess mass	
			$n = 50$	0.044(0.018)	0.164(0.032)	0.284(0.040)
			$n = 100$	0.208(0.036)	0.438(0.043)	0.554(0.044)
			$n = 200$	0.578(0.043)	0.796(0.035)	0.870(0.029)
MC15	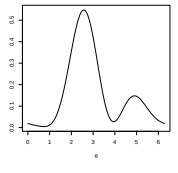	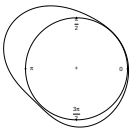			U^2 statistic	
			$n = 50$	0.678(0.041)	0.852(0.031)	0.908(0.025)
			$n = 100$	0.894(0.027)	0.956(0.018)	0.968(0.015)
			$n = 200$	0.986(0.010)	0.996(0.006)	0.998(0.004)
					Excess mass	
			$n = 50$	0.026(0.014)	0.118(0.028)	0.212(0.036)
			$n = 100$	0.128(0.029)	0.318(0.041)	0.452(0.044)
			$n = 200$	0.406(0.043)	0.644(0.042)	0.752(0.038)

Table 3.3: Percentages of rejections for testing unimodality, with 500 simulations (1.96 times their estimated standard deviation in parenthesis) and $B = 500$ bootstrap samples.

			α	0.01	0.05	0.10
MC11	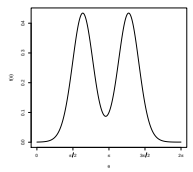	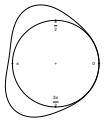			U^2 statistic	
			$n = 50$	0.006(0.007)	0.024(0.013)	0.066(0.022)
			$n = 200$	0.024(0.013)	0.064(0.021)	0.090(0.025)
			$n = 1000$	0.038(0.017)	0.094(0.026)	0.132(0.030)
					Excess mass	
			$n = 50$	0.010(0.009)	0.034(0.016)	0.068(0.022)
			$n = 200$	0.002(0.004)	0.024(0.013)	0.058(0.020)
			$n = 1000$	0(0)	0.038(0.016)	0.074(0.023)
MC12	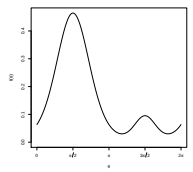	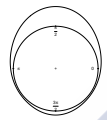			U^2 statistic	
			$n = 50$	0.012(0.010)	0.048(0.019)	0.096(0.026)
			$n = 200$	0.010(0.009)	0.032(0.015)	0.066(0.022)
			$n = 1000$	0(0)	0.004(0.006)	0.022(0.013)
					Excess mass	
			$n = 50$	0.002(0.004)	0.028(0.014)	0.060(0.021)
			$n = 200$	0.006(0.007)	0.030(0.015)	0.082(0.024)
			$n = 1000$	0.004(0.006)	0.040(0.017)	0.088(0.025)
MC13	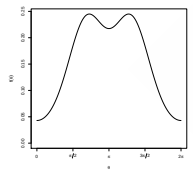	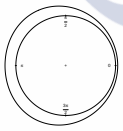			U^2 statistic	
			$n = 50$	0.006(0.007)	0.026(0.014)	0.058(0.020)
			$n = 200$	0.002(0.004)	0.020(0.012)	0.048(0.019)
			$n = 1000$	0.014(0.010)	0.044(0.018)	0.098(0.026)
					Excess mass	
			$n = 50$	0.004(0.006)	0.042(0.018)	0.100(0.026)
			$n = 200$	0.008(0.008)	0.046(0.018)	0.104(0.027)
			$n = 1000$	0.006(0.007)	0.056(0.020)	0.112(0.028)
MC14	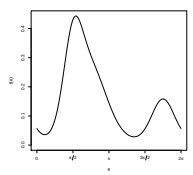	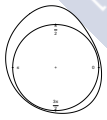			U^2 statistic	
			$n = 50$	0.014(0.010)	0.060(0.021)	0.100(0.026)
			$n = 200$	0.002(0.004)	0.020(0.012)	0.046(0.018)
			$n = 1000$	0(0)	0.012(0.010)	0.030(0.015)
					Excess mass	
			$n = 50$	0.004(0.006)	0.034(0.016)	0.054(0.020)
			$n = 200$	0.004(0.006)	0.036(0.016)	0.086(0.025)
			$n = 1000$	0.002(0.004)	0.034(0.016)	0.082(0.024)
MC15	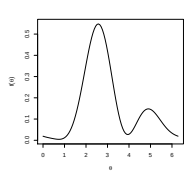	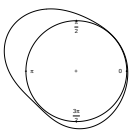			U^2 statistic	
			$n = 50$	0.048(0.019)	0.152(0.031)	0.238(0.037)
			$n = 200$	0.040(0.017)	0.100(0.026)	0.170(0.033)
			$n = 1000$	0.002(0.004)	0.036(0.016)	0.076(0.023)
					Excess mass	
			$n = 50$	0.008(0.008)	0.028(0.014)	0.066(0.022)
			$n = 200$	0.012(0.010)	0.034(0.016)	0.074(0.023)
			$n = 1000$	0.010(0.009)	0.040(0.017)	0.092(0.025)

Table 3.4: Percentages of rejections for testing bimodality, with 500 simulations (1.96 times their estimated standard deviation in parenthesis) and $B = 500$ bootstrap samples.

			α	0.01	0.05	0.10
MC16	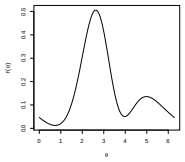	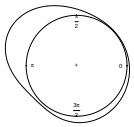			U^2 statistic	
			$n = 50$	0.030(0.015)	0.084(0.024)	0.156(0.032)
			$n = 200$	0.026(0.014)	0.068(0.022)	0.118(0.028)
			$n = 1000$	0.002(0.004)	0.010(0.009)	0.034(0.016)
					Excess mass	
			$n = 50$	0.006(0.007)	0.024(0.013)	0.060(0.021)
			$n = 200$	0.002(0.004)	0.040(0.017)	0.078(0.024)
			$n = 1000$	0.010(0.009)	0.048(0.019)	0.100(0.026)
MC17	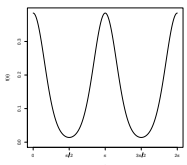	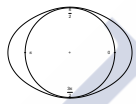			U^2 statistic	
			$n = 50$	0.004(0.006)	0.012(0.010)	0.044(0.018)
			$n = 200$	0(0)	0.012(0.010)	0.030(0.015)
			$n = 1000$	0.002(0.004)	0.022(0.013)	0.052(0.019)
					Excess mass	
			$n = 50$	0.004(0.006)	0.030(0.015)	0.080(0.024)
			$n = 200$	0.004(0.006)	0.036(0.016)	0.066(0.022)
			$n = 1000$	0.002(0.004)	0.032(0.015)	0.072(0.023)
MC18	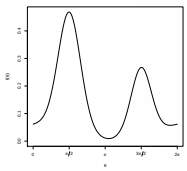	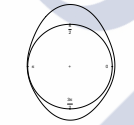			U^2 statistic	
			$n = 50$	0.002(0.004)	0.036(0.016)	0.088(0.025)
			$n = 200$	0.008(0.008)	0.046(0.018)	0.126(0.029)
			$n = 1000$	0.012(0.010)	0.070(0.022)	0.122(0.029)
					Excess mass	
			$n = 50$	0.010(0.009)	0.036(0.016)	0.072(0.023)
			$n = 200$	0.008(0.008)	0.044(0.018)	0.074(0.023)
			$n = 1000$	0.014(0.010)	0.042(0.017)	0.090(0.025)
MC19	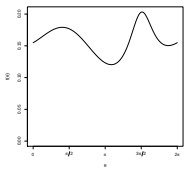	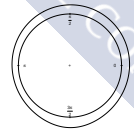			U^2 statistic	
			$n = 50$	0.010(0.009)	0.044(0.018)	0.098(0.026)
			$n = 200$	0.016(0.011)	0.052(0.019)	0.100(0.026)
			$n = 1000$	0.016(0.011)	0.068(0.022)	0.122(0.029)
					Excess mass	
			$n = 50$	0.006(0.007)	0.046(0.018)	0.096(0.026)
			$n = 200$	0.008(0.008)	0.062(0.021)	0.118(0.028)
			$n = 1000$	0.012(0.010)	0.058(0.020)	0.110(0.027)
MC20	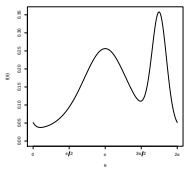	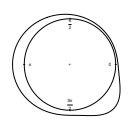			U^2 statistic	
			$n = 50$	0.032(0.015)	0.144(0.031)	0.214(0.036)
			$n = 200$	0.054(0.020)	0.144(0.031)	0.230(0.037)
			$n = 1000$	0.024(0.013)	0.102(0.027)	0.192(0.035)
					Excess mass	
			$n = 50$	0.018(0.012)	0.078(0.024)	0.140(0.030)
			$n = 200$	0.016(0.011)	0.064(0.021)	0.126(0.029)
			$n = 1000$	0.006(0.007)	0.040(0.017)	0.092(0.025)

Table 3.5: Percentages of rejections for testing bimodality, with 500 simulations (1.96 times their estimated standard deviation in parenthesis) and $B = 500$ bootstrap samples.

			α	0.01	0.05	0.10
MC21	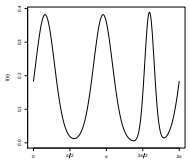	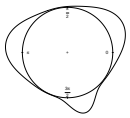			U^2 statistic	
			$n = 50$	0.870(0.029)	0.964(0.016)	0.978(0.013)
			$n = 100$	0.998(0.004)	1(0)	1(0)
			$n = 200$	1(0)	1(0)	1(0)
					Excess mass	
			$n = 50$	0.600(0.043)	0.782(0.036)	0.842(0.032)
			$n = 100$	0.942(0.020)	0.978(0.013)	0.992(0.008)
			$n = 200$	1(0)	1(0)	1(0)
MC22	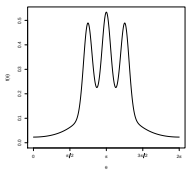	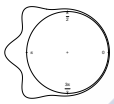			U^2 statistic	
			$n = 50$	0.050(0.019)	0.180(0.034)	0.288(0.040)
			$n = 100$	0.130(0.029)	0.392(0.043)	0.556(0.044)
			$n = 200$	0.344(0.042)	0.700(0.040)	0.852(0.031)
					Excess mass	
			$n = 50$	0.062(0.021)	0.204(0.035)	0.282(0.039)
			$n = 100$	0.184(0.034)	0.380(0.043)	0.506(0.044)
			$n = 200$	0.436(0.043)	0.692(0.040)	0.780(0.036)
MC23	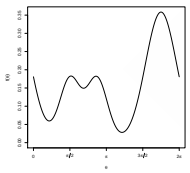	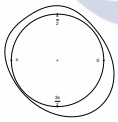			U^2 statistic	
			$n = 50$	0.032(0.015)	0.102(0.027)	0.164(0.032)
			$n = 100$	0.058(0.020)	0.160(0.032)	0.218(0.036)
			$n = 200$	0.060(0.021)	0.188(0.034)	0.262(0.039)
					Excess mass	
			$n = 50$	0.008(0.008)	0.054(0.020)	0.102(0.027)
			$n = 100$	0.018(0.012)	0.066(0.022)	0.124(0.029)
			$n = 200$	0.036(0.016)	0.088(0.025)	0.178(0.034)
MC24	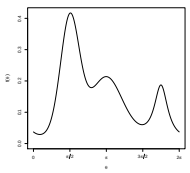	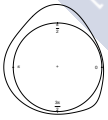			U^2 statistic	
			$n = 50$	0.880(0.028)	0.962(0.017)	0.978(0.013)
			$n = 100$	1(0)	1(0)	1(0)
			$n = 200$	1(0)	1(0)	1(0)
					Excess mass	
			$n = 50$	0.002(0.004)	0.058(0.020)	0.108(0.027)
			$n = 100$	0.022(0.013)	0.078(0.024)	0.154(0.032)
			$n = 200$	0.036(0.016)	0.126(0.029)	0.200(0.035)
MC25	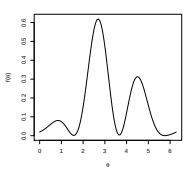	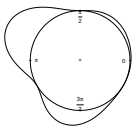			U^2 statistic	
			$n = 50$	0.782(0.036)	0.918(0.024)	0.950(0.019)
			$n = 100$	0.980(0.012)	1(0)	1(0)
			$n = 200$	0.998(0.004)	1(0)	1(0)
					Excess mass	
			$n = 50$	0.030(0.015)	0.160(0.032)	0.244(0.038)
			$n = 100$	0.154(0.032)	0.340(0.042)	0.448(0.044)
			$n = 200$	0.456(0.044)	0.660(0.042)	0.746(0.038)

Table 3.6: Percentages of rejections for testing bimodality, with 500 simulations (1.96 times their estimated standard deviation in parenthesis) and $B = 500$ bootstrap samples.

3.4.1 Fires dataset

The studied dataset contains the location and date of all active fires detected by the MODIS from 10 July 2002 to 9 July 2012. The MODIS algorithm identifies pixels where one or more fires are actively burning at the time of satellite overpass, based on the contrasting responses of the middle-infrared and longwave infrared bands in areas containing hot targets. Cloud and water pixels are previously excluded from analysis using multiple numerical thresholds on visible and near–infrared reflectance, and thermal infrared temperature values. The size of the smallest flaming fire having at least a 50% chance of being detected by the MODIS algorithm, under both ideal daytime and nighttime conditions is approximately 100 m^2. For further details about the MODIS active fire detection algorithm, see Giglio et al. (2003) or Oom and Pereira (2013).

MODIS data are provided in a discretized scale, so in order to apply the testing procedure, it is necessary to recover the continuous underlying structure. For that purpose, denote by $(X_1, \ldots, X_n)$ the days of the year when the n recorded fires occurred, with $X_i \in \{1, \ldots, 366\}$. The dataset used for the study of the number of fire seasons is the following

$$\Theta_i = 2\pi(X_i + \mathcal{E}_i)/366; \text{ with } i = 1, \ldots n,$$

being $\mathcal{E}_i$ generated from the uniform distribution $U(-1, 0)$. This means that it is assumed that fires were produced at any time of the day. Provided that data are not repeated, as this can considerably alter the test statistic, other ways of modifying the data can be considered, but, in general, this perturbation does not show relevant impacts in the results.

Once this modification is done, the analysed area is divided in grid cells of size $0.5°$. Then, from the resulting $(360 \cdot 720)$ cells, those ones with low fire incidence, i.e., cells having fewer than ten fires in more than 7 out of ten years, will not be considered in the study. This leaves 23,987 grid cells in the area, each one having between 37 and 20,120 fires. A map including the world map with a summary of fire counts is included in Figure 3.2.

3.4.2 Spatial False Discovered Rate

As it was mentioned, removing the low fire incidence cells, the fires sample $\{\Theta_i; i = 1, \ldots, 4.17 \cdot 10^7\}$ is organized in $2.4 \cdot 10^4$ cells. Hence, the proposed testing procedure (see Section 3.2) will be applied systematically over these groups. It is clear then

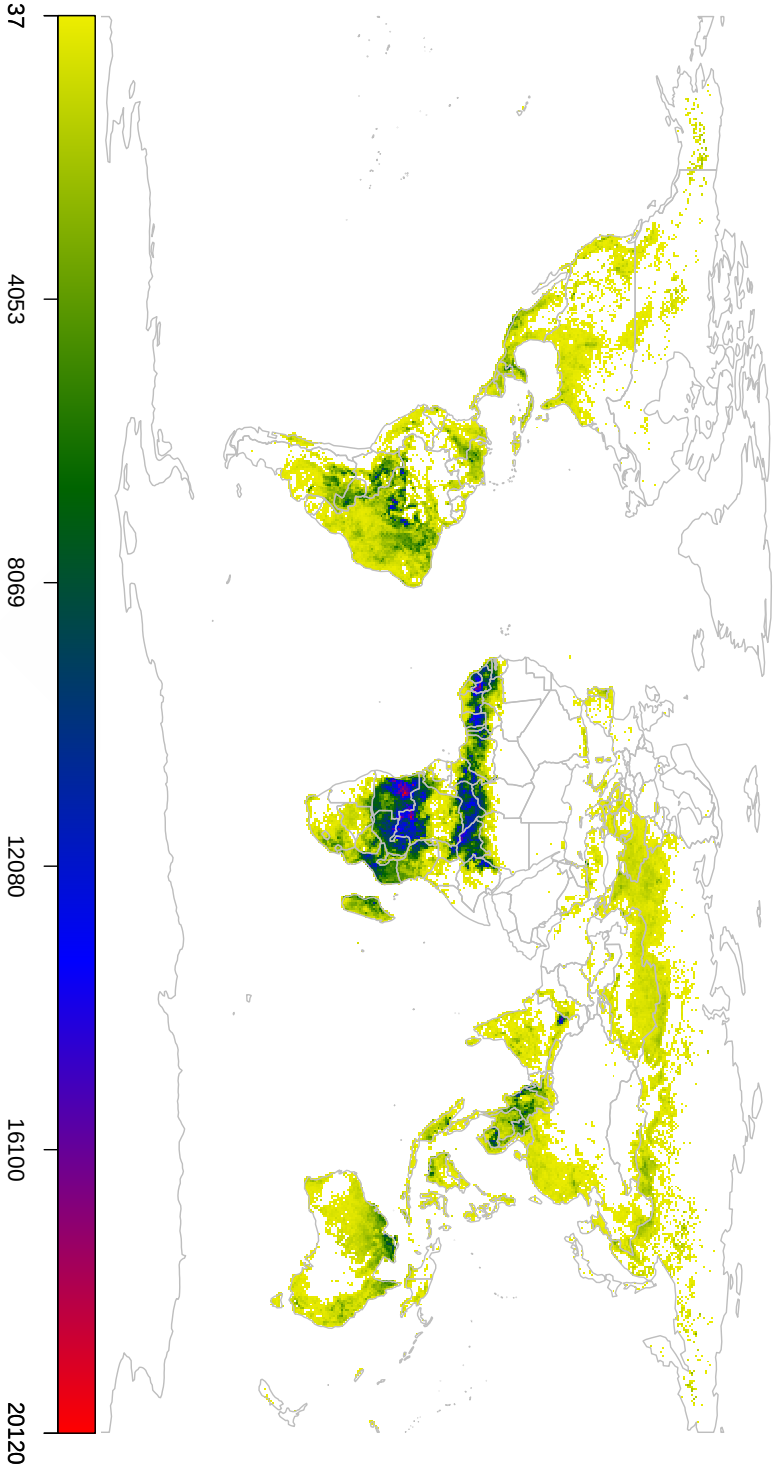

Figure 3.2: Number of fires detected by the MODIS in the different cells of the world from from 10 July 2002 to 9 July 2012 (in colour, as reflected in the bottom legend). In white, cells with low fire incidence.

that a FDR correction must be applied. In addition, the provided separation in grid cells is not necessarily designed for producing "independent" areas in the sense that occurrence of fires in a cell may not be independent of occurrence in the neighbouring ones. So the spatial dependence must be taken into account for correcting the FDR procedure. This will be done following the ideas by Benjamini and Heller (2007) (procedure 3), with some modifications. Their method allows to control the FDR accounting for the spatial dependence of the data, employing prior information about the aggregation of different locations (where the size and shape of the different groups do not need to be equal). This is the case in our study, as it is expected that the behaviour of the fires will be similar in regions where the land is used for the same purpose. Once the aggregation is done, Benjamini and Heller (2007) propose testing first on those large units, allowing to have a single p–value for the large area. Then, if the null hypothesis is rejected, it controls the dependence of the aggregate and the p–values in the inside locations, in order to correct them in the multiple testing problem and properly detect the rejected locations.

The method employed can be outlined as follows: in an initial step (Step 1), the testing procedure is applied, locally, to each cell, obtaining the corresponding p–value. Secondly (Step 2), *fire patches* by land cover are defined in order to create groups of cells that are related. Finally (Step 3), a hierarchical testing procedure (similar to that one of Benjamini and Heller, 2007) is applied. This final step consists in, first, deciding in which of the previous patches the null hypothesis is rejected (patch testing; Step 3a) and, secondly, within each rejected patch, determining in which of its cells H_0 is rejected (trimming procedure; Step 3b). Further details in the specific problem and solution are provided below.

Step 1. Local application of the test. In each of the $2.4 \cdot 10^4$ grid cells, the method proposed in Section 3.2 will be used (with $B = 5000$ bootstrap replicates) for obtaining the corresponding p–values when it is tested if there is one season of fires or more.

Step 2. Fire patches. To define the fire patches, a rule for determining the cells expected to display "similar" fire season modality patterns must be established. The fire patches were constructed using the information of the land cover data provided by the European Space Agency Climate Change Initiative project (*Land Cover version 1.6.1*, data from 2008 to 2012[1]), which describes the physical material at the surface of the earth, including various types of vegetation, bare rock and soil, water, snow and ice, and artificial surfaces. Its construction is divided in two steps. First, since the original land cover database is divided in pixels of size 300 meters is necessary to define the principal land cover of the 0.5° cell. Second, the land cover cells are

[1]Available in `http://www.esa-landcover-cci.org`

grouped into homogeneous patches, where it is expected that they will display similar fire season modality patterns.

Then, the first objective is to decide which is the principal land cover in a given cell. For that purpose the original labels of the 300m–pixel, represented in Figure 3.3 (top–left), are divided in six classes: *cropland* (rainfed; irrigated or post–flooding), *forest* (tree cover; broadleaved, needleleaved or mixed leaf type; evergreen or deciduous; closed or open), *shrubland*, *grassland* (herbaceous cover, grassland), *lichens and mosses* and *low vegetation* (sparse vegetation; tree cover, flooded; urban areas; bare areas; water bodies; permanent snow and ice). Also, some of the 300m–pixels have a mixed label, e. g., "Mosaic tree and shrub ($> 50\%$) / herbaceous cover ($< 50\%$)", in that case the 75% of the pixel is catalogued as the principal use and the 25% of the pixel is catalogued as the secondary use. Also, if the principal or the secondary use belong to a mixed label (in the last example the principal use is a mix of forest and shrubland), then its percentage is divided according to the surrounding (180×180) 300m–pixels in the 0.5°–cell. In the last example if $20,000$ (out of 180×180) surrounding pixels are forest and $10,000$ shrubland, then the $75 \cdot 20,000/30,000 = 50\%$ of the pixel is catalogued as forest and the 25% as shrubland. Once the (180×180) 300m–pixels inside a given 0.5°–cell are catalogued, if at least the 60% of the land cover is of one type, then the cell is labelled like most pixels. If both the principal and secondary land cover are greater than 30% and lower than 60% (and not the principal nor the secondary land covers are low vegetation), then the cell is catalogued with a mixed label. Otherwise, the cell is labelled as *mixed vegetation*. This classification leaves the 12 land covers represented in Figure 3.3 (top–right) for the north–western part of the Iberian Peninsula and in Figure 3.4 for the entire world.

Now, in order to create the homogeneous land cover patches, given the grid cells surrounding a selected cell, if at least one of them has the same label as the selected one, then both cells will be considered in the same patch. Fire patches are created as follows: fix a cell and consider the eight surrounding cells; check which surrounding cells belong to the same class as the focal cell. All of them will be part of the same patch. This is shown in Figure 3.3 (bottom–right). Taking as a reference the central cell, it is going to form part of the same fire patch as the red cells in the bottom. The rest of the cells are going to be outside the patch: the blue ones have a different classification and the dark grey cell is outside of the studied area. Then, part of the border of this patch (green line) is determined by these non–red cells. This procedure leaves 4177 different fire patches. A representation of these patches for the north–west of the Iberian Peninsula is given in Figure 3.3 (bottom–left).

Step 3. Hierarchical testing procedure. Some notation is required for this part. Let $\mathfrak{j} = 1, \ldots, J$ be the different patches created in Step 2, $\mathfrak{l} = 1, \ldots, L_{\mathfrak{j}}$ be the

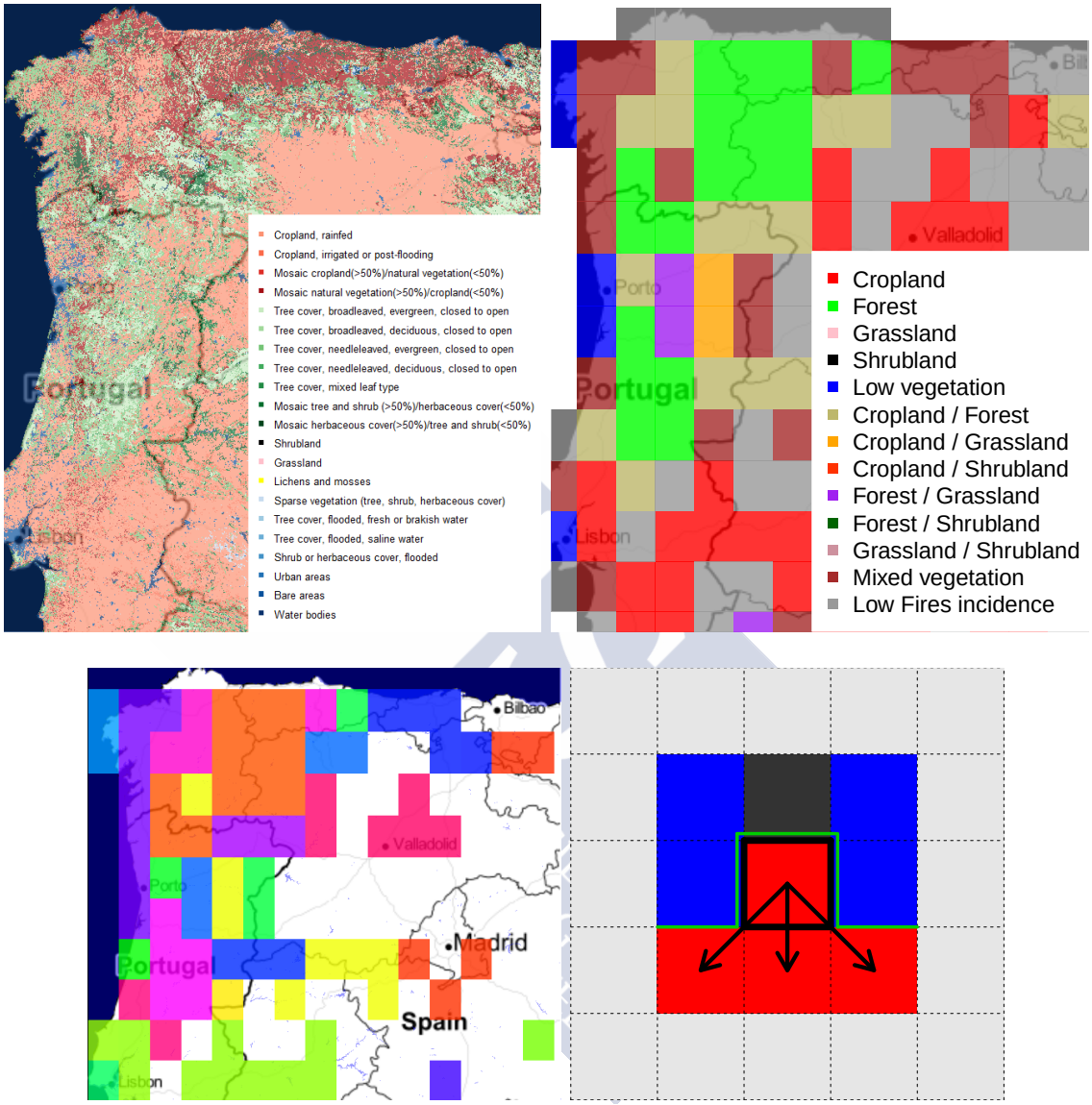

Figure 3.3: Top and bottom–left: north–west of the Iberian Peninsula (the background map was obtained with OpenStreetMap contributors, 2017). Top: land cover as specified in the legend. Top–left: original land cover database (300m–pixel). Top right: principal land cover in each 0.5° cell. Bottom–left: each translucent colour represents a fire patch; in white, cells with low fire incidence. Bottom right: construction of the fire patch; the cells are separated by dashed lines; in the middle (black square): focus cell; red and blue: different land uses in the cells; grey: not considered cells; dark grey: region outside the studied area; the arrows indicate cells to be aggregated into a homogeneous land cover patch; green lines: part of the border of the patch.

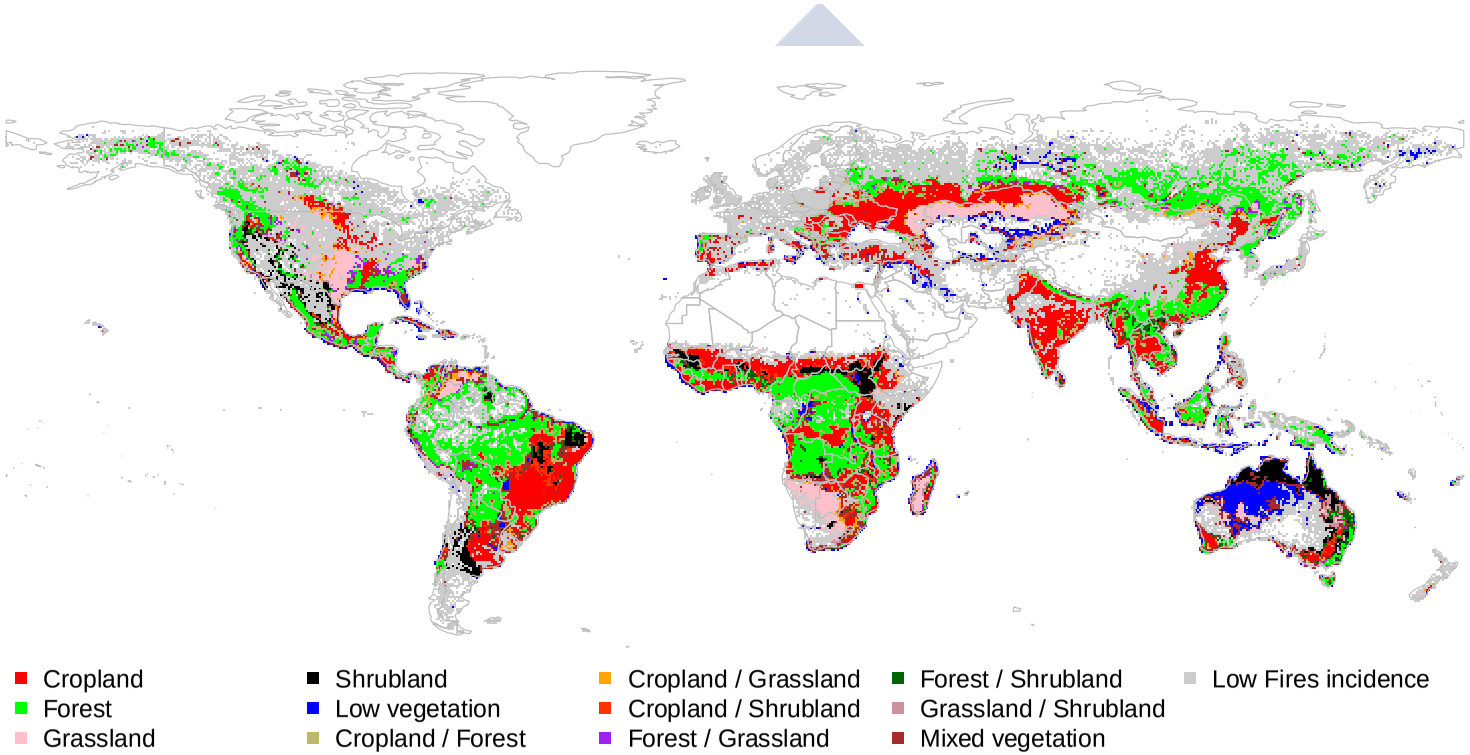

Figure 3.4: Land cover of each 0.5° cell of the world and low fire incidence cells (in colour, as reflected in the bottom legend). In white, cells with no fires.

cells in the patch $\mathfrak{j}$ and $\tilde{p}_{\mathfrak{l}\mathfrak{j}}$ the p–value obtained in Step 1 for the cell $\mathfrak{l}$ in the patch $\mathfrak{j}$. Then, $z_{\mathfrak{l}\mathfrak{j}} = \Phi^{-1}(1 - \tilde{p}_{\mathfrak{l}\mathfrak{j}})$ will be the corresponding z–score for the cell $\mathfrak{l}$ in patch $\mathfrak{j}$, where Φ is the cumulative distribution of a standard normal distribution. Note that since a bootstrap procedure is used to approximate the p–values $\tilde{p}_{\mathfrak{l}\mathfrak{j}}$, they can be equal to 0 or 1 and, in that case, the z–score is non–finite. In order to correct that, if $\tilde{p}_{\mathfrak{l}\mathfrak{j}}$ is equal to 0, following the ideas of Jeffreys (1946) prior, this p–value is replaced by a random value from the distribution $\text{Beta}(1/2, B + 1/2)$ and if it is equal to one then a random value from $\text{Beta}(B + 1/2, 1/2)$ is taken. Once the z–scores for each cell in the different patches are calculated, a hierarchical method will be employed. The testing procedure is divided in two steps: first it tests at significance level α_c in which fire patches the null hypothesis can be rejected (Step 3a) and then tests H_0 at level α_r the cells within the rejected patches (Step 3b).

Step 3a. Patch testing. In this stage, fire patches where the null hypothesis is rejected are identified. This step consists in computing a global p–value for each patch and then, since each patch has a different number of cells, the weighted FDR procedure of Benjamini and Hochberg (1997) at level α_c will be applied in order to correct for multiple testing. The global p–value of the patch $\mathfrak{j}$ is calculated as $\tilde{\Phi}(\bar{Z}_{\mathfrak{j}}/\hat{\sigma}_{\bar{Z}_{\mathfrak{j}}})$, that is, the right tail probability of the standard normal distribution calculated in the standardized z–score average of the cells in a fire patch. More precisely:

1. In each patch $\mathfrak{j}$, with $\mathfrak{j} \in \{1, \ldots, J\}$, calculate the z–score average: $\bar{Z}_{\mathfrak{j}} = (1/L_{\mathfrak{j}}) \sum_{\mathfrak{l}=1}^{L_{\mathfrak{j}}} z_{\mathfrak{l}\mathfrak{j}}$, where $z_{\mathfrak{l}\mathfrak{j}}$ are the z–scores defined above.

2. Compute its standard error: $\hat{\sigma}_{\bar{Z}_{\mathfrak{j}}} = (\hat{\sigma}_{\mathfrak{j}}/L_{\mathfrak{j}}) \sqrt{L_{\mathfrak{j}} + 2 \sum_{\mathfrak{l}=1}^{L_{\mathfrak{j}}} \sum_{\mathfrak{m}=1}^{\mathfrak{l}-1} \hat{\rho}^{\mathfrak{j}}_{\mathfrak{l},\mathfrak{m}}}$, where $\hat{\rho}^{\mathfrak{j}}_{\mathfrak{l},\mathfrak{m}} = 1 - \hat{\gamma}(s_{\mathfrak{l}\mathfrak{j}} - s_{\mathfrak{m}\mathfrak{j}})/\hat{\sigma}_{\mathfrak{j}}$ is the estimated correlation between cell $\mathfrak{l}$ and $\mathfrak{m}$ in the patch $\mathfrak{j}$, $\hat{\gamma}(s_{\mathfrak{l}\mathfrak{j}} - s_{\mathfrak{m}\mathfrak{j}})$ is an estimation of the semivariogram evaluated at the distance (of the centroids in the map) between cells $\mathfrak{l}$ and $\mathfrak{m}$, within patch $\mathfrak{j}$, and $\hat{\sigma}_{\mathfrak{j}}$ the estimated variance of the cells in patch $\mathfrak{j}$. The semivariogram estimator is obtained by (weighted) least squares on an exponential family, in order to ensure that such an estimator is indeed a valid semivariogram (something that may be not satisfied by nonparametric estimators) and to control the parameters of interest. Specifically, in an exponential family, two parameters drive the behaviour of the spatial covariance: the point variance and the range. Hence, the estimated variance is obtained from this parametric procedure. It should be noted that least squares procedures for variogram estimation require the use of a nonpametric pilot estimator. In this case, the robust version of the empirical variogram was used (see Cressie, 1993, Ch.2).

3. The weighted FDR procedure at level α_c is applied on the p–values $\breve{p}_{\mathfrak{j}} = \tilde{\Phi}(\bar{Z}_{\mathfrak{j}}/\hat{\sigma}_{\bar{Z}_{\mathfrak{j}}})$, being the weight proportional to the size of the patches. Given

the ordered p–values $\breve{p}_{(1)} \leq \ldots \leq \breve{p}_{(J)}$, unimodality is rejected in the $\mathfrak{k}$ patches with the smallest p–values, being $\mathfrak{k} = \max\{\upsilon : \breve{p}_{(\upsilon)} \leq (\sum_{\mathfrak{j}=1}^{\upsilon} L_{(\mathfrak{j})} / \sum_{\mathfrak{j}=1}^{J} L_{(\mathfrak{j})})\alpha_c\}$ and $L_{(\mathfrak{j})}$ the number of cells in the fire patch associated with $\breve{p}_{(\mathfrak{j})}$.

Step 3b. Trimming procedure. Once a decision about which patches are candidates for rejecting the null hypothesis (and hence exhibiting a multimodal fire pattern), specific cells where this rejection holds are identified. It should be noted that the cell test statistic is correlated with the test statistic at the patch level. This means that a FDR correction cannot be directly applied over all the cells belonging to the same patch and a correction is proposed by Benjamini and Hochberg (1997). First, calculate the conditional p–value of a cell within a patch that was rejected, $\hat{p}_{\mathfrak{l}\mathfrak{j}}$. Then, over these p–values, apply the two–stage procedure introduced by Benjamini et al. (2006), at level α_r, to enhance the power. This last method in its first stage consists in estimating the sum of weights of null cells, using for that purpose the classical FDR procedure at level α_r and then using this quantity in a second stage to determine the number of rejected cells within the patch. To be more precise and summarize Step 3b, the following steps are detailed:

4. Calculate the conditional p–value of each cell $\mathfrak{l}$ within the patch that was rejected $\mathfrak{j}$ ($\hat{p}_{\mathfrak{l}\mathfrak{j}}$). P–values can be estimated as follows:

$$\hat{p}_{\mathfrak{l}\mathfrak{j}} = \int_{z_{\mathfrak{l}\mathfrak{j}}}^{\infty} \left(\frac{\hat{J}_0}{J} \tilde{\Phi} \left(\frac{\tilde{\Phi}^{-1}(u_1) - \hat{\rho}_{\mathfrak{l}\mathfrak{j}} u}{\sqrt{1 - \hat{\rho}_{\mathfrak{l}\mathfrak{j}}^2}} \right) + \right.$$
$$\left. + \left(1 - \frac{\hat{J}_0}{J}\right) \tilde{\Phi} \left(\frac{\tilde{\Phi}^{-1}(u_1) - \hat{\rho}_{\mathfrak{l}\mathfrak{j}} u - \hat{\mu}_{\mathfrak{j}}}{\sqrt{1 - \hat{\rho}_{\mathfrak{l}\mathfrak{j}}^2}} \right) \right) \phi(u) du \cdot$$
$$\cdot \left(\frac{\hat{J}_0}{J} u_1 + \left(1 - \frac{\hat{J}_0}{J}\right) \tilde{\Phi} \left(\tilde{\Phi}^{-1}(u_1) - \hat{\mu}_{\mathfrak{j}} \right) \right)^{-1},$$

being ϕ a standard normal density and noting that

(a) $u_1 = (\sum_{\mathfrak{j}=1}^{\mathfrak{k}} L_{(\mathfrak{j})} / \sum_{\mathfrak{j}=1}^{J} L_{(\mathfrak{j})})\alpha_c$ is the cutoff point of the largest p–value rejected in Step 3a.

(b) $\hat{J}_0 = (J - \mathfrak{k})/(1 - \alpha_c)$ is the estimated sum of weights of null patches.

(c) $\hat{\mu}_{\mathfrak{j}} = ((\sum_{\mathfrak{j}=1}^{J} \sum_{\mathfrak{l}=1}^{L_{\mathfrak{j}}} z_{\mathfrak{l}\mathfrak{j}}) / (\sum_{\mathfrak{j}=1}^{J} L_{\mathfrak{j}})) / \hat{\sigma}_{\bar{Z}_{\mathfrak{j}}}$ is the estimation of the standardized expectation of the patch test statistic under the alternative.

(d) $\hat{\rho}_{\mathfrak{l}\mathfrak{j}} = (1+\sum_{\mathfrak{m}=1,\mathfrak{m}\neq\mathfrak{l}}^{L_\mathfrak{j}} \hat{\rho}^{\mathfrak{j}}_{\mathfrak{l},\mathfrak{m}})\hat{\sigma}_\mathfrak{j}/(L_\mathfrak{j}\hat{\sigma}_{\bar{Z}_\mathfrak{j}})$ is the estimated correlation between the z-score in a given cell and the average z-score of the patch.

5. Given these $L_\mathfrak{j}$ p–values in the patch $\mathfrak{j}$, apply a two–stage procedure at level α_r:

   (a) Apply the classic FDR procedure, at level $\alpha'_r = \alpha_r/(1+\alpha_r)$. Given the ordered p–values $\hat{p}_{(1)\mathfrak{j}} \leq \ldots \leq \hat{p}_{(L_\mathfrak{j})\mathfrak{j}}$, let $\mathfrak{k}_{1\mathfrak{j}} = \max\{\upsilon : \hat{p}_{(\upsilon)\mathfrak{j}} \leq (\upsilon/L_\mathfrak{j})\alpha'_r\}$.

   (b) Apply again the classic FDR procedure at level α'_r, being in this case the sum of weights of null cells: $\hat{J}_{0\mathfrak{j}} = L_\mathfrak{j} - \mathfrak{k}_{1\mathfrak{j}}$. Reject the unimodality in the $\mathfrak{k}_{2\mathfrak{j}}$ cells with the smallest p–values, being $\mathfrak{k}_{2\mathfrak{j}} = \max\{\upsilon : \hat{p}_{(\upsilon)\mathfrak{j}} \leq (\upsilon/\hat{J}_{0\mathfrak{j}})\alpha'_r\}$.

3.4.3 Results

Employing our new proposal for testing the number of modes and correcting the FDR accounting for the spatial dependence of the data, bellow is summarized how it is applied to the wildfires dataset described in Section 3.4.1. As a first step, the p–values applying the new procedure provided in Section 3.2 (with $B = 5000$ bootstrap replicates) were computed in all the cells of the world. In a second step, the different fires patches were created using the land cover database. Finally, the hierarchical testing procedure was applied. First, to determine in which of the previously created patches the null hypothesis is rejected at significance level $\alpha_c = 0.01$. Second, within the rejected patches, it was determined which cells can be rejected at the trimming significance level $\alpha_r = 0.01$. The rejected cells are shown in green colour in Figure 3.5.

The first main conclusion, when the modality map is observed, is that in almost all the globe, where the wildfires are present, the pattern is clearly multimodal, suggesting the prevalence of fire use as a land management tool at global scale. Although a second step indicating which is the "relevance" of each mode is needed, this map leads to the important conclusion that human are altering the fire seasonality all around the world. Although most of the non–rejected regions are scattered, one can see some areas with high–concentrated non–rejected cells. Looking at these regions, one should be careful about the conclusions related with the agricultural activity in the areas where the humans are not altering the fire seasonality. That is the case of the west coast of India, one of the largest areas with non–rejected cells, where a high number of millet crops can be found (see Leff et al., 2004), or some parts in the Central and Northern Hemisphere South America and the Indonesia islands (such us Java), as they are large producers of coffee.

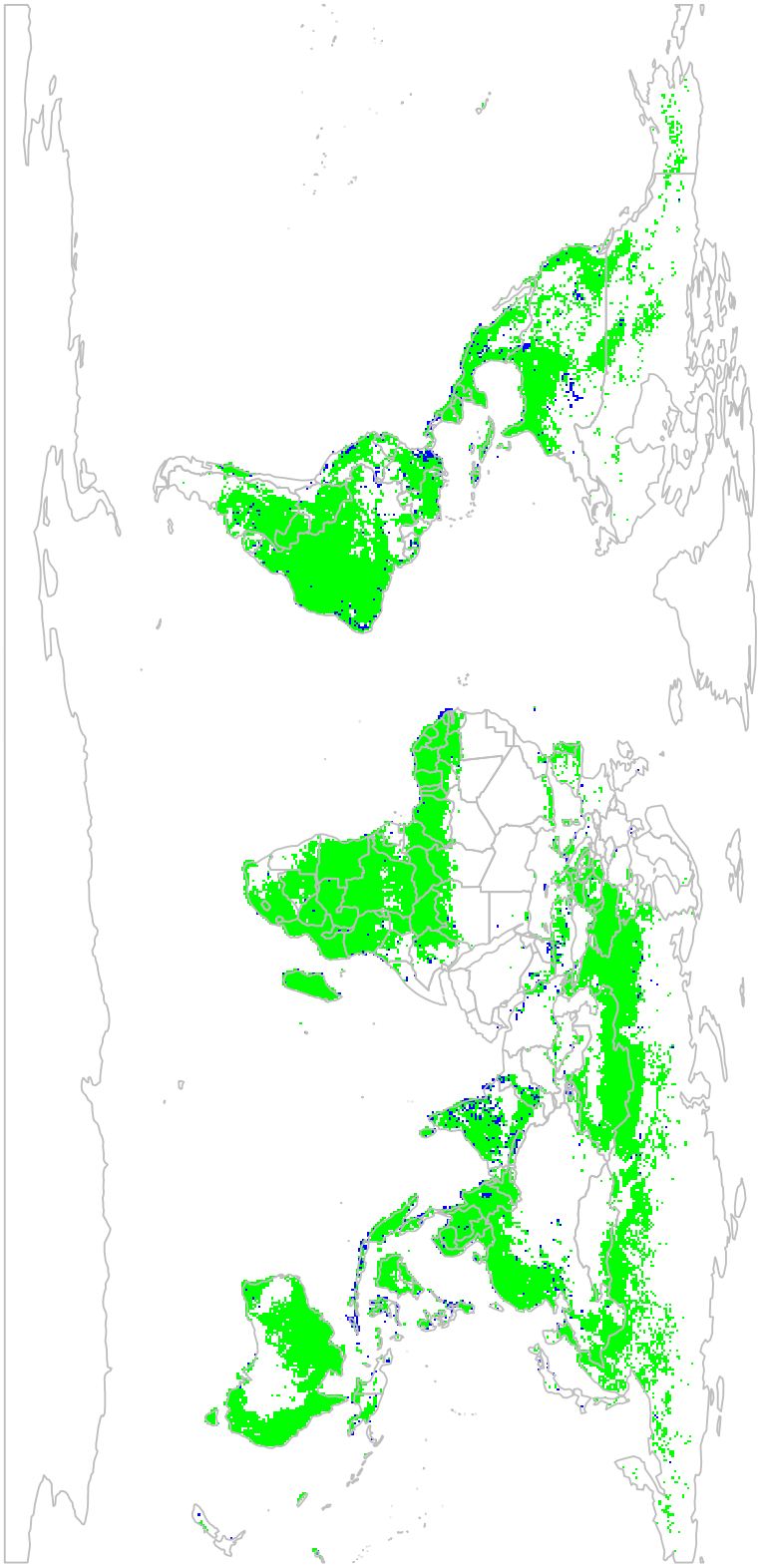

Figure 3.5: Results after applying the procedure described in Section 3.4.2, with $\alpha_c = 0.01$ and $\alpha_r = 0.01$, in the world, divided in grids of size 0.5°. In green: cells where H_0 is rejected. In blue: cells where there is no evidence to reject H_0. In white, cells with low fire incidence.

Chapter 4

Symmetry testing in circular data

Once a conclusion about the number of modes is obtained, symmetry, or more precisely reflective symmetry, is another of these most frequently encountered simplifying assumptions. When dealing with real data it is important to see if the distribution of the sample is equal at the left and the right handsides of some central direction as it may help for a better understanding. In addition, when one is trying to figure out the underlying model of the data, the rejection of this hypothesis often leads to the subsequent exploration of models with more parameters than their symmetric counterparts. As mentioned in the Introduction, in the statistical literature, several proposals were made for testing symmetry in the linear setting. Unlike in the modality testing field, quite a few of them present a correct calibration and the issue then is trying to get the most powerful test. Related with this issue, as mentioned in the Introduction, in the linear case, some optimal, in the maximin sense (see Section 1.2.3), test have been proposed, for the two available scenarios if one wants to test symmetry: when the central location is known and when it is completely unknown. For circular data, the situation is quite different as there are just a few proposals for testing circular symmetry. Referring to the most general case, testing reflective symmetry when the central direction is unknown, just Pewsey (2002) has proposed a simple omnibus test based on the sample second sine moment about the mean direction. Following the Le Cam methodology (see Appendix D for a brief introduction to this topic), the aim of this chapter is to present new optimal tests of the null hypothesis that the circular random variable is reflectively symmetric about an unknown central direction, against the alternative hypothesis that the distribution is an asymmetric case of the `k`–sine–skewed family of distributions. It will be also seen that the proposal of Pewsey (2002) is (asymptotically) a particular case of the tests presented in this chapter.

The chapter is organized as follows. The uniform local asymptotic normality property for the k–sine–skewed family is established in Section 4.1. In Section 4.2 optimal parametric tests for circular reflective symmetry about an unknown central direction are developed, first, in Section 4.2.1, assuming that the form of the base symmetric unimodal circular density is known. Then, relaxing this assumption in Section 4.2.2 similar results are derived. In this section, the optimal semi–parametric tests for circular reflective symmetry about an unknown central direction are developed, assuming that the form of the base symmetric unimodal circular density is unknown. In Section 4.3, the results from a simulation study are presented. The simulation study is designed to explore and compare the calibration and power of the tests proposed in this chapter with those of Ley and Verdebout (2014) (when the central direction is known). In Section 4.4, the tests developed in this chapter are applied in the analysis of a circular dataset from an study about the cracks in cemented femoral components.

Contents

4.1 ULAN property of k–sine–skewed densities

Let $\Theta_1, \ldots, \Theta_n$ be independent and identically distributed circular observations with common density the k–sine–skewed model (1.2.9), that is,

$$f^{\mathtt{k}}_{\mu,\lambda}(\theta) = f_0(\theta-\mu)[1+\lambda\sin(\mathtt{k}(\theta-\mu))],$$

where $\mu \in [0, 2\pi)$ is the location parameter, $f_0 \in \mathcal{F}$ a given reflectively symmetric unimodal base density and $\mathtt{k} \in \mathbb{N}_0$ and $\lambda \in [-1, 1]$ parameters controlling the number of modes and the symmetry. For any $f_0 \in \mathcal{F}$ and any $\mathtt{k} \in \mathbb{N}_0$, denote the joint distribution of the n–tuple $\Theta_1, \ldots, \Theta_n$ by $\mathrm{P}^{(n)}_{\boldsymbol{\vartheta};f_0,\mathtt{k}}$, where $\boldsymbol{\vartheta} = (\mu, \lambda)' \in [0, 2\pi) \times [-1, 1]$. Since $f^k_{\mu,\lambda} = f_0$ when $\lambda = 0$, and hence does not depend on k, the index k can be dropped and simply write $\mathrm{P}^{(n)}_{\boldsymbol{\vartheta};f_0}$ at $\boldsymbol{\vartheta} = \boldsymbol{\vartheta}_0 = (\mu, 0)'$. Any pair $(f_0, \mathtt{k})$ induces the *parametric* model

$$\mathcal{P}^{(n)}_{f_0,\mathtt{k}} = \left\{ \mathrm{P}^{(n)}_{\boldsymbol{\vartheta};f_0,\mathtt{k}} : \boldsymbol{\vartheta} \in [0, 2\pi) \times [-1, 1] \right\},$$

whereas any $\mathtt{k} \in \mathbb{N}_0$ induces the *semi–parametric* model $\mathcal{P}_k^{(n)} = \cup_{f_0 \in \mathcal{F}} \mathcal{P}_{f_0,\mathtt{k}}^{(n)}$.

The *uniform local asymptotic normality* (ULAN) property (see Appendix D) of the parametric model $\mathcal{P}_{f_0,\mathtt{k}}^{(n)}$ in the vicinity of unimodal reflective symmetry, i.e. around $\lambda = 0$, was established by Ley and Verdebout (2014). This property of k–sine–skewed distributions is crucial in the development of the tests proposed. The derivation of the ULAN property requires the following regularity condition on the base density f_0 to hold.

ASSUMPTION A: *The base density $f_0(\theta)$ is a.e. a class–one function over $[0, 2\pi)$, or equivalently over $\mathbb{R}$ by periodicity, with a.e.–derivative f_0'.*

Most classical reflectively symmetric unimodal densities, such us, the von Mises, the cardioid, the wrapped normal or the wrapped Cauchy, satisfy this requirement. Note that the continuously differentiable condition over the circle, combined with the fact that $f_0 > 0$, implies that the Fisher information quantity for location, $I_{f_0} = \int_0^{2\pi} \varphi_{f_0}^2(\theta) f_0(\theta) d\theta$, where $\varphi_{f_0} = -f_0'/f_0$, is finite. The ULAN property of the parametric model $\mathcal{P}_{f_0,\mathtt{k}}^{(n)}$ with respect to $\boldsymbol{\vartheta} = (\mu, \lambda)'$, in the vicinity of unimodal reflective symmetry, then takes the form showed in the following theorem.

Theorem 4.1.1. *Let $f_0 \in \mathcal{F}$, $\mathtt{k} \in \mathbb{N}_0$ and Assumption A holds. Then, for any $\mu \in [0, 2\pi)$, the parametric family of densities $\mathcal{P}_{f_0,\mathtt{k}}^{(n)}$ is ULAN at $\boldsymbol{\vartheta}_0 = (\mu, 0)'$ with central sequence*

$$\boldsymbol{\Delta}_{f_0,\mathtt{k}}^{(n)}(\mu) = \begin{pmatrix} \Delta_{f_0,\mathtt{k};1}^{(n)}(\mu) \\ \Delta_{\mathtt{k};2}^{(n)}(\mu) \end{pmatrix} = \frac{1}{\sqrt{n}} \sum_{i=1}^{n} \begin{pmatrix} \varphi_{f_0}(\Theta_i - \mu) \\ \sin(\mathtt{k}(\Theta_i - \mu)) \end{pmatrix},$$

and corresponding Fisher information matrix

$$\boldsymbol{\Gamma}_{f_0,\mathtt{k}} = \begin{pmatrix} \Gamma_{f_0,\mathtt{k};11} & \Gamma_{f_0,\mathtt{k};12} \\ \Gamma_{f_0,\mathtt{k};12} & \Gamma_{f_0,\mathtt{k};22} \end{pmatrix},$$

where $\Gamma_{f_0,\mathtt{k};11} = I_{f_0}$, $\Gamma_{f_0,\mathtt{k};12} = -\int_0^{2\pi} \sin(\mathtt{k}\theta) f_0'(\theta) d\theta$ and $\Gamma_{f_0,\mathtt{k};22} = \int_0^{2\pi} \sin^2(\mathtt{k}\theta) f_0(\theta) d\theta$.

More precisely, for any $\mu^{(n)} = \mu + O(n^{-1/2})$ and for any bounded sequence $\boldsymbol{\tau}^{(n)} = (\tau_1^{(n)}, \tau_2^{(n)})' \in \mathbb{R}^2$ such that $\mu^{(n)} + n^{-1/2}\tau_1^{(n)}$ remains in $[0, 2\pi)$, then

$$\begin{aligned} \Lambda^{(n)}_{(\mu^{(n)}+n^{-1/2}\tau_1^{(n)}, n^{-1/2}\tau_2^{(n)})'/(\mu^{(n)},0)';f_{0,\mathtt{k}}} &= \log\left(d\mathrm{P}^{(n)}_{(\mu^{(n)}+n^{-1/2}\tau_1^{(n)}, n^{-1/2}\tau_2^{(n)})';f_{0,\mathtt{k}}} / d\mathrm{P}^{(n)}_{(\mu^{(n)},0)';f_0} \right) \\ &= \boldsymbol{\tau}^{(n)\prime} \boldsymbol{\Delta}_{f_0,\mathtt{k}}^{(n)}(\mu^{(n)}) - (1/2)\boldsymbol{\tau}^{(n)\prime} \boldsymbol{\Gamma}_{f_0,\mathtt{k}} \boldsymbol{\tau}^{(n)} + o_{\mathrm{P}}(1) \end{aligned} \tag{4.1.1}$$

and $\boldsymbol{\Delta}_{f_0,\mathtt{k}}^{(n)}(\mu^{(n)}) \xrightarrow{\mathcal{L}} \mathcal{N}_2(\mathbf{0}, \boldsymbol{\Gamma}_{f_0,\mathtt{k}})$, both under $\mathrm{P}^{(n)}_{(\mu^{(n)},0)';f_0}$ as $n \to \infty$.

Theorem 4.1.1 is the key for providing the test statistic that will be employed and its asymptotic distribution under the null. Its proof is given in Ley and Verdebout (2014), where a brief discussion about the minimal conditions required for the ULAN property to hold are also presented. The Fisher information for departures from unimodal reflective symmetry, $\Gamma_{f_0,\mathtt{k};22}$, and hence the cross–information quantity, $\Gamma_{f_0,\mathtt{k};12}$, can easily be shown to be finite by bounding $\sin^2$ by 1 under the integral sign. Note that the constant $\mathtt{k}$ has no effect on the validity of Theorem 4.1.1.

For ULAN to make sense, the Fisher information matrix $\mathbf{\Gamma}_{f_0,\mathtt{k}}$ must be non–singular. This is always the case, as shown in Theorem 6.1 of Ley and Verdebout (2014), except when f_0 is the von Mises circular density and $\mathtt{k} = 1$. As it will be seen in the sequel, this singularity issue plays no role for tests for reflective symmetry about a known location but precludes the construction of a powerful test for reflective symmetry against von–Mises–based sine–skewed alternatives when the location is unknown.

4.2 Optimal tests for reflective symmetry

Locally (around $\boldsymbol{\vartheta}_0$) and asymptotically optimal (maximin) tests, in the Le Cam sense (see Appendix D), for reflective symmetry within the class of sine–skewed distributions which assume that μ is *known* were proposed in Ley and Verdebout (2014). In this section, the *parametric* testing problem is first considered

$$H_{0;f_0} : \lambda = 0 \quad \text{vs.} \quad H_{a;f_0,\mathtt{k}} : \lambda \neq 0, \text{ for a given } f_0 \in \mathcal{F} \text{ and } \mathtt{k} \in \mathbb{N}_0, \tag{4.2.2}$$

that is, it is studied if the underlying density of the data is f_0 against the alternative that it follows a $\mathtt{k}$–sine–skewed version of this density, where f_0 is a specified density belonging to $\mathcal{F}$ and the unknown central direction under $H_{0;f_0}$ is estimated.

A drawback of the above tests is that they are only valid under the parametric null hypothesis $H_{0;f_0}$ with f_0 specified. In order to tackle the more general null hypothesis of reflective symmetry, a test statistic whose asymptotic distribution is valid under any symmetric density $g_0 \in \mathcal{F}$ is needed. Thus, next the more demanding testing problem is considered

$$H_0 : \lambda = 0 \quad \text{vs.} \quad H_{a;\mathtt{k}} : \lambda \neq 0, \text{ for any } g_0 \in \mathcal{F} \text{ and } \mathtt{k} \in \mathbb{N}_0 \tag{4.2.3}$$

in which both, the location parameter μ and the density g_0, take on nuisance roles.

For both problems, the ULAN property of Theorem 4.1.1 is used to derive tests that are valid under the null hypotheses considered and achieve local and asymptotic

Location	Data density	Central seq.	Statistic	Test	Section
Known	Known	$\Delta^{(n)}_{\mathtt{k};2}(\mu)$	$Q^{(n);\mu;g_0}_{\mathtt{k}} = \lvert\Delta^{(n)}_{\mathtt{k};2}(\mu)\rvert/\Gamma^{1/2}_{f_0,\mathtt{k};22}$	$\phi^{(n);\mu;g_0}_{\mathtt{k}}$	3 of LV
	Unknown	$\Delta^{(n)}_{\mathtt{k};2}(\mu)$	$Q^{*(n);\mu}_{\mathtt{k}} = \frac{\lvert\Delta^{(n)}_{\mathtt{k};2}(\mu)\rvert}{(\sum_{i=1}^{n}\sin^2(\mathtt{k}(\Theta_i-\mu)))^{1/2}}$	$\phi^{*(n);\mu}_{\mathtt{k}}$	3 of LV
Unknown	Known	$\Delta^{(n)eff}_{f_0,\mathtt{k};2}(\mu)$	$Q^{(n);g_0}_{\mathtt{k}}$	$\phi^{(n);g_0}_{\mathtt{k}}$	4.2.1
	Unknown	$\Delta^{(n)ecd}_{f_0,g_0,\mathtt{k};2}(\mu)$	$Q^{*(n)}_{f_0,\mathtt{k}}$	$\phi^{*(n)}_{f_0,\mathtt{k}}$	4.2.2

Table 4.1: Summary of the different tests for assessing asymmetry. LV refers to Ley and Verdebout (2014); location (μ) and the data underlying density ($g_0 \in \mathcal{F}$) must be previously known; $\mathtt{k} \in \mathbb{N}_0$ and $f_0 \in \mathcal{F}$ are selected by the user, where it is recommended to use $\mathtt{k} = 2$ and VM_κ as f_0 when this information is unknown.

parametric optimality against a $\mathtt{k}$–sine–skewed alternative characterized by the fixed couple $(f_0, \mathtt{k}) \in (\mathcal{F} \times \mathbb{N}_0)$. In the semi–parametric testing problem (4.2.3), f_0 and $\mathtt{k}$ are chosen *a priori* by the practitioner and, from these choices, tests that are asymptotically optimal against the $(f_0, \mathtt{k})$–sine–skewed alternative are derived. Such tests are valid under any density $g_0 \in \mathcal{F}$.

In order to clarify the notation in the next sections, it should be noted that Δ denotes the central limit sequences. From them, the test statistics (denoted by Q) will be constructed, and the formal test with the asymptotic distribution (which is a standard normal for all cases) is denoted by ϕ. As also the Ley and Verdebout (2014) proposals will be compared in the simulation study (see Section 4.3), this will lead to a total of four different tests, reflected in Table 4.1. For Q and ϕ, the superindex indicates if $\mu \in [0, 2\pi)$ or the base density of the data, $g_0 \in \mathcal{F}$, must be known and, with a subindex, the imposed value of $\mathtt{k} \in \mathbb{N}_0$ and/or the base density, not depending on the data, $f_0 \in \mathcal{F}$.

4.2.1 Optimal tests: the specified density case

For the testing problem (4.2.2), the tests are constructed using a $\sqrt{n}$ consistent and discretized (see Assumption B below) estimator $\hat{\mu}^{(n)}$. The main reason why this testing problem is more demanding than the fixed–μ problem considered in Ley and Verdebout (2014) is due to the fact that the Fisher information matrix $\mathbf{\Gamma}_{f_0,\mathtt{k}}$ is not, in general, diagonal. If the information matrix $\mathbf{\Gamma}_{f_0,\mathtt{k}}$ is diagonal, the substitution of $\hat{\mu}^{(n)}$ for μ would, asymptotically, have no influence on the behavior of the central sequence

for departures from unimodal reflective symmetry $\Delta^{(n)}_{\mathtt{k};2}(\mu)$.

Note that the information matrix $\mathbf{\Gamma}_{f_0,\mathtt{k}}$ is never diagonal if $\mathtt{k}=1$. This can be seen by noting that $\sin(\theta)\varphi_{f_0}(\theta)f_0(\theta) > 0$ over $(0,2\pi)$. On the other hand, when $\mathtt{k}>1$ densities for which $\Gamma_{f_0,\mathtt{k};12}=0$ can be found. If the density function is square integrable on $[0,2\pi)$, this happens when the trigonometric moment $\alpha_{\mathtt{k}} = \mathbb{E}(\cos \mathtt{k}\Theta) = 0$ for $\Theta \sim f_0$, which can be proved using the Fourier expansion (see Jammalamadaka and Sengupta, 2001, Section 2.1). Given any value of $\mathtt{k}$ with $\mathtt{k}>1$, an example where this occurs is the cardioid density for which $\alpha_1=\rho$ and $\alpha_p=0$ if $p>1$.

According to that, the covariance $\Gamma_{f_0,\mathtt{k};12}$ is only rarely null. Hence, a local perturbation of μ has the same asymptotic impact on $\Delta^{(n)}_{\mathtt{k};2}(\mu)$ as a local perturbation of $\lambda=0$. It follows that the effect of ignoring the value of μ is strictly positive when performing inference on λ: the stronger the correlation between μ and λ, the larger that cost. The worst case occurs when the information matrix is singular (that is when f_0 is the von Mises and $\mathtt{k}=1$, see Section 4.1), which leads to asymptotic local powers equal to the nominal level α. This scenario implies that the best possible test is the trivial one, that is, the test that discards the observations and rejects the null hypothesis with probability α.

The cost of estimating μ can be avoided by removing the effect of the location central sequence $\Delta^{(n)}_{f_0,\mathtt{k};1}(\mu)$ from the skewness central sequence $\Delta^{(n)}_{\mathtt{k};2}(\mu)$. To this end a Gram–Schmidt orthogonalization approach is used. This is done projecting $\Delta^{(n)}_{\mathtt{k};2}(\mu)$ onto the subspace orthogonal to $\Delta^{(n)}_{f_0,\mathtt{k};1}(\mu)$, which ensures that the resulting f_0–*efficient central sequence for skewness* $\Delta^{(n)eff}_{f_0,\mathtt{k};2}(\mu)$ and $\Delta^{(n)}_{f_0,\mathtt{k};1}(\mu)$ are asymptotically uncorrelated. This new central sequence is thus of the form

$$\begin{aligned}\Delta^{(n)eff}_{f_0,\mathtt{k};2}(\mu) &= \Delta^{(n)}_{\mathtt{k};2}(\mu) - \frac{\Gamma_{f_0,\mathtt{k};12}}{\Gamma_{f_0,\mathtt{k};11}}\Delta^{(n)}_{f_0,\mathtt{k};1}(\mu) \\ &= n^{-1/2}\sum_{i=1}^{n}\left(\sin(\mathtt{k}(\Theta_i-\mu)) - \frac{\Gamma_{f_0,\mathtt{k};12}}{\Gamma_{f_0,\mathtt{k};11}}\varphi_{f_0}(\Theta_i-\mu)\right). \qquad (4.2.4)\end{aligned}$$

At this point, another important consequence of the ULAN property should be employed, the *asymptotic linearity property* (see Appendix D):

$$\Delta^{(n)}_{f_0,\mathtt{k}}(\mu + n^{-1/2}\tau^{(n)}_1) - \Delta^{(n)}_{f_0,\mathtt{k}}(\mu) = -\Gamma_{f_0,\mathtt{k}}(\tau^{(n)}_1,0)' + o_{\mathrm{P}}(1) \qquad (4.2.5)$$

under $\mathrm{P}^{(n)}_{(\mu,0)';f_0}$ as $n\to\infty$, with $\tau^{(n)}_1 \in \mathbb{R}$ as in Theorem 4.1.1. See Sections 2 and 3 of Koudou and Ley (2014) for further explanations on these issues. It is now not difficult to derive from (4.2.5) the asymptotic linearity property of $\Delta^{(n)eff}_{f_0,\mathtt{k};2}(\mu)$:

$$\Delta^{(n)eff}_{f_0,\mathtt{k};2}(\mu + n^{-1/2}\tau^{(n)}_1) - \Delta^{(n)eff}_{f_0,\mathtt{k};2}(\mu) = o_{\mathrm{P}}(1) \qquad (4.2.6)$$

under $\mathrm{P}^{(n)}_{(\mu,0)';f_0}$ as $n \to \infty$. Now consider replacing the non–random bounded sequence $\tau_1^{(n)}$ with $n^{1/2}(\hat{\mu}^{(n)} - \mu)$ for some $\sqrt{n}$ consistent estimator $\hat{\mu}^{(n)}$. The latter is bounded in probability and, via Lemma 4.4 of Kreiss (1987), serves as a candidate for $\tau_1^{(n)}$ provided the following assumption holds.

ASSUMPTION B: *The sequence of estimators $\hat{\mu}^{(n)}$ is (i) $\sqrt{n}$ consistent, i.e., $n^{1/2}(\hat{\mu}^{(n)} - \mu) = O_{\mathrm{P}}(1)$ as $n \to \infty$, under $\mathrm{P}^{(n)}_{(\mu,0)';f_0}$, and (ii) locally asymptotically discrete, meaning that, for all $\mu \in [0, 2\pi)$ and all $c > 0$, there exists an $M = M(c) > 0$ such that the number of possible values of $\hat{\mu}^{(n)}$ in intervals of the form $\{t \in \mathbb{R} : n^{1/2}|t - \mu| \leq c\}$ is bounded by M, uniformly as $n \to \infty$.*

Note that Assumption B (ii) is a purely technical requirement, with little practical implication. Indeed, for fixed sample size, any estimator can be considered part of a locally asymptotically discrete sequence. However, it is precisely this assumption that allows us to replace $\tau_1^{(n)}$ by $n^{1/2}(\hat{\mu}^{(n)} - \mu)$ in (4.2.6) thanks to the aforementioned Lemma 4.4 of Kreiss (1987), yielding

$$\Delta^{(n)eff}_{f_0,\mathtt{k};2}(\hat{\mu}^{(n)}) - \Delta^{(n)eff}_{f_0,\mathtt{k};2}(\mu) = o_{\mathrm{P}}(1) \tag{4.2.7}$$

under $\mathrm{P}^{(n)}_{(\mu,0)';f_0}$ as $n \to \infty$. The locally (around $\lambda = 0$) and asymptotically maximin f_0–parametric test $\phi^{(n);f_0}_{\mathtt{k}}$ can be built. It rejects $H_{0;f_0}$ at asymptotic level α whenever the statistic

$$Q^{(n);f_0}_{\mathtt{k}} = \frac{|\Delta^{(n)eff}_{f_0,\mathtt{k};2}(\hat{\mu}^{(n)})|}{\Gamma^{1/2}_{f_0,\mathtt{k};22.1}}$$

exceeds the upper $\alpha/2$ quantile of the standard normal distribution, $z_{1-\alpha/2}$, where $\Gamma_{f_0,\mathtt{k};22.1} = \Gamma_{f_0,\mathtt{k};22} - \Gamma^2_{f_0,\mathtt{k};12}/\Gamma_{f_0,\mathtt{k};11}$ is the asymptotic variance of $\Delta^{(n)eff}_{f_0,\mathtt{k};2}(\mu)$ under $\mathrm{P}^{(n)}_{(\mu,0)';f_0}$. Optimal properties of this test statistic will be described in a more flexible scenario in Section 4.2.2.

Depending on the choice of f_0 and $\mathtt{k}$, there are different constructions of the test statistic $Q^{(n);f_0}_{\mathtt{k}}$. Among the possible base symmetric densities, here the test statistic is described for three of the most well–known distributions: the von Mises, the cardioid and the wrapped Cauchy.

Von Mises distribution

For the von Mises distribution, it is obtained that $\varphi_{f_{\mathrm{VM}_\kappa}}(\theta) = \kappa \sin(\theta)$, $\Gamma_{f_{\mathrm{VM}_\kappa},\mathtt{k};11} = \kappa I_1(\kappa)/I_0(\kappa)$, $\Gamma_{f_{\mathrm{VM}_\kappa},\mathtt{k};12} = \mathtt{k} I_k(\kappa)/I_0(\kappa)$ and $\Gamma_{f_{\mathrm{VM}_\kappa},\mathtt{k};22} = (1 - I_{2k}(\kappa)/I_0(\kappa))/2$, where I_k denotes the modified Bessel function of the first kind and order $\mathtt{k}$. As it was

mentioned before, when $\mathtt{k}=1$ the Fisher information matrix is singular, then, in this case, the resulting test coincides with the trivial test. For $\mathtt{k}>1$ the test statistic is equal to

$$Q_{\mathtt{k}}^{(n);f_{\mathrm{VM}_\kappa}}=\frac{n^{-1/2}\sum_{i=1}^{n}\left(\sin(\mathtt{k}(\Theta_i-\hat{\mu}^{(n)}))-\frac{\mathtt{k}I_k(\kappa)}{\kappa I_1(\kappa)}\kappa\sin(\Theta_i-\hat{\mu}^{(n)})\right)}{\sqrt{\frac{1}{2}\left(1-\frac{I_{2k}(\kappa)}{I_0(\kappa)}\right)-\frac{(\mathtt{k}I_k(\kappa))^2}{\kappa I_1(\kappa)I_0(\kappa)}}}.$$

To make a more flexible parametric scenario, one can replace in the previous expression κ by the $\sqrt{n}$ consistent estimator $\hat{\kappa}^{(n)}=A^{-1}(\bar{R})$, with $A(x)=I_1(x)/I_0(x)$ and being $\bar{R}$ the mean resultant length. Then, the null hypothesis will be rejected when $|Q_{\mathtt{k}}^{(n);f_{\mathrm{VM}_{\hat{\kappa}^{(n)}}}}|$ exceeds $z_{\alpha/2}$. The steps to see that the replacement of κ by $\hat{\kappa}^{(n)}$ has asymptotically no effect are similar to the previous calculations and hence omitted. For this purpose, it is necessary to stablish the ULAN property, in the vicinity of symmetry, of the parametric location–concentration–skewness von Mises model

$$\mathcal{P}_{f_{\mathrm{VM},\mathtt{k}}}^{(n)}=\left\{\mathrm{P}_{(\mu,\kappa,\lambda);f_{\mathrm{VM},\mathtt{k}}}^{(n)}:\mu\in[0,2\pi),\kappa>0,\lambda\in[-1,1]\right\},$$

and then notice that the central sequence for concentration is asymptotically independent of the central sequences for location and skewness.

Cardioid distribution

When the cardioid is taken as the base distribution and $\mathtt{k}>1$ the same statistic as in the Ley and Verdebout (2014) proposal is obtained replacing μ by the $\sqrt{n}$ estimator $\hat{\mu}^{(n)}$. Since $\Gamma_{f_{\mathrm{C}_\rho},\mathtt{k};22}=1/2$ the test statistic when $\mathtt{k}>1$ is

$$Q_{\mathtt{k}}^{(n);f_{\mathrm{C}_\rho}}=\sqrt{2}n^{-1/2}\sum_{i=1}^{n}\sin(\mathtt{k}(\Theta_i-\hat{\mu}^{(n)})).$$

When $\mathtt{k}=2$, if the estimator of μ is obtained with the method of moments, then the test using this test statistic and the $\bar{b}_2$ test of Pewsey (2002) are asymptotically equivalent. When $\mathtt{k}=1$ straightforward calculations yield $\varphi_{f_{\mathrm{C}_\rho}}(\theta)=2\rho\sin(\theta)/(1+2\rho\cos(\theta))$, $\Gamma_{f_{\mathrm{C}_\rho},1;11}=1-\sqrt{1-4\rho^2}$ and $\Gamma_{f_{\mathrm{C}_\rho},1;12}=\rho$. Then, the test statistic is equal to

$$Q_1^{(n);f_{\mathrm{C}_\rho}}=\frac{n^{-1/2}\sum_{i=1}^{n}\left(\sin(\mathtt{k}(\Theta_i-\hat{\mu}^{(n)}))-\frac{2\rho^2\sin(\Theta_i-\hat{\mu}^{(n)})}{\left(1-\sqrt{1-4\rho^2}\right)(1+2\rho\cos(\Theta_i-\hat{\mu}^{(n)}))}\right)}{\sqrt{\frac{1}{2}-\frac{\rho^2}{1-\sqrt{1-4\rho^2}}}}.$$

Wrapped Cauchy distribution

In the case of the wrapped Cauchy, the following results are obtained, $\varphi_{f_{\mathrm{WC}_\rho}}(\theta) = 2\rho\sin(\theta)/(1+\rho^2-2\rho\cos(\theta))$, $\Gamma_{f_{\mathrm{WC}_\rho},\mathtt{k};11} = 2\rho^2/(1-\rho^2)^2$, $\Gamma_{f_{\mathrm{WC}_\rho},\mathtt{k};12} = \mathtt{k}\rho^{\mathtt{k}}$ and $\Gamma_{f_{\mathrm{WC}_\rho},\mathtt{k};22} = (1-\rho^2)\cdot(\sum_{l=1}^{\mathtt{k}}\rho^{2(l-1)})/2$. Thus, the test statistic for the wrapped Cauchy distribution is

$$Q_{\mathtt{k}}^{(n);f_{\mathrm{WC}_\rho}} = \frac{n^{-1/2}\sum_{i=1}^n\left(\sin(\mathtt{k}(\Theta_i-\hat{\mu}^{(n)})) - (\mathtt{k}\rho^{\mathtt{k}-1}(1-\rho^2)^2)\,\frac{\sin(\Theta_i-\hat{\mu}^{(n)})}{1+\rho^2-2\rho\cos(\Theta_i-\hat{\mu}^{(n)})}\right)}{\sqrt{\frac{1-\rho^2}{2}\left(\left(\sum_{l=1}^{\mathtt{k}}\rho^{2(l-1)}\right) - \mathtt{k}^2\rho^{2(\mathtt{k}-1)}(1-\rho^2)\right)}}.$$

4.2.2 Optimal tests: the unspecified density case

Consider now the testing problem (4.2.3). Here the objective is to construct tests that are still locally and asymptotically maximin for detecting an alternative characterized by a specified couple $(f_0,\mathtt{k}) \in (\mathcal{F}\times\mathbb{N}_0)$. However the main difference with respect to the parametric problem considered in Section 4.2.1 is that the objective is to build a test that is asymptotically valid under any $g_0 \in \mathcal{F}$. Specifically, it is needed to allow the substitution of μ by $\hat{\mu}^{(n)}$ in $\Delta_{\mathtt{k};2}^{(n)}(\mu)$ under $\mathrm{P}_{(\mu,0)';g_0}^{(n)}$ with possibly $g_0 \neq f_0$. The ULAN property combined with Lemma 4.4 of Kreiss (1987) directly entails that

$$\Delta_{\mathtt{k};2}^{(n)}\left(\hat{\mu}^{(n)}\right) - \Delta_{\mathtt{k};2}^{(n)}(\mu) = -\Gamma_{g_0,\mathtt{k};12}n^{1/2}\left(\hat{\mu}^{(n)}-\mu\right) + o_P(1), \tag{4.2.8}$$

under $\mathrm{P}_{(\mu,0)';g_0}^{(n)}$ as $n\to\infty$, provided that $\hat{\mu}^{(n)}$ satisfies Assumption B. Therefore, the substitution of μ by $\hat{\mu}^{(n)}$ under $P_{(\mu,0)',g_0}^{(n)}$ has no asymptotic cost only if

$$\Gamma_{g_0,\mathtt{k};12} = 0. \tag{4.2.9}$$

As seen in Section 4.2.1, the situation described by (4.2.9) rarely occurs. In order to circumvent this problem and eliminate the asymptotic covariance $\Gamma_{g_0,\mathtt{k};12}$ while keeping the $(f_0,\mathtt{k})$ target in mind, it is considered an *efficient central sequence*

$$\Delta_{f_0,g_0,\mathtt{k};2}^{(n);ecd}(\mu) = n^{-1/2}\sum_{i=1}^n\left(\sin(\mathtt{k}(\Theta_i-\mu)) - \eta\varphi_{f_0}(\Theta_i-\mu)\right),$$

where letting

$$\Gamma_{f_0,g_0,\mathtt{k};11} = \int_0^{2\pi}\varphi_{f_0}(\theta)\varphi_{g_0}(\theta)g_0(\theta)d\theta,$$

$\eta = \Gamma_{g_0,\mathtt{k};12}/\Gamma_{f_0,g_0,\mathtt{k};11}$. Since f_0 and g_0 are periodic class one functions over a bounded set and $f_0, g_0 > 0$, this cross–information quantity $\Gamma_{f_0,g_0,\mathtt{k};11}$ is finite. Then note that

if $g_0 = f_0$ then $\Gamma_{f_0,f_0,\mathtt{k};11} = \Gamma_{f_0,\mathtt{k};11}$, so that $\Delta^{(n)ecd}_{f_0,f_0,\mathtt{k};2}(\mu)$ will coincide with $\Delta^{(n)eff}_{f_0,\mathtt{k};2}(\mu)$ under $P^{(n)}_{(\mu,0)',f_0}$ which is key for maintaining the asymptotic optimality against $(f_0,\mathtt{k})$ alternatives as it will be seen in the sequel. Integrating by parts,

$$\Gamma_{g_0,\mathtt{k};12} = \int_0^{2\pi} \sin(\mathtt{k}\theta)\varphi_{g_0}(\theta)g_0(\theta)d\theta = \mathtt{k}\int_0^{2\pi} \cos(\mathtt{k}\theta)g_0(\theta)d\theta = \mathtt{k}\mathrm{E}_{g_0}[\cos(\mathtt{k}(\Theta_i-\mu))] \tag{4.2.10}$$

and

$$\begin{aligned}\Gamma_{f_0,g_0,\mathtt{k};11} &= \int_0^{2\pi} \varphi_{f_0}(\theta)\varphi_{g_0}(\theta)g_0(\theta)d\theta = [\varphi_{f_0}(\theta)g_0(\theta)]_0^{2\pi} + \int_0^{2\pi} \varphi'_{f_0}(\theta)g_0(\theta)d\theta \\ &= \int_0^{2\pi} \varphi'_{f_0}(\theta)g_0(\theta)d\theta = \mathrm{E}_{g_0}[\varphi'_{f_0}(\theta)] \end{aligned} \tag{4.2.11}$$

provided that the following assumption hold.

Assumption C. The mapping $\theta \mapsto \varphi_{f_0}(\theta)$ is almost everywhere class on over $[0,2\pi)$ with almost everywhere derivative $\varphi'_{f_0}(\theta)$, where $f_0 \in \mathcal{F}$

In the following result, it is showed that the estimators

$$\hat{\Gamma}_{g_0,k;12} = n^{-1}\sum_{i=1}^{n} k\cos\left(k\left(\Theta_i - \hat{\mu}^{(n)}\right)\right) \quad \text{and} \quad \hat{\Gamma}_{f_0,g_0,k;11} = n^{-1}\sum_{i=1}^{n} \varphi'_{f_0}\left(\Theta_i - \hat{\mu}^{(n)}\right)$$

are consistent estimators of $\Gamma_{g_0,k;12}$ and $\Gamma_{f_0,g_0,k;11}$ in (4.2.10) and (4.2.11), respectively.

Lemma 4.2.1. *Suppose $k \in \mathbb{N}_0$, $f_0, g_0 \in \mathcal{F}$ and Assumptions A, B and C hold. Then $\hat{\Gamma}_{g_0,\mathtt{k};12} - \Gamma_{g_0,\mathtt{k};12} = o_{\mathrm{P}}(1)$ and $\hat{\Gamma}_{f_0,g_0,\mathtt{k};11} - \Gamma_{f_0,g_0,\mathtt{k};11} = o_{\mathrm{P}}(1)$ as $n \to \infty$ under $\mathrm{P}^{(n)}_{(\mu,0);g_0}$.*

The proof is provided in B.2.1. Using these estimators, our test is based on the estimated version of the efficient central sequence

$$\Delta^{*(n);ecd}_{f_0,\mathtt{k};2}(\mu) = n^{-1/2}\sum_{i=1}^{n}\left(\sin(\mathtt{k}(\Theta_i-\mu)) - \hat{\eta}\varphi_{f_0}(\Theta_i-\mu)\right), \tag{4.2.12}$$

where $\hat{\eta} = \hat{\Gamma}_{g_0,\mathtt{k};12}/\hat{\Gamma}_{f_0,g_0,\mathtt{k};11}$. The test $\phi^{*(n)}_{f_0,\mathtt{k}}$ rejects H_0 at asymptotic level α whenever the test statistic $|Q^{*(n)}_{f_0,\mathtt{k}}| > z_{1-\alpha/2}$, where

$$\begin{aligned} Q^{*(n)}_{f_0,\mathtt{k}} &= \frac{\Delta^{*(n);ecd}_{f_0,\mathtt{k};2}\left(\hat{\mu}^{(n)}\right)}{\left(C^{*(n)}_{f_0,\mathtt{k}}\left(\hat{\mu}^{(n)}\right)\right)^{1/2}} \\ &= \frac{n^{-1/2}\sum_{i=1}^{n}\left(\sin(\mathtt{k}(\Theta_i-\hat{\mu}^{(n)})) - \hat{\eta}\varphi_{f_0}\left(\Theta_i-\hat{\mu}^{(n)}\right)\right)}{\left(n^{-1}\sum_{i=1}^{n}\left(\sin(\mathtt{k}(\Theta_i-\hat{\mu}^{(n)})) - \hat{\eta}\varphi_{f_0}\left(\Theta_i-\hat{\mu}^{(n)}\right)\right)^2\right)^{1/2}}. \end{aligned} \tag{4.2.13}$$

The asymptotic distribution is formally established in Theorem 4.2.1, where the optimality properties of $\phi^{*(n)}_{f_0,\mathtt{k}}$ are proved. Before doing so, first the following result on the efficient central sequence in (4.2.12) is provided, the proof of this result is given in B.2.2.

Lemma 4.2.2. *Suppose* $\mathtt{k} \in \mathbb{N}_0$, $f_0, g_0 \in \mathcal{F}$ *and Assumptions A, B and C hold. Then, as* $n \to \infty$ *under* $\mathrm{P}^{(n)}_{(\mu,0);g_0}$*: (i)* $\Delta^{*(n);ecd}_{f_0,\mathtt{k};2}\left(\hat{\mu}^{(n)}\right) - \Delta^{(n);ecd}_{f_0,g_0,\mathtt{k};2}(\mu) = o_{\mathrm{P}}(1)$*; (ii)* $C^{*(n)}_{f_0,\mathtt{k}}\left(\hat{\mu}^{(n)}\right) - C^{(n)}_{f_0,g_0,\mathtt{k}}(\mu) = o_{\mathrm{P}}(1)$*, where*

$$C^{(n)}_{f_0,g_0,\mathtt{k}}(\mu) = n^{-1}\sum_{i=1}^{n}\left(\sin(\mathtt{k}(\Theta_i-\mu)) - \frac{\Gamma_{g_0,\mathtt{k};12}}{\Gamma_{f_0,g_0,\mathtt{k};11}}\varphi_{f_0}(\Theta_i-\mu)\right)^2.$$

Using Lemma 4.2.2, the optimality properties of the semi-parametric test $\phi^{*(n)}_{f_0,\mathtt{k}}$ can be established. Given a posited base density $f_0 \in \mathcal{F}$ and value of $\mathtt{k}$, in Theorem 4.2.1 the asymptotic properties of the test statistic $Q^{*(n)}_{f_0,\mathtt{k}}$ are provided both under H_0 and a sequence of contiguous alternatives.

Theorem 4.2.1. *Suppose* $\mathtt{k} \in \mathbb{N}_0$*, the posited base density* $f_0 \in \mathcal{F}$ *and Assumptions A, B and C hold. Then:*

(i) under H_0, $Q^{*(n)}_{f_0,\mathtt{k}} \xrightarrow{\mathcal{D}} \mathcal{N}(0,1)$ *as* $n \to \infty$*, so that the test* $\phi^{*(n)}_{f_0,\mathtt{k}}$ *has asymptotic level* α *under* H_0*;*

(ii) under $\cup_{\mu\in[-\pi,\pi)}\mathrm{P}^{(n)}_{(\mu,n^{-1/2}\tau_2^{(n)})';g_0,\mathtt{k}'}$ *with* $g_0 \in \mathcal{F}$, $\mathtt{k}' \in \mathbb{N}_0$ *and* $\tau_2^{(n)}$ *a bounded sequence as in Theorem 4.1.1,* $Q^{*(n)}_{f_0,\mathtt{k}}$ *is asymptotically normal with mean* $V^{g_0}_{f_0}(\mathtt{k})^{-1/2}C^{g_0}_{f_0}(\mathtt{k},\mathtt{k}')\tau_2$ *and variance 1, where* $\tau_2 = \lim_{n\to\infty}\tau_2^{(n)}$*,*

$$V^{g_0}_{f_0}(\mathtt{k}) = \int_{-\pi}^{\pi}\left(\sin(\mathtt{k}\theta) - \frac{\Gamma_{g_0,\mathtt{k};12}}{\Gamma_{f_0,g_0,\mathtt{k};11}}\varphi_{f_0}(\theta)\right)^2 g_0(\theta)d\theta,$$

and

$$C^{g_0}_{f_0}(\mathtt{k},\mathtt{k}') = \int_{-\pi}^{\pi}\left(\sin(\mathtt{k}\theta) - \frac{\Gamma_{g_0,\mathtt{k};12}}{\Gamma_{f_0,g_0,\mathtt{k};11}}\varphi_{f_0}(\theta)\right)\sin(\mathtt{k}'\theta)g_0(\theta)d\theta,$$

(both finite) ;

(iii) the test $\phi^{*(n)}_{f_0,\mathtt{k}}$ *is locally and asymptotically maximin at asymptotic level* α *when testing* H_0 *against* $H_{a;f_0,\mathtt{k}}$*.*

The proof of Theorem 4.2.1 is given in B.2.3. Theorem 4.2.1 states that $\phi^{*(n)}_{f_0,\mathtt{k}}$ is valid under the entire null hypothesis H_0, and so is asymptotically distribution and

location free. The asymptotic power of $\phi^{*(n)}_{f_0,\mathtt{k}}$ against local alternatives of the form $\cup_{\mu\in[-\pi,\pi)}\mathrm{P}^{(n)}_{(\mu,n^{-1/2}\tau_2^{(n)});g_0,\mathtt{k}'}$ as a function of the posited f_0 can be calculated using the result provided in Theorem 4.2.1 (ii).

Clearly, the actual form of the test statistic $Q^{*(n)}_{f_0,\mathtt{k}}$ is independent of the true underlying density g_0 but will depend on the posited density f_0 and the value of $\mathtt{k}$. Then, unlike the fixed location test, two choices must be done. Here, as in Section 4.2.1, the test statistics, using the von Mises, the cardioid and the wrapped Cauchy as posited densities, are described.

Von Mises distribution

For the von Mises distribution, $\varphi'_{f_{\mathrm{VM}_\kappa}}(\theta)=\kappa\sin(\theta)$. When $\mathtt{k}=1$, again, as in the parametric case, it is obtained the trivial test. For $\mathtt{k}>1$, independently on the value of κ, the numerator of the test statistic, $\Delta^{*(n);ecd}_{\mathrm{VM}_\kappa,\mathtt{k};2}(\hat\mu^{(n)})$, becomes

$$n^{-1/2}\sum_{i=1}^{n}\left(\sin(\mathtt{k}(\Theta_i-\hat\mu^{(n)}))-\left[\frac{\sum_{l=1}^{n}\mathtt{k}\cos\left(\mathtt{k}\left(\Theta_l-\hat\mu^{(n)}\right)\right)}{\sum_{m=1}^{n}\cos(\Theta_m-\hat\mu^{(n)})}\right]\sin(\Theta_i-\hat\mu^{(n)})\right).$$

In this case, for the von Mises base density, when $\mathtt{k}=2$ and the method of moments estimator of μ is used, $Q^{*(n)}_{f_{\mathrm{VM}_\kappa},2}$ is asymptotically equivalent (in the sense that the difference is $o_{\mathrm{P}}(1)$ as $n\to\infty$) to the test statistic used in the $\bar b_2$ test of Pewsey (2002). The later test statistic is of the form

$$\frac{n^{-1/2}\sum_{i=1}^{n}\sin(2(\Theta_i-\hat\mu^{(n)}))}{\sqrt{M_n}},$$

where M_n is such that $M_n-n^{-1}\sum_{i=1}^{n}\left(\sin(2(\Theta_i-\hat\mu^{(n)}))\right)^2$ is $o_{\mathrm{P}}(1)$ as $n\to\infty$ under $\mathrm{P}^{(n)}_{(\mu,0)';g_0}$ for any g_0. Therefore the $\bar b_2$ test is locally and asymptotically maximin against von-Mises 2–sine–skewed alternatives for the μ–unspecified problem.

Cardioid distribution

Taking the cardioid as the base density, the derivative of $\varphi_{f_{\mathrm{C}_\rho}}$ with respect to θ is $\varphi'_{f_{\mathrm{C}_\rho}}(\theta)=2\rho(2\rho+\cos(\theta))/(1+2\rho\cos(\theta))^2$, and, then, the numerator of the test statistic, $\Delta^{*(n);ecd}_{\mathrm{C}_\rho,\mathtt{k};2}(\hat\mu^{(n)})$, becomes

$$n^{-1/2}\sum_{i=1}^{n}\left(\sin(\mathtt{k}(\Theta_i-\hat\mu^{(n)}))-\left[\frac{\sum_{l=1}^{n}\mathtt{k}\cos\left(\mathtt{k}\left(\Theta_l-\hat\mu^{(n)}\right)\right)}{\sum_{m=1}^{n}\frac{(2\rho+\cos(\Theta_m-\hat\mu^{(n)}))}{(1+2\rho\cos(\Theta_m-\hat\mu^{(n)}))^2}}\right]\frac{\sin(\Theta_i-\hat\mu^{(n)})}{1+2\rho\cos(\Theta_i-\hat\mu^{(n)})}\right).$$

Note that if the underlying density g_0 is cardioid, then for $\mathtt{k} > 1$, $\Gamma_{g_0,\mathtt{k};12} = 0$, and so $\eta = 0$ in this case. The various results of the Section then directly imply that

$$Q^{*(n)}_{f_0,\mathtt{k}} = \frac{n^{-1/2}\sum_{i=1}^n \sin(\mathtt{k}(\Theta_i - \hat{\mu}^{(n)}))}{\left(n^{-1}\sum_{i=1}^n \left(\sin(\mathtt{k}(\Theta_i - \hat{\mu}^{(n)}))\right)^2\right)^{1/2}} + o_{\mathrm{P}}(1)$$

as $n \to \infty$ under $\mathrm{P}^{(n)}_{(\mu,0)';f_{\mathrm{C}_\rho}}$ still for $\mathtt{k} > 1$ and any posited density f_0. This implies in particular that for fixed $\mathtt{k} > 1$, the choice of f_0 in $Q^{*(n)}_{f_0,\mathtt{k}}$ under cardioid distributions is irrelevant since it has no impact on the local power. For $\mathtt{k} = 2$, the local asymptotic powers of tests based on $Q^{*(n)}_{f_0,\mathtt{k}}$ for any f_0 in the cardioid case are the same as the local asymptotic powers of the Pewsey (2002) $\bar{b}_2$ test and also therefore of the $\phi^{*(n)}_{f_{\mathrm{VM}_\kappa},2}$.

Wrapped Cauchy distribution

For the wrapped Cauchy model, $\varphi'_{f_{\mathrm{WC}_\rho}}(\theta) = 2\rho(-2\rho + (1+\rho^2)\cos(\theta))/(1+\rho^2 - 2\rho\cos(\theta))^2$. The numerator of the test statistic takes then the form

$$n^{-1/2}\sum_{i=1}^n \left(\sin(\mathtt{k}(\Theta_i - \hat{\mu}^{(n)})) - \left[\frac{\sum_{l=1}^n \mathtt{k}\cos\left(\mathtt{k}\left(\Theta_l - \hat{\mu}^{(n)}\right)\right)}{\sum_{m=1}^n \frac{2\rho(-2\rho+(1+\rho^2)\cos(\Theta_m - \hat{\mu}^{(n)}))}{(1+\rho^2-2\rho\cos(\Theta_m - \hat{\mu}^{(n)}))^2}}\right]\frac{\sin(\Theta_i - \hat{\mu}^{(n)})}{1+2\rho\cos(\Theta_i - \hat{\mu}^{(n)})}\right).$$

4.3 Simulation study

In order to investigate the performance of the semi–parametric test ($\phi^{*(n)}_{f_0,\mathtt{k}}$) and compare it with its parametric counterpart ($\phi^{(n);g_0}_{\mathtt{k}}$), as well as with their analogues proposed by Ley and Verdebout (2014) for when μ is specified ($\phi^{*(n);\mu}_{\mathtt{k}}$ and $\phi^{(n);\mu;g_0}_{\mathtt{k}}$, respectively), a Monte Carlo experiment was carried out. When conducting this study, in general (Tables 4.5–4.14), samples of size $n = 30, 100, 500$ from $\mathtt{k}'$–sine–skewed distributions were simulated, with $\mu = 0$, $\lambda = 0, 0.2, 0.4, 0.6$, $\mathtt{k}' = 1, 2, 3$ and, for the underlying symmetric density g_0, the f_{VM_1}, $f_{\mathrm{VM}_{10}}$, $f_{\mathrm{C}_{0.45}}$, $f_{\mathrm{WN}_{0.5}}$, $f_{\mathrm{WN}_{0.9}}$ and $f_{\mathrm{WC}_{0.5}}$ densities (see Figure 4.1 or Appendix A for a representation of these densities and their alternatives). These sample sizes, smaller that those used in previous chapters, were selected following the selection in Ley and Verdebout (2014) and since, in general, the objective is seeing the power of the tests. Finally, for each $(n, \lambda, \mathtt{k}', g_0)$ combination 1000 samples were simulated and it is shown in each table the percentage of rejections for a nominal significance level of $\alpha = 0.05$. The models under the null hypothesis correspond to $\lambda = 0$ and, because of the form of (1.2.9), are $\mathtt{k}'$–invariant. For the parametric test when the underlying density is the von Mises and $\mathtt{k} = 1$,

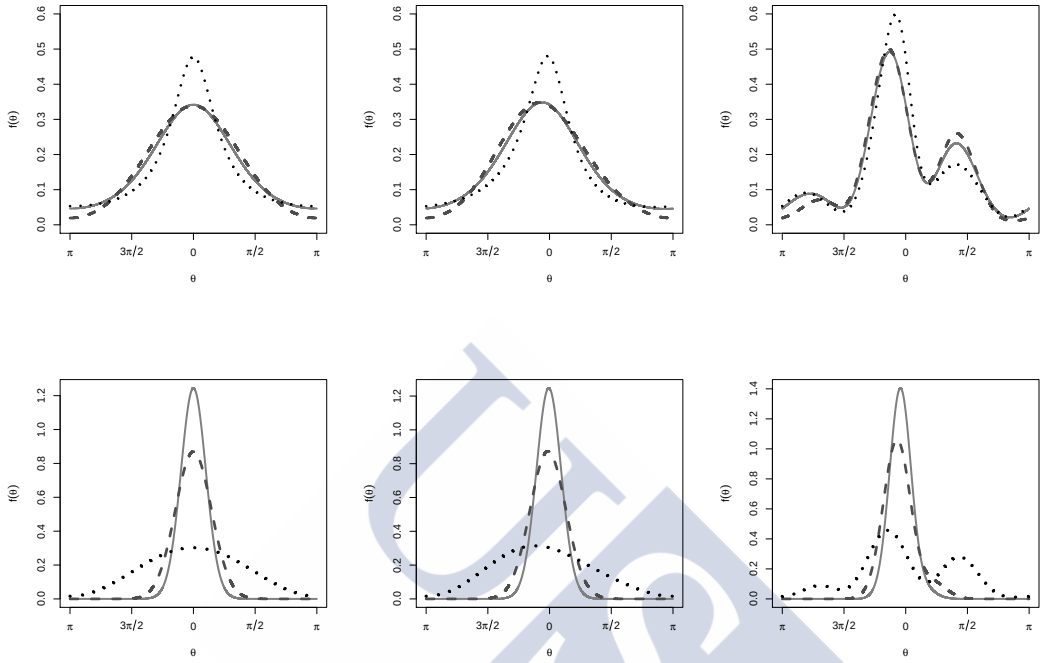

Figure 4.1: Examples of k–sine–skewed distributions. Left: $\lambda = 0$ (symmetric). Center: $\lambda = 0.2$ and $\mathtt{k} = 1$ ("low" asymmetry). Right: $\lambda = 0.6$ and $\mathtt{k} = 3$ ("high" asymmetry). First row: f_{VM_1} (solid line), $f_{\mathrm{WN}_{0.5}}$ (dashed line) and $f_{\mathrm{WC}_{0.5}}$ (dotted line). Second row: $f_{\mathrm{VM}_{10}}$ (solid line), $f_{\mathrm{WN}_{0.9}}$ (dashed line) and $f_{\mathrm{C}_{0.45}}$ (dotted line).

$\phi_1^{(n);f_{\mathrm{VM}_\kappa}}$, the resulting test coincides with the trivial test and for that reason is not showed on the simulation results in Table 4.5.

General conclusions. First, as mentioned in the previous section, two decisions must be done, selecting the base density f_0 (in the semiparametric test for unknown location) and the value of k. Broadly, as it will be seen later in this simulation study, when the value of k is unknown the best power results are achieved when $\mathtt{k} = 2$. Although it will be seen that, in practice, the selection of the base density f_0 in the semiparametric scenario has little impact on the test statistic, our suggestion is employ the von Mises density as, independently on the concentration parameter, it is optimal against all the kind of von-Mises and cardioid 2–sine–skewed alternatives.

From the results reported in Tables 4.2–4.4 it may seem that the calibration of the tests is correct; although for the scenarios in which the value of μ is unspecified, the $\phi_2^{(n);g_0}$ and $\phi_{f_{\mathrm{VM}_\kappa};2}^{*(n)}$ tests are somewhat conservative for $n = 30$. As might be expected, the rejection rates of all four tests increase with the sample size, n, and

the value of λ, and are generally higher when the posited value of $\mathtt{k}$ coincides with the true value of $\mathtt{k}'$. In general, knowing the form of the underlying distribution has little effect on the relative performance of the two pairs of tests. Again as might be expected, the rejection rates are higher for the tests for which the centre, μ, is correctly imposed. For those two test, $\phi_{\mathtt{k}}^{(n);g_0}$ and $\phi_{f_{\mathrm{VM}_\kappa};\mathtt{k}}^{*(n)}$, the power is lowest when the underlying distribution is highly concentrated, as it is for the $f_{\mathrm{VM}_{10}}$ and $f_{\mathrm{WN}_{0.9}}$ cases. The reason for this lower power can be appreciated from a comparison of their densities in the graphics showed in Figure 4.1. Clearly, there is very little difference between the shape of the base symmetric density and the shapes of the other densities, corresponding to different values of λ, portrayed in those graphics. Overall, however, $\phi_{f_{\mathrm{VM}_\kappa};\mathtt{k}}^{*(n)}$ provides a relatively competitive test compared with $\phi_{\mathtt{k}}^{(n);g_0}$ for the scenario in which μ is unspecified.

Selection of $\mathtt{k}$. In this part of the simulation study, the four tests for reflective symmetry assuming that $\mathtt{k}$ was 1, 2 and 3 and imposing the cardioid $\mathrm{C}_{0.25}$ as the base density for the semi–parametric test, $\phi_{f_{\mathrm{C}_{0.25}};\mathtt{k}}^{*(n)}$. This base density was chosen as, when $\mathtt{k}=2$, it presents similar results to those achieved with the von Mises base density and, unlike this density, it also allows to impose $\mathtt{k}=1$ in the construction of the test. The rejection rates obtained for the different values of $\mathtt{k}$ and a nominal significance level of $\alpha=0.05$ are reproduced in Tables 4.5 and 4.6 (for $\mathtt{k}=1$), Tables 4.2–4.4 (for $\mathtt{k}=2$) and in Tables 4.7 and 4.8 (for $\mathtt{k}=3$).

From the results reported in Tables 4.2–4.8 it may seem that the rejection rates of all four tests are generally highest when the posited value of $\mathtt{k}$ coincides with the true value of $\mathtt{k}'$. Some exceptions to this rule can be found in the concentrated densities $f_{\mathrm{VM}_{10}}$ and $f_{\mathrm{WN}_{0.9}}$. For example, for these two densities, in Tables 4.2–4.6, when $\mathtt{k}=1,2$; the $\phi_{\mathtt{k}}^{(n);\mu;g_0}$ and $\phi_{\mathtt{k}}^{*(n);\mu}$ tests perform better for $\mathtt{k}'=3$, rather than for $\mathtt{k}'=\mathtt{k}$. When $k\neq k'$, some of the tests perform, at best, like the trivial test. This is the case, in Tables 4.2–4.8, for the $\phi_{\mathtt{k}}^{(n);g_0}$ and $\phi_{f_{\mathrm{C}_{0.25}};\mathtt{k}}^{*(n)}$ tests when $k'=1$ and, again, g_0 is the highly concentrated $f_{\mathrm{VM}_{10}}$ or $f_{\mathrm{WN}_{0.9}}$ density. This last case also occurs for other densities as, for example, the $\phi_1^{(n);\mu;g_0}$ and $\phi_1^{*(n);\mu}$ tests when $g_0=f_{\mathrm{C}_{0.45}}$ and $k'=3$, in Table 4.5; $\phi_3^{(n);\mu;g_0}$, $\phi_3^{*(n);\mu}$, $\phi_3^{(n);g_0}$ and $\phi_{f_{\mathrm{C}_{0.25}};3}^{*(n)}$ tests when $g_0=f_{\mathrm{C}_{0.45}}$ and $k'=1$, in Table 4.7; $\phi_3^{(n);g_0}$ and $\phi_{f_{\mathrm{C}_{0.25}};3}^{*(n)}$ tests when $g_0=f_{\mathrm{WN}_{0.5}}$ or $g_0=f_{\mathrm{WN}_{0.9}}$ and $k'=1$, in Table 4.8.

Using the asymptotic distribution for calibrating the test. To improve the calibration results when the sample size is too small ($n=30$), one can think in nonparametric techniques. Replicating the proposal of Pewsey (2002), the employed method, for generating resamples under the null hypothesis of symmetry, was sampling with replacement from $\{\Theta_1,\ldots,\Theta_n,2\hat{\mu}^{(n)}-\Theta_1,2\hat{\mu}^{(n)}-\Theta_n\}$ to generate the

new bootstrap resamples of size n and, then, compute their associated test statistic value. Observing the obtained results in Table 4.9, the conclusion is that it is not worthwhile the extra computational time to obtain the p–value with the bootstrap method.

Wrong selection of the base density in the parametric test. In order to determine the behaviour of the parametric tests for reflective symmetry under different densities from those used as base symmetric densities, in Tables 4.10, 4.11 and 4.12, the parametric test (with $\mathtt{k} = 2$) was used for computing the percentage of rejections, using as f_0 the following densities: $f_{\mathrm{VM}_{10}}$, f_{C_ρ} and $f_{\mathrm{WC}_{0.5}}$. In Tables 4.10–4.12, it is observed the high impact of wrongly determine the base density on the parametric test statistic, specially when the location parameter is unknown, a clear example of this fact can be found (in Table 4.12) in the poor calibration of the parametric test (using the wrong underlying density) when the sample is generated from the wrapped normal density with concentration parameter 0.9.

Using other base densities in the semiparametric test. Tables 4.13 and 4.14 together with Tables 4.2–4.4 can be used to compare the percentage of rejections of the semiparametric proposal with unknown central direction (and $\mathtt{k} = 2$) under other base densities f_0: $f_{\mathrm{C}_{0.45}}$ and $f_{\mathrm{WC}_{0.5}}$. From Tables 4.13 and 4.14, the little impact of the base density in the semiparametric scenario is observed, since they all provide, in the reported scenarios, a similar percentage of rejections as in Tables 4.2–4.4.

Using the Ley and Verdebout (2014) proposal when μ is unknown. Also, Tables 4.13 and 4.14 report the percentage of rejections when it is used the semiparametric proposal with "known" central direction estimated from the sample, $\phi_2^{*(n);\hat{\mu}^{(n)}}$, in order to analyse the impact of estimating μ in the Ley and Verdebout (2014) proposal. On these tables, the already mentioned high impact of using the test with known location parameter, when it is unknown (estimating it), is observed. A clear example of the bad calibration using the Ley and Verdebout (2014) proposal estimating the location parameter from the sample can be found when the data is generated from concentrated densities as $f_{\mathrm{WN}_{0.9}}$ (Table 4.17).

In Tables 4.15 and 4.16 the behaviour of the known location test when imposing a wrong parameter of μ can be observed. In most of the cases, even an slight perturbation in the location parameter has an important effect in the calibration of the test. For example, imposing a wrong location, translated by $\pi/16$, for large sample sizes ($n = 500$) in all the simulated densities, with the exception of $f_{\mathrm{C}_{0.45}}$, the percentage of rejections under the null is always above the significance level. Suggesting that the Ley and Verdebout (2014) proposal should not be used unless the location parameter is clearly known.

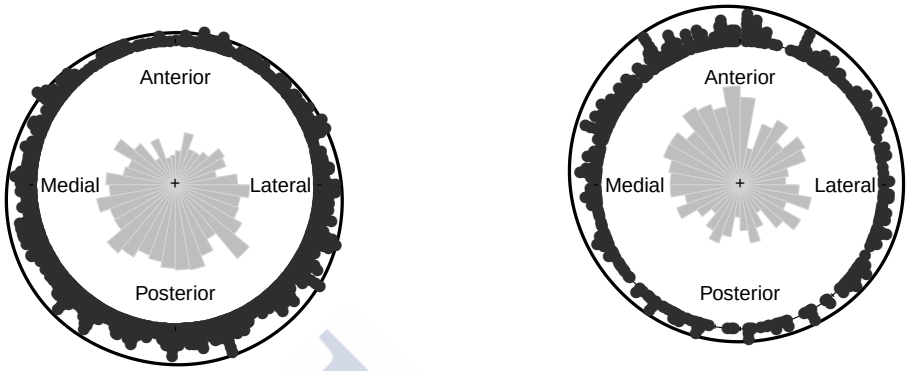

Figure 4.2: Raw circular plot, rose diagram and density estimate for the cracks in the cemented femoral components in the proximal (left) and the distal region (right).

Behaviour of the test under other models. In Table 4.17, the percentage of rejections using the semiparametric test with known and unknown central direction are calculated under other alternatives. With this objective, it was simulated samples of size $n = 30, 100, 500$ from the Kato and Jones (2012) distribution, with parameters $\mu = 0$, $r = 0.5$, $\kappa = 0.5, 0.9$ and skewness parameter $\nu = 0, 0.2, 0.4, 0.6$; and the three–parameter asymmetric submodel given in the Equation (7) of Kato and Jones (2015), with parameters $\mu = 0$, $\gamma = 0.5, 0.9$, $\bar{\beta}_2 = \nu\gamma(1-\gamma)$ and skewness parameter $\nu = 0, 0.2, 0.4, 0.6$ (see Appendix A). Under these other alternatives, the test with known and unknown central location provides, in general, good results as the power increases with the sample size and the skewness of the model.

4.4 Cracks in cemented femoral components

To illustrate the application of the new test for circular symmetry, the angles of the fatigue cracks around the cemented femoral components, described in Section 1.3.4, will be considered. The objective is to test if these cracks are symmetrically distributed around a central direction in both regions distinguished in the femur (proximal, close to the hip, and distal, close to the knee). In this study the entire sample will be taken, with the exception of an outlier bone, as Mann et al. (2003) reported that this specimen had an inferior cement mantle with substantial stem–cement voids and,

	λ	0			0.2			0.4			0.6		
	n	30	100	500	30	100	500	30	100	500	30	100	500
	$\mathtt{k}'$	$g_0 = f_{\mathrm{VM}_1}$											
$Q_2^{(n);\mu;g_0}$	1	0.050	0.046	0.050	0.057	0.087	0.306	0.097	0.232	0.797	0.145	0.463	0.990
$Q_2^{*(n);\mu}$		0.053	0.043	0.048	0.051	0.088	0.298	0.095	0.232	0.802	0.148	0.473	0.990
$Q_2^{(n);g_0}$		0.057	0.043	0.056	0.046	0.046	0.054	0.046	0.044	0.068	0.036	0.064	0.219
$Q_{f_{\mathrm{VM}_\kappa};2}^{*(n)}$		0.033	0.036	0.050	0.029	0.043	0.056	0.038	0.038	0.068	0.044	0.079	0.248
$Q_{f_{\mathrm{C}_{0.25}};2}^{*(n)}$		0.033	0.037	0.048	0.030	0.045	0.056	0.039	0.040	0.066	0.045	0.078	0.250
$Q_2^{(n);\mu;g_0}$	2	0.050	0.046	0.050	0.100	0.295	0.895	0.349	0.825	1	0.648	0.994	1
$Q_2^{*(n);\mu}$		0.053	0.043	0.048	0.111	0.293	0.897	0.347	0.826	1	0.646	0.995	1
$Q_2^{(n);g_0}$		0.057	0.043	0.056	0.069	0.211	0.783	0.195	0.605	0.999	0.351	0.826	1
$Q_{f_{\mathrm{VM}_\kappa};2}^{*(n)}$		0.033	0.036	0.050	0.039	0.183	0.777	0.139	0.550	0.999	0.235	0.747	1
$Q_{f_{\mathrm{C}_{0.25}};2}^{*(n)}$		0.033	0.037	0.048	0.043	0.180	0.773	0.140	0.551	0.999	0.237	0.758	1
$Q_2^{(n);\mu;g_0}$	3	0.050	0.046	0.050	0.062	0.100	0.321	0.103	0.256	0.823	0.164	0.475	0.991
$Q_2^{*(n);\mu}$		0.053	0.043	0.048	0.061	0.105	0.319	0.107	0.259	0.823	0.172	0.482	0.991
$Q_2^{(n);g_0}$		0.057	0.043	0.056	0.053	0.077	0.293	0.086	0.218	0.794	0.122	0.405	0.982
$Q_{f_{\mathrm{VM}_\kappa};2}^{*(n)}$		0.033	0.036	0.050	0.032	0.065	0.288	0.057	0.198	0.777	0.086	0.343	0.975
$Q_{f_{\mathrm{C}_{0.25}};2}^{*(n)}$		0.033	0.037	0.048	0.029	0.059	0.262	0.058	0.182	0.725	0.082	0.306	0.952
	$\mathtt{k}'$	$g_0 = f_{\mathrm{VM}_{10}}$											
$Q_2^{(n);\mu;g_0}$	1	0.049	0.046	0.044	0.060	0.085	0.282	0.097	0.233	0.786	0.163	0.476	0.983
$Q_2^{*(n);\mu}$		0.051	0.042	0.044	0.058	0.090	0.282	0.095	0.234	0.791	0.162	0.464	0.986
$Q_2^{(n);g_0}$		0.050	0.047	0.040	0.045	0.045	0.034	0.045	0.040	0.039	0.047	0.036	0.044
$Q_{f_{\mathrm{VM}_\kappa};2}^{*(n)}$		0.028	0.040	0.040	0.029	0.037	0.034	0.029	0.030	0.041	0.027	0.038	0.053
$Q_{f_{\mathrm{C}_{0.25}};2}^{*(n)}$		0.028	0.041	0.039	0.029	0.037	0.034	0.028	0.031	0.041	0.027	0.038	0.053
$Q_2^{(n);\mu;g_0}$	2	0.049	0.046	0.044	0.083	0.183	0.694	0.222	0.586	0.998	0.417	0.911	1
$Q_2^{*(n);\mu}$		0.051	0.042	0.044	0.083	0.190	0.699	0.230	0.586	0.998	0.431	0.918	1
$Q_2^{(n);g_0}$		0.050	0.047	0.040	0.052	0.053	0.044	0.045	0.051	0.070	0.032	0.040	0.053
$Q_{f_{\mathrm{VM}_\kappa};2}^{*(n)}$		0.028	0.040	0.040	0.029	0.044	0.046	0.038	0.042	0.068	0.037	0.047	0.068
$Q_{f_{\mathrm{C}_{0.25}};2}^{*(n)}$		0.028	0.041	0.039	0.028	0.044	0.045	0.037	0.042	0.068	0.035	0.047	0.067
$Q_2^{(n);\mu;g_0}$	3	0.049	0.046	0.044	0.107	0.238	0.843	0.273	0.728	1	0.575	0.977	1
$Q_2^{*(n);\mu}$		0.051	0.042	0.044	0.104	0.243	0.842	0.280	0.743	1	0.581	0.982	1
$Q_2^{(n);g_0}$		0.050	0.047	0.040	0.061	0.058	0.138	0.050	0.098	0.412	0.059	0.138	0.543
$Q_{f_{\mathrm{VM}_\kappa};2}^{*(n)}$		0.028	0.040	0.040	0.034	0.057	0.146	0.033	0.087	0.397	0.031	0.091	0.524
$Q_{f_{\mathrm{C}_{0.25}};2}^{*(n)}$		0.028	0.041	0.039	0.033	0.057	0.144	0.033	0.086	0.400	0.030	0.089	0.524

Table 4.2: Percentages of rejections for testing symmetry, with 1000 simulations.

	λ	0			0.2			0.4			0.6		
	n	30	100	500	30	100	500	30	100	500	30	100	500
	k′	$g_0 = f_{\mathrm{C}_{0.45}}$											
$Q_2^{(n);\mu;g_0}$	1	0.056	0.057	0.042	0.068	0.090	0.285	0.106	0.260	0.814	0.175	0.489	0.993
$Q_2^{*(n);\mu}$		0.061	0.057	0.041	0.070	0.093	0.287	0.103	0.252	0.811	0.171	0.484	0.992
$Q_2^{(n);g_0}$		0.054	0.061	0.044	0.041	0.064	0.246	0.042	0.101	0.485	0.025	0.055	0.338
$Q_{f_{\mathrm{VM}_\kappa};2}^{*(n)}$		0.049	0.057	0.038	0.045	0.067	0.269	0.055	0.148	0.577	0.048	0.118	0.488
$Q_{f_{\mathrm{C}_{0.25}};2}^{*(n)}$		0.049	0.057	0.038	0.044	0.067	0.272	0.056	0.150	0.586	0.048	0.120	0.504
$Q_2^{(n);\mu;g_0}$	2	0.056	0.057	0.042	0.120	0.289	0.905	0.336	0.830	1	0.661	0.991	1
$Q_2^{*(n);\mu}$		0.061	0.057	0.041	0.119	0.292	0.905	0.342	0.834	1	0.667	0.991	1
$Q_2^{(n);g_0}$		0.054	0.061	0.044	0.073	0.261	0.890	0.200	0.729	1	0.402	0.948	1
$Q_{f_{\mathrm{VM}_\kappa};2}^{*(n)}$		0.049	0.057	0.038	0.083	0.274	0.901	0.205	0.763	1	0.373	0.950	1
$Q_{f_{\mathrm{C}_{0.25}};2}^{*(n)}$		0.049	0.057	0.038	0.084	0.275	0.901	0.210	0.767	1	0.378	0.957	1
$Q_2^{(n);\mu;g_0}$	3	0.056	0.057	0.042	0.057	0.094	0.296	0.113	0.237	0.829	0.157	0.493	0.989
$Q_2^{*(n);\mu}$		0.061	0.057	0.041	0.058	0.100	0.299	0.112	0.237	0.832	0.157	0.496	0.988
$Q_2^{(n);g_0}$		0.054	0.061	0.044	0.051	0.092	0.287	0.070	0.217	0.816	0.105	0.435	0.987
$Q_{f_{\mathrm{VM}_\kappa};2}^{*(n)}$		0.049	0.057	0.038	0.050	0.085	0.302	0.074	0.215	0.802	0.106	0.408	0.981
$Q_{f_{\mathrm{C}_{0.25}};2}^{*(n)}$		0.049	0.057	0.038	0.046	0.086	0.302	0.075	0.213	0.806	0.107	0.399	0.984
	k′	$g_0 = f_{\mathrm{WN}_{0.5}}$											
$Q_2^{(n);\mu;g_0}$	1	0.054	0.048	0.052	0.066	0.113	0.354	0.117	0.292	0.894	0.202	0.578	0.997
$Q_2^{*(n);\mu}$		0.052	0.053	0.049	0.065	0.112	0.351	0.111	0.294	0.895	0.212	0.579	0.998
$Q_2^{(n);g_0}$		0.036	0.047	0.052	0.040	0.059	0.145	0.033	0.066	0.223	0.021	0.040	0.112
$Q_{f_{\mathrm{VM}_\kappa};2}^{*(n)}$		0.030	0.041	0.050	0.039	0.059	0.148	0.037	0.077	0.257	0.041	0.058	0.167
$Q_{f_{\mathrm{C}_{0.25}};2}^{*(n)}$		0.028	0.042	0.049	0.040	0.060	0.149	0.036	0.077	0.268	0.043	0.062	0.170
$Q_2^{(n);\mu;g_0}$	2	0.054	0.048	0.052	0.116	0.289	0.894	0.327	0.826	1	0.656	0.995	1
$Q_2^{*(n);\mu}$		0.052	0.053	0.049	0.112	0.289	0.896	0.329	0.825	1	0.669	0.996	1
$Q_2^{(n);g_0}$		0.036	0.047	0.052	0.090	0.243	0.864	0.210	0.717	1	0.399	0.941	1
$Q_{f_{\mathrm{VM}_\kappa};2}^{*(n)}$		0.030	0.041	0.050	0.084	0.249	0.866	0.186	0.728	1	0.355	0.930	1
$Q_{f_{\mathrm{C}_{0.25}};2}^{*(n)}$		0.028	0.042	0.049	0.085	0.254	0.869	0.187	0.731	1	0.359	0.935	1
$Q_2^{(n);\mu;g_0}$	3	0.054	0.048	0.052	0.062	0.118	0.364	0.114	0.284	0.889	0.187	0.553	0.999
$Q_2^{*(n);\mu}$		0.052	0.053	0.049	0.061	0.118	0.363	0.114	0.277	0.889	0.189	0.558	0.999
$Q_2^{(n);g_0}$		0.036	0.047	0.052	0.050	0.112	0.354	0.084	0.265	0.893	0.167	0.531	0.999
$Q_{f_{\mathrm{VM}_\kappa};2}^{*(n)}$		0.030	0.041	0.050	0.062	0.111	0.387	0.086	0.269	0.912	0.165	0.534	1
$Q_{f_{\mathrm{C}_{0.25}};2}^{*(n)}$		0.028	0.042	0.049	0.062	0.108	0.374	0.082	0.259	0.903	0.152	0.509	1

Table 4.3: Percentages of rejections for testing symmetry, with 1000 simulations.

	λ	0			0.2			0.4			0.6		
	n	30	100	500	30	100	500	30	100	500	30	100	500
	k′	$g_0 = f_{\mathrm{WN}_{0.9}}$											
$Q_2^{(n);\mu;g_0}$	1	0.043	0.047	0.053	0.059	0.109	0.437	0.109	0.339	0.954	0.227	0.671	1
$Q_2^{*(n);\mu}$		0.050	0.041	0.055	0.069	0.112	0.434	0.100	0.340	0.953	0.230	0.679	1
$Q_2^{(n);g_0}$		0.052	0.050	0.059	0.044	0.047	0.051	0.047	0.041	0.058	0.030	0.031	0.051
$Q_{f_{\mathrm{VM}_\kappa};2}^{*(n)}$		0.024	0.044	0.060	0.033	0.044	0.055	0.032	0.039	0.063	0.033	0.036	0.065
$Q_{f_{\mathrm{C}_{0.25}};2}^{*(n)}$		0.024	0.046	0.057	0.032	0.044	0.055	0.028	0.039	0.065	0.032	0.035	0.063
$Q_2^{(n);\mu;g_0}$	2	0.043	0.047	0.053	0.089	0.219	0.824	0.263	0.717	1	0.564	0.982	1
$Q_2^{*(n);\mu}$		0.050	0.041	0.055	0.091	0.227	0.825	0.263	0.731	1	0.571	0.983	1
$Q_2^{(n);g_0}$		0.052	0.050	0.059	0.050	0.068	0.128	0.055	0.088	0.354	0.051	0.124	0.446
$Q_{f_{\mathrm{VM}_\kappa};2}^{*(n)}$		0.024	0.044	0.060	0.043	0.051	0.133	0.031	0.066	0.357	0.024	0.104	0.462
$Q_{f_{\mathrm{C}_{0.25}};2}^{*(n)}$		0.024	0.046	0.057	0.042	0.050	0.129	0.030	0.063	0.359	0.023	0.098	0.463
$Q_2^{(n);\mu;g_0}$	3	0.043	0.047	0.053	0.097	0.233	0.829	0.275	0.737	1	0.599	0.986	1
$Q_2^{*(n);\mu}$		0.050	0.041	0.055	0.096	0.232	0.824	0.280	0.741	1	0.608	0.988	1
$Q_2^{(n);g_0}$		0.052	0.050	0.059	0.073	0.113	0.483	0.131	0.326	0.951	0.194	0.546	0.998
$Q_{f_{\mathrm{VM}_\kappa};2}^{*(n)}$		0.024	0.044	0.060	0.049	0.123	0.486	0.077	0.297	0.958	0.123	0.497	0.997
$Q_{f_{\mathrm{C}_{0.25}};2}^{*(n)}$		0.024	0.046	0.057	0.048	0.120	0.483	0.076	0.291	0.956	0.122	0.493	0.997
	k′	$g_0 = f_{\mathrm{WC}_{0.5}}$											
$Q_2^{(n);\mu;g_0}$	1	0.058	0.041	0.045	0.061	0.098	0.241	0.092	0.222	0.682	0.132	0.389	0.959
$Q_2^{*(n);\mu}$		0.054	0.043	0.047	0.062	0.097	0.241	0.084	0.213	0.691	0.133	0.387	0.962
$Q_2^{(n);g_0}$		0.045	0.054	0.043	0.046	0.064	0.162	0.059	0.122	0.507	0.083	0.264	0.894
$Q_{f_{\mathrm{VM}_\kappa};2}^{*(n)}$		0.038	0.053	0.053	0.051	0.069	0.227	0.077	0.187	0.719	0.120	0.427	0.979
$Q_{f_{\mathrm{C}_{0.25}};2}^{*(n)}$		0.038	0.053	0.050	0.051	0.071	0.220	0.076	0.187	0.703	0.117	0.412	0.974
$Q_2^{(n);\mu;g_0}$	2	0.058	0.041	0.045	0.114	0.294	0.852	0.322	0.807	1	0.629	0.985	1
$Q_2^{*(n);\mu}$		0.054	0.043	0.047	0.110	0.292	0.852	0.325	0.808	1	0.624	0.987	1
$Q_2^{(n);g_0}$		0.045	0.054	0.043	0.069	0.144	0.478	0.113	0.372	0.957	0.219	0.628	0.997
$Q_{f_{\mathrm{VM}_\kappa};2}^{*(n)}$		0.038	0.053	0.053	0.060	0.123	0.417	0.106	0.310	0.910	0.160	0.467	0.990
$Q_{f_{\mathrm{C}_{0.25}};2}^{*(n)}$		0.038	0.053	0.050	0.064	0.130	0.432	0.107	0.320	0.914	0.168	0.485	0.991
$Q_2^{(n);\mu;g_0}$	3	0.058	0.041	0.045	0.067	0.113	0.334	0.110	0.290	0.857	0.186	0.531	0.997
$Q_2^{*(n);\mu}$		0.054	0.043	0.047	0.067	0.114	0.336	0.110	0.289	0.859	0.190	0.543	0.996
$Q_2^{(n);g_0}$		0.045	0.054	0.043	0.046	0.061	0.057	0.056	0.060	0.088	0.047	0.060	0.127
$Q_{f_{\mathrm{VM}_\kappa};2}^{*(n)}$		0.038	0.053	0.053	0.051	0.074	0.152	0.074	0.128	0.413	0.097	0.206	0.679
$Q_{f_{\mathrm{C}_{0.25}};2}^{*(n)}$		0.038	0.053	0.050	0.049	0.072	0.127	0.072	0.111	0.323	0.088	0.169	0.552

Table 4.4: Percentages of rejections for testing symmetry, with 1000 simulations.

	λ	0			0.2			0.4			0.6		
	n	30	100	500	30	100	500	30	100	500	30	100	500
	k′	$g_0 = f_{\mathrm{VM}_1}$											
$Q_1^{(n);\mu;g_0}$	1	0.040	0.050	0.052	0.125	0.302	0.862	0.326	0.788	1	0.636	0.995	1
$Q_1^{*(n);\mu}$		0.043	0.052	0.052	0.115	0.302	0.865	0.330	0.791	1	0.650	0.996	1
$Q_{f_{\mathrm{C}_{0.25}};1}^{*(n)}$		0.033	0.036	0.045	0.035	0.043	0.052	0.045	0.040	0.065	0.046	0.073	0.245
$Q_1^{(n);\mu;g_0}$	2	0.040	0.050	0.052	0.076	0.116	0.337	0.127	0.281	0.845	0.196	0.512	0.993
$Q_1^{*(n);\mu}$		0.043	0.052	0.052	0.074	0.114	0.334	0.127	0.279	0.845	0.190	0.516	0.992
$Q_{f_{\mathrm{C}_{0.25}};1}^{*(n)}$		0.033	0.036	0.045	0.045	0.177	0.740	0.133	0.535	0.998	0.220	0.753	1
$Q_1^{(n);\mu;g_0}$	3	0.040	0.050	0.052	0.058	0.061	0.084	0.052	0.051	0.131	0.060	0.083	0.204
$Q_1^{*(n);\mu}$		0.043	0.052	0.052	0.060	0.060	0.085	0.049	0.057	0.127	0.061	0.084	0.203
$Q_{f_{\mathrm{C}_{0.25}};1}^{*(n)}$		0.033	0.036	0.045	0.029	0.050	0.105	0.044	0.082	0.263	0.042	0.109	0.462
	k′	$g_0 = f_{\mathrm{VM}_{10}}$											
$Q_1^{(n);\mu;g_0}$	1	0.051	0.046	0.043	0.059	0.093	0.282	0.101	0.241	0.788	0.168	0.491	0.984
$Q_1^{*(n);\mu}$		0.045	0.043	0.044	0.057	0.095	0.285	0.101	0.235	0.793	0.167	0.482	0.986
$Q_{f_{\mathrm{C}_{0.25}};1}^{*(n)}$		0.027	0.039	0.038	0.028	0.036	0.035	0.028	0.031	0.041	0.027	0.037	0.052
$Q_1^{(n);\mu;g_0}$	2	0.051	0.046	0.043	0.082	0.179	0.681	0.224	0.575	0.998	0.413	0.903	1
$Q_1^{*(n);\mu}$		0.045	0.043	0.044	0.078	0.186	0.693	0.218	0.584	0.997	0.434	0.913	1
$Q_{f_{\mathrm{C}_{0.25}};1}^{*(n)}$		0.027	0.039	0.038	0.028	0.043	0.043	0.034	0.041	0.068	0.034	0.046	0.065
$Q_1^{(n);\mu;g_0}$	3	0.051	0.046	0.043	0.101	0.221	0.811	0.259	0.702	1	0.535	0.970	1
$Q_1^{*(n);\mu}$		0.045	0.043	0.044	0.101	0.231	0.808	0.263	0.718	1	0.563	0.975	1
$Q_{f_{\mathrm{C}_{0.25}};1}^{*(n)}$		0.027	0.039	0.038	0.032	0.058	0.142	0.033	0.078	0.393	0.030	0.088	0.521
	k′	$g_0 = f_{\mathrm{C}_{0.45}}$											
$Q_1^{(n);\mu;g_0}$	1	0.039	0.053	0.057	0.123	0.299	0.876	0.334	0.829	1	0.673	0.996	1
$Q_1^{*(n);\mu}$		0.036	0.050	0.056	0.121	0.306	0.880	0.332	0.834	1	0.679	0.998	1
$Q_1^{(n);g_0}$		0.059	0.052	0.052	0.046	0.087	0.311	0.048	0.133	0.630	0.035	0.069	0.499
$Q_{f_{\mathrm{C}_{0.25}};1}^{*(n)}$		0.048	0.057	0.046	0.048	0.088	0.311	0.052	0.180	0.685	0.051	0.162	0.648
$Q_1^{(n);\mu;g_0}$	2	0.039	0.053	0.057	0.063	0.088	0.311	0.105	0.239	0.812	0.179	0.461	0.988
$Q_1^{*(n);\mu}$		0.036	0.050	0.056	0.059	0.091	0.311	0.108	0.242	0.811	0.177	0.466	0.989
$Q_1^{(n);g_0}$		0.059	0.052	0.052	0.083	0.193	0.764	0.169	0.588	1	0.321	0.903	1
$Q_{f_{\mathrm{C}_{0.25}};1}^{*(n)}$		0.048	0.057	0.046	0.086	0.264	0.884	0.209	0.750	1	0.366	0.958	1
$Q_1^{(n);\mu;g_0}$	3	0.039	0.053	0.057	0.057	0.048	0.064	0.067	0.042	0.053	0.059	0.052	0.038
$Q_1^{*(n);\mu}$		0.036	0.050	0.056	0.055	0.048	0.063	0.068	0.045	0.052	0.064	0.048	0.036
$Q_1^{(n);g_0}$		0.059	0.052	0.052	0.048	0.054	0.066	0.040	0.045	0.037	0.039	0.047	0.045
$Q_{f_{\mathrm{C}_{0.25}};1}^{*(n)}$		0.048	0.057	0.046	0.046	0.068	0.123	0.056	0.085	0.327	0.057	0.178	0.605

Table 4.5: Percentages of rejections for testing symmetry, with 1000 simulations.

	λ	0			0.2			0.4			0.6		
	n	30	100	500	30	100	500	30	100	500	30	100	500
	k′	$g_0 = f_{\mathrm{WN}_{0.5}}$											
$Q_1^{(n);\mu;g_0}$	1	0.045	0.048	0.046	0.114	0.238	0.879	0.301	0.792	1	0.629	0.990	1
$Q_1^{*(n);\mu}$		0.046	0.049	0.047	0.109	0.233	0.880	0.303	0.789	1	0.647	0.991	1
$Q_1^{(n);g_0}$		0.039	0.047	0.063	0.052	0.048	0.155	0.041	0.065	0.276	0.022	0.044	0.152
$Q_{f_{\mathrm{C}_{0.25}};1}^{*(n)}$		0.019	0.048	0.058	0.043	0.056	0.168	0.033	0.090	0.312	0.036	0.068	0.222
$Q_1^{(n);\mu;g_0}$	2	0.045	0.048	0.046	0.052	0.113	0.357	0.119	0.296	0.913	0.209	0.586	0.999
$Q_1^{*(n);\mu}$		0.046	0.049	0.047	0.057	0.112	0.354	0.120	0.301	0.914	0.207	0.588	0.999
$Q_1^{(n);g_0}$		0.039	0.047	0.063	0.083	0.218	0.783	0.176	0.626	0.998	0.361	0.902	1
$Q_{f_{\mathrm{C}_{0.25}};1}^{*(n)}$		0.019	0.048	0.058	0.080	0.243	0.851	0.177	0.714	1	0.353	0.939	1
$Q_1^{(n);\mu;g_0}$	3	0.045	0.048	0.046	0.049	0.043	0.057	0.051	0.048	0.088	0.041	0.049	0.109
$Q_1^{*(n);\mu}$		0.046	0.049	0.047	0.051	0.045	0.060	0.050	0.049	0.089	0.047	0.052	0.107
$Q_1^{(n);g_0}$		0.039	0.047	0.063	0.050	0.064	0.088	0.047	0.070	0.186	0.044	0.100	0.353
$Q_{f_{\mathrm{C}_{0.25}};1}^{*(n)}$		0.019	0.048	0.058	0.058	0.084	0.169	0.052	0.140	0.525	0.095	0.237	0.866
	k′	$g_0 = f_{\mathrm{WN}_{0.9}}$											
$Q_1^{(n);\mu;g_0}$	1	0.037	0.042	0.055	0.064	0.117	0.460	0.111	0.367	0.966	0.236	0.694	1
$Q_1^{*(n);\mu}$		0.048	0.043	0.054	0.067	0.115	0.462	0.113	0.364	0.967	0.253	0.703	1
$Q_1^{(n);g_0}$		0.051	0.056	0.052	0.045	0.049	0.052	0.043	0.041	0.062	0.032	0.030	0.045
$Q_{f_{\mathrm{C}_{0.25}};1}^{*(n)}$		0.023	0.043	0.057	0.029	0.038	0.053	0.020	0.037	0.061	0.029	0.031	0.059
$Q_1^{(n);\mu;g_0}$	2	0.037	0.042	0.055	0.098	0.213	0.787	0.239	0.685	1	0.532	0.974	1
$Q_1^{*(n);\mu}$		0.048	0.043	0.054	0.093	0.212	0.789	0.249	0.703	1	0.558	0.979	1
$Q_1^{(n);g_0}$		0.051	0.056	0.052	0.048	0.068	0.133	0.054	0.087	0.349	0.055	0.140	0.460
$Q_{f_{\mathrm{C}_{0.25}};1}^{*(n)}$		0.023	0.043	0.057	0.037	0.046	0.126	0.028	0.057	0.355	0.020	0.092	0.470
$Q_1^{(n);\mu;g_0}$	3	0.037	0.042	0.055	0.085	0.183	0.705	0.223	0.637	1	0.470	0.946	1
$Q_1^{*(n);\mu}$		0.048	0.043	0.054	0.081	0.191	0.708	0.237	0.640	1	0.505	0.947	1
$Q_1^{(n);g_0}$		0.051	0.056	0.052	0.073	0.108	0.446	0.128	0.308	0.941	0.189	0.519	0.998
$Q_{f_{\mathrm{C}_{0.25}};1}^{*(n)}$		0.023	0.043	0.057	0.041	0.104	0.470	0.071	0.275	0.948	0.111	0.480	0.995
	k′	$g_0 = f_{\mathrm{WC}_{0.5}}$											
$Q_1^{(n);\mu;g_0}$	1	0.051	0.056	0.046	0.098	0.241	0.763	0.268	0.708	1	0.544	0.963	1
$Q_1^{*(n);\mu}$		0.050	0.055	0.044	0.092	0.231	0.763	0.273	0.716	1	0.561	0.967	1
$Q_1^{(n);g_0}$		0.037	0.048	0.052	0.041	0.072	0.263	0.062	0.173	0.742	0.102	0.363	0.979
$Q_{f_{\mathrm{C}_{0.25}};1}^{*(n)}$		0.036	0.056	0.045	0.050	0.068	0.198	0.062	0.163	0.616	0.098	0.358	0.949
$Q_1^{(n);\mu;g_0}$	2	0.051	0.056	0.046	0.066	0.083	0.257	0.103	0.233	0.769	0.165	0.454	0.982
$Q_1^{*(n);\mu}$		0.050	0.055	0.044	0.061	0.090	0.259	0.114	0.227	0.768	0.171	0.456	0.981
$Q_1^{(n);g_0}$		0.037	0.048	0.052	0.047	0.077	0.271	0.090	0.217	0.707	0.137	0.344	0.892
$Q_{f_{\mathrm{C}_{0.25}};1}^{*(n)}$		0.036	0.056	0.045	0.063	0.132	0.450	0.100	0.324	0.923	0.163	0.506	0.994
$Q_1^{(n);\mu;g_0}$	3	0.051	0.056	0.046	0.055	0.057	0.093	0.046	0.110	0.256	0.067	0.148	0.534
$Q_1^{*(n);\mu}$		0.050	0.055	0.044	0.055	0.051	0.097	0.054	0.110	0.262	0.076	0.152	0.533
$Q_1^{(n);g_0}$		0.037	0.048	0.052	0.047	0.119	0.392	0.111	0.326	0.897	0.184	0.546	0.990
$Q_{f_{\mathrm{C}_{0.25}};1}^{*(n)}$		0.036	0.056	0.045	0.041	0.064	0.057	0.056	0.067	0.105	0.057	0.066	0.157

Table 4.6: Percentages of rejections for testing symmetry, with 1000 simulations.

	λ	0			0.2			0.4			0.6		
	n	30	100	500	30	100	500	30	100	500	30	100	500
	k′	$g_0 = f_{\mathrm{VM}_1}$											
$Q_3^{(n);\mu;g_0}$	1	0.044	0.072	0.056	0.048	0.047	0.049	0.041	0.058	0.092	0.050	0.081	0.153
$Q_3^{*(n);\mu}$		0.043	0.070	0.056	0.043	0.048	0.049	0.046	0.061	0.091	0.053	0.083	0.150
$Q_3^{(n);g_0}$		0.045	0.069	0.064	0.046	0.040	0.038	0.051	0.046	0.056	0.053	0.056	0.088
$Q_{f_{\mathrm{C}_{0.25}};3}^{*(n)}$		0.025	0.040	0.062	0.028	0.034	0.033	0.024	0.037	0.059	0.027	0.048	0.094
$Q_3^{(n);\mu;g_0}$	2	0.044	0.072	0.056	0.056	0.096	0.298	0.088	0.240	0.818	0.148	0.480	0.994
$Q_3^{*(n);\mu}$		0.043	0.070	0.056	0.065	0.096	0.299	0.090	0.245	0.818	0.149	0.474	0.994
$Q_3^{(n);g_0}$		0.045	0.069	0.064	0.054	0.074	0.220	0.059	0.146	0.530	0.080	0.221	0.672
$Q_{f_{\mathrm{C}_{0.25}};3}^{*(n)}$		0.025	0.040	0.062	0.029	0.052	0.247	0.035	0.159	0.697	0.074	0.282	0.924
$Q_3^{(n);\mu;g_0}$	3	0.044	0.072	0.056	0.118	0.298	0.897	0.313	0.812	1	0.651	0.990	1
$Q_3^{*(n);\mu}$		0.043	0.070	0.056	0.124	0.299	0.896	0.318	0.810	1	0.660	0.992	1
$Q_3^{(n);g_0}$		0.045	0.069	0.064	0.091	0.231	0.875	0.196	0.700	1	0.397	0.936	1
$Q_{f_{\mathrm{C}_{0.25}};3}^{*(n)}$		0.025	0.040	0.062	0.047	0.180	0.850	0.096	0.581	1	0.226	0.797	1
	k′	$g_0 = f_{\mathrm{VM}_{10}}$											
$Q_3^{(n);\mu;g_0}$	1	0.054	0.046	0.040	0.055	0.084	0.255	0.081	0.209	0.746	0.138	0.440	0.971
$Q_3^{*(n);\mu}$		0.051	0.046	0.041	0.055	0.088	0.255	0.082	0.214	0.746	0.135	0.432	0.972
$Q_3^{(n);g_0}$		0.044	0.051	0.033	0.040	0.048	0.035	0.043	0.043	0.037	0.043	0.038	0.044
$Q_{f_{\mathrm{C}_{0.25}};3}^{*(n)}$		0.028	0.045	0.040	0.029	0.037	0.033	0.029	0.033	0.038	0.028	0.042	0.053
$Q_3^{(n);\mu;g_0}$	2	0.054	0.046	0.040	0.081	0.177	0.680	0.206	0.553	0.997	0.394	0.902	1
$Q_3^{*(n);\mu}$		0.051	0.046	0.041	0.082	0.182	0.682	0.213	0.563	0.997	0.412	0.905	1
$Q_3^{(n);g_0}$		0.044	0.051	0.033	0.050	0.052	0.043	0.044	0.046	0.066	0.035	0.040	0.049
$Q_{f_{\mathrm{C}_{0.25}};3}^{*(n)}$		0.028	0.045	0.040	0.030	0.045	0.044	0.041	0.042	0.064	0.041	0.049	0.066
$Q_3^{(n);\mu;g_0}$	3	0.054	0.046	0.040	0.102	0.247	0.858	0.287	0.758	0.999	0.568	0.985	1
$Q_3^{*(n);\mu}$		0.051	0.046	0.041	0.101	0.250	0.859	0.289	0.758	0.999	0.590	0.985	1
$Q_3^{(n);g_0}$		0.044	0.051	0.033	0.057	0.060	0.143	0.049	0.106	0.399	0.061	0.139	0.513
$Q_{f_{\mathrm{C}_{0.25}};3}^{*(n)}$		0.028	0.045	0.040	0.037	0.057	0.152	0.035	0.085	0.408	0.037	0.095	0.512
	k′	$g_0 = f_{\mathrm{C}_{0.45}}$											
$Q_3^{(n);\mu;g_0}$	1	0.056	0.052	0.046	0.059	0.044	0.050	0.053	0.040	0.044	0.049	0.043	0.041
$Q_3^{*(n);\mu}$		0.052	0.052	0.047	0.054	0.044	0.050	0.049	0.042	0.042	0.049	0.045	0.041
$Q_3^{(n);g_0}$		0.047	0.053	0.043	0.050	0.041	0.057	0.046	0.035	0.047	0.048	0.032	0.035
$Q_{f_{\mathrm{C}_{0.25}};3}^{*(n)}$		0.031	0.041	0.039	0.028	0.036	0.054	0.026	0.029	0.040	0.030	0.021	0.033
$Q_3^{(n);\mu;g_0}$	2	0.056	0.052	0.046	0.061	0.092	0.314	0.108	0.260	0.819	0.186	0.473	0.992
$Q_3^{*(n);\mu}$		0.052	0.052	0.047	0.061	0.092	0.314	0.118	0.250	0.819	0.174	0.476	0.992
$Q_3^{(n);g_0}$		0.047	0.053	0.043	0.061	0.075	0.268	0.098	0.181	0.645	0.119	0.247	0.754
$Q_{f_{\mathrm{C}_{0.25}};3}^{*(n)}$		0.031	0.041	0.039	0.030	0.064	0.283	0.073	0.187	0.786	0.098	0.337	0.962
$Q_3^{(n);\mu;g_0}$	3	0.056	0.052	0.046	0.134	0.307	0.897	0.361	0.814	1	0.660	0.993	1
$Q_3^{*(n);\mu}$		0.052	0.052	0.047	0.140	0.306	0.898	0.363	0.811	1	0.674	0.993	1
$Q_3^{(n);g_0}$		0.047	0.053	0.043	0.100	0.246	0.889	0.224	0.694	1	0.429	0.938	1
$Q_{f_{\mathrm{C}_{0.25}};3}^{*(n)}$		0.031	0.041	0.039	0.054	0.195	0.889	0.127	0.586	1	0.260	0.838	1

Table 4.7: Percentages of rejections for testing symmetry, with 1000 simulations.

	λ	0			0.2			0.4			0.6		
	n	30	100	500	30	100	500	30	100	500	30	100	500
	k′	$g_0 = f_{\mathrm{WN}_{0.5}}$											
$Q_3^{(n);\mu;g_0}$	1	0.034	0.048	0.041	0.050	0.062	0.056	0.048	0.055	0.071	0.046	0.054	0.092
$Q_3^{*(n);\mu}$		0.031	0.047	0.041	0.051	0.063	0.053	0.051	0.060	0.069	0.044	0.057	0.092
$Q_3^{(n);g_0}$		0.034	0.051	0.045	0.054	0.061	0.056	0.045	0.053	0.056	0.044	0.039	0.036
$Q_{f_{\mathrm{C}_{0.25}};3}^{*(n)}$		0.026	0.038	0.042	0.039	0.051	0.054	0.029	0.045	0.054	0.032	0.036	0.038
$Q_3^{(n);\mu;g_0}$	2	0.034	0.048	0.041	0.072	0.116	0.369	0.122	0.316	0.880	0.217	0.586	0.995
$Q_3^{*(n);\mu}$		0.031	0.047	0.041	0.069	0.112	0.370	0.128	0.311	0.879	0.220	0.583	0.995
$Q_3^{(n);g_0}$		0.034	0.051	0.045	0.076	0.105	0.329	0.088	0.227	0.747	0.127	0.294	0.861
$Q_{f_{\mathrm{C}_{0.25}};3}^{*(n)}$		0.026	0.038	0.042	0.051	0.093	0.355	0.066	0.254	0.837	0.117	0.408	0.982
$Q_3^{(n);\mu;g_0}$	3	0.034	0.048	0.041	0.121	0.334	0.884	0.347	0.807	1	0.679	0.989	1
$Q_3^{*(n);\mu}$		0.031	0.047	0.041	0.124	0.333	0.886	0.346	0.810	1	0.679	0.990	1
$Q_3^{(n);g_0}$		0.034	0.051	0.045	0.101	0.307	0.866	0.235	0.737	1	0.472	0.971	1
$Q_{f_{\mathrm{C}_{0.25}};3}^{*(n)}$		0.026	0.038	0.042	0.057	0.261	0.869	0.152	0.661	1	0.294	0.910	1
	k′	$g_0 = f_{\mathrm{WN}_{0.9}}$											
$Q_3^{(n);\mu;g_0}$	1	0.045	0.058	0.053	0.066	0.098	0.320	0.084	0.242	0.867	0.176	0.517	0.996
$Q_3^{*(n);\mu}$		0.048	0.058	0.054	0.061	0.097	0.320	0.083	0.237	0.872	0.172	0.517	0.996
$Q_3^{(n);g_0}$		0.052	0.057	0.060	0.040	0.051	0.060	0.049	0.037	0.061	0.033	0.031	0.053
$Q_{f_{\mathrm{C}_{0.25}};3}^{*(n)}$		0.030	0.050	0.066	0.040	0.048	0.056	0.040	0.041	0.064	0.039	0.040	0.070
$Q_3^{(n);\mu;g_0}$	2	0.045	0.058	0.053	0.081	0.216	0.753	0.229	0.654	1	0.496	0.956	1
$Q_3^{*(n);\mu}$		0.048	0.058	0.054	0.078	0.214	0.751	0.219	0.656	1	0.496	0.956	1
$Q_3^{(n);g_0}$		0.052	0.057	0.060	0.047	0.064	0.121	0.048	0.078	0.326	0.045	0.098	0.380
$Q_{f_{\mathrm{C}_{0.25}};3}^{*(n)}$		0.030	0.050	0.066	0.047	0.058	0.127	0.039	0.069	0.342	0.031	0.107	0.415
$Q_3^{(n);\mu;g_0}$	3	0.045	0.058	0.053	0.101	0.263	0.881	0.300	0.815	1	0.676	0.992	1
$Q_3^{*(n);\mu}$		0.048	0.058	0.054	0.103	0.262	0.884	0.296	0.816	1	0.675	0.993	1
$Q_3^{(n);g_0}$		0.052	0.057	0.060	0.071	0.123	0.488	0.132	0.333	0.959	0.195	0.537	0.995
$Q_{f_{\mathrm{C}_{0.25}};3}^{*(n)}$		0.030	0.050	0.066	0.057	0.121	0.494	0.086	0.308	0.955	0.139	0.501	0.995
	k′	$g_0 = f_{\mathrm{WC}_{0.5}}$											
$Q_3^{(n);\mu;g_0}$	1	0.069	0.055	0.065	0.052	0.077	0.086	0.067	0.109	0.218	0.091	0.142	0.406
$Q_3^{*(n);\mu}$		0.067	0.055	0.067	0.053	0.078	0.087	0.068	0.108	0.222	0.084	0.146	0.412
$Q_3^{(n);g_0}$		0.051	0.058	0.061	0.044	0.057	0.121	0.054	0.100	0.380	0.069	0.151	0.683
$Q_{f_{\mathrm{C}_{0.25}};3}^{*(n)}$		0.041	0.053	0.054	0.038	0.063	0.217	0.051	0.162	0.648	0.079	0.311	0.936
$Q_3^{(n);\mu;g_0}$	2	0.069	0.055	0.065	0.066	0.131	0.301	0.126	0.271	0.848	0.205	0.546	0.996
$Q_3^{*(n);\mu}$		0.067	0.055	0.067	0.064	0.122	0.308	0.122	0.276	0.847	0.197	0.547	0.996
$Q_3^{(n);g_0}$		0.051	0.058	0.061	0.035	0.061	0.049	0.051	0.051	0.051	0.042	0.056	0.057
$Q_{f_{\mathrm{C}_{0.25}};3}^{*(n)}$		0.041	0.053	0.054	0.031	0.053	0.138	0.049	0.101	0.400	0.075	0.153	0.617
$Q_3^{(n);\mu;g_0}$	3	0.069	0.055	0.065	0.133	0.317	0.873	0.334	0.822	1	0.654	0.991	1
$Q_3^{*(n);\mu}$		0.067	0.055	0.067	0.129	0.317	0.876	0.340	0.821	1	0.657	0.994	1
$Q_3^{(n);g_0}$		0.051	0.058	0.061	0.082	0.203	0.726	0.179	0.585	0.997	0.343	0.826	1
$Q_{f_{\mathrm{C}_{0.25}};3}^{*(n)}$		0.041	0.053	0.054	0.063	0.161	0.627	0.126	0.444	0.969	0.221	0.573	0.996

Table 4.8: Percentages of rejections for testing symmetry, with 1000 simulations.

	λ	0			0.2			0.4			0.6		
	n	30	100	500	30	100	500	30	100	500	30	100	500
	k′	$g_0 = f_{\mathrm{VM}_1}$											
$Q^{*(n)}_{f_{\mathrm{C}_{0.25}};2}$	1	0.037	0.037	0.051	0.038	0.048	0.056	0.044	0.044	0.068	0.049	0.080	0.245
$Q^{*(n)}_{f_{\mathrm{C}_{0.25}};2}$	2	0.033	0.038	0.056	0.047	0.175	0.771	0.147	0.551	0.999	0.241	0.746	1
$Q^{*(n)}_{f_{\mathrm{C}_{0.25}};2}$	3	0.037	0.037	0.054	0.039	0.064	0.260	0.065	0.188	0.718	0.089	0.306	0.949
	k′	$g_0 = f_{\mathrm{VM}_{10}}$											
$Q^{*(n)}_{f_{\mathrm{C}_{0.25}};2}$	1	0.029	0.047	0.044	0.029	0.039	0.037	0.035	0.037	0.041	0.026	0.044	0.051
$Q^{*(n)}_{f_{\mathrm{C}_{0.25}};2}$	2	0.029	0.042	0.039	0.032	0.045	0.042	0.039	0.041	0.070	0.041	0.046	0.069
$Q^{*(n)}_{f_{\mathrm{C}_{0.25}};2}$	3	0.025	0.044	0.041	0.038	0.055	0.144	0.038	0.081	0.393	0.033	0.090	0.528
	k′	$g_0 = f_{\mathrm{C}_{0.45}}$											
$Q^{*(n)}_{f_{\mathrm{C}_{0.25}};2}$	1	0.058	0.057	0.043	0.047	0.071	0.268	0.063	0.144	0.584	0.060	0.126	0.512
$Q^{*(n)}_{f_{\mathrm{C}_{0.25}};2}$	2	0.061	0.058	0.041	0.090	0.274	0.900	0.215	0.767	1	0.382	0.955	1
$Q^{*(n)}_{f_{\mathrm{C}_{0.25}};2}$	3	0.059	0.060	0.040	0.052	0.085	0.290	0.076	0.208	0.795	0.106	0.405	0.986
	k′	$g_0 = f_{\mathrm{WN}_{0.5}}$											
$Q^{*(n)}_{f_{\mathrm{C}_{0.25}};2}$	1	0.029	0.046	0.052	0.044	0.063	0.151	0.044	0.082	0.269	0.048	0.059	0.173
$Q^{*(n)}_{f_{\mathrm{C}_{0.25}};2}$	2	0.033	0.048	0.049	0.091	0.254	0.867	0.198	0.734	1	0.355	0.933	1
$Q^{*(n)}_{f_{\mathrm{C}_{0.25}};2}$	3	0.033	0.044	0.052	0.068	0.112	0.376	0.089	0.262	0.908	0.165	0.517	1
	k′	$g_0 = f_{\mathrm{WN}_{0.9}}$											
$Q^{*(n)}_{f_{\mathrm{C}_{0.25}};2}$	1	0.028	0.049	0.054	0.033	0.041	0.056	0.031	0.040	0.062	0.037	0.040	0.063
$Q^{*(n)}_{f_{\mathrm{C}_{0.25}};2}$	2	0.031	0.048	0.057	0.046	0.056	0.130	0.034	0.073	0.362	0.028	0.097	0.467
$Q^{*(n)}_{f_{\mathrm{C}_{0.25}};2}$	3	0.031	0.050	0.059	0.047	0.118	0.479	0.078	0.305	0.955	0.119	0.492	0.997
	k′	$g_0 = f_{\mathrm{WC}_{0.5}}$											
$Q^{*(n)}_{f_{\mathrm{C}_{0.25}};2}$	1	0.043	0.054	0.052	0.057	0.072	0.214	0.082	0.186	0.700	0.127	0.409	0.975
$Q^{*(n)}_{f_{\mathrm{C}_{0.25}};2}$	2	0.044	0.055	0.054	0.068	0.128	0.431	0.107	0.306	0.914	0.158	0.479	0.990
$Q^{*(n)}_{f_{\mathrm{C}_{0.25}};2}$	3	0.042	0.057	0.046	0.060	0.075	0.123	0.071	0.112	0.327	0.093	0.163	0.546

Table 4.9: Percentages of rejections for testing symmetry, with 1000 simulations.

	λ	0			0.2			0.4			0.6		
	n	30	100	500	30	100	500	30	100	500	30	100	500
	k′	$g_0 = f_{\mathrm{VM}_1}$											
$Q_2^{(n);\mu;f_{\mathrm{VM}_{10}}}$	1	0.152	0.131	0.147	0.170	0.203	0.471	0.226	0.402	0.905	0.312	0.635	0.998
$Q_2^{(n);\mu;f_{C_\rho}}$		0.050	0.046	0.049	0.057	0.086	0.305	0.095	0.230	0.796	0.145	0.463	0.990
$Q_2^{(n);\mu;f_{\mathrm{WC}_{0.5}}}$		0.061	0.054	0.060	0.069	0.098	0.325	0.111	0.248	0.821	0.159	0.488	0.991
$Q_2^{(n);f_{\mathrm{VM}_{10}}}$		0.820	0.820	0.817	0.802	0.833	0.821	0.810	0.834	0.835	0.829	0.833	0.914
$Q_2^{(n);f_{C_\rho}}$		0.027	0.026	0.028	0.024	0.027	0.030	0.025	0.025	0.040	0.022	0.040	0.154
$Q_2^{(n);f_{\mathrm{WC}_{0.5}}}$		0.041	0.039	0.041	0.042	0.048	0.045	0.038	0.035	0.052	0.035	0.048	0.184
$Q_2^{(n);\mu;f_{\mathrm{VM}_{10}}}$	2	0.152	0.131	0.147	0.246	0.488	0.961	0.544	0.920	1	0.825	1	1
$Q_2^{(n);\mu;f_{C_\rho}}$		0.050	0.046	0.049	0.100	0.293	0.894	0.347	0.825	1	0.647	0.994	1
$Q_2^{(n);\mu;f_{\mathrm{WC}_{0.5}}}$		0.061	0.054	0.060	0.116	0.323	0.912	0.381	0.838	1	0.672	0.994	1
$Q_2^{(n);f_{\mathrm{VM}_{10}}}$		0.820	0.820	0.817	0.860	0.920	0.997	0.901	0.978	1	0.946	0.992	1
$Q_2^{(n);f_{C_\rho}}$		0.027	0.026	0.028	0.043	0.161	0.701	0.134	0.512	0.998	0.262	0.768	1
$Q_2^{(n);f_{\mathrm{WC}_{0.5}}}$		0.041	0.039	0.041	0.073	0.196	0.712	0.163	0.550	0.999	0.319	0.817	1
$Q_2^{(n);\mu;f_{\mathrm{VM}_{10}}}$	3	0.152	0.131	0.147	0.160	0.227	0.501	0.241	0.424	0.922	0.336	0.680	0.994
$Q_2^{(n);\mu;f_{C_\rho}}$		0.050	0.046	0.049	0.061	0.100	0.318	0.102	0.255	0.822	0.164	0.475	0.991
$Q_2^{(n);\mu;f_{\mathrm{WC}_{0.5}}}$		0.061	0.054	0.060	0.072	0.116	0.342	0.114	0.273	0.836	0.187	0.498	0.991
$Q_2^{(n);f_{\mathrm{VM}_{10}}}$		0.820	0.820	0.817	0.828	0.855	0.933	0.846	0.905	0.994	0.858	0.964	0.999
$Q_2^{(n);f_{C_\rho}}$		0.027	0.026	0.028	0.023	0.051	0.216	0.049	0.156	0.716	0.077	0.299	0.969
$Q_2^{(n);f_{\mathrm{WC}_{0.5}}}$		0.041	0.039	0.041	0.034	0.054	0.085	0.046	0.079	0.217	0.046	0.099	0.409
	k′	$g_0 = f_{\mathrm{VM}_{10}}$											
$Q_2^{(n);\mu;f_{\mathrm{VM}_{10}}}$	1	0.049	0.046	0.044	0.060	0.085	0.282	0.097	0.233	0.786	0.163	0.476	0.983
$Q_2^{(n);\mu;f_{C_\rho}}$		0.011	0.005	0.008	0.010	0.016	0.105	0.016	0.086	0.564	0.046	0.218	0.939
$Q_2^{(n);\mu;f_{\mathrm{WC}_{0.5}}}$		0.013	0.006	0.012	0.013	0.021	0.119	0.022	0.099	0.601	0.057	0.243	0.949
$Q_2^{(n);f_{\mathrm{VM}_{10}}}$		0.050	0.047	0.040	0.045	0.045	0.034	0.045	0.040	0.039	0.047	0.036	0.044
$Q_2^{(n);f_{C_\rho}}$		0	0	0	0	0	0	0	0	0	0	0	0
$Q_2^{(n);f_{\mathrm{WC}_{0.5}}}$		0	0	0	0	0	0	0	0	0	0	0	0
$Q_2^{(n);\mu;f_{\mathrm{VM}_{10}}}$	2	0.049	0.046	0.044	0.083	0.183	0.694	0.222	0.586	0.998	0.417	0.911	1
$Q_2^{(n);\mu;f_{C_\rho}}$		0.011	0.005	0.008	0.014	0.060	0.411	0.063	0.314	0.986	0.180	0.757	1
$Q_2^{(n);\mu;f_{\mathrm{WC}_{0.5}}}$		0.013	0.006	0.012	0.019	0.072	0.441	0.075	0.339	0.989	0.205	0.785	1
$Q_2^{(n);f_{\mathrm{VM}_{10}}}$		0.050	0.047	0.040	0.052	0.053	0.044	0.045	0.051	0.070	0.032	0.040	0.053
$Q_2^{(n);f_{C_\rho}}$		0	0	0	0	0	0	0	0	0	0	0	0
$Q_2^{(n);f_{\mathrm{WC}_{0.5}}}$		0	0	0	0	0	0	0	0	0	0	0	0
$Q_2^{(n);\mu;f_{\mathrm{VM}_{10}}}$	3	0.049	0.046	0.044	0.107	0.238	0.843	0.273	0.728	1	0.575	0.977	1
$Q_2^{(n);\mu;f_{C_\rho}}$		0.011	0.005	0.008	0.024	0.089	0.616	0.100	0.485	0.998	0.291	0.908	1
$Q_2^{(n);\mu;f_{\mathrm{WC}_{0.5}}}$		0.013	0.006	0.012	0.031	0.101	0.648	0.120	0.520	0.999	0.320	0.925	1
$Q_2^{(n);f_{\mathrm{VM}_{10}}}$		0.050	0.047	0.040	0.061	0.058	0.138	0.050	0.098	0.412	0.059	0.138	0.543
$Q_2^{(n);f_{C_\rho}}$		0	0	0	0	0	0	0	0	0	0	0	0
$Q_2^{(n);f_{\mathrm{WC}_{0.5}}}$		0	0	0	0	0	0	0	0	0	0	0	0

Table 4.10: Percentages of rejections for testing symmetry, with 1000 simulations.

	λ	0			0.2			0.4			0.6		
	n	30	100	500	30	100	500	30	100	500	30	100	500
	$\mathtt{k}'$	$g_0 = f_{\mathrm{C}_{0.45}}$											
$Q_2^{(n);\mu;f_{\mathrm{VM}_{10}}}$	1	0.141	0.142	0.139	0.162	0.206	0.487	0.246	0.425	0.917	0.327	0.671	1
$Q_2^{(n);\mu;f_{\mathrm{C}_\rho}}$		0.056	0.057	0.042	0.068	0.090	0.285	0.106	0.260	0.814	0.175	0.489	0.993
$Q_2^{(n);\mu;f_{\mathrm{WC}_{0.5}}}$		0.065	0.065	0.048	0.080	0.098	0.308	0.119	0.276	0.826	0.189	0.510	0.994
$Q_2^{(n);f_{\mathrm{VM}_{10}}}$		0.839	0.858	0.836	0.827	0.860	0.932	0.824	0.875	0.979	0.821	0.848	0.968
$Q_2^{(n);f_{\mathrm{C}_\rho}}$		0.054	0.061	0.044	0.041	0.064	0.246	0.042	0.101	0.485	0.025	0.055	0.338
$Q_2^{(n);f_{\mathrm{WC}_{0.5}}}$		0.068	0.082	0.079	0.062	0.101	0.341	0.055	0.167	0.621	0.041	0.094	0.482
$Q_2^{(n);\mu;f_{\mathrm{VM}_{10}}}$	2	0.141	0.142	0.139	0.259	0.482	0.956	0.534	0.923	1	0.843	0.996	1
$Q_2^{(n);\mu;f_{\mathrm{C}_\rho}}$		0.056	0.057	0.042	0.120	0.289	0.905	0.336	0.830	1	0.661	0.991	1
$Q_2^{(n);\mu;f_{\mathrm{WC}_{0.5}}}$		0.065	0.065	0.048	0.134	0.310	0.911	0.359	0.848	1	0.688	0.991	1
$Q_2^{(n);f_{\mathrm{VM}_{10}}}$		0.839	0.858	0.836	0.874	0.930	0.998	0.931	0.996	1	0.965	0.999	1
$Q_2^{(n);f_{\mathrm{C}_\rho}}$		0.054	0.061	0.044	0.073	0.261	0.890	0.200	0.729	1	0.402	0.948	1
$Q_2^{(n);f_{\mathrm{WC}_{0.5}}}$		0.068	0.082	0.079	0.099	0.292	0.907	0.266	0.772	1	0.463	0.966	1
$Q_2^{(n);\mu;f_{\mathrm{VM}_{10}}}$	3	0.141	0.142	0.139	0.161	0.223	0.494	0.245	0.415	0.910	0.324	0.677	0.995
$Q_2^{(n);\mu;f_{\mathrm{C}_\rho}}$		0.056	0.057	0.042	0.057	0.094	0.296	0.113	0.237	0.829	0.157	0.493	0.989
$Q_2^{(n);\mu;f_{\mathrm{WC}_{0.5}}}$		0.065	0.065	0.048	0.069	0.114	0.319	0.127	0.261	0.842	0.175	0.515	0.992
$Q_2^{(n);f_{\mathrm{VM}_{10}}}$		0.839	0.858	0.836	0.839	0.856	0.937	0.864	0.926	0.998	0.888	0.971	1
$Q_2^{(n);f_{\mathrm{C}_\rho}}$		0.054	0.061	0.044	0.051	0.092	0.287	0.070	0.217	0.816	0.105	0.435	0.987
$Q_2^{(n);f_{\mathrm{WC}_{0.5}}}$		0.068	0.082	0.079	0.074	0.084	0.157	0.077	0.121	0.361	0.081	0.188	0.648
	$\mathtt{k}'$	$g_0 = f_{\mathrm{WN}_{0.5}}$											
$Q_2^{(n);\mu;f_{\mathrm{VM}_{10}}}$	1	0.138	0.133	0.165	0.161	0.254	0.547	0.246	0.479	0.964	0.395	0.747	1
$Q_2^{(n);\mu;f_{\mathrm{C}_\rho}}$		0.054	0.048	0.052	0.066	0.113	0.354	0.117	0.292	0.894	0.202	0.578	0.997
$Q_2^{(n);\mu;f_{\mathrm{WC}_{0.5}}}$		0.061	0.058	0.059	0.074	0.125	0.376	0.128	0.317	0.903	0.229	0.602	0.998
$Q_2^{(n);f_{\mathrm{VM}_{10}}}$		0.831	0.819	0.819	0.823	0.845	0.866	0.836	0.854	0.903	0.791	0.821	0.887
$Q_2^{(n);f_{\mathrm{C}_\rho}}$		0.023	0.031	0.034	0.027	0.034	0.106	0.016	0.044	0.154	0.011	0.023	0.070
$Q_2^{(n);f_{\mathrm{WC}_{0.5}}}$		0.032	0.039	0.048	0.035	0.046	0.133	0.034	0.062	0.200	0.016	0.031	0.120
$Q_2^{(n);\mu;f_{\mathrm{VM}_{10}}}$	2	0.138	0.133	0.165	0.249	0.516	0.960	0.540	0.924	1	0.817	0.998	1
$Q_2^{(n);\mu;f_{\mathrm{C}_\rho}}$		0.054	0.048	0.052	0.116	0.289	0.894	0.327	0.826	1	0.656	0.995	1
$Q_2^{(n);\mu;f_{\mathrm{WC}_{0.5}}}$		0.061	0.058	0.059	0.132	0.317	0.905	0.350	0.835	1	0.676	0.996	1
$Q_2^{(n);f_{\mathrm{VM}_{10}}}$		0.831	0.819	0.819	0.846	0.927	1	0.923	0.990	1	0.967	1	1
$Q_2^{(n);f_{\mathrm{C}_\rho}}$		0.023	0.031	0.034	0.051	0.172	0.801	0.150	0.634	1	0.311	0.907	1
$Q_2^{(n);f_{\mathrm{WC}_{0.5}}}$		0.032	0.039	0.048	0.078	0.208	0.819	0.173	0.658	1	0.352	0.922	1
$Q_2^{(n);\mu;f_{\mathrm{VM}_{10}}}$	3	0.138	0.133	0.165	0.155	0.251	0.545	0.238	0.469	0.958	0.395	0.751	1
$Q_2^{(n);\mu;f_{\mathrm{C}_\rho}}$		0.054	0.048	0.052	0.062	0.118	0.364	0.114	0.284	0.889	0.187	0.553	0.999
$Q_2^{(n);\mu;f_{\mathrm{WC}_{0.5}}}$		0.061	0.058	0.059	0.068	0.129	0.381	0.136	0.304	0.899	0.208	0.586	0.999
$Q_2^{(n);f_{\mathrm{VM}_{10}}}$		0.831	0.819	0.819	0.812	0.870	0.958	0.859	0.921	1	0.917	0.979	1
$Q_2^{(n);f_{\mathrm{C}_\rho}}$		0.023	0.031	0.034	0.036	0.073	0.318	0.058	0.221	0.884	0.125	0.486	1
$Q_2^{(n);f_{\mathrm{WC}_{0.5}}}$		0.032	0.039	0.048	0.035	0.062	0.140	0.047	0.105	0.423	0.061	0.196	0.764

Table 4.11: Percentages of rejections for testing symmetry, with 1000 simulations.

	λ	0			0.2			0.4			0.6		
	n	30	100	500	30	100	500	30	100	500	30	100	500
	k′	$g_0 = f_{\mathrm{WN}_{0.9}}$											
$Q_2^{(n);\mu;f_{\mathrm{VM}_{10}}}$	1	0.096	0.105	0.110	0.117	0.199	0.562	0.187	0.481	0.981	0.342	0.792	1
$Q_2^{(n);\mu;f_{\mathrm{C}_\rho}}$		0.028	0.030	0.032	0.041	0.078	0.360	0.076	0.271	0.931	0.165	0.585	1
$Q_2^{(n);\mu;f_{\mathrm{WC}_{0.5}}}$		0.035	0.034	0.039	0.047	0.088	0.381	0.088	0.291	0.938	0.189	0.619	1
$Q_2^{(n);f_{\mathrm{VM}_{10}}}$		0.315	0.352	0.389	0.296	0.348	0.379	0.291	0.350	0.386	0.298	0.333	0.342
$Q_2^{(n);f_{\mathrm{C}_\rho}}$		0	0	0	0	0	0	0	0	0	0	0	0
$Q_2^{(n);f_{\mathrm{WC}_{0.5}}}$		0	0	0	0	0	0	0	0	0	0	0	0
$Q_2^{(n);\mu;f_{\mathrm{VM}_{10}}}$	2	0.096	0.105	0.110	0.174	0.328	0.886	0.378	0.830	1	0.689	0.994	1
$Q_2^{(n);\mu;f_{\mathrm{C}_\rho}}$		0.028	0.030	0.032	0.061	0.176	0.751	0.198	0.645	1	0.464	0.963	1
$Q_2^{(n);\mu;f_{\mathrm{WC}_{0.5}}}$		0.035	0.034	0.039	0.068	0.189	0.765	0.216	0.668	1	0.495	0.972	1
$Q_2^{(n);f_{\mathrm{VM}_{10}}}$		0.315	0.352	0.389	0.304	0.398	0.541	0.309	0.446	0.783	0.296	0.470	0.817
$Q_2^{(n);f_{\mathrm{C}_\rho}}$		0	0	0	0	0	0	0	0	0	0	0	0
$Q_2^{(n);f_{\mathrm{WC}_{0.5}}}$		0	0	0	0	0	0	0	0	0	0	0	0
$Q_2^{(n);\mu;f_{\mathrm{VM}_{10}}}$	3	0.096	0.105	0.110	0.177	0.355	0.908	0.415	0.848	1	0.720	0.996	1
$Q_2^{(n);\mu;f_{\mathrm{C}_\rho}}$		0.028	0.030	0.032	0.058	0.176	0.768	0.208	0.666	1	0.502	0.977	1
$Q_2^{(n);\mu;f_{\mathrm{WC}_{0.5}}}$		0.035	0.034	0.039	0.065	0.190	0.784	0.230	0.692	1	0.533	0.979	1
$Q_2^{(n);f_{\mathrm{VM}_{10}}}$		0.315	0.352	0.389	0.366	0.500	0.855	0.452	0.731	0.997	0.522	0.870	1
$Q_2^{(n);f_{\mathrm{C}_\rho}}$		0	0	0	0	0	0	0	0	0	0	0	0
$Q_2^{(n);f_{\mathrm{WC}_{0.5}}}$		0	0	0	0	0	0	0	0	0	0	0	0
	k′	$g_0 = f_{\mathrm{WC}_{0.5}}$											
$Q_2^{(n);\mu;f_{\mathrm{VM}_{10}}}$	1	0.144	0.119	0.133	0.143	0.194	0.388	0.190	0.354	0.815	0.260	0.555	0.988
$Q_2^{(n);\mu;f_{\mathrm{C}_\rho}}$		0.051	0.035	0.038	0.055	0.088	0.227	0.083	0.203	0.667	0.115	0.366	0.952
$Q_2^{(n);\mu;f_{\mathrm{WC}_{0.5}}}$		0.058	0.041	0.045	0.061	0.098	0.241	0.092	0.222	0.682	0.132	0.389	0.959
$Q_2^{(n);f_{\mathrm{VM}_{10}}}$		0.836	0.828	0.822	0.835	0.848	0.918	0.856	0.903	0.995	0.887	0.959	1
$Q_2^{(n);f_{\mathrm{C}_\rho}}$		0.036	0.045	0.042	0.038	0.058	0.207	0.051	0.140	0.664	0.084	0.313	0.966
$Q_2^{(n);f_{\mathrm{WC}_{0.5}}}$		0.045	0.054	0.043	0.046	0.064	0.162	0.059	0.122	0.507	0.083	0.264	0.894
$Q_2^{(n);\mu;f_{\mathrm{VM}_{10}}}$	2	0.144	0.119	0.133	0.238	0.454	0.934	0.492	0.911	1	0.802	0.998	1
$Q_2^{(n);\mu;f_{\mathrm{C}_\rho}}$		0.051	0.035	0.038	0.096	0.271	0.836	0.306	0.787	1	0.592	0.980	1
$Q_2^{(n);\mu;f_{\mathrm{WC}_{0.5}}}$		0.058	0.041	0.045	0.114	0.294	0.852	0.322	0.807	1	0.629	0.985	1
$Q_2^{(n);f_{\mathrm{VM}_{10}}}$		0.836	0.828	0.822	0.823	0.897	0.976	0.870	0.949	1	0.925	0.981	1
$Q_2^{(n);f_{\mathrm{C}_\rho}}$		0.036	0.045	0.042	0.053	0.113	0.402	0.110	0.319	0.919	0.188	0.529	0.994
$Q_2^{(n);f_{\mathrm{WC}_{0.5}}}$		0.045	0.054	0.043	0.069	0.144	0.478	0.113	0.372	0.957	0.219	0.628	0.997
$Q_2^{(n);\mu;f_{\mathrm{VM}_{10}}}$	3	0.144	0.119	0.133	0.150	0.232	0.500	0.222	0.459	0.944	0.346	0.708	1
$Q_2^{(n);\mu;f_{\mathrm{C}_\rho}}$		0.051	0.035	0.038	0.060	0.100	0.305	0.097	0.269	0.845	0.163	0.511	0.996
$Q_2^{(n);\mu;f_{\mathrm{WC}_{0.5}}}$		0.058	0.041	0.045	0.067	0.113	0.334	0.110	0.290	0.857	0.186	0.531	0.997
$Q_2^{(n);f_{\mathrm{VM}_{10}}}$		0.836	0.828	0.822	0.837	0.838	0.878	0.842	0.889	0.969	0.876	0.913	0.989
$Q_2^{(n);f_{\mathrm{C}_\rho}}$		0.036	0.045	0.042	0.035	0.064	0.137	0.055	0.103	0.412	0.061	0.202	0.717
$Q_2^{(n);f_{\mathrm{WC}_{0.5}}}$		0.045	0.054	0.043	0.046	0.061	0.057	0.056	0.060	0.088	0.047	0.060	0.127

Table 4.12: Percentages of rejections for testing symmetry, with 1000 simulations.

	λ	0			0.2			0.4			0.6		
	n	30	100	500	30	100	500	30	100	500	30	100	500
	k′	$g_0 = f_{\mathrm{VM}_1}$											
$Q^{*(n)}_{f_{\mathrm{C}_{0,45}};2}$	1	0.030	0.040	0.049	0.031	0.045	0.055	0.043	0.038	0.066	0.039	0.083	0.248
$Q^{*(n)}_{f_{\mathrm{WC}_{0.5}};2}$		0.031	0.040	0.048	0.027	0.044	0.053	0.037	0.046	0.064	0.043	0.074	0.239
$Q^{*(n);\hat{\mu}^{(n)}}_2$		0.026	0.026	0.026	0.026	0.029	0.030	0.026	0.025	0.039	0.022	0.041	0.154
$Q^{*(n)}_{f_{\mathrm{C}_{0,45}};2}$	2	0.030	0.040	0.049	0.047	0.179	0.755	0.141	0.512	0.995	0.227	0.704	0.999
$Q^{*(n)}_{f_{\mathrm{WC}_{0.5}};2}$		0.031	0.040	0.048	0.040	0.185	0.762	0.127	0.532	0.999	0.225	0.743	1
$Q^{*(n);\hat{\mu}^{(n)}}_2$		0.026	0.026	0.026	0.044	0.157	0.703	0.133	0.512	0.999	0.275	0.784	1
$Q^{*(n)}_{f_{\mathrm{C}_{0,45}};2}$	3	0.030	0.040	0.049	0.032	0.049	0.178	0.047	0.128	0.508	0.069	0.196	0.782
$Q^{*(n)}_{f_{\mathrm{WC}_{0.5}};2}$		0.031	0.040	0.048	0.030	0.050	0.161	0.048	0.125	0.481	0.063	0.183	0.785
$Q^{*(n);\hat{\mu}^{(n)}}_2$		0.026	0.026	0.026	0.024	0.046	0.220	0.051	0.162	0.732	0.089	0.320	0.970
	k′	$g_0 = f_{\mathrm{VM}_{10}}$											
$Q^{*(n)}_{f_{\mathrm{C}_{0,45}};2}$	1	0.028	0.039	0.039	0.028	0.037	0.034	0.028	0.031	0.041	0.027	0.037	0.053
$Q^{*(n)}_{f_{\mathrm{WC}_{0.5}};2}$		0.035	0.043	0.041	0.042	0.045	0.032	0.043	0.040	0.034	0.037	0.053	0.059
$Q^{*(n);\hat{\mu}^{(n)}}_2$		0	0	0	0	0	0	0	0	0	0	0	0
$Q^{*(n)}_{f_{\mathrm{C}_{0,45}};2}$	2	0.028	0.039	0.039	0.029	0.044	0.044	0.036	0.043	0.068	0.035	0.046	0.066
$Q^{*(n)}_{f_{\mathrm{WC}_{0.5}};2}$		0.035	0.043	0.041	0.045	0.053	0.047	0.049	0.048	0.062	0.046	0.056	0.053
$Q^{*(n);\hat{\mu}^{(n)}}_2$		0	0	0	0	0	0	0	0	0	0	0	0
$Q^{*(n)}_{f_{\mathrm{C}_{0,45}};2}$	3	0.028	0.039	0.039	0.033	0.057	0.143	0.033	0.085	0.395	0.030	0.090	0.521
$Q^{*(n)}_{f_{\mathrm{WC}_{0.5}};2}$		0.035	0.043	0.041	0.044	0.059	0.108	0.045	0.080	0.249	0.051	0.077	0.241
$Q^{*(n);\hat{\mu}^{(n)}}_2$		0	0	0	0	0	0	0	0	0	0	0	0
	k′	$g_0 = f_{\mathrm{C}_{0.45}}$											
$Q^{*(n)}_{f_{\mathrm{C}_{0,45}};2}$	1	0.050	0.058	0.038	0.050	0.074	0.280	0.056	0.155	0.624	0.047	0.140	0.599
$Q^{*(n)}_{f_{\mathrm{WC}_{0.5}};2}$		0.052	0.057	0.040	0.043	0.070	0.274	0.047	0.162	0.605	0.052	0.136	0.567
$Q^{*(n);\hat{\mu}^{(n)}}_2$		0.053	0.059	0.040	0.041	0.068	0.247	0.043	0.100	0.478	0.028	0.058	0.333
$Q^{*(n)}_{f_{\mathrm{C}_{0,45}};2}$	2	0.050	0.058	0.038	0.088	0.281	0.902	0.219	0.773	1	0.387	0.954	1
$Q^{*(n)}_{f_{\mathrm{WC}_{0.5}};2}$		0.052	0.057	0.040	0.086	0.273	0.903	0.201	0.772	1	0.369	0.962	1
$Q^{*(n);\hat{\mu}^{(n)}}_2$		0.053	0.059	0.040	0.072	0.258	0.893	0.204	0.734	1	0.400	0.947	1
$Q^{*(n)}_{f_{\mathrm{C}_{0,45}};2}$	3	0.050	0.058	0.038	0.047	0.089	0.289	0.072	0.202	0.816	0.093	0.402	0.987
$Q^{*(n)}_{f_{\mathrm{WC}_{0.5}};2}$		0.052	0.057	0.040	0.045	0.085	0.290	0.070	0.197	0.814	0.090	0.384	0.985
$Q^{*(n);\hat{\mu}^{(n)}}_2$		0.053	0.059	0.040	0.054	0.096	0.290	0.079	0.223	0.814	0.122	0.438	0.987

Table 4.13: Percentages of rejections for testing symmetry, with 1000 simulations.

	λ	0			0.2			0.4			0.6		
	n	30	100	500	30	100	500	30	100	500	30	100	500
	k′	$g_0 = f_{\mathrm{WN}_{0.5}}$											
$Q^{*(n)}_{f_{\mathrm{C}_{0,45}};2}$	1	0.028	0.045	0.054	0.040	0.060	0.161	0.035	0.081	0.289	0.037	0.067	0.207
$Q^{*(n)}_{f_{\mathrm{WC}_{0.5}};2}$		0.027	0.045	0.055	0.039	0.052	0.155	0.037	0.083	0.277	0.038	0.062	0.190
$Q^{*(n);\hat{\mu}^{(n)}}_{2}$		0.021	0.033	0.032	0.028	0.034	0.107	0.016	0.045	0.152	0.012	0.024	0.069
$Q^{*(n)}_{f_{\mathrm{C}_{0,45}};2}$	2	0.028	0.045	0.054	0.077	0.253	0.870	0.186	0.715	1	0.363	0.927	1
$Q^{*(n)}_{f_{\mathrm{WC}_{0.5}};2}$		0.027	0.045	0.055	0.077	0.247	0.866	0.185	0.724	1	0.344	0.941	1
$Q^{*(n);\hat{\mu}^{(n)}}_{2}$		0.021	0.033	0.032	0.056	0.174	0.796	0.153	0.643	1	0.324	0.908	1
$Q^{*(n)}_{f_{\mathrm{C}_{0,45}};2}$	3	0.028	0.045	0.054	0.063	0.103	0.321	0.076	0.213	0.858	0.135	0.451	0.997
$Q^{*(n)}_{f_{\mathrm{WC}_{0.5}};2}$		0.027	0.045	0.055	0.054	0.097	0.305	0.072	0.201	0.829	0.125	0.434	0.994
$Q^{*(n);\hat{\mu}^{(n)}}_{2}$		0.021	0.033	0.032	0.039	0.076	0.317	0.070	0.223	0.886	0.131	0.491	1
	k′	$g_0 = f_{\mathrm{WN}_{0.9}}$											
$Q^{*(n)}_{f_{\mathrm{C}_{0,45}};2}$	1	0.024	0.046	0.053	0.031	0.042	0.054	0.026	0.038	0.061	0.032	0.035	0.063
$Q^{*(n)}_{f_{\mathrm{WC}_{0.5}};2}$		0.027	0.042	0.054	0.037	0.038	0.063	0.032	0.040	0.043	0.033	0.047	0.050
$Q^{*(n);\hat{\mu}^{(n)}}_{2}$		0	0	0	0	0	0	0	0	0	0	0	0
$Q^{*(n)}_{f_{\mathrm{C}_{0,45}};2}$	2	0.024	0.046	0.053	0.041	0.049	0.127	0.030	0.059	0.360	0.022	0.095	0.467
$Q^{*(n)}_{f_{\mathrm{WC}_{0.5}};2}$		0.027	0.042	0.054	0.036	0.041	0.061	0.031	0.043	0.072	0.033	0.038	0.045
$Q^{*(n);\hat{\mu}^{(n)}}_{2}$		0	0	0	0	0	0	0	0	0	0	0	0
$Q^{*(n)}_{f_{\mathrm{C}_{0,45}};2}$	3	0.024	0.046	0.053	0.047	0.113	0.481	0.076	0.287	0.952	0.117	0.485	0.996
$Q^{*(n)}_{f_{\mathrm{WC}_{0.5}};2}$		0.027	0.042	0.054	0.041	0.059	0.170	0.047	0.094	0.280	0.059	0.078	0.169
$Q^{*(n);\hat{\mu}^{(n)}}_{2}$		0	0	0	0	0	0	0	0	0	0	0	0.028
	k′	$g_0 = f_{\mathrm{WC}_{0.5}}$											
$Q^{*(n)}_{f_{\mathrm{C}_{0,45}};2}$	1	0.038	0.058	0.045	0.053	0.070	0.203	0.065	0.152	0.606	0.107	0.347	0.945
$Q^{*(n)}_{f_{\mathrm{WC}_{0.5}};2}$		0.040	0.053	0.046	0.046	0.066	0.167	0.060	0.133	0.534	0.091	0.301	0.905
$Q^{*(n);\hat{\mu}^{(n)}}_{2}$		0.041	0.056	0.046	0.040	0.064	0.218	0.056	0.149	0.676	0.089	0.325	0.967
$Q^{*(n)}_{f_{\mathrm{C}_{0,45}};2}$	2	0.038	0.058	0.045	0.058	0.129	0.431	0.103	0.303	0.902	0.169	0.469	0.986
$Q^{*(n)}_{f_{\mathrm{WC}_{0.5}};2}$		0.040	0.053	0.046	0.056	0.132	0.468	0.102	0.343	0.953	0.169	0.558	0.997
$Q^{*(n);\hat{\mu}^{(n)}}_{2}$		0.041	0.056	0.046	0.055	0.123	0.432	0.109	0.350	0.932	0.206	0.574	0.995
$Q^{*(n)}_{f_{\mathrm{C}_{0,45}};2}$	3	0.038	0.058	0.045	0.046	0.062	0.059	0.061	0.069	0.107	0.064	0.064	0.149
$Q^{*(n)}_{f_{\mathrm{WC}_{0.5}};2}$		0.040	0.053	0.046	0.044	0.066	0.053	0.055	0.064	0.100	0.047	0.067	0.174
$Q^{*(n);\hat{\mu}^{(n)}}_{2}$		0.041	0.056	0.046	0.047	0.070	0.154	0.069	0.129	0.449	0.074	0.226	0.762

Table 4.14: Percentages of rejections for testing symmetry, with 1000 simulations.

	λ	0			0.2			0.4			0.6		
	n	30	100	500	30	100	500	30	100	500	30	100	500
Test	k'	$g_0 = f_{\mathrm{VM}_1}$											
$\phi_2^{(n);\pi/32}$	1	0.062	0.052	0.101	0.073	0.134	0.540	0.122	0.317	0.933	0.171	0.550	0.999
$\phi_2^{(n);\pi/16}$		0.071	0.078	0.228	0.089	0.184	0.732	0.145	0.388	0.968	0.208	0.612	1
$\phi_2^{(n);\pi/8}$		0.095	0.178	0.656	0.122	0.298	0.934	0.177	0.486	0.988	0.239	0.646	1
$\phi_2^{(n);\pi/4}$		0.126	0.336	0.911	0.126	0.290	0.927	0.120	0.312	0.925	0.126	0.325	0.920
$\phi_2^{(n);\pi/32}$	2	0.062	0.052	0.101	0.142	0.394	0.966	0.388	0.883	1	0.694	0.996	1
$\phi_2^{(n);\pi/16}$		0.071	0.078	0.228	0.162	0.471	0.988	0.404	0.892	1	0.706	0.997	1
$\phi_2^{(n);\pi/8}$		0.095	0.178	0.656	0.191	0.531	0.997	0.375	0.866	1	0.600	0.990	1
$\phi_2^{(n);\pi/4}$		0.126	0.336	0.911	0.126	0.310	0.931	0.129	0.318	0.917	0.143	0.316	0.932
$\phi_2^{(n);\pi/32}$	3	0.062	0.052	0.101	0.074	0.152	0.539	0.132	0.342	0.931	0.197	0.560	0.996
$\phi_2^{(n);\pi/16}$		0.071	0.078	0.228	0.090	0.216	0.730	0.151	0.398	0.977	0.208	0.627	0.997
$\phi_2^{(n);\pi/8}$		0.095	0.178	0.656	0.124	0.321	0.932	0.168	0.453	0.993	0.226	0.644	0.998
$\phi_2^{(n);\pi/4}$		0.126	0.336	0.911	0.122	0.314	0.915	0.131	0.330	0.917	0.142	0.335	0.929
Test	k'	$g_0 = f_{\mathrm{VM}_{10}}$											
$\phi_2^{(n);\pi/32}$	1	0.355	0.820	1	0.475	0.960	1	0.607	0.991	1	0.732	0.998	1
$\phi_2^{(n);\pi/16}$		0.908	1	1	0.942	1	1	0.979	1	1	0.989	1	1
$\phi_2^{(n);\pi/8}$		1	1	1	1	1	1	1	1	1	1	1	1
$\phi_2^{(n);\pi/4}$		1	1	1	1	1	1	1	1	1	1	1	1
$\phi_2^{(n);\pi/32}$	2	0.355	0.820	1	0.580	0.980	1	0.792	0.998	1	0.929	1	1
$\phi_2^{(n);\pi/16}$		0.908	1	1	0.967	1	1	0.991	1	1	1	1	1
$\phi_2^{(n);\pi/8}$		1	1	1	1	1	1	1	1	1	1	1	1
$\phi_2^{(n);\pi/4}$		1	1	1	1	1	1	1	1	1	1	1	1
$\phi_2^{(n);\pi/32}$	3	0.355	0.820	1	0.623	0.989	1	0.856	1	1	0.965	1	1
$\phi_2^{(n);\pi/16}$		0.908	1	1	0.976	1	1	0.998	1	1	1	1	1
$\phi_2^{(n);\pi/8}$		1	1	1	1	1	1	1	1	1	1	1	1
$\phi_2^{(n);\pi/4}$		1	1	1	1	1	1	1	1	1	1	1	1
Test	k'	$g_0 = f_{\mathrm{C}_{0.45}}$											
$\phi_2^{(n);\pi/32}$	1	0.058	0.057	0.041	0.066	0.089	0.277	0.106	0.254	0.803	0.171	0.475	0.991
$\phi_2^{(n);\pi/16}$		0.051	0.052	0.042	0.063	0.084	0.248	0.096	0.228	0.748	0.151	0.430	0.983
$\phi_2^{(n);\pi/8}$		0.044	0.055	0.043	0.060	0.071	0.160	0.088	0.152	0.502	0.117	0.269	0.854
$\phi_2^{(n);\pi/4}$		0.051	0.054	0.042	0.057	0.048	0.042	0.047	0.053	0.051	0.051	0.045	0.048
$\phi_2^{(n);\pi/32}$	2	0.058	0.057	0.041	0.108	0.283	0.894	0.325	0.810	1	0.641	0.987	1
$\phi_2^{(n);\pi/16}$		0.051	0.052	0.042	0.110	0.248	0.861	0.279	0.765	1	0.596	0.980	1
$\phi_2^{(n);\pi/8}$		0.044	0.055	0.043	0.079	0.166	0.611	0.186	0.528	0.997	0.378	0.868	1
$\phi_2^{(n);\pi/4}$		0.051	0.054	0.042	0.049	0.047	0.046	0.047	0.054	0.060	0.048	0.050	0.046
$\phi_2^{(n);\pi/32}$	3	0.058	0.057	0.041	0.063	0.092	0.285	0.107	0.229	0.807	0.150	0.465	0.987
$\phi_2^{(n);\pi/16}$		0.051	0.052	0.042	0.062	0.088	0.255	0.094	0.204	0.736	0.133	0.412	0.975
$\phi_2^{(n);\pi/8}$		0.044	0.055	0.043	0.054	0.069	0.149	0.072	0.134	0.464	0.090	0.241	0.815
$\phi_2^{(n);\pi/4}$		0.051	0.054	0.042	0.039	0.043	0.046	0.049	0.049	0.055	0.045	0.051	0.052

Table 4.15: Percentages of rejections for testing symmetry, with 1000 simulations.

	λ	0			0.2			0.4			0.6		
	n	30	100	500	30	100	500	30	100	500	30	100	500
Test	k'	$g_0 = f_{\mathrm{WN}_{0.5}}$											
$\phi_2^{(n);\pi/32}$	1	0.058	0.055	0.064	0.071	0.151	0.496	0.125	0.343	0.940	0.231	0.638	0.999
$\phi_2^{(n);\pi/16}$		0.058	0.062	0.112	0.070	0.177	0.618	0.121	0.372	0.963	0.219	0.643	1
$\phi_2^{(n);\pi/8}$		0.073	0.095	0.267	0.075	0.199	0.704	0.126	0.352	0.959	0.195	0.571	0.999
$\phi_2^{(n);\pi/4}$		0.075	0.137	0.493	0.076	0.119	0.510	0.070	0.122	0.503	0.076	0.120	0.482
$\phi_2^{(n);\pi/32}$	2	0.058	0.055	0.064	0.122	0.352	0.939	0.334	0.857	1	0.677	0.996	1
$\phi_2^{(n);\pi/16}$		0.058	0.062	0.112	0.133	0.377	0.960	0.327	0.848	1	0.655	0.995	1
$\phi_2^{(n);\pi/8}$		0.073	0.095	0.267	0.125	0.367	0.960	0.264	0.739	1	0.488	0.971	1
$\phi_2^{(n);\pi/4}$		0.075	0.137	0.493	0.071	0.134	0.488	0.078	0.123	0.485	0.072	0.126	0.489
$\phi_2^{(n);\pi/32}$	3	0.058	0.055	0.064	0.068	0.146	0.483	0.126	0.317	0.923	0.207	0.590	1
$\phi_2^{(n);\pi/16}$		0.058	0.062	0.112	0.076	0.168	0.599	0.126	0.334	0.946	0.219	0.567	1
$\phi_2^{(n);\pi/8}$		0.073	0.095	0.267	0.077	0.193	0.688	0.118	0.339	0.935	0.185	0.489	0.997
$\phi_2^{(n);\pi/4}$		0.075	0.137	0.493	0.073	0.132	0.493	0.070	0.131	0.491	0.066	0.127	0.492
Test	k'	$g_0 = f_{\mathrm{WN}_{0.9}}$											
$\phi_2^{(n);\pi/32}$	1	0.184	0.490	0.992	0.299	0.820	1	0.450	0.963	1	0.652	0.996	1
$\phi_2^{(n);\pi/16}$		0.552	0.982	1	0.724	1	1	0.855	1	1	0.943	1	1
$\phi_2^{(n);\pi/8}$		0.990	1	1	0.993	1	1	0.997	1	1	1	1	1
$\phi_2^{(n);\pi/4}$		1	1	1	1	1	1	1	1	1	1	1	1
$\phi_2^{(n);\pi/32}$	2	0.184	0.490	0.992	0.402	0.920	1	0.680	0.997	1	0.913	1	1
$\phi_2^{(n);\pi/16}$		0.552	0.982	1	0.796	0.999	1	0.951	1	1	0.995	1	1
$\phi_2^{(n);\pi/8}$		0.990	1	1	0.994	1	1	1	1	1	1	1	1
$\phi_2^{(n);\pi/4}$		1	1	1	1	1	1	1	1	1	1	1	1
$\phi_2^{(n);\pi/32}$	3	0.184	0.490	0.992	0.398	0.928	1	0.674	0.996	1	0.903	1	1
$\phi_2^{(n);\pi/16}$		0.552	0.982	1	0.782	1	1	0.938	1	1	0.991	1	1
$\phi_2^{(n);\pi/8}$		0.990	1	1	0.997	1	1	1	1	1	1	1	1
$\phi_2^{(n);\pi/4}$		1	1	1	1	1	1	1	1	1	1	1	1
Test	k'	$g_0 = f_{\mathrm{WC}_{0.5}}$											
$\phi_2^{(n);\pi/32}$	1	0.076	0.110	0.349	0.103	0.253	0.780	0.153	0.439	0.973	0.221	0.648	1
$\phi_2^{(n);\pi/16}$		0.133	0.280	0.894	0.171	0.473	0.986	0.243	0.678	1	0.337	0.838	1
$\phi_2^{(n);\pi/8}$		0.295	0.739	1	0.342	0.833	1	0.425	0.912	1	0.508	0.966	1
$\phi_2^{(n);\pi/4}$		0.493	0.959	1	0.478	0.944	1	0.471	0.946	1	0.483	0.953	1
$\phi_2^{(n);\pi/32}$	2	0.076	0.110	0.349	0.203	0.539	0.997	0.461	0.943	1	0.771	1	1
$\phi_2^{(n);\pi/16}$		0.133	0.280	0.894	0.312	0.745	1	0.569	0.983	1	0.843	1	1
$\phi_2^{(n);\pi/8}$		0.295	0.739	1	0.480	0.926	1	0.684	0.996	1	0.863	1	1
$\phi_2^{(n);\pi/4}$		0.493	0.959	1	0.480	0.951	1	0.486	0.951	1	0.484	0.954	1
$\phi_2^{(n);\pi/32}$	3	0.076	0.110	0.349	0.107	0.308	0.851	0.190	0.537	0.994	0.300	0.756	1
$\phi_2^{(n);\pi/16}$		0.133	0.280	0.894	0.181	0.518	0.996	0.276	0.738	1	0.396	0.880	1
$\phi_2^{(n);\pi/8}$		0.295	0.739	1	0.353	0.828	1	0.422	0.923	1	0.520	0.964	1
$\phi_2^{(n);\pi/4}$		0.493	0.959	1	0.485	0.942	1	0.472	0.948	1	0.473	0.946	1

Table 4.16: Percentages of rejections for testing symmetry, with 1000 simulations.

ν	0			0.2			0.4			0.6		
n	30	100	500	30	100	500	30	100	500	30	100	500
	$\mathrm{KJ}_{10}(0, 0.5, 0.5, \nu)$											
$Q_2^{*(n);\mu}$	0.053	0.051	0.058	0.194	0.538	0.995	0.524	0.962	1	0.747	0.997	1
$Q_{f_{\mathrm{VM}_\kappa};2}^{*(n)}$	0.044	0.057	0.050	0.047	0.057	0.040	0.053	0.059	0.047	0.044	0.061	0.067
	$\mathrm{KJ}_{10}(0, 0.9, 0.5, \nu)$											
$Q_2^{*(n);\mu}$	0.048	0.038	0.059	0.271	0.724	1	0.707	0.997	1	0.916	1	1
$Q_{f_{\mathrm{VM}_\kappa};2}^{*(n)}$	0.049	0.042	0.053	0.053	0.048	0.062	0.052	0.067	0.085	0.064	0.070	0.142
	$\mathrm{KJ}_{15}(0, 0.5, \nu)$											
$Q_2^{*(n);\mu}$	0.054	0.043	0.047	0.070	0.103	0.399	0.127	0.307	0.923	0.199	0.569	0.999
$Q_{f_{\mathrm{VM}_\kappa};2}^{*(n)}$	0.038	0.053	0.053	0.069	0.113	0.364	0.103	0.296	0.895	0.175	0.567	1
	$\mathrm{KJ}_{15}(0, 0.9, \nu)$											
$Q_2^{*(n);\mu}$	0.064	0.049	0.036	0.051	0.067	0.165	0.066	0.154	0.496	0.123	0.263	0.791
$Q_{f_{\mathrm{VM}_\kappa};2}^{*(n)}$	0.025	0.045	0.062	0.032	0.058	0.173	0.048	0.157	0.516	0.061	0.279	0.867

Table 4.17: Percentages of rejections for testing symmetry, with 1000 simulations.

for that reason, it was also excluded from their study, which aimed to check if the cracks were uniformly distributed. This leaves a total number of cement cracks equal to 2388: 1567 in the proximal region, and 434 in the distal region. Circular data plots for the two regions, together with rose diagrams and kernel density estimates obtained using the plug–in rule of Oliveira et al. (2012) to select the concentration parameter, are portrayed in Figure 4.2.

Since neither the mean direction, nor the underlying distribution, nor the value of $\mathtt{k}$ are assumed to be known, the $\phi_{f_{\mathrm{VM}_\kappa};2}^{*(n)}$ test was applied as it is a powerful omnibus test under such circumstances. The p–value obtained for the directions of the cracks in the proximal region was 0.6096, whilst for those in the distal region the p–value was 0.0483. Clearly, there is no significant evidence to reject underlying reflective symmetry for the distribution of the directions of the cracks in the proximal region. On the other hand, for a significance level of the 5% the test rejects reflective symmetry for the distribution of the crack directions in the distal region. Observing the p–values obtained, for other values of $\mathtt{k}$, when the $\phi_{f_{\mathrm{C}_{0.25}};\mathtt{k}}^{*(n)}$ test is used, in the proximal region there are still no evidences for rejecting the reflective symmetry, as for $\mathtt{k} = 1$ the p–value is 0.7543, for $\mathtt{k} = 2$ it is 0.6058 and for $\mathtt{k} = 3$ it is 0.5730. Now, in the distal region, the conclusion is not so clear as the p–values are 0.0345 (for $\mathtt{k} = 1$), 0.0451 (for $\mathtt{k} = 2$) and 0.9507 (for $\mathtt{k} = 3$). The distal sample can be seen as another good example of why the multimodality test are not only important *per se*, applying the new test proposed in Section 3.2 for $H_0 : j = 1$ (with $B = 1000$), the p–value was 0.259 so there is no evidence for rejecting the null hypothesis of unimodality. As, usually, the $\mathtt{k}$–sine–skewed are unimodal when $\mathtt{k} = 1$ (if the data is not "too" concentrated

around the central direction), in this case, it seems that the most powerful test can be obtained with a low value of `k`, which supports the evidences against the null for a significance level of the 5%. These findings provide further evidence to complement the results presented in Mann et al. (2003) regarding the different distributions of the crack directions in the two regions. It seems that cracks in the proximal and distal region are not equally distributed just with a translation in the central direction.

Chapter 5

Conclusions and discussion

This essay was focused on assessing simplifying hypothesis in density estimation for linear and circular data. The main statistical contributions that have been achieved in this PhD thesis are summed up in the following points.

Testing the number of modes for linear data. The objective was to provide a nonparametric tool for testing if the linear random variable has k modes. In addition, the proposed procedure has been compared with the existing methods, outperforming all of them in a wide range of scenarios. This goal corresponds to the contents in Chapter 2.

Testing the number of modes for circular data. The second goal was to extend the previous testing procedure to the circular setting. Since the final objective of this part was to determine if, in each region of the world, there is one season of fires or more, it was also studied how to handle the multiple testing problem with spatially correlated data. The results achieved in this point are collected in Chapter 3.

Testing reflective symmetry for circular data. The third objective was to introduce a new proposal for testing circular symmetry when the central location is unknown. The development of this point is provided in Chapter 4.

In what follows, some final comments and discussion on each chapter are presented.

5.1 Multimodality tests for linear data

Determining the number of modes in a distribution is a relevant practical problem in many applied sciences. The proposal presented in Chapter 2 provides a good performance for the testing problem (1.1.3), being in the case of a general number of modes k the only alternative with a reasonable behaviour. The totally nonparametric testing procedure can be extended to other contexts where a natural nonparametric estimator under the null hypothesis is available, as it was done in Chapter 3 for circular data.

The relevance of the developed techniques was shown in two datasets. First, in a classical example in the philatelic field, given an answer about the number of modes with a well–calibrated test. Second, showing the method potential for determining if the malaria is not eradicated in a given population. With the aim of making this procedure accessible for the scientific community, and therefore, enabling its use in other practical problems, the R package **multimode** was developed and it is presented in Appendix C.

Future research on this topic includes the extension of this techniques to the d–dimensional case (with $d > 1$). The excess mass statistic can be adapted in this setting, but there is not a clear definition of the critical bandwidth. In fact, using the Gaussian kernel, for the simplest case in the bidimensional setting, where a single value of h is taken in both dimensions, in Scott (2015, Sect. 9.2.4), an counterexample where the monotony in the number of modes is not satisfied can be found. Then, empirical approximations must be developed for tackling this problem.

5.2 Multimodality tests for circular data

As mentioned in the Introduction, asymmetric and multimodal distribution occur frequently in practice in the circular setting. In Chapters 3 and 4 different tests were developed for testing both hypothesis in a flexible way. The growing interest in the last few years in more flexible models in circular data, give to these methods a special relevance as a preliminary tool before applying more complicated methods. The proposal presented in Chapter 3 shows how the method presented in Chapter 2 can be extended to other settings, having a correct behaviour in the circular setting.

The detailed method, adapting the proposal of Benjamini and Heller (2007), provides a useful algorithm for correcting the FDR accounting for the spatial dependence of the data in other contexts where prior information about the neighbouring

locations is known. Related with the last point, future research on this topic includes trying to integrate the spatial correlation in the test statistic before making the FDR correction.

The map shown in Section 3.4.3 provides new conclusions about how human activity modifies fire seasonality. Related with this application, as it is expected that the circular kernel density estimator provides good estimation of the location of the modes and antimodes, future research may include the use of multimodality test as a preliminary tool for exploring when the peaks of fires are produced and also its associated mass. This will allow review different works in the forest field with nonparametric techniques. For instance, one can determine when the principal peaks of fires are produced in each 0.5° cell (Le Page et al., 2010), the delay of the agricultural fires with respect to the climatological ones (Magi et al., 2012) or the mass associated to each peak for better understanding the importance of the different human activities (Korontzi et al., 2006).

Other possible approach for solving the last questions can be done using a mixture of flexible parametric distributions. In particular, a future objective includes trying to model the wildfires distribution using Hidden Markov Models (HMM). The conclusions about the number of modes can be used as a preliminary tool for determining how many components should be used in the mixture distribution used in the HMM.

Finally, in future updates of the R package, the objective will be include different tools for determining the number of modes in the circular setting.

5.3 Symmetry tests in the circular setting

Test for circular reflective symmetry have been developed in Chapter 4. Specifically, such tests consider an unknown centre of symmetry and are optimal against `k`–sine–skewed alternatives. Recommendations for their use, as well as other tests that have been proposed in the literature, were established in the light of the simulation based results reported in Section 4.3. As mentioned there, the proposed tests are generally conservative when the sample size is of the order of 30. For that reason, future research may involve more sophisticated methods for generating the bootstrap resamples in order to better approximate the distribution of the test statistic under the null (improving the bootstrap method mentioned in Section 4.3) and also for having a complete non–parametric approach.

Circular data are just one class of directional data. Others include bivariate circular data distributed on the torus, cylindrical data, spherical data and data distributed

on the surfaces of the extensions of such Riemannian manifolds. The development of tests for reflective symmetry on such manifolds would be of considerable interest. Ideas underpinning such tests are explored in Jupp and Spurr (1983) and Jupp et al. (2016).

Appendices

USC
UNIVERSIDADE
DE SANTIAGO
DE COMPOSTELA

Appendix A

Models for simulation studies

The specific formulas of those models considered in the simulation studies carried out in Section 2.2, 3.3 and 4.3 are given here. The notation for the mixture models is $\sum_{i=1}^{m} p_i \cdot \psi_i$, where each ψ_i represents the density of the mixture component and p_i are the weights of these different components, with $i = 1, \ldots, m$, satisfying $\sum_{i=1}^{m} p_i = 1$.

The unimodal linear density functions used as ψ_i are the following models, as defined in Johnson et al. (1995): Beta(θ_i, ϕ_i), Gamma(α_i, β_i), Weibull(δ_i, c_i) and N(μ_i, σ_i^2). All the linear models were created in such a way that $f(0) \approx f(1) \approx 0.1 \max_{x \in (0,1)} f(x)$. This last reason and the aim of producing a rich family of models with different shapes are the explanation of why most of these densities have peculiar parameters. The unimodal linear probability density functions are represented in Figure A.1, the bimodal and trimodal models appear in Figure A.2.

Unimodal linear models:

- M1: $0.44 \cdot \mathrm{N}(0.372, 0.03) + 0.44 \cdot \mathrm{N}(0.67, 0.022) + 0.12 \cdot \mathrm{N}(0.5, 0.2)$.
- M2: $0.9 \cdot \mathrm{N}(0.5, 0.05) + 0.05 \cdot \mathrm{N}(0.197, 0.01) + 0.05 \cdot \mathrm{N}(0.803, 0.01)$.
- M3: $0.6 \cdot \mathrm{N}(0.62, 0.04) + 0.2 \cdot \mathrm{N}(0.218, 0.1) + 0.2 \cdot \mathrm{N}(0.5, 0.00795)$.
- M4: $\mathrm{N}(0.5, 0.05428)$.
- M5: $0.9 \cdot \mathrm{N}(0.5, 0.0485) + 0.1 \cdot \mathrm{N}(0.5, 0.47)$.
- M6: $0.6 \cdot \mathrm{N}(0.5, 0.0502) + 0.2 \cdot \mathrm{N}(0.3, 0.02) + 0.2 \cdot \mathrm{N}(0.7, 0.02)$.
- M7: $0.5 \cdot \mathrm{Beta}(10, 3) + 0.5 \cdot \mathrm{N}(0.5, 0.137)$.

- M8: $0.6 \cdot \mathrm{N}(0.4985, 0.0793) + 0.4 \cdot \mathrm{Weibull}(3, 0.5)$.
- M9: $0.5 \cdot \mathrm{N}(0.5, 0.3) + 0.45 \cdot \mathrm{N}(0.5, 0.045) + 0.05 \cdot \mathrm{N}(0.5, 0.000135)$.
- M10: $0.6 \cdot \mathrm{N}(0.307, 0.0518) + 0.4 \cdot \mathrm{Gamma}(4, 8)$.
- M26: $0.58 \cdot \mathrm{N}(0.61, 0.035) + 0.2 \cdot \mathrm{N}(0.232, 0.04) + 0.2 \cdot \mathrm{N}(0.5, 0.00795) + 0.01 \cdot \mathrm{N}(0.15, 0.0028) + 0.01 \cdot \mathrm{N}(0.98, 0.0028)$.

Bimodal linear models:

- M11: $0.75 \cdot \mathrm{N}(0.458, 0.0546) + 0.25 \cdot \mathrm{N}(0.85, 0.0041)$.
- M12: $0.5 \cdot \mathrm{N}(0.211, 0.012) + 0.3 \cdot \mathrm{N}(0.75, 0.062) + 0.2 \cdot \mathrm{Beta}(5, 2)$.
- M13: $0.95 \cdot \mathrm{N}(0.3035, 0.02) + 0.05 \cdot \mathrm{N}(0.96757, 0.0004)$.
- M14: $0.5 \cdot \mathrm{N}(0.776, 0.0109) + 0.3 \cdot \mathrm{N}(0.3, 0.04) + 0.1 \cdot \mathrm{N}(0.25, 0.0025) + 0.1 \cdot \mathrm{N}(0.35, 0.0025)$.
- M15: $0.3 \cdot \mathrm{N}(0.13, 0.1) + 0.3 \cdot \mathrm{N}(0.81, 0.1) + 0.2 \cdot \mathrm{Gamma}(3, 9) + 0.2 \cdot \mathrm{Beta}(7, 2)$.
- M16: $0.6 \cdot \mathrm{N}(0.384, 0.01202) + 0.2 \cdot \mathrm{N}(0.2, 0.05) + 0.2 \cdot \mathrm{N}(0.9, 0.00272)$.
- M17: $0.5 \cdot \mathrm{N}(0.3, 0.0197) + 0.5 \cdot \mathrm{N}(0.7, 0.0197)$.
- M18: $0.5 \cdot \mathrm{N}(0.18, 0.007) + 0.5 \cdot \mathrm{N}(0.82, 0.007)$.
- M19: $0.5 \cdot \mathrm{N}(0.06787, 0.001) + 0.5 \cdot \mathrm{N}(0.93213, 0.001)$.
- M20: $0.48 \cdot \mathrm{N}(0.06777, 0.001) + 0.48 \cdot \mathrm{N}(0.93223, 0.001) + 0.02 \cdot \mathrm{Beta}(1.1, 2.37558) + 0.02 \cdot \mathrm{Beta}(2.37558, 1.1)$.

Trimodal linear models:

- M21: $0.45 \cdot \mathrm{N}(0.26, 0.01476) + 0.33 \cdot \mathrm{N}(0.79145, 0.01) + 0.22 \cdot \mathrm{N}(0.5, 0.007)$.
- M22: $0.68 \cdot \mathrm{N}(0.6, 0.0025) + 0.22 \cdot \mathrm{N}(0.10245, 0.01588) + 0.1 \cdot \mathrm{N}(0.93, 0.0015)$.
- M23: $0.45 \cdot \mathrm{N}(0.25, 0.015) + 0.45 \cdot \mathrm{N}(0.6, 0.015) + 0.1 \cdot \mathrm{N}(0.95222, 0.00049)$.
- M24: $0.55 \cdot \mathrm{N}(0.5, 0.08425) + 0.15 \cdot \mathrm{N}(0.3, 0.004) + 0.15 \cdot \mathrm{N}(0.5, 0.004) + 0.15 \cdot \mathrm{N}(0.7, 0.004)$.

- M25: $0.6 \cdot \mathrm{N}(0.7749, 0.011) + 0.2 \cdot \mathrm{N}(0.1345, 0.006) + 0.2 \cdot \mathrm{N}(0.36, 0.006)$.

In the circular setting, the density functions used as ψ_i (symmetric with respect to μ_i and unimodal), are the following models, as defined in 1.2: von Mises $\mathrm{VM}(\mu_i, \kappa_i)$, with $\kappa_i > 0$; wrapped normal $\mathrm{WN}(\mu_i, \rho_i)$, with $\rho_i \in (0, 1)$; wrapped Cauchy $\mathrm{WC}(\mu_i, \rho_i)$, with $\rho_i \in (0, 1)$; and cardioid $\mathrm{C}(\mu_i, \rho_i)$, with $\rho_i \in (0, 0.5)$. Also, to see the behaviour of the test in reflective asymmetric models, it was employed the k–sine–skewed wrapped normal $\mathtt{k}ss\mathrm{WN}(\mu, \rho, \lambda, \mathtt{k})$ and the k–sine–skewed von Mises $\mathtt{k}ss\mathrm{VM}(\mu, \kappa, \lambda, \mathtt{k})$. The linear representation of the unimodal circular probability density functions are showed in Figure A.3, the bimodal and trimodal models appears in Figure A.4. The circular representation of the unimodal models appear in Figure A.5, the bimodal and trimodal models appear in Figure A.6.

Unimodal circular models:

- MC1: $\mathrm{VM}(\pi, 1)$
- MC2: $\mathrm{WN}(\pi, 0.9)$
- MC3: $\mathrm{WC}(\pi, 0.8)$
- MC4: $\mathrm{C}(\pi, 0.5)$
- MC5: $0.9 \cdot \mathrm{VM}(\pi, 10) + 0.1 \cdot \mathrm{VM}(\pi, 1)$.
- MC6: $0.2 \cdot \mathrm{VM}(2\pi/3, 3) + 0.6 \cdot \mathrm{VM}(\pi, 1.4) + 0.2 \cdot \mathrm{VM}(4\pi/3, 3)$.
- MC7: $0.05 \cdot \mathrm{VM}(2\pi/3, 7) + 0.9 \cdot \mathrm{VM}(\pi, 1) + 0.05 \cdot \mathrm{VM}(4\pi/3, 7)$.
- MC8: $0.05 \cdot \mathrm{VM}(2\pi/3, 4) + 0.9 \cdot \mathrm{VM}(\pi, 1) + 0.05 \cdot \mathrm{VM}(4\pi/3, 7)$.
- MC9: $\mathtt{k}ss\mathrm{WN}(\pi, 0.4, 0.99, 1)$.
- MC10: $\mathtt{k}ss\mathrm{VM}(\pi, 1, 0.9, 1)$.

Bimodal circular models:

- MC11: $0.5 \cdot \mathrm{VM}(2, 5) + 0.5 \cdot \mathrm{VM}(4, 5)$.
- MC12: $0.9 \cdot \mathrm{VM}(\pi/2, 2) + 0.1 \cdot \mathrm{VM}(3\pi/2, 5)$.
- MC13: $0.5 \cdot \mathrm{VM}(\pi - 1, 1.5) + 0.5 \cdot \mathrm{VM}(\pi + 1, 1.5)$.

- MC14: $0.3 \cdot \mathrm{VM}(\pi/2, 6) + 0.5 \cdot \mathrm{VM}(3\pi/4, 2) + 0.2 \cdot \mathrm{VM}(7\pi/4, 4)$.
- MC15: $\mathtt{k}ss\mathrm{WN}(\pi, 0.5, 0.9, 2)$.
- MC16: $\mathtt{k}ss\mathrm{VM}(\pi, 1, 0.8, 2)$.
- MC17: $0.5 \cdot \mathrm{VM}(0, 4) + 0.5 \cdot \mathrm{VM}(\pi, 4)$.
- MC18: $0.1 \cdot \mathrm{VM}(0, 2) + 0.6 \cdot \mathrm{VM}(\pi/2, 4) + 0.3 \cdot \mathrm{VM}(3\pi/2, 5)$.
- MC19: $0.5 \cdot \mathrm{VM}(0, 0.2) + 0.25 \cdot \mathrm{WN}(\pi/2, 0.5) + 0.25 \cdot \mathrm{WC}(3\pi/2, 0.5)$.
- MC20: $0.75 \cdot \mathrm{VM}(\pi, 1) + 0.25 \cdot \mathrm{VM}(7\pi/4, 10)$.

Trimodal circular models:

- MC21: $0.4 \cdot \mathrm{VM}(0.5, 6) + 0.4 \cdot \mathrm{VM}(3, 6) + 0.2 \cdot \mathrm{VM}(5, 24)$.
- MC22: $(1/6) \cdot \mathrm{VM}(\pi - 0.8, 30) + 0.5 \cdot \mathrm{VM}(\pi, 1) + (1/6) \cdot \mathrm{VM}(\pi, 30) + (1/6) \cdot \mathrm{VM}(\pi + 0.8, 30)$.
- MC23: $0.2 \cdot \mathrm{VM}(\pi/2, 5) + 0.2 \cdot \mathrm{VM}(7\pi/8, 5) + 0.6 \cdot \mathrm{WN}(7\pi/4, 0.8)$.
- MC24: $0.2 \cdot \mathrm{VM}(\pi/2, 6) + 0.2 \cdot \mathrm{VM}(7\pi/8, 2) + 0.6 \cdot \mathrm{WC}(7\pi/4, 0.7)$.
- MC25: $\mathtt{k}ss\mathrm{WN}(\pi, 0.5, 0.99, 3)$.

The used models in Section 4.3 were the $\mathtt{k}'$–sine–skewed alternatives of the von Mises $\mathtt{k}ss\mathrm{VM}(\mu, \kappa, \lambda, \mathtt{k}')$, cardioid $\mathtt{k}ss\mathrm{C}(\mu, \rho, \lambda, \mathtt{k}')$, wrapped normal $\mathtt{k}ss\mathrm{WN}(\mu, \rho, \lambda, \mathtt{k}')$ and wrapped Cauchy $\mathtt{k}ss\mathrm{WC}(\mu, \rho, \lambda, \mathtt{k}')$. It was also used the Kato and Jones (2012) distribution: $\mathrm{KJ}_{10}(\mu, \kappa, r, \nu)$, which probability density function is

$$f(\theta; \mu, \kappa, r, \nu) = \frac{1 - r^2}{2\pi I_0(\kappa)} \cdot \frac{1}{1 + r^2 - 2r\cos(\theta - \gamma)} \cdot \exp\left(\frac{\kappa\xi\cos(\theta - \eta) - 2r\cos\nu}{1 + r^2 - 2r\cos(\theta - \gamma)}\right),$$

where $0 \leq \mu, \nu < 2\pi$, $\kappa > 0$, $r \in [0, 1)$, $\gamma = \mu + \nu$, $\xi = \sqrt{r^4 + 2r^2\cos(2\nu) + 1}$ and $\eta = \mu + \arg[r^2(\cos(2\nu) + i\sin(2\nu)) + 1]$; and the three–parameter asymmetric submodel given in the Equation (7) of Kato and Jones (2015): $\mathrm{KJ}_{15}(\mu, \gamma, \nu)$, which probability density function is

$$f(\theta; \mu, \gamma, \nu) = \frac{1}{2\pi}\left(1 + 2\gamma^3 \frac{\cos(\theta - \mu) - \gamma}{\gamma^4 + \gamma^2 + \bar{\beta}_2^2 - 2\gamma(\gamma^2\cos(\theta - \mu) + \bar{\beta}_2\sin(\theta - \mu))}\right),$$

where $\mu \in [0, 2\pi)$, $0 \leq \gamma < 1$, $\bar{\beta}_2 = \nu\gamma(1-\gamma)$ and $|\nu| \leq 1$. The symmetry in this two models is obtained when $\nu = 0$, further discussion about the meaning of the parameters can be seen in Kato and Jones (2012) and Kato and Jones (2015). The linear representation of these circular probability density functions are shown in Figures A.7 and A.8, in these graphics the axes were moved in order to show, more clearly, the shape of the densities. The circular representation can be seen in Figures A.9 and A.10.

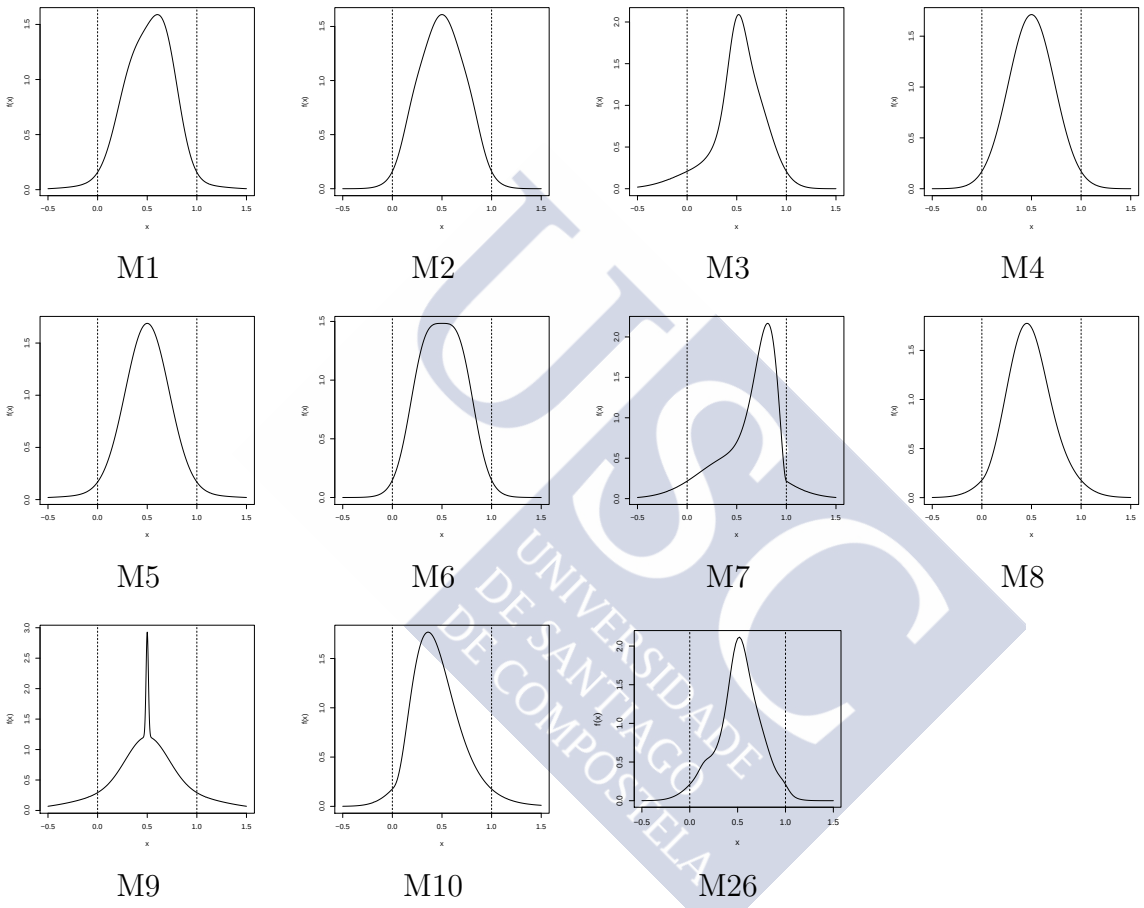

Figure A.1: Unimodal linear density functions: M1–M10 and M26. These models were used in Section 1.1 for illustration purposes and in Section 2.2 as part of the simulation study carried out for comparing the calibration of the different procedures for testing the number of modes in the linear case.

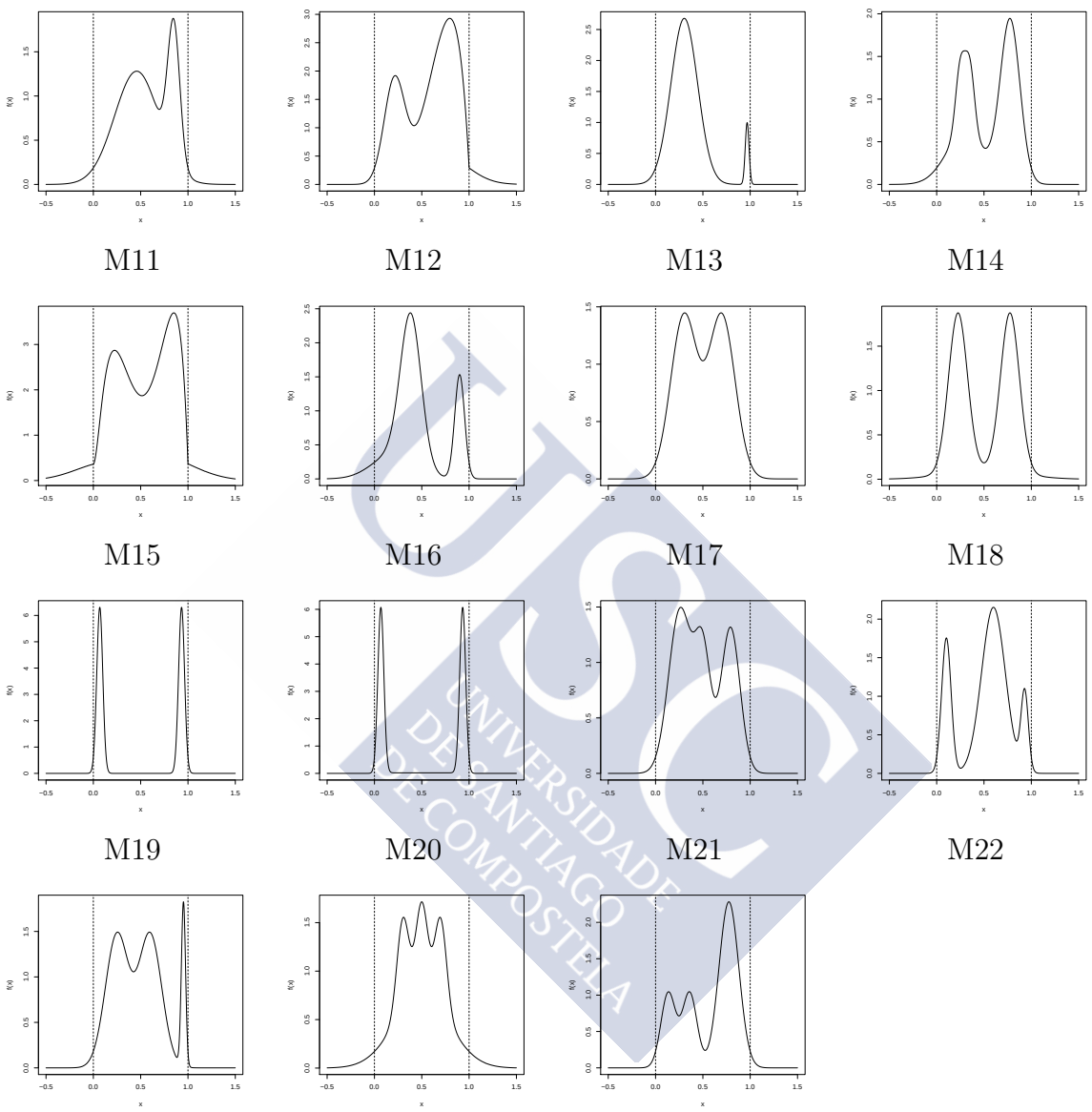

Figure A.2: Linear density functions. M11–M20: bimodal models. M21–M25: trimodal models. These models were used in Sections 1.1 and 2.1.3 for illustration purposes and in Section 2.2 as part of the simulation study comparing, in terms of empirical size and power, the different procedures for testing the number of modes in the linear case.

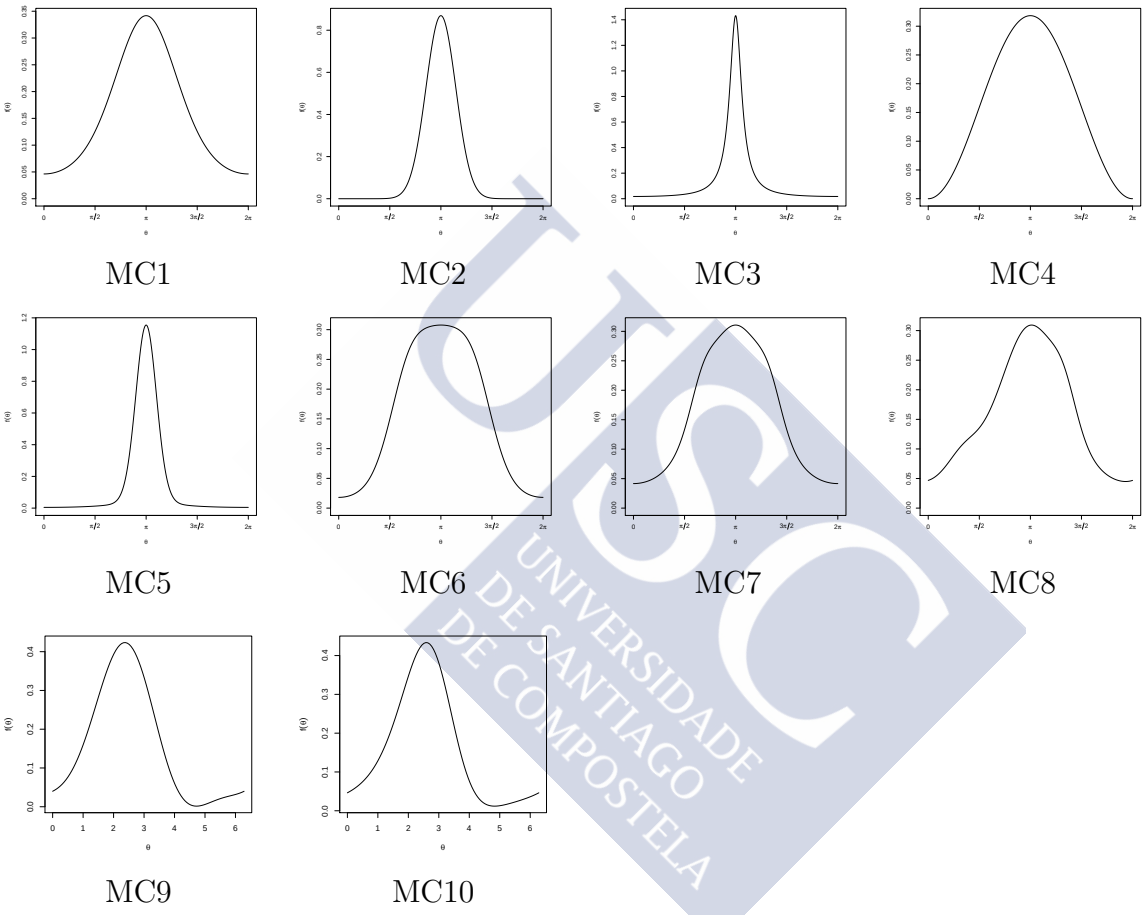

Figure A.3: Linear representation of the unimodal circular denstity functions: MC1–MC10. These models were used in Section 1.2 and 3.2 for illustration purposes and in Section 3.3 as part of the simulation study carried out for comparing the calibration of the different procedures for testing the number of modes in the circular case.

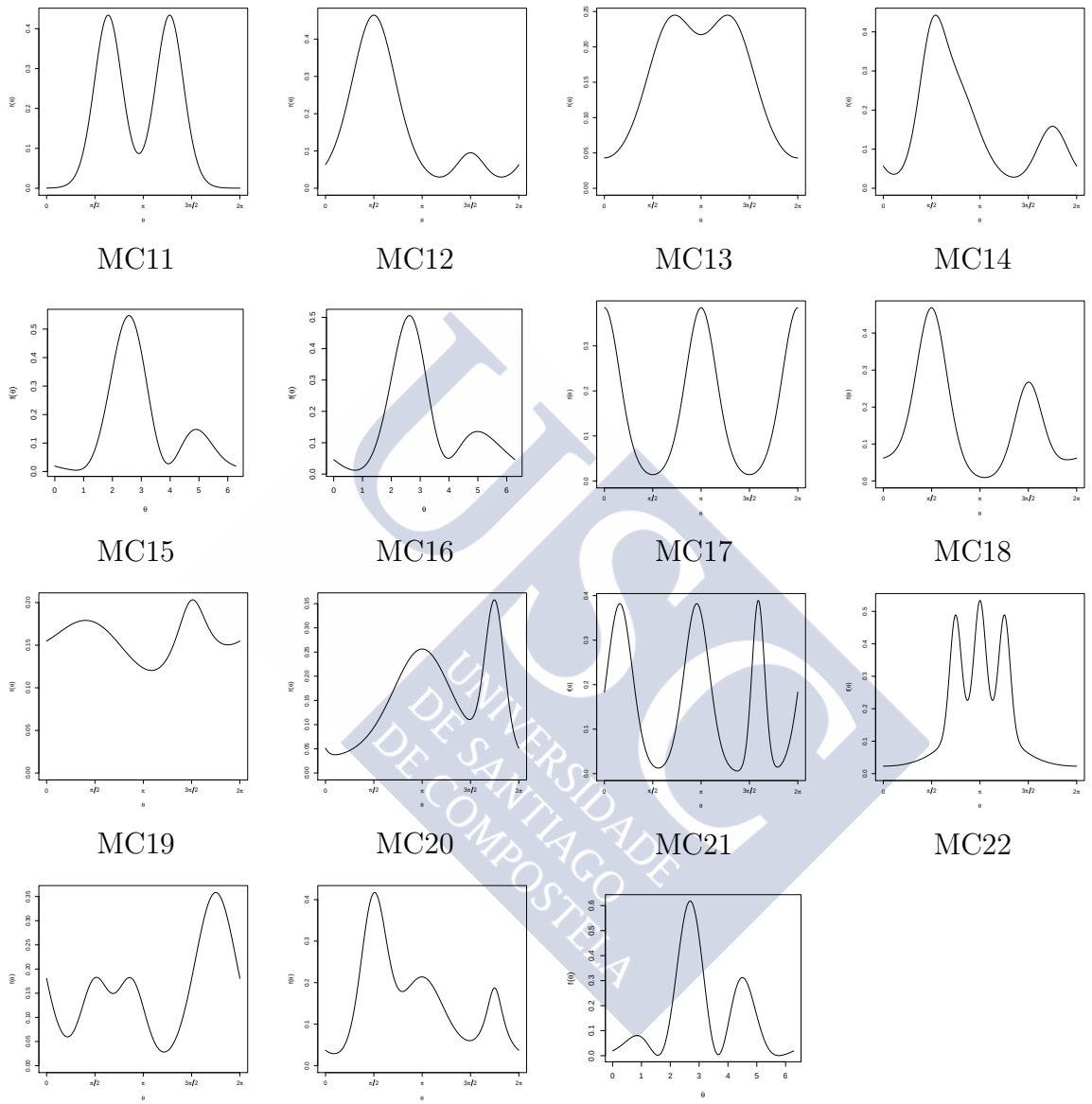

Figure A.4: Linear representation of circular density functions. MC11–MC20: bimodal models. MC21–MC25: trimodal models. These models were used in Section 3.3 as part of the simulation study comparing, in terms of empirical size and power, the different procedures for testing the number of modes in the circular case.

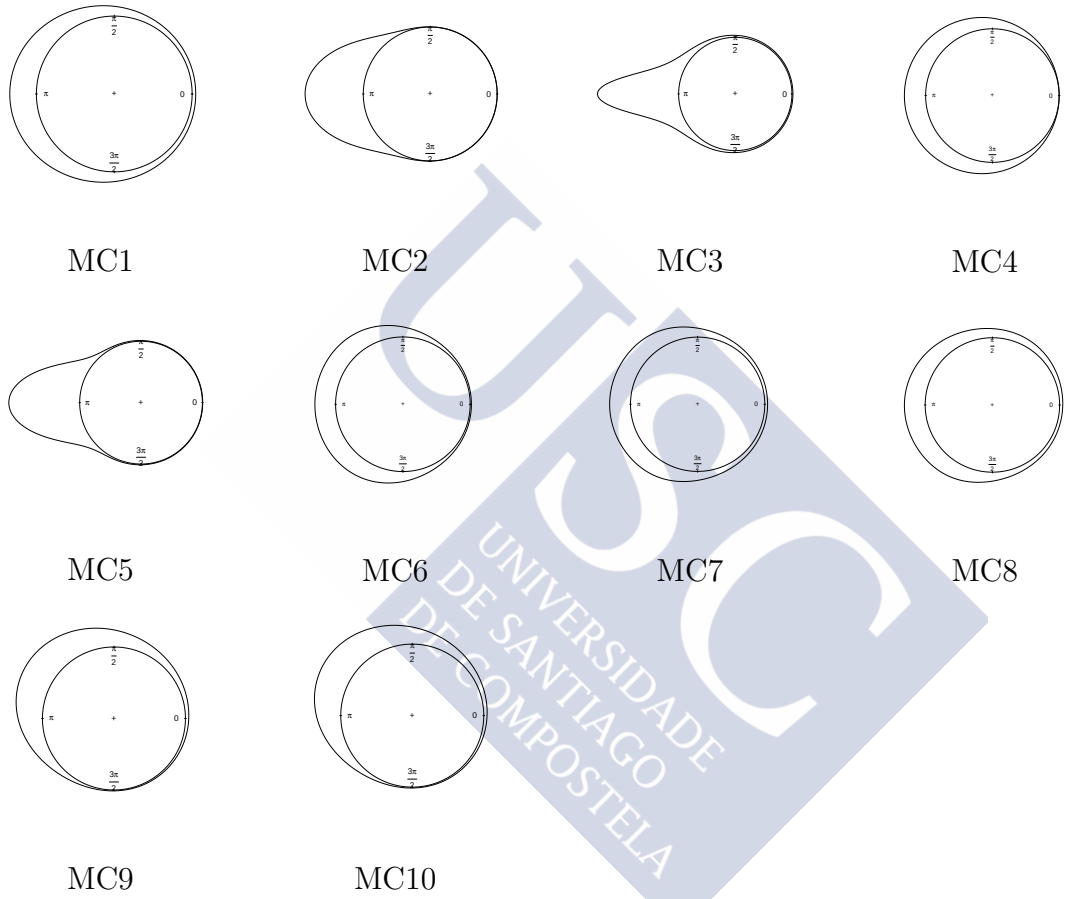

Figure A.5: Circular representation of the unimodal density functions: MC1–MC10. These models were used in Section 1.2 and 3.2 for illustration purposes and in Section 3.3 as part of the simulation study carried out for comparing the calibration of the different procedures for testing the number of modes in the circular case.

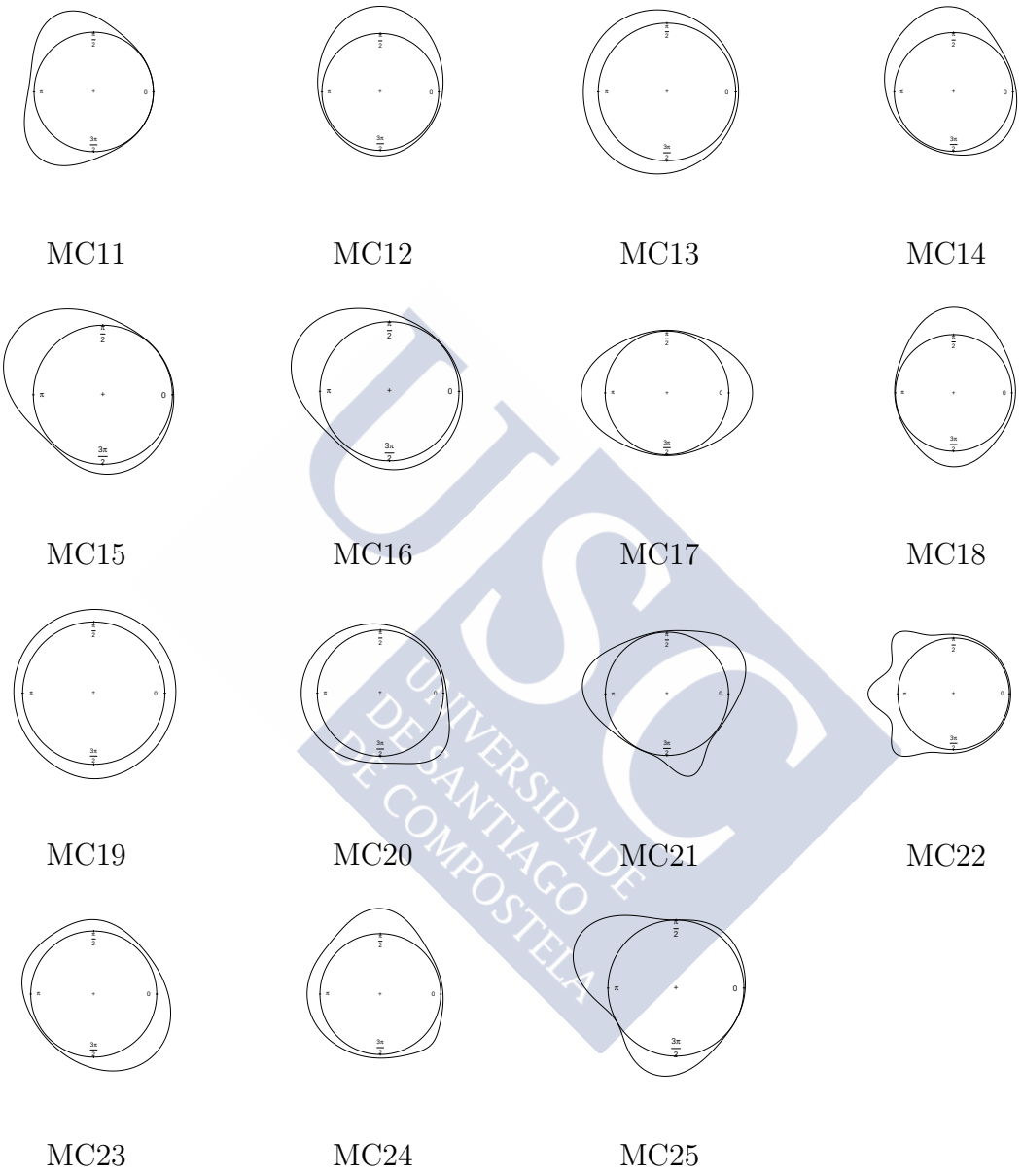

Figure A.6: Circular representation of some density functions. MC11–MC20: bimodal models. MC21–MC25: trimodal models. These models were used in Section 3.3 as part of the simulation study comparing, in terms of empirical size and power, the different procedures for testing the number of modes in the circular case.

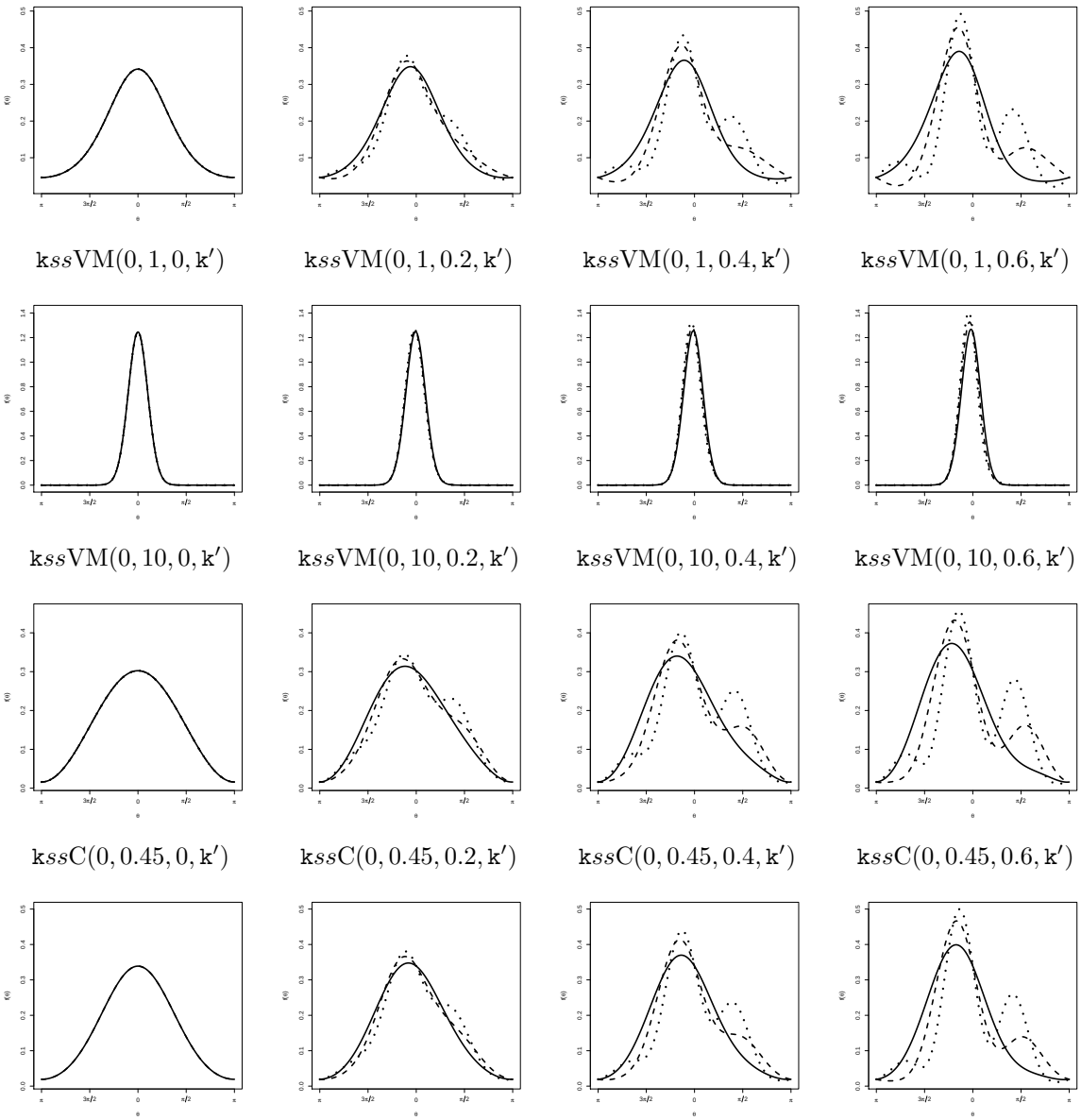

Figure A.7: Linear representation of k–sine–skewed models. solid line: $\mathtt{k}' = 1$. Dashed line: $\mathtt{k}' = 2$. Pointed line: $\mathtt{k}' = 3$. These models were used in Section 4.3 as part of the simulation study comparing, in terms of empirical size and power, the different procedures for testing reflective symmetry in the circular case.

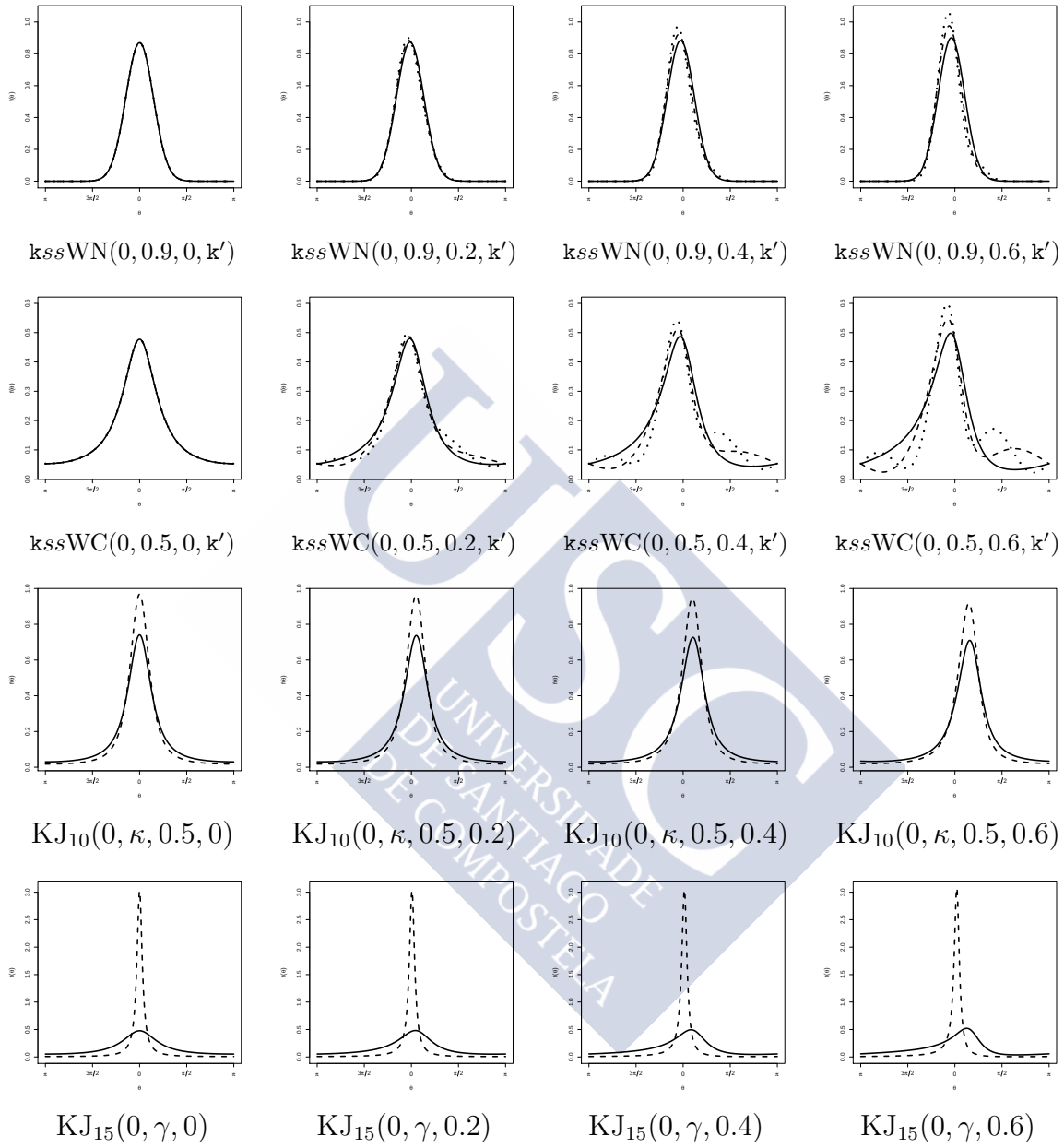

Figure A.8: Linear representation of k–sine–skewed and Kato Jones models. First two columns: solid line, $\mathtt{k}' = 1$; dashed line, $\mathtt{k}' = 2$; pointed line, $\mathtt{k}' = 3$. Third column: solid line, $\kappa = 0.5$; dashed line, $\kappa = 0.9$. Forth column: solid line, $\gamma = 0.5$; dashed line, $\gamma = 0.9$. These models were used in Section 4.3 as part of the simulation study comparing, in terms of empirical size and power, the different procedures for testing reflective symmetry in the circular case.

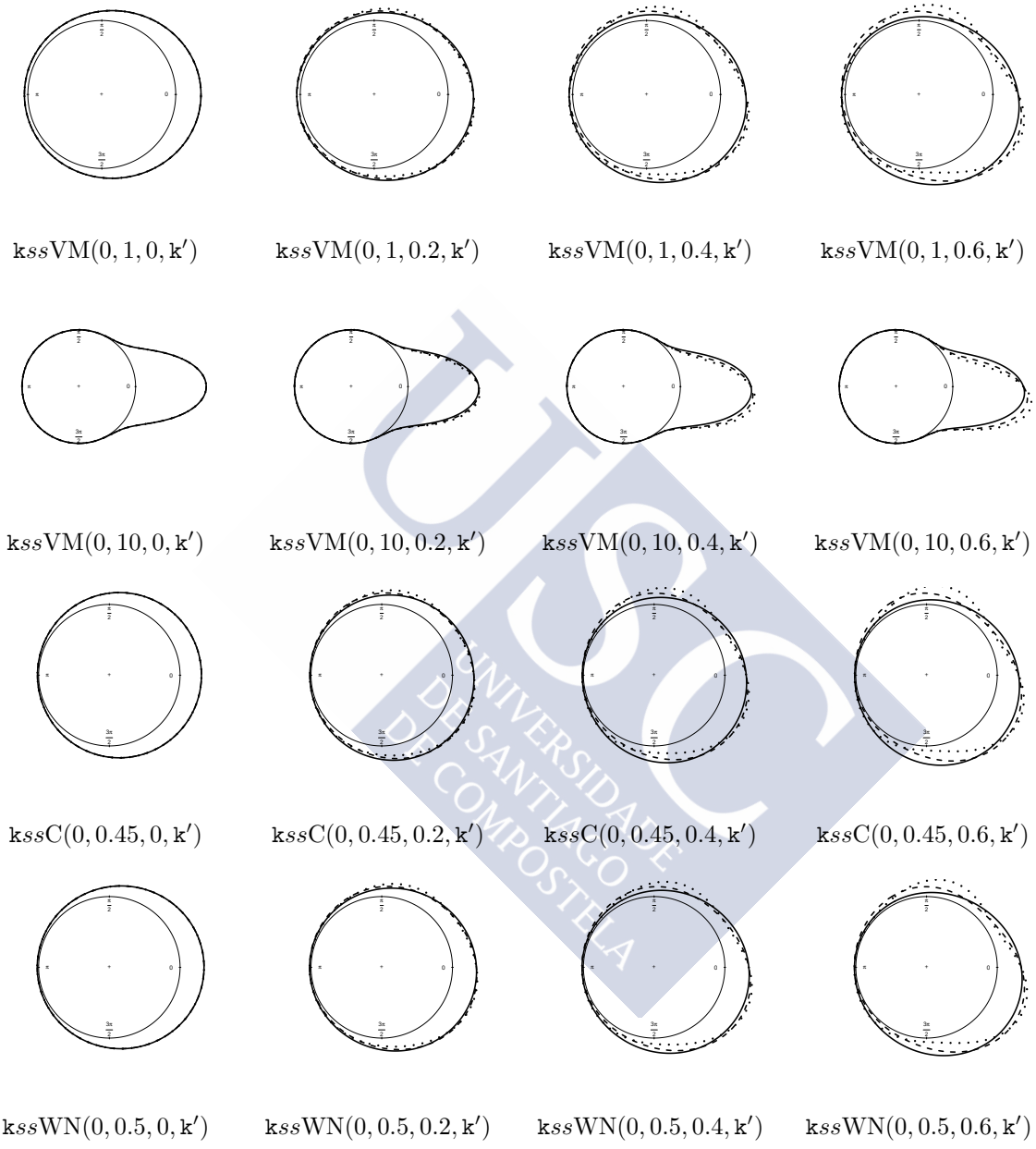

kssVM$(0, 1, 0, \mathtt{k}')$ kssVM$(0, 1, 0.2, \mathtt{k}')$ kssVM$(0, 1, 0.4, \mathtt{k}')$ kssVM$(0, 1, 0.6, \mathtt{k}')$

kssVM$(0, 10, 0, \mathtt{k}')$ kssVM$(0, 10, 0.2, \mathtt{k}')$ kssVM$(0, 10, 0.4, \mathtt{k}')$ kssVM$(0, 10, 0.6, \mathtt{k}')$

kssC$(0, 0.45, 0, \mathtt{k}')$ kssC$(0, 0.45, 0.2, \mathtt{k}')$ kssC$(0, 0.45, 0.4, \mathtt{k}')$ kssC$(0, 0.45, 0.6, \mathtt{k}')$

kssWN$(0, 0.5, 0, \mathtt{k}')$ kssWN$(0, 0.5, 0.2, \mathtt{k}')$ kssWN$(0, 0.5, 0.4, \mathtt{k}')$ kssWN$(0, 0.5, 0.6, \mathtt{k}')$

Figure A.9: Circular representation of k–sine–skewed models. solid line: $\mathtt{k}' = 1$. Dashed line: $\mathtt{k}' = 2$. Pointed line: $\mathtt{k}' = 3$. These models were used in Section 4.3 as part of the simulation study comparing, in terms of empirical size and power, the different procedures for testing reflective symmetry in the circular case.

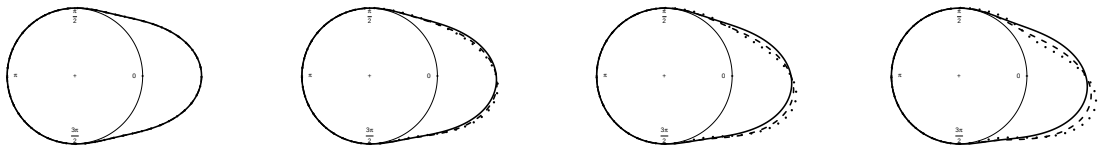

$\mathtt{k}ss\mathrm{WN}(0, 0.9, 0, \mathtt{k}')$ $\mathtt{k}ss\mathrm{WN}(0, 0.9, 0.2, \mathtt{k}')$ $\mathtt{k}ss\mathrm{WN}(0, 0.9, 0.4, \mathtt{k}')$ $\mathtt{k}ss\mathrm{WN}(0, 0.9, 0.6, \mathtt{k}')$

$\mathtt{k}ss\mathrm{WC}(0, 0.5, 0, \mathtt{k}')$ $\mathtt{k}ss\mathrm{WC}(0, 0.5, 0.2, \mathtt{k}')$ $\mathtt{k}ss\mathrm{WC}(0, 0.5, 0.4, \mathtt{k}')$ $\mathtt{k}ss\mathrm{WC}(0, 0.5, 0.6, \mathtt{k}')$

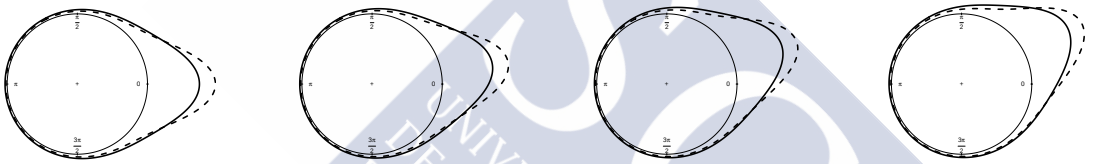

$\mathrm{KJ}_{10}(0, \kappa, 0.5, 0)$ $\mathrm{KJ}_{10}(0, \kappa, 0.5, 0.2)$ $\mathrm{KJ}_{10}(0, \kappa, 0.5, 0.4)$ $\mathrm{KJ}_{10}(0, \kappa, 0.5, 0.6)$

$\mathrm{KJ}_{15}(0, \gamma, 0)$ $\mathrm{KJ}_{15}(0, \gamma, 0.2)$ $\mathrm{KJ}_{15}(0, \gamma, 0.4)$ $\mathrm{KJ}_{15}(0, \gamma, 0.6)$

Figure A.10: Circular representation of k–sine–skewed and Kato Jones models. First two columns: solid line, $\mathtt{k}' = 1$; dashed line, $\mathtt{k}' = 2$; pointed line, $\mathtt{k}' = 3$. Third column: solid line, $\kappa = 0.5$; dashed line, $\kappa = 0.9$. Forth column: solid line, $\gamma = 0.5$; dashed line, $\gamma = 0.9$. These models were used in Section 4.3 as part of the simulation study comparing, in terms of empirical size and power, the different procedures for testing reflective symmetry in the circular case.

USC
UNIVERSIDADE
DE SANTIAGO
DE COMPOSTELA

Appendix B

Some theoretical results

This appendix is devoted to proof different results obtained in Chapters 2 and 4. In Section B.1, for the linear case, it is obtained the asymptotic convergence, in probability, of $\hat{d}_i$ to d_i (2.1.8), for all the modes and antimodes of f. This includes the convergence of the estimated modes and antimodes to the real turning points when the critical bandwidth of Hall and York (2001) is employed. In section B.2 is proved some results given in Chapter 4 to get the optimality and the asymptotic distribution under the null and under the ~~k–sine–skewed~~ alternatives of the test statistic for testing circular symmetry.

B.1 Proofs for the linear multimodality test

The complementary results needed to prove that $\hat{d}_i$ converge, in probability, to d_i, as $n \to \infty$, for $i = 1, \ldots, (2j-1)$, where j is the number of modes of f, are given in this part. These proves are based on some results of Romano (1988). In order to provide the different demonstrations, some further conditions must be considered:

(C1) f is a bounded and derivable density function.

(C2) The second derivative of f is continuous in a neighbourhood of the order points $x_1, \ldots, x_{2j-1}$. For all these points, f satisfies $f(x_i) \cdot f''(x_i) \neq 0$, $f'(x_i) = 0$ and $\text{Sign}\{f'(x_i+)\} = -\text{Sign}\{f'(x_i-)\}$. In addition, $f'(x) \neq 0$ if $x \notin \{x_1, \ldots, x_{2j-1}\}$.

(C3) f has a bounded support $[a, b]$.

(C4) $f'(a+) > 0$ and $f'(b-) < 0$.

(C5) f is twice continuously differentiable on $[a, b]$.

(C6) Denoting as a_n and b_n the fixed sequence of numbers such as $(nb_n^2)/(\log(n)a_n) \to \infty$ and $a_n \to 0$. The bandwidth $h_{(n)}$ satisfies $b_n \leq h_{(n)} \leq a_n$ and $f_{h_{(n)}}$ has j modes and $(j-1)$ antimodes.

(C7) Let $S_n = S_n(X_1, \ldots, X_n)$ be any statistic such that for some real values s_1 and s_2,

$$0 < s_1 \leq \liminf_{n\to\infty} S_n \leq \limsup_{n\to\infty} S_n \leq s_2 < \infty \quad a.s.$$

(C8) Let $\eta_{(n;l)}$ be a fixed sequence of numbers with $\eta_{(n;l)} \to 0$ and $n{\eta_{(n;l)}}^{2l+1}/\log(n) \to \infty$.

Under assumptions (C1), (C2) and (C6), denoting as $\widehat{x_i}$ to the nearest mode or antimode of $\hat{f}_{h_{(n)}}$ to x_i, for $i \in \{1, \ldots, 2j-1\}$, then

(R1) $\widehat{x_i} \to x_i \quad a.s.$

(R2) $\hat{f}_{h_{(n)}}(\widehat{x_i}) \to f(\widehat{x_i}) \quad a.s$

Also, if (R1) is satisfied, employing the Proposition 2.1. of Romano (1988), given the order of the derivative l, and under the assumptions (C2), (C7) and (C8), taking the bandwidth $h_{(n;l)} = \eta_{(n;l)} \cdot S_n$ the following convergence is obtained, for all $i \in \{1, \ldots, 2j-1\}$,

(R3) $\hat{f}^{(l)}_{h_{(n;l)}}(\widehat{x_i}) \to f^{(l)}(x_i) \quad a.s..$

Note that under (C7) and (C8), taking $a_n = \eta_{(n;0)} \cdot s_2$ and $b_n = \eta_{(n;0)} \cdot s_1$, the first part of condition (C6) is also satisfied, so employing the bandwidth $h_{(n;0)} = \eta_{(n;0)} \cdot S_n$, if it has j modes and $(j-1)$ antimodes, (C6) can be replaced by (C7) and (C8).

Although, in this essay, the results are given under more general conditions, for the important case of the critical bandwidth h_j, employing the results of Mammen et al. (1992), under (C1)–(C5), h_j always satisfy (C6). Based on this fact, combined with previous results, it is concluded that, under (C1)–(C5), $\hat{d}_i$ converge in probability to d_i, as $n \to \infty$, for $i = 1, \ldots, (2j-1)$. Note that for having this last result no more conditions that those ones given as *Assumptions* in Mammen et al. (1992) are needed.

To prove the results given in (R1) and (R2), in this thesis, the focus will be when x_i is a mode, that is, $i = 1, 3, \ldots, 2j-1$. The proof for the antimodes is analogue to the given one. To begin the proof, first, it will be introduced the following function

$$f_h(t) = \frac{1}{h}\int_{-\infty}^{\infty} K\left(\frac{t-y}{h}\right) f(y)dy.$$

Taking $x_0 = 2a - x_1$ and $x_{2j} = 2b - x_{2j-1}$ (note that condition (C3) is not needed in this case, if the support is unbounded these values can be replace conveniently with other values $x_0 < x_1$ and $x_{2j} > x_{2j-1}$), let δ_i be the values such as $\delta_i \leq \min\{(x_i - x_{i-1})/2, (x_{i+1} - x_i)/2\}$ and also the following conditions are satisfied (see Romano, 1988, Proposition 5.1. and Corollary 5.1.)

$$\lim_{n\to\infty} \sup_{\{h:b_n\leq h\leq a_n\}} \sup_{\{t:|t-x_i|<\delta_i\}} |f_h(t) - f(t)| \leq \lim_{n\to\infty} \sup_{\{h:0<h\leq a_n\}} \sup_{\{t:|t-x_i|<\delta_i\}} |f_h(t) - f(t)| = 0. \quad \text{(B.1.1)}$$

$$\sup_{\{h:b_n\leq h\leq a_n\}} \sup_{\{t:|t-x_i|<\delta_i\}} |\hat{f}_h(t) - f_h(t)| \leq \sup_{\{h:b_n\leq h\leq a_n\}} \sup_t |\hat{f}_h(t) - f_h(t)| \to 0 \quad c.s. \quad \text{(B.1.2)}$$

Combining (B.1.1) and (B.1.2), it is obtained that

$$\mathbb{P}\left(\lim_{n\to\infty} \sup_{\{h:b_n\leq h\leq a_n\}} \sup_{\{t:|t-x_i|<\delta_i\}} |\hat{f}_h(t) - f(t)| = 0\right) = 1 \quad \text{(B.1.3)}$$

Using that, by definition, fixed $i \in \{1, 3, \ldots, 2j-1\}$, for any $\delta \in (0, \delta_i)$,

$$\sup_{t:\delta<|t-x_i|<\delta_i} f(t) < f(x_i),$$

the continuity of f, its Taylor expansion and $\int_{-\infty}^{\infty} K(z)dz = 1$, the following inequality is satisfied,

$$\lim_{n\to\infty} \sup_{\{h:b_n\leq h\leq a_n\}} \sup_{\{t:\delta\leq|t-x_i|<\delta_i\}} f_h(t) \leq \lim_{n\to\infty} \sup_{\{h:0<h\leq a_n\}} \sup_{\{t:\delta\leq|t-x_i|<\delta_i\}} \int_{-\infty}^{\infty} K(z)\, f(t-zh)dz < f(x_i). \quad \text{(B.1.4)}$$

Combining (B.1.2) and (B.1.4) yields

$$\mathbb{P}\left(\lim_{n\to\infty} \sup_{\{h:b_n\leq h\leq a_n\}} \sup_{\{t:\delta\leq|t-x_i|<\delta_i\}} \hat{f}_h(t) < f(x_i)\right) = 1 \quad \text{(B.1.5)}$$

Denoting as $\hat{l}_{i,h}$ the point, in the interval $(x_i - \delta, x_i + \delta)$, where the supreme of $\hat{f}_h$ is obtained for a given value of h, satisfying $b_n \leq h \leq a_n$, and then combining (B.1.3)

and (B.1.5), it yields

$$\mathbb{P}\left(\lim_{n\to\infty}\sup_{\{h:b_n\leq h\leq a_n\}}|\hat{l}_{i,h}-x_i|\geq\delta\right)=0$$

Since this can be done for any $\delta\in(0,\delta_i)$, this proves

$$\sup_{\{h:b_n\leq h\leq a_n\}}|\hat{l}_{i,h}-x_i|\to 0\quad a.s,$$

now, employing (B.1.3) and (B.1.5) with the fact that $\hat{f}_h$ is continuous, for each $i\in\{1,3,\ldots,(2j-1)\}$, yields that $\hat{l}_{i,h}$ is a mode of $\hat{f}_h$ and it is satisfied

$$\sup_{\{h:b_n\leq h\leq a_n\}}\sup_{\{t:|t-x_i|<\delta_i\}}\hat{f}_h(t)\to f(t)\quad a.s,\tag{B.1.6}$$

Finally, using that $\hat{f}_{h_{(n)}}$ has j modes and $\widehat{x_i}$ was defined as the closest mode of $\hat{f}_{h_{(n)}}$ to x_i necessarily

$$|\hat{x}_i-x_i|=|\hat{l}_{i,h_{(n)}}-x_i|\leq\sup_{\{h:b_n<h\leq a_n\}}|\hat{l}_{i,h}-x_i|\to 0\quad c.s.\tag{B.1.7}$$

Results (R1) and (R2) are derived from (B.1.6) and (B.1.7). □

B.2 Proofs for the circular symmetry test

This part is devoted to proof different results achieved in Section 4.2. These proofs are needed to demonstrate the asymptotic distribution under the null and under the contiguous alternatives and in order to proof that the proposed test is optimal in the maximin sense.

B.2.1 Proof of Lemma 4.2.1

The first part of Lemma 4.2.1, that is, $\hat{\Gamma}_{f_0,g_0,\mathbf{k};11}-\Gamma_{f_0,g_0,\mathbf{k};11}=o_{\mathrm{P}}(1)$ as $n\to\infty$ under $\mathrm{P}^{(n)}_{(\mu,0);g_0}$ is showed bellow. The proof of $\hat{\Gamma}_{g_0,\mathbf{k};12}-\Gamma_{g_0,\mathbf{k};12}=o_{\mathrm{P}}(1)$ as $n\to\infty$ under $\mathrm{P}^{(n)}_{(\mu,0);g_0}$ can be done along the same lines. In this proof, it is taken $\mu^{(n)}=\mu+n^{-1/2}\tau_1^{(n)}$,

for some bounded sequence $\tau_1^{(n)}$ as in Theorem 4.1.1. Due to the local discreteness of $\hat{\mu}^{(n)}$ (Assumption B), it is sufficient to show that

$$\frac{1}{n}\sum_{i=1}^{n}\dot{\varphi}_{f_0}\left(\Theta_i-\mu^{(n)}\right)-\mathrm{E}_{g_0}[\dot{\varphi}_{f_0}\left(\Theta_i-\mu\right)]=o_{\mathrm{P}}(1)$$

as $n\to\infty$ under $\mathrm{P}^{(n)}_{(\mu,0);g_0}$. The law of large numbers directly entails that

$$\frac{1}{n}\sum_{i=1}^{n}\dot{\varphi}_{f_0}\left(\Theta_i-\mu\right)-\mathrm{E}_{g_0}[\dot{\varphi}_{f_0}\left(\Theta_i-\mu\right)]=o_{\mathrm{P}}(1)$$

as $n\to\infty$ under $\mathrm{P}^{(n)}_{(\mu,0);g_0}$ so that it only remains to show that

$$S_n=\frac{1}{n}\sum_{i=1}^{n}(\dot{\varphi}_{f_0}\left(\Theta_i-\mu^{(n)}\right)-\dot{\varphi}_{f_0}\left(\Theta_i-\mu\right))$$

is $o_{\mathrm{P}}(1)$ as $n\to\infty$ under $\mathrm{P}^{(n)}_{(\mu,0);g_0}$. Since the Θ_i are independent independent and identically distributed,

$$\begin{aligned}\mathrm{E}[|S_n|] &\leq \frac{1}{n}\sum_{i=1}^{n}\mathrm{E}[|(\dot{\varphi}_{f_0}\left(\Theta_i-\mu^{(n)}\right)-\dot{\varphi}_{f_0}\left(\Theta_i-\mu\right))|]\\ &= \mathrm{E}[|(\dot{\varphi}_{f_0}\left(\Theta_1-\mu^{(n)}\right)-\dot{\varphi}_{f_0}\left(\Theta_1-\mu\right))|].\end{aligned}$$

Since $\dot{\varphi}_{f_0}$ is continuous on a compact support, it is bounded; the result then follows by applying the Lebesgue Dominated Convergence Theorem.

□

B.2.2 Proof of Lemma 4.2.2

For proving (i), first, it is showed that $\Delta^{(n);ecd}_{f_0,g_0,\mathtt{k};2}\left(\hat{\mu}^{(n)}\right)-\Delta^{(n);ecd}_{f_0,g_0,\mathtt{k};2}(\mu)=o_{\mathrm{P}}(1)$ under $\mathrm{P}^{(n)}_{(\mu,0);g_0}$ as $n\to\infty$. For doing so note that Assumption C directly entails that under $\mathrm{P}^{(n)}_{(\mu,0);g_0}$, as $n\to\infty$,

$$\begin{aligned}n^{-1/2}\sum_{i=1}^{n}\varphi_{f_0}(\Theta_i-\hat{\mu}^{(n)}) &= \Delta^{(n)}_{f_0,\mathtt{k};1}-\mathrm{E}_{g_0}[\dot{\varphi}_{f_0}(\Theta_i-\mu)]n^{1/2}(\hat{\mu}^{(n)}-\mu)+o_{\mathrm{P}}(1)\\ &= \Delta^{(n)}_{f_0,\mathtt{k};1}-\Gamma_{f_0,g_0,\mathtt{k};11}n^{1/2}(\hat{\mu}^{(n)}-\mu)+o_{\mathrm{P}}(1). \qquad \text{(B.2.8)}\end{aligned}$$

Therefore, combining (4.2.8) and (B.2.8), it follows that

$$\begin{aligned}\Delta^{(n);ecd}_{f_0,g_0,\mathtt{k};2}\left(\hat{\mu}^{(n)}\right) &= \Delta^{(n)}_{\mathtt{k};2}(\mu) - \eta\Delta^{(n)}_{f_0,\mathtt{k};1} - (\Gamma_{g_0,\mathtt{k};12} - \eta\Gamma_{f_0,g_0,\mathtt{k};11})n^{1/2}(\hat{\mu}^{(n)} - \mu) + o_{\mathrm{P}}(1) \\ &= \Delta^{(n);ecd}_{f_0,g_0,\mathtt{k};2}(\mu) + o_{\mathrm{P}}(1),\end{aligned}$$

since $(\Gamma_{g_0,\mathtt{k};12} - \eta\Gamma_{f_0,g_0,\mathtt{k};11}) = 0$. It remains to show that

$$\Delta^{*(n);ecd}_{f_0,\mathtt{k};2}\left(\hat{\mu}^{(n)}\right) - \Delta^{(n);ecd}_{f_0,g_0,\mathtt{k};2}\left(\hat{\mu}^{(n)}\right) = -\left(\frac{\hat{\Gamma}_{g_0,\mathtt{k};12}}{\hat{\Gamma}_{f_0,g_0,\mathtt{k};11}} - \frac{\Gamma_{g_0,\mathtt{k};12}}{\Gamma_{f_0,g_0,\mathtt{k};11}}\right)\Delta^{(n)}_{f_0,\mathtt{k};1}\left(\hat{\mu}^{(n)}\right) = o_{\mathrm{P}}(1) \tag{B.2.9}$$

under $\mathrm{P}^{(n)}_{(\mu,0);g_0}$ as $n \to \infty$. To prove (B.2.9), first note that (B.2.8) and the Central Limit Theorem readily imply that $\Delta^{(n)}_{f_0,\mathtt{k};1}\left(\hat{\mu}^{(n)}\right)$ is $O_{\mathrm{P}}(1)$ under $\mathrm{P}^{(n)}_{(\mu,0);g_0}$ as $n \to \infty$. Therefore, it is only needed to show that

$$\frac{\hat{\Gamma}_{g_0,\mathtt{k};12}}{\hat{\Gamma}_{f_0,g_0,\mathtt{k};11}} - \frac{\Gamma_{g_0,\mathtt{k};12}}{\Gamma_{f_0,g_0,\mathtt{k};11}} = o_{\mathrm{P}}(1) \tag{B.2.10}$$

as $n \to \infty$ under $\mathrm{P}^{(n)}_{(\mu,0);g_0}$ as $n \to \infty$. Since

$$\frac{\hat{\Gamma}_{g_0,\mathtt{k};12}}{\hat{\Gamma}_{f_0,g_0,\mathtt{k};11}} - \frac{\Gamma_{g_0,\mathtt{k};12}}{\Gamma_{f_0,g_0,\mathtt{k};11}} = \frac{\hat{\Gamma}_{g_0,\mathtt{k};12} - \Gamma_{g_0,\mathtt{k};12}}{\hat{\Gamma}_{f_0,g_0,\mathtt{k};11}} - \frac{\Gamma_{g_0,\mathtt{k};12}\left(\hat{\Gamma}_{f_0,g_0,\mathtt{k};11} - \Gamma_{f_0,g_0,\mathtt{k};11}\right)}{\hat{\Gamma}_{f_0,g_0,\mathtt{k};11}\Gamma_{f_0,g_0,\mathtt{k};11}},$$

the results directly follows from Lemma 4.2.1.

Turning to the proof of (ii), working along the same lines as at the end of the proof of Lemma 4.2.1, it is easy to obtain that

$$n^{-1}\sum_{i=1}^{n}\varphi^2_{f_0}(\Theta_i - \hat{\mu}^{(n)}) - \mathrm{E}_{g_0}[\varphi^2_{f_0}(\Theta_i - \mu)] \tag{B.2.11}$$

and

$$n^{-1}\sum_{i=1}^{n}\sin(\mathtt{k}(\Theta_i - \hat{\mu}^{(n)}))\varphi_{f_0}(\Theta_i - \hat{\mu}^{(n)}) - \mathrm{E}_{g_0}[\sin(\mathtt{k}(\Theta_i - \mu))\varphi_{f_0}(\Theta_i - \mu)] \tag{B.2.12}$$

are $o_{\mathrm{P}}(1)$ under $\mathrm{P}^{(n)}_{(\mu,0);g_0}$ as $n \to \infty$. It directly follows that $C^{(n)}_{f_0,g_0,\mathtt{k}}\left(\hat{\mu}^{(n)}\right) - C^{(n)}_{f_0,g_0,\mathtt{k}}(\mu) = o_{\mathrm{P}}(1)$ under $\mathrm{P}^{(n)}_{(\mu,0);g_0}$ as $n \to \infty$. Therefore it remains to show that $C^{*(n)}_{f_0,\mathtt{k}}\left(\hat{\mu}^{(n)}\right) - C^{(n)}_{f_0,g_0,\mathtt{k}}\left(\hat{\mu}^{(n)}\right)$ is $o_{\mathrm{P}}(1)$ under $\mathrm{P}^{(n)}_{(\mu,0);g_0}$ as $n \to \infty$. This last result is obtained showing that

$$\begin{aligned}C^{*(n)}_{f_0,\mathtt{k}}\left(\hat{\mu}^{(n)}\right) - C^{(n)}_{f_0,g_0,\mathtt{k}}\left(\hat{\mu}^{(n)}\right) &= \left(\frac{\hat{\Gamma}^2_{g_0,\mathtt{k};12}}{\hat{\Gamma}^2_{f_0,g_0,\mathtt{k};11}} - \frac{\Gamma^2_{g_0,\mathtt{k};12}}{\Gamma^2_{f_0,g_0,\mathtt{k};11}}\right)n^{-1}\sum_{i=1}^{n}\varphi^2_{f_0}(\Theta_i - \hat{\mu}^{(n)}) \\ &-2\left(\frac{\hat{\Gamma}_{g_0,\mathtt{k};12}}{\hat{\Gamma}_{f_0,g_0,\mathtt{k};11}} - \frac{\Gamma_{g_0,\mathtt{k};12}}{\Gamma_{f_0,g_0,\mathtt{k};11}}\right)n^{-1}\sum_{i=1}^{n}\sin(\mathtt{k}(\Theta_i - \hat{\mu}^{(n)}))\varphi_{f_0}(\Theta_i - \hat{\mu}^{(n)}),\end{aligned}$$

now, using (B.2.11) and (B.2.12) together with (B.2.10) and the continuous mapping theorem directly imply that $C^{*(n)}_{f_0,\mathtt{k}}\left(\hat{\mu}^{(n)}\right) - C^{(n)}_{f_0,g_0,\mathtt{k}}\left(\hat{\mu}^{(n)}\right)$ is $o_{\mathrm{P}}(1)$ under $\mathrm{P}^{(n)}_{(\mu,0);g_0}$ as $n \to \infty$. The result follows.

□

B.2.3 Proof of Theorem 4.2.1

Fix $g_0 \in \mathcal{F}$ and $\mu \in [-\pi, \pi)$. Lemma 4.2.2 combined with Slutski's Lemma leads to

$$Q^{*(n)}_{f_0,\mathtt{k}} = \frac{\Delta^{(n);ecd}_{f_0,g_0,\mathtt{k};2}(\mu)}{C^{(n)}_{f_0,g_0,\mathtt{k}}(\mu)} + o_P(1) = \frac{\Delta^{(n);ecd}_{f_0,g_0,\mathtt{k};2}(\mu)}{V^{g_0}_{f_0}(\mathtt{k})} + o_P(1) \tag{B.2.13}$$

as $n \to \infty$ under $\mathrm{P}^{(n)}_{(\mu,0)';g_0}$. Part (i) then follows from the Central Limit Theorem.

Part (ii) is obtained via Le Cam's Third Lemma. First, it is necessary to calculate the joint distribution of $\Delta^{*(n);ecd}_{f_0,\mathtt{k};2}\left(\hat{\mu}^{(n)}\right)$ and $\log(d\mathrm{P}^{(n)}_{(\mu,n^{-1/2}\tau_2^{(n)})';g_0,\mathtt{k}'}/d\mathrm{P}^{(n)}_{(\mu,0)';g_0})$ under $\mathrm{P}^{(n)}_{(\mu,0)';g_0}$. For doing so, the Lemma 4.2.2 and the multivariate Central Limit Theorem can be used for obtaining that

$$\frac{1}{\sqrt{n}}\sum_{i=1}^{n}\begin{pmatrix}\sin(\mathtt{k}(\Theta_i-\mu)) - \eta\varphi_{f_0}(\Theta_i-\mu)\\ \tau_2^{(n)}\sin(\mathtt{k}'(\Theta_i-\mu))\end{pmatrix} - \begin{pmatrix}0\\ \frac{1}{2}(\tau_2^{(n)})^2\Gamma_{g_0,\mathtt{k}';22}\end{pmatrix} \xrightarrow{\mathcal{D}}$$
$$\mathcal{N}_2\left(\begin{pmatrix}0\\ -\frac{1}{2}(\tau_2)^2\Gamma_{g_0,\mathtt{k}';22}\end{pmatrix}, \begin{pmatrix}V^{g_0}_{f_0}(\mathtt{k}) & \tau_2 C^{g_0}_{f_0}(\mathtt{k},\mathtt{k}')\\ \tau_2 C^{g_0}_{f_0}(\mathtt{k},\mathtt{k}') & (\tau_2)^2\Gamma_{g_0,\mathtt{k}';22}\end{pmatrix}\right)$$

as $n \to \infty$ under $\mathrm{P}^{(n)}_{(\mu,0)';g_0}$. Now, since $\mathrm{P}^{(n)}_{(\mu,0)';g_0}$ and $\mathrm{P}^{(n)}_{(\mu,n^{-1/2}\tau_2^{(n)})';g_0,\mathtt{k}'}$ are mutually contiguous, the result $\Delta^{*(n);ecd}_{f_0,\mathtt{k};2}\left(\hat{\mu}^{(n)}\right) \xrightarrow{\mathcal{D}} \mathcal{N}(\tau_2 C^{g_0}_{f_0}(\mathtt{k},\mathtt{k}'), V^{g_0}_{f_0}(\mathtt{k}))$ under $\mathrm{P}^{(n)}_{(\mu,n^{-1/2}\tau_2^{(n)})';g_0,\mathtt{k}'}$ as $n \to \infty$ is obtained applying the Third Le Cam Lemma.

Part (iii) is proved combining the result (B.2.13) under $\mathrm{P}^{(n)}_{(\mu,0)';f_0}$ with the result mentioned at the beginning of Section 4.2.2, that is, $\Delta^{(n);ecd}_{f_0,f_0,\mathtt{k};2}(\mu) - \Delta^{(n)eff}_{f_0,\mathtt{k};2}(\mu) = o_{\mathrm{P}}(1)$ as $n \to \infty$ under $\mathrm{P}^{(n)}_{(\mu,0)',f_0}$ (and therefore under contiguous alternatives), and the optimality of the parametric test $\phi^{(n)}_{f_0,\mathtt{k}}$.

□

USC
UNIVERSIDADE
DE SANTIAGO
DE COMPOSTELA

Appendix C

Software: multimode package

With the aim of making the mode testing procedures for linear data accessible for the scientific community, and therefore, enabling its use in practical problems, an R package has been developed (R Core Team, 2017). This appendix is intended for presenting the utilities of package **multimode**, which has been implemented collecting the contributions from Chapter 2 on testing the number of modes, and some already existing (exploratory and testing) methods. The package will be released under GPL–3 license and uploaded to CRAN in due course. Future extensions of the package will include the testing procedure introduced in Chapter 3. Specifically, in its current version, the package includes the datasets and the functions shown in Table C.1. The contents of this appendix are organized in two parts. First, a brief demonstration of the package capabilities will be given. Second, some numerical approximations must be done in order to get the critical bandwidth and the excess mass in the **multimode** package and for the simulation study in Section 2.2 and those ones are described in Section C.2.

C.1 Using multimode

A complete description of **multimode** capabilities is provided in this section. First, the different datasets available in the package will be described. Second, the usage of different functions for exploring the number of modes will be illustrated. Finally, the functions for testing multimodality and estimating the location of modes and antimodes will be introduced.

Dataset	Description
`acidity`	Acid–neutralizing capacity
`chondrite`	Percentage of silica in chondrite meteors
`enzyme`	Blood enzymatic activity
`galaxy`	Velocities of galaxies
`geyser`	Waiting time between geyser eruptions
`stamps`	Stamps thickness
Function	**Description**
`critbw`	Critical bandwidth computation
`excessmass`	Excess mass statistic
`locmodes`	Location of modes and antimodes
`modeforest`	Mode forest
`modetest`	Test for the number of modes
`modetree`	Mode tree
`nmodes`	Number of modes
`sizer`	SiZer map

Table C.1: Summary of **multimode** package contents.

C.1.1 Data description

The package **multimode** includes some classical datasets for which determining the number of different groups in the sample and/or exploring the location of modes and antimodes are relevant issues. The first dataset, `acidity`, analysed by Crawford (1994), contains, on the log scale, the Acid–Neutralizing Capacity (ANC) measured in a sample of 155 lakes in North–Central Wisconsin (USA). ANC describes the capability of a lake to absorb acid, where low ANC values may lead to a loss of biological resources. The dataset `chondrite`, included in Table 2 of Good and Gaskins (1980), contains the percentage silica (in %) in 22 chondrite meteors. The dataset `enzyme`, introduced by Bechtel et al. (1993), collects a sample with the distribution of enzymatic activity in the blood, for an enzyme involved in the metabolism of carcinogenic substances. The dataset `galaxy` contains the velocities in km/sec of different galaxies (diverging away from our own galaxy) from the unfilled survey of the Corona Borealis region. In this dataset introduced by Postman et al. (1986) and further studied by Roeder (1990), multimodality is an evidence for voids and superclusters in the universe. The dataset in `geyser` contains the interval times between the starts of the geyser eruptions collected during different periods on the Old Faithful Geyser in Yellowstone National Park, Wyoming, USA. The included periods are: October 1980, obtained from Table 3 of Härdle (2012) and the supplementary material of Weisberg (2005); and August 1985, from Table 1 in Azzalini and Bowman (1990). Finally, the dataset `stamps`, introduced in Section 1.3.1, analysed in Izenman and Sommer (1988) and in Section 2.3 of

this manuscript, consists of thickness measurements (in millimetres) of 485 unwatermarked used white wove stamps of the 1872 Hidalgo stamp issue of Mexico. All of them had an overprint with the year (1872 or either an 1873 or 1874) and some of them were watermarked (Papel Sellado or LA+-F), being this information also included inside `stamps`.

Some of these datasets (`acidity`, `enzyme`, `galaxy` or `stamps`), were used in the statistical literature for illustrating mixtures of parametric models. Then, the nonparametric (both exploratory and inferential) tools included in **multimode** could be seen as a preliminary tool for determining the number of components. Some references can be found in, for example, McLachlan and Peel (2000) or Richardson and Green (1997). In other datasets (`chondrite`, `geyser` or `stamps`), testing or exploring the number of modes is an important problem *per se*. Some examples of their employment can be found in Chaudhuri and Marron (1999), Müller and Sawitzki (1991) or Scott (2015, Sect. 9.2). In the subsequent sections, the `stamps` dataset will be used for illustrating the functions available in the **multimode** package.

C.1.2 Exploring data with multimode

When the objective is exploring the number of modes in a sample, as mentioned in the Introduction, a simple exploratory solution might be to observe the number of peaks in the kernel density estimation for different values of h. In order to facilitate this task, using the Gaussian kernel and a given bandwidth parameter `bw`, the function `nmodes` computes the estimated number of modes in the real line or in a support bounded by `lowsup` and `uppsup`. This kernel density estimation is calculated in `n` equally spaced points of the variable for computational reasons (as in the `density` function from the **stats** package). For instance, using the code below, it is obtained that the estimated number of modes using the rule of thumb and the plug–in rule (`bw.nrd0` and `bw.SJ` from the **stats** package and illustrated in Figure 2.1, left panels) is, respectively, two and nine.

```
R> data(stamps)
R> bwRT <- bw.nrd0(stamps) ; bwPI <- bw.SJ(stamps)
R> nmodes(data=stamps,bw=bwRT,lowsup=-Inf,uppsup=Inf,n=2^15)
R> nmodes(data=stamps,bw=bwPI,lowsup=-Inf,uppsup=Inf,n=2^15)
```

Based on the idea of exploring the number of modes (and their location) for different values of h, in **multimode** there are implemented three graphical tools: `modetree`, `modeforest` and `sizer`. Below, these exploratory functions and their arguments are further explained. The common characteristics, in the three of them, are: the exploratory features will be calculated in a finite number of grid points (the common argument is the first element of `gridsize`); the number of modes will be determined according to a value of h and the employed bandwidth values can be chosen by the practitioner (`bws`, `cbw1`, `cbw2` and second

element `gridsize`); a graphical display is generated (or added to the current graphic) with different plot arguments (`display`, `logbw`, `xlab`, `ylab`); an output related with the modes location is returned.

The different exploratory tools (`modetree`, `modeforest` and `sizer`) allow three options for providing the bandwidths. The first one is to use a range of bandwidth parameters in the argument `bws` and the exploratory tool is computed in a grid of h between the given values and size equal to the second element of the argument `gridsize`. By default, a grid of size 151 is computed between a lower bandwidth equal to twice the distance between the grid points used for estimating the density and upper bandwidth equal to the data range. The second option considers the critical bandwidths for `cbw1` and `cbw2` modes as the range of bandwidths. The third method is to include a vector of bandwidths in the argument `bws` with size greater than two. Then, these exploratory tools are represented (using a $\log_{10}$ scale for the bandwidths if `logbw=TRUE`) when the argument `display` is `TRUE` with the titles in the x and y axis provided by `xlab` and `ylab`.

The mode tree introduced by Minnotte and Scott (1993) and implemented in the function `modetree`, shows with continuous lines the estimated mode locations for each bandwidth. In addition, it represents, with horizontal dashed lines, how each mode splits into more modes as the bandwidth decreases. For `modetree`, the first element of `gridsize` is equal to the number of equally spaced points at which the density is to be estimated. Moreover, the mode tree can be added to other plot when the argument `addplot` is `TRUE`. Also, the colour lines in the mode tree can be chosen with the argument `col.lines`. Below, an example with the code lines for computing the mode tree for the `stamps` dataset between the bandwidths $7.5 \cdot 10^{-4}$ and $7.5 \cdot 10^{-3}$ is shown and its representation appears in Figure C.1 (left).

```
R> mtstamps <- modetree(data=stamps,bws=c(0.00075,0.0075),
+    gridsize=c(512,151),cbw1=NULL,cbw2=NULL,display=TRUE,
+    logbw=FALSE,addplot=FALSE,xlab="Thickness (in mm)",
+    ylab=NULL,col.lines="black")
R> names(mtstamps)

[1] "locations"  "bandwidths"
```

This function returns a list containing the following components: `locations`, a matrix with the estimated mode locations for each bandwidth; and `bandwidths`, the bandwidths employed for computing the mode tree. The plot and the argument `locations` returned by the function `modetree` can be useful for exploring where the different modes are when the number of modes is not clear and one wants to explore different possibilities. In this case, the principal mode appears between the values 0.0765 and 0.0793, the secondary mode between 0.0986 and 0.1011, and so forth.

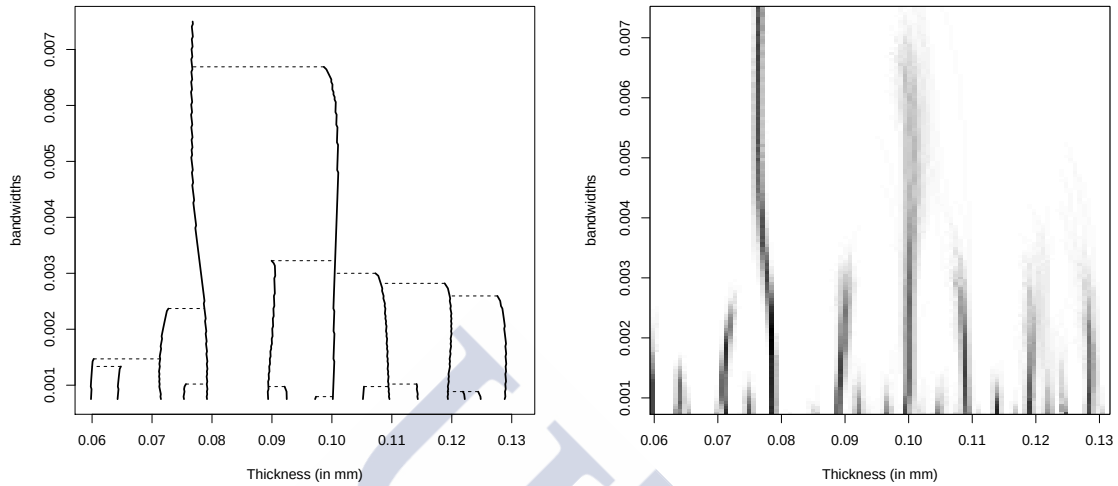

Figure C.1: Mode tree (left) and forest (right) for the sample of 485 stamps from the 1872 Hidalgo Issue of Mexico between the bandwidths $7.5 \cdot 10^{-4}$ and $7.5 \cdot 10^{-3}$. For each bandwidth, the estimated modes location are, in the left, continuous lines and, in the right, dark grey pixels. The horizontal discontinuous lines (left) indicate how each mode is split.

The mode forest, introduced by Minnotte et al. (1998), is provided by `modeforest`. The mode forest is generated by looking simultaneously at a collection of mode trees generated by the original sample and `B` random resamples drawn with replacement from the original one. This tool represents the number of times that an estimated mode falls in each location–bandwidth (horizontal–vertical axis) pixel. The pixels are then shaded proportionally to counts (large counts corresponding to darker pixels and low counts to lighter ones).

In the case of the `modeforest` and `sizer`, the first element of `gridsize` is equal to the number of grid points in the horizontal (values of the variable) axis. In both cases, the horizontal values plotted are bounded by the interval (`from`,`to`), being this interval equal to the data range by default. In the `modeforest` function, the number of equally spaced points at which the density is to be estimated is chosen by the argument `n`. The mode forest for the `stamps` dataset between the bandwidths $7.5 \cdot 10^{-4}$ and $7.5 \cdot 10^{-3}$ and represented in Figure C.1 (right) can be obtained as follows:

```
R> mfstamps <- modeforest(data=stamps,bws=c(0.00075,0.0075),
+    gridsize=c(100,151),B=99,n=512,cbw1=NULL,cbw2=NULL,
+    display=TRUE,logbw=FALSE,from=NULL,to=NULL,
+    xlab="Thickness (in mm)",ylab=NULL)
```

```
R> names(mfstamps)

[1] "modeforest" "range.x"    "range.bws"
```

Once computed the `modeforest` function, it provides a matrix (`modeforest`) including the percentage of times that an estimated mode falls in each location–bandwidth pixel. The functions `modeforest` and `sizer` return `range.x` (the employed location values to represent the mode forest or the SiZer map) and `range.bws` (the used bandwidths to compute the exploratory tool). In the `modeforest` plot, modes can be detected observing the dark grey areas, but one should be careful with the very dark areas (as that one before 0.06) since, due to the resampling algorithm, it is possible that spurious modes (created by some atypical data points) may seem visually more prominent than real modes (as pointed out by Minnotte et al., 1998). Observing Figure C.1 (right), the mode forest suggests at least seven modes for the `stamps` dataset.

With the `sizer` function the assessment of SIgnificant ZERo crossing of the derivative of the smoothed curve is computed for a given sample. At a given location (horizontal axis) and using a specified bandwidth parameter (vertical axis), the SiZer map, introduced by Chaudhuri and Marron (1999), represents where the smoothed curve is significantly increasing (blue colour by default), decreasing (red by default) or not significantly different from zero (orchid, a light tone of purple, by default). Thus, for a given bandwidth, a region significantly increasing followed by a region significantly decreasing (blue–red pattern by default) indicates where there is a significant peak.

The confidence limits of $\hat{f}'_h(x)$, used for determining the behaviour of the smoothed curve, are of the form $\mathrm{CI}^{\pm}(x,h) = \hat{f}'_h(x) \pm \mathrm{quantile}(\alpha) \cdot \widehat{\mathrm{SD}}(\hat{f}'_h(x))$, where $\widehat{\mathrm{SD}}$ is the estimated standard deviation and α is the significance level (selected by the argument `alpha`). For calculating these quantiles Chaudhuri and Marron (1999) proposed four different methods, all implemented in the `sizer` function using the argument `method`. The available quantiles are: the pointwise Gaussian quantiles (q_1), when `method=1`; approximate simultaneous over x Gaussian quantiles (q_2), when `method=2`; bootstrap quantile simultaneous over x (q_3), when `method=3`; and bootstrap quantile simultaneous over x and h (q_4), when `method=4`. Bootstrap quantiles q_3 and q_4 are computed generating `B` random samples drawn with replacement from the sample.

Areas with too sparse data for meaningful inference are identified for q_2, q_3 and q_4 (and marked with grey colour by default). A location–bandwidth pixel is classified in this category when the estimated Effective Sample Size is less than a value n_0 (argument `n0`, see Chaudhuri and Marron, 1999).

The different colours showing the significance features of the smoothed curve can be replaced using the `col.sizer` argument. A legend indicating the meaning of the different colours is also provided in the plot position given in `poslegend` when the argument `addlegend` is `TRUE`. The different SiZer maps for the `stamps` dataset between the band-

widths $7.5 \cdot 10^{-4}$ and 0.02 and represented in Figure C.2 can be obtained as shown below (varying the value of `method` between 1 and 4). For computing the quantiles q_2, q_3 and q_4 it was taken $n_0 = 5$ as suggested by Chaudhuri and Marron (1999) and the number of bootstrap replicas in methods q_3 and q_4 is $B = 500$.

```
R> sizerstamps <- sizer(data,method=1,bws=c(0.00075,0.0075),
+    gridsize=NULL,alpha=0.05,B=NULL,n0=NULL,cbw1=NULL,cbw2=NULL,
+    display=TRUE,logbw=TRUE,from=NULL,to=NULL,col.sizer=NULL,
+    xlab="Thickness (in mm)",ylab=NULL,addlegend=TRUE,
+    poslegend="topright")
R> names(sizerstamps)

[1] "sizer"     "lower.CI"  "estimate"  "upper.CI"  "ESS"
[6] "range.x"   "range.bws"
```

Apart from the already described arguments, `sizer` returns a list with five matrices containing different information in each location–bandwidth pixel: `sizer`, with the significant behaviours of the smoothed curve; `lower.CI` with the lower limits of the confidence interval, $\mathrm{CI}^-(x,h)$; `estimate`, with the derivative values of the kernel density estimation, $\hat{f}'_h(x)$; `upper.CI` with the upper limits of the confidence interval, $\mathrm{CI}^+(x,h)$; and `ESS`, with the Effective Sample Size.

As noted before, in the SiZer maps (represented in Figure C.2), blue colour indicates locations where, for a given bandwidth, the smoothed curve is significantly increasing, red colour shows where it is significantly decreasing and purple (orchid) indicates where it is not significantly different from zero. Then, given a value of $\log_{10}(h)$, modes can be detected in the blue–red patterns. In this case, the SiZer maps computed with Gaussian quantiles just detect, at most, one mode around the value 0.08. The conclusion with those ones constructed with bootstrap confidence intervals vary with the bandwidth. For all the bandwidth values, both methods capture the principal mode before the value 0.08 and for several bandwidth parameters is also detected a secondary mode around 0.10. The third and the fourth mode (around 0.09 and 0.11) that appears in the mode tree (Figure C.1, left) are only significant modes for some bandwidth parameters for q_3. Finally, both methods, q_3 and q_4, detect another mode near 0.07 for some bandwidth values. Then, depending on the bandwidth parameter, the conclusion using the quantile q_3 is that there are between one and five modes (in order of appearance, around 0.08, 0.10, 0.09, 0.11 and 0.07), while q_4 detects between one and three modes (around 0.08, 0.10 and 0.07).

C.1.3 Testing and locating modes with multimode

The **multimode** package has implemented all the test presented in the Chapter 2. In particular, it allows to compute both test statistics: the critical bandwidth of Silverman (1981)

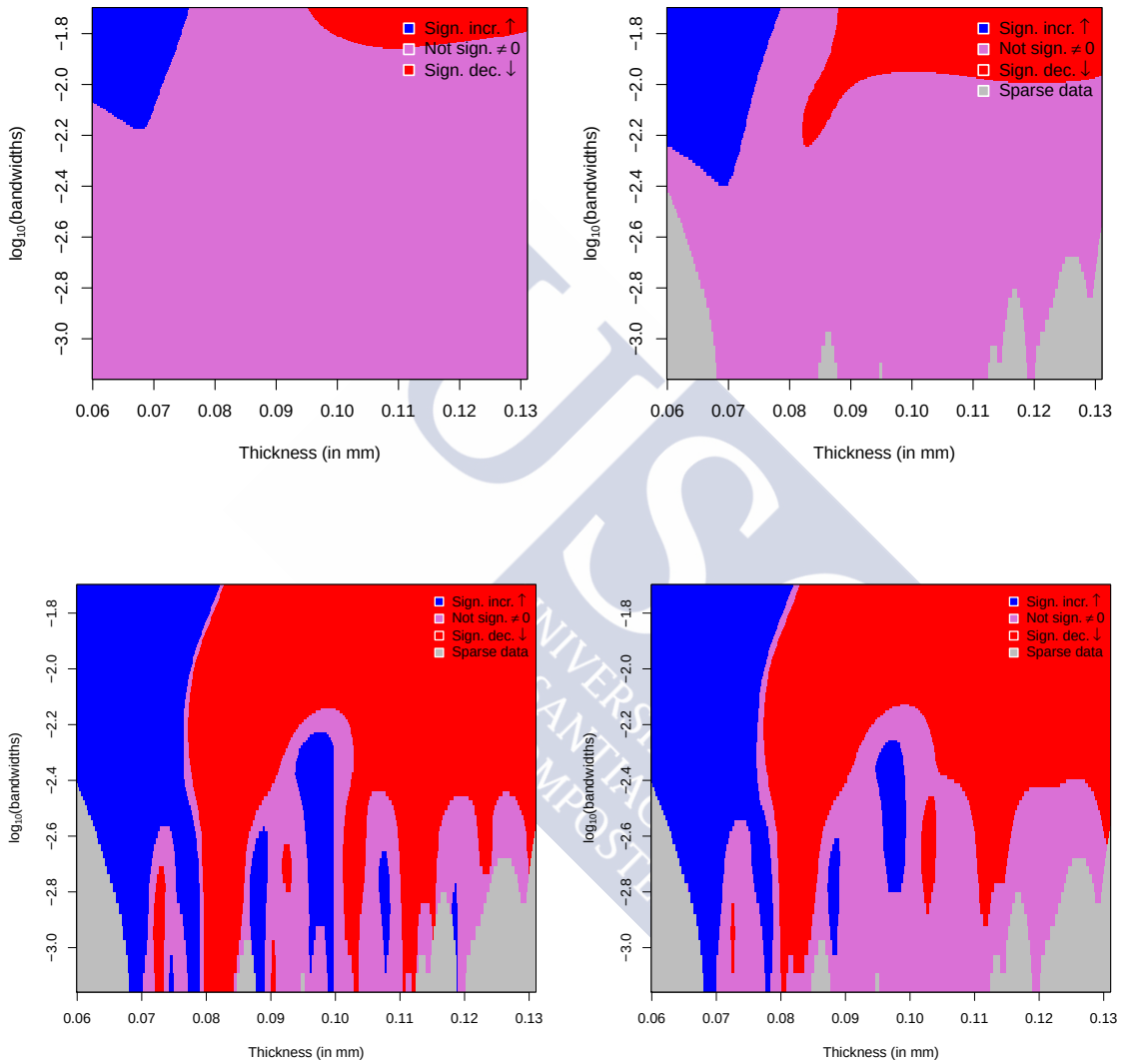

Figure C.2: SiZer maps for the sample of 485 stamps from the 1872 Hidalgo Issue of Mexico between the bandwidths $\log_{10}(h) = -3.12$ ($h = 7.5 \cdot 10^{-4}$) and $\log_{10}(h) = -1.70$ ($h = 0.02$). Given a value of $\log_{10}(h)$, modes can be detected in the blue–red patterns. Top: Gaussian quantiles q_1 (left) and q_2 (right). Bottom: bootstrap quantiles q_3 (left) and q_4 (right).

and Hall and York (2001) (with the function `bw.crit`) and the excess mass of Müller and Sawitzki (1991) (with `excessmass`). Their associated p–values can be also obtained using different testing proposals (with `modetest`).

For the three functions (`bw.crit`, `excessmass` and `modetest`), the number of modes for computing the statistic or for testing can be specified in the argument `mod0`.

For `bw.crit` and for the testing proposals using the critical bandwidth in `modetest`, when the compact support is unknown, the critical bandwidth introduced by Silverman (1981) is computed and if the finite values of the support limits are provided (via arguments `lowsup` and `uppsup`) that one of Hall and York (2001) is calculated. Being both arguments necessary in `modetest` when employing the Hall and York (2001) proposal or for computing the new proposal when the compact support is known (see Section 2.1.3.1). As in the `nmodes` function, the number of equally spaced points at which the density is to be estimated is chosen by the argument `n`. Since a dichotomy method is employed for computing the critical bandwidth (see Appendix C.2), the parameter `tol` is used to determine a stopping time in such a way that the error committed in the computation of the critical bandwidth is less than `tol`.

For `excessmass` and in the testing proposals using the excess mass in `modetest`, when there are repeated data in the sample or the distance between different pairs of data points shows ties, a data perturbation is applied. This modification is made in order to avoid the discretization of the data which has important effects on the computation of the test statistic. The perturbed sample is obtained by adding a sample from the uniform distribution in the support minus/plus a half of the minimum of the positive distances between two sample points (as done in Section 2.3).

Using the `stamps` dataset, below how to obtain the test statistics is shown. In the first place, the critical bandwidth of Silverman (1981) and Hall and York (2001), in the interval $I = [0.04, 0.15]$, is computed for one mode. Secondly, the excess mass statistic of Müller and Sawitzki (1991) for one mode is obtained.

```
R> bw.crit(data=stamps,mod0=1,lowsup=-Inf,uppsup=Inf,n=2^15,tol=10^(-5))
R> bw.crit(data=stamps,mod0=1,lowsup=0.04,uppsup=0.15,n=2^15,tol=10^(-5))
R> excessmass(data=stamps,mod0=1)
```

Once the different test statistics are computed, the number of modes for the underlying density of given sample can be tested with the function `modetest`. The different proposals that can be used for testing the number of modes (using the argument `method`) are those ones introduced in Section 2.1. The available methods, based on the critical bandwidth (see Section 2.1.1), include: Silverman (1981) (`SI`), Hall and York (2001) (`HY`) and Fisher and Marron (2001) (`FM`). Based on the excess mass (Section 2.1.2): Hartigan and Hartigan (1985) (`HH`, equivalent to the proposal of Müller and Sawitzki, 1991) and Cheng and Hall

(1998) (CH). Finally, the new proposal described in Section 2.1.3 (NP) is also included. For calculating the corresponding p–value, all the available proposals require bootstrap or Monte Carlo resamples, the number of replicates can be specified with the argument B.

As pointed out before, the bounded support (lowsup and uppsup) is necessary when the Hall and York (2001) proposal (HY) is employed and they can be also used with the NP proposal. In the NP case, the parameter tol2 is the accuracy required in the integration of the calibration function when the compact support is known (see Section 2.1.3.1). For the HY test, the two suggested methods for computing the λ_α factor (see Section 2.1.1) are implemented using the argument methodhy. The methodhy 1 corresponds with the asymptotic correction of Silverman (1981) test based on the limiting distribution of the test statistic. When methodhy=1, the significance level must be previously determined with alpha. The methodhy 2 is based on Monte Carlo techniques. For this reason, when methodhy=2, the number of replicates (nMC) and the number of bootstrap resamples (BMC) used for computing the p–value in each Monte Carlo sample are needed.

Finally, the modetest function includes the argument full.result. When this argument equals TRUE, the function returns a list with both, the test statistic (statistic) and the associated p–value (p.value); when it is FALSE, just the p.value is returned.

The different p–values obtained with the new proposal in Section 2.3 and reproduced in Table C.3 can be obtained as follows (varying the value of mod0 between 1 and 9):

```
R> modeteststamps <- modetest(data=stamps,mod0=1,method="NP",B=500,
+    full.result=TRUE,n=2^10,tol=10^(-5))
R> names(modeteststamps)

[1] "p.value"   "statistic"
```

Assuming that the compact support for the stamps dataset is $I = [0.04, 0.15]$, the modification of the new proposal presented in Section 2.1.3.1 can be obtained as follows

```
R> modetest(data=stamps,mod0=1,method="NP",B=500,full.result=FALSE,
+    lowsup=0.04,uppsup=0.15,n=2^10,tol=10^(-5),tol2=10^(-5))
```

The p–values of the other proposals allowing for testing a general number of modes (SI and FM) are obtained with the below code lines (varying the value of mod0 between 1 and 9).

```
R> modetest(data=stamps,mod0=1,method="SI",B=500,full.result=FALSE,
+    n=2^10,tol=10^(-5))
R> modetest(data=stamps,mod0=1,method="FM",B=500,full.result=FALSE,
+    n=2^10,tol=10^(-5))
```

method	SI	HY		FM	HH	CH	NP
methodhy		1	2				
P–value	0.002	0	0	0	0.030	0	0

Table C.2: P–values obtained using different proposals for testing unimodality, generated using $B = 500$ resamples.

The other critical bandwidth proposal, `HY`, only can be used for testing unimodality when the compact support of the variable is known (see Section 2.1.1). In this case, the test with both alternatives for approximating the λ_α: a first approach based on a polynomial approximation (`methodhy=1`) and a second option using Monte Carlo techniques (`methodhy=2`), can be computed as follows:

```
R> modetest(data=stamps,method="HY",B=500,full.result=FALSE,lowsup=0.04,
+    uppsup=0.15,n=2^10,tol=10^(-5),methodhy=1,alpha=0.05)
R> modetest(data=stamps,method="HY",B=500,full.result=FALSE,lowsup=0.04,
+    uppsup=0.15,n=2^10,tol=10^(-5),methodhy=2,nMC=100,BMC=100)
```

The p–values of the unimodality test based on the excess mass (`HH` and `CH`) can be obtained with the following code lines:

```
R> modetest(data=stamps,method="HH",B=500,full.result=FALSE)
R> modetest(data=stamps,method="CH",B=500,full.result=FALSE)
```

Table C.2 shows the `p.values` obtained for all the unimodality tests available. For all of them the null hypothesis of unimodality is rejected for a significance level $\alpha = 0.05$.

The results for the tests (`SI`, `FM` and `NP`) that allow testing k–modality, with $k > 1$, are in Table C.3 (with k between one and nine). In the case of the `FM` proposal, for reproducing the Fisher and Marron (2001) results, the `stamps` data were also perturbed as done with the `excessmass` function. Similar results are obtained for the `SI` proposal, when perturbing and not the data; and for the `NP` proposal when the support is not employed and using the approach presented in Section 2.1.3.1 with $I = [0.04, 0.15]$. Fixing a significance level $\alpha = 0.05$, there is not a clear conclusion when using `SI` and `FM`. In the `SI` case the null hypothesis is non–rejected when $k = 2, 3, 7, 8, 9$ and for the `FM`, using the perturbed sample, it is non–rejected just when $k = 7$. While, in the unique proposal well calibrated (`NP`), the null hypothesis is rejected until $k = 3$ and it is not for $k \geq 4$, indicating that the number of modes is (at least) equal to four.

Once the number of modes is known, the function `locmodes` provides the estimation of the location of modes and antimodes and their density value. In this case, since it is

k	1	2	3	4	5	6	7	8	9
SI	0.006	0.348	0.092	0.016	0.006	0.002	0.494	0.308	0.616
FM	0	0.006	0	0	0	0	0	0	0
FM*	0	0	0	0	0	0	0.096	0.014	0.046
NP*	0	0.022	0.004	0.506	0.574	0.566	0.376	0.886	0.808

Table C.3: P–values obtained using different proposals for testing k–modality, with k between 1 and 9, generated using $B = 500$ resamples. The asterisk (*) denotes the tests where the original sample was perturbed.

known, the compact support of the variable can be used to obtain a good estimator of the location of the modes (see Appendix B). In other situations, one should be careful about the conclusions as the critical bandwidth of Silverman (1981) may create artificial modes in the tails.

The arguments of the `locmodes` function include those ones mentioned in the `bw.crit` function: `mod0`, `lowsup`, `uppsup`, `n` and `tol`. It also allows the representation of the estimation (for the number of modes indicated in `mod0`) of the density, modes and antimodes with the argument `display`. The rest of the included graphical arguments (`addplot`, `xlab`, `ylab`, `addLegend`, `posLegend`) were already described in the `modetree` and `sizer` functions.

The estimation of the location of modes and antimodes and their density value assuming four (`mod0=4`, Ameijeiras-Alonso et al., 2016) and seven (`mod0=7`, Izenman and Sommer, 1988) modes, and plotted in Figure C.3 can be obtained as follows:

```
R> lms <- locmodes(data=stamps,mod0=4,lowsup=0.04,uppsup=0.15,n=2^15,
+    tol=10^(-5),display=TRUE,addplot=FALSE,xlab="Thickness (in mm)",
+    ylab=NULL,addLegend=TRUE,posLegend="topright")
R> names(lms)

[1] "locations" "fvalue"    "cbw"
```

This function returns: in `locations`, a vector with the estimated locations of modes (odd positions of the vector) and antimodes (even positions); in `fvalue`, a vector with their estimated density values; and `cbw`, the critical bandwidth of the sample for `mod0` modes. Attending to the obtained results assuming that the distribution has four modes, the estimated modes (odd positions of `locations`) are: 0.07857, 0.09065, 0.1006 and 0.1083.

The results obtained after applying the `modetest` function can help also to have a better interpretation of the SiZer map (Figure C.1). If the conclusion is that there are four modes, the most plausible results are obtained with the bootstrap quantiles q_3 and, in that case, the

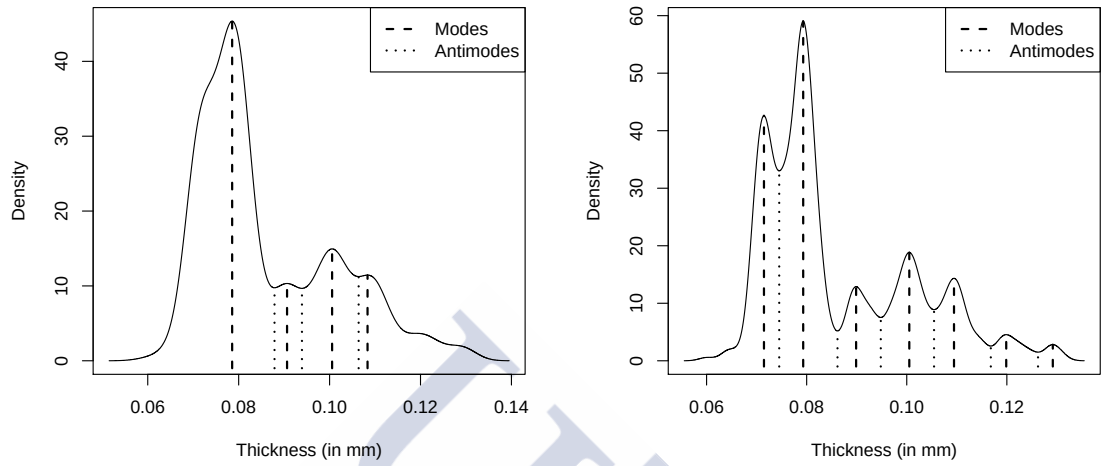

Figure C.3: Estimation of the density, modes and antimodes for the sample of 485 stamps from the 1872 Hidalgo Issue of Mexico, obtained with the function `locmodes`. Left: assuming four modes. Right: assuming seven modes.

estimated modes (in `locmodes`) coincides with those ones observed when a value of $\log_{10}(h)$ close to -2.7 is taken.

C.2 Numerical approximations

Details of the numerical approaches used in the **multimode** package and in Section 2.2 can be found below.

Practical computation of the critical bandwidth. To obtain both the critical bandwidth of Silverman (1981) and that one of Hall and York (2001), a binary search procedure is used. In each step of the algorithm, denoting h_a as the bandwidth in such a way than $\widehat{f}_{h_a}$ has at most k modes and h_b the bandwidth for which the kernel density estimation has more than k modes (both in the interval I if the critical bandwidth of Hall and York, 2001, is being calculated). Then the dichotomy algorithm is stopped when $(h_b - h_a) <$`tol`, being the parameter `tol` equal to $(h_{a_0}/2^{10})$ in Section 2.2, where h_{a_0} is the initial value of h_a. The last calculated value of h_a is the one employed as the critical bandwidth. The number of points where the kernel density estimators where calculated in Section 2.2 is equal to 2^{15}.

Practical computation of the excess mass. To obtain the excess mass defined by

Müller and Sawitzki (1991) when the null hypothesis of unimodality is being tested, the following result is used: the value of the excess mass statistic is exactly twice the value of the *dip* statistic introduced by Hartigan and Hartigan (1985). The value of the *dip* was obtained using the **diptest** package implemented by Maechler (2015).

For the general case, the following algorithm will be employed to obtain the excess mass statistic when the null hypothesis $H_0 : j = k$, with $k > 1$, is tested. First, assume that $d_k(p)$ is the minimum distance of the union of k intervals containing p data points. To get the possible values of λ corresponding to $E_{n,k}(\mathbb{P}_n, \lambda)$, and candidates to minimize the difference

$$D_{n,k+1}(\lambda) = \{E_{n,k+1}(\mathbb{P}_n, \lambda) - E_{n,k}(\mathbb{P}_n, \lambda)\},$$

the first step begins in $q_k(1) = n$ (where the number in parenthesis is the current iteration). Then, it search from $q_k(1) - 1$ until $(k + 1)$ the integer $q_k(2)$ minimizing the following expression

$$\lambda_k(1) = \min_{q_k(2)} \frac{q_k(1) - q_k(2)}{n(d_k(q_k(1)) - d_k(q_k(2)))},$$

the value of $\lambda_k(1)$ is one of the possible values of λ minimizing $D_{n,k+1}(\lambda)$. Then, if $q_k(2) = (k + 1)$ is the value minimizing the previous expression, the algorithm will be stopped, otherwise it is continued until $q_k(t_k) = (k+1)$ (where t_k is the realised number of iterations). After obtaining the vector $\boldsymbol{\lambda}_k$ of possible values of λ minimizing $D_{n,k+1}(\lambda)$, the algorithm is repeated for $(k + 1)$ to get the vector $\boldsymbol{\lambda}_{k+1}$. Then the excess mass statistic is easy to obtain using that

$$\Delta_{n,k+1} = \min_{\boldsymbol{\lambda}_k \cup \boldsymbol{\lambda}_{k+1}} D_{n,k+1}(\lambda).$$

To get the values of $d_k(p)$, one can obtain the exact result of the excess mass employing the algorithm provided by Müller and Sawitzki (1991). A similar algorithm was implemented and employed to get the exact results in Section 2.3 and in the computation of this test statistic in **multimode**. The problem of employing this algorithm is the high computational cost for an extensive study. For this reason an approximation was used in Section 2.2 to get the excess mass statistic, $\Delta_{n,3}$. The new algorithm consist in, first, calculate $d_1(p)$ to obtain the exact values of $\boldsymbol{\lambda}_1$ and secondly create a grid of l possible values between each $\lambda_1(j)$ and $\lambda_1(j+1)$, with j and entire value between 1 and $(t_k - 1)$. Finally, to get the test statistic, that value of λ belonging the entire grid and minimising $D_{n,3}(\lambda)$ is chosen. The employed size l was: $l = 100$ when $n = 50$, $l = 40$ for $n = 100$, $l = 20$ if $n = 200$ and $l = 5$ when $n = 1000$. This selection of points represents a balance between the accuracy and the computation time, as, in general, if n is large then the length of the vector t_k is also large.

Appendix D

Introduction on Le Cam theory

The central idea of Le Cam theory is to approximate a family of parametric measures by a simple Gaussian shift model, that is the *Uniform Local Asymptotic Normality* (ULAN) property. In the case considered in Chapter 4 the location–skewness family of `k`–sine–skewed models is locally (around $\lambda = 0$) and asymptotically equivalent to this Gaussian. The ULAN property is a key point to provide the optimal test (against the `k`–sine–skewed alternatives) and it implies the *asymptotic linearity property* which allows to see the influence of estimating the location parameter. Apart from that, the known as *Le Cam Lemmas* are also useful to provide the asymptotic distribution of the test statistic under the *contiguous* alternatives (when $\lambda \neq 0$). A formal definition of the four terms in italics are provided below as an introduction of Le Cam theory focused in the results given in Chapter 4.

To start the introduction of Le Cam theory, the first important point is to understand the concept of *contiguity* introduced by Le Cam (1960). Let $P^{(n)}$ and $Q^{(n)}$ be two sequences of probability distributions defined on measurable spaces $(\Omega_n, \mathcal{A}_n)$. The sequence $Q^{(n)}$ is contiguous to $P^{(n)}$ if $P^{(n)}(A_n) \to 0$ implies $Q^{(n)}(A_n) \to 0$ for every sequence of measurable sets $A_n \in \mathcal{A}_n$. In that case, the contiguity is denoted as $Q^{(n)} \lhd P^{(n)}$. If both sequences are contiguous between themselves, $Q^{(n)} \lhd P^{(n)}$ and $P^{(n)} \lhd Q^{(n)}$, it is said that $P^{(n)}$ and $Q^{(n)}$ are mutually contiguous, and denoted as $Q^{(n)} \lhd \rhd P^{(n)}$.

The second important point are the Le Cam Lemmas. Two of the three Le Cam Lemmas are introduced in this part as they will be needed to provide the following results and that ones in Chapter 4. First Le Cam lemma provides sufficient conditions to proof the contiguity between two sequences of probability measures and some properties for the likelihood ratio $dP^{(n)}/dQ^{(n)}$.

Lemma D.0.1. *(First Le Cam Lemma) Given two sequences of probability measures $P^{(n)}$ and $Q^{(n)}$ defined on measurable spaces $(\Omega_n, \mathcal{A}_n)$. The following conditions are equivalent:*

(i) $Q^{(n)} \lhd P^{(n)}$

(ii) $P^{(n)}/Q^{(n)}$ *converges weakly (under* $Q^{(n)}$*) to a random variable* U *along a subsequence, then* $\mathbb{P}(U > 0) = 1$.

(iii) $Q^{(n)}/P^{(n)}$ *converges weakly (under* $P^{(n)}$*) to a random variable* V *along a subsequence, then* $\mathbb{E}[V] = 1$.

(iv) Any statistic $\mathbf{S_n} : \Omega_n \to \mathbb{R}^p$ *is such that if* $\mathbf{S_n} = o_P(1)$ *under* $P^{(n)}$*, then* $\mathbf{S_n} = o_P(1)$ *under* $Q^{(n)}$.

Given two sequences of probability measures $P^{(n)}$ and $Q^{(n)}$, First Le Cam Lemma implies that if

$$\log\left(\frac{dP^{(n)}}{dQ^{(n)}}\right) \xrightarrow{\mathcal{D}} \mathrm{N}(\mu, \sigma^2), \text{ under } Q^{(n)} \text{ as } n \to \infty,$$

being N the normal distribution, with $\mu \in \mathbb{R}$ and $\sigma^2 > 0$; then $Q^{(n)} \lhd P^{(n)}$. Furthermore, if it is also satisfied that $\mu = -\sigma^2/2$, then $Q^{(n)} \lhd \rhd P^{(n)}$. Once the contiguity $Q^{(n)} \lhd P^{(n)}$ is proven, if the asymptotic distribution of a test statistic S_n under $P^{(n)}$ is known, the Third Le Cam Lemma can be used to provide the distribution of S_n under the contiguous alternatives $Q^{(n)}$.

Lemma D.0.2. *(Third Le Cam Lemma) Given two sequences of probability measures* $P^{(n)}$ *and* $Q^{(n)}$ *defined on measurable spaces* $(\Omega_n, \mathcal{A}_n)$*. If* $\mathbf{S_n} : \Omega_n \to \mathbb{R}^p$ *is a test statistic and it is satisfied both* $Q^{(n)} \lhd P^{(n)}$ *and*

$$\begin{pmatrix} \mathbf{S_n} \\ \log\left(dP^{(n)}/dQ^{(n)}\right) \end{pmatrix} \xrightarrow{\mathcal{D}} N_{p+1}\left(\begin{pmatrix} \boldsymbol{\mu} \\ -\sigma^2/2 \end{pmatrix}, \begin{pmatrix} \boldsymbol{\Sigma} & \boldsymbol{\tau} \\ \boldsymbol{\tau}' & \sigma^2 \end{pmatrix}\right),$$

under $P^{(n)}$ *as* $n \to \infty$*, being* N_{p+1} *the* $(p+1)$*–dimensional normal distribution and with* $\boldsymbol{\mu}, \boldsymbol{\tau} \in \mathbb{R}^p$*,* $\sigma^2 > 0$ *and* $\boldsymbol{\sigma}$ *a symmetric positive defined matrix of dimension* p*; then* $\mathbf{S_n} \xrightarrow{\mathcal{D}} N_p(\boldsymbol{\mu} + \boldsymbol{\tau}, \boldsymbol{\Sigma})$ *under* $Q^{(n)}$ *as* $n \to \infty$.

The third Le Cam Lemma is useful to provide the distribution of a test statistic under contiguous alternatives.

The third important point of Le Cam theory is the concept of *Local Asymptotic Normality* (LAN) and Uniform Local Asymptotic Normality (ULAN). Let $(\Theta_1, ..., \Theta_n)$ be an independent and identically distributed sample from a parametric distribution $\mathrm{P}_{\boldsymbol{\vartheta}}$, with $\boldsymbol{\vartheta} \in \mathcal{V} \subset \mathbb{R}^p$ and $\mathrm{P}^{(n)}_{\boldsymbol{\vartheta}}$ their joint distribution. The family of probability distributions $\mathcal{P}^{(n)} = \{\mathrm{P}^{(n)}_{\boldsymbol{\vartheta}} : \boldsymbol{\vartheta} \in \mathcal{V} \subset \mathbb{R}^p\}$ is LAN if for all the possible $\boldsymbol{\vartheta} \in \mathcal{V}$ there exist: (i) a sequence $\boldsymbol{\nu}^{(n)}$ of (non–random) $p \times p$ matrices such that the Frobenius norm $\|\boldsymbol{\nu}^{(n)}\|_F = \sqrt{\sum_{i=1}^p \sum_{j=1}^p |\boldsymbol{\nu}^{(n)}_{ij}|^2} \to 0$ as $n \to \infty$; (ii) a central sequence (of random vectors) $\boldsymbol{\Delta}^{(n)}(\boldsymbol{\vartheta})$;

(iii) the (non–random) Fisher information matrix $\boldsymbol{\Gamma}(\boldsymbol{\vartheta})$; such that for every bounded sequence of vectors $\boldsymbol{\tau}^{(n)} \in \mathbb{R}^p$ it is satisfied

$$\log\left(\frac{\mathrm{dP}^{(n)}_{\boldsymbol{\vartheta}+\boldsymbol{\nu}^{(n)}\boldsymbol{\tau}^{(n)}}}{\mathrm{dP}^{(n)}_{\boldsymbol{\vartheta}}}\right)(\boldsymbol{\tau}^{(n)})'\boldsymbol{\Delta}^{(n)}(\boldsymbol{\vartheta}) - \frac{1}{2}(\boldsymbol{\tau}^{(n)})'\boldsymbol{\Gamma}(\boldsymbol{\vartheta})\boldsymbol{\tau}^{(n)} + o_{\mathrm{P}}(1),$$

and $\boldsymbol{\Delta}^{(n)}(\boldsymbol{\vartheta}) \xrightarrow{\mathcal{D}} \mathcal{N}_p(0, \boldsymbol{\Gamma}(\boldsymbol{\vartheta}))$, both under $\mathrm{P}^{(n)}_{\boldsymbol{\vartheta}}$ as $n \to \infty$. In particular, the LAN property implies that the Third Le Cam Lemma is applicable. If the LAN property holds uniformly in a neighbourhood of the parameter $\boldsymbol{\vartheta}$, $\mathcal{P}^{(n)}$ will be ULAN. $\mathcal{P}^{(n)}$ is ULAN if for every $\boldsymbol{\vartheta} \in \mathcal{V}$, given any sequence of the form $\boldsymbol{\vartheta}^{(n)} = \boldsymbol{\vartheta} + O(\|\boldsymbol{\nu}^{(n)}\|)$ and any bounded sequence $\boldsymbol{\tau}^{(n)}$ it is satisfied

$$\log\left(\frac{\mathrm{dP}^{(n)}_{\boldsymbol{\vartheta}^{(n)}+\boldsymbol{\nu}^{(n)}\boldsymbol{\tau}^{(n)}}}{\mathrm{dP}^{(n)}_{\boldsymbol{\vartheta}^{(n)}}}\right) = (\boldsymbol{\tau}^{(n)})'\boldsymbol{\Delta}^{(n)}(\boldsymbol{\vartheta}^{(n)}) - \frac{1}{2}(\boldsymbol{\tau}^{(n)})'\boldsymbol{\Gamma}(\boldsymbol{\vartheta})\boldsymbol{\tau}^{(n)} + o_{\mathrm{P}}(1),$$

under $\mathrm{P}^{(n)}_{\boldsymbol{\vartheta}}$ as $n \to \infty$. As it was pointed out, stablish the ULAN property is a fundamental key in Le Cam theory and, also, because it implies the asymptotic linearity property, that is,

$$\boldsymbol{\Delta}^{(n)}_{\boldsymbol{\vartheta}+\boldsymbol{\nu}^{(n)}\boldsymbol{\tau}^{(n)}} - \boldsymbol{\Delta}^{(n)}_{\boldsymbol{\vartheta}} = \boldsymbol{\Gamma}(\boldsymbol{\vartheta})\boldsymbol{\tau}^{(n)} + o_{\mathrm{P}}(1)$$

under $\mathrm{P}^{(n)}_{\boldsymbol{\vartheta}}$ as $n \to \infty$. The asymptotic linearity property is essential when the central direction needs to be estimated with a $\sqrt{n}$ consistent estimator of μ.

USC
UNIVERSIDADE
DE SANTIAGO
DE COMPOSTELA

Resumen en castellano

El análisis estadístico clásico de datos continuos y unidimensionales está, normalmente, centrado en el estudio de fenómenos que están distribuidos de forma simétrica y que están concentrados alrededor de un único punto. Sin embargo, cuando son aplicados a los datos reales, estos modelos pueden fallar. Para resolver este problema, han sido diseñadas diversas distribuciones que tratan de capturar aquellas situaciones en las que lo datos no se distribuyen de igual manera a la izquierda y a la derecha de un eje central (asimetría) o cuando estos están concentrados alrededor de más de un valor (multimodalidad). Este tipo de problemática también puede ocurrir en datos que presentan estructuras más complejas, como es el caso de los datos circulares, cuyas muestras pueden ser representadas como puntos en la circunferencia del círculo unidad. De hecho, una de las primeras referencias en este contexto, recogiendo los primeros avances realizados en el campo de los datos circulares en las décadas de 1950 y 1960 (Mardia, 1972, Cap. 1), trata esta temática desde el inicio ya que las distribuciones asimétricas y multimodales son habituales en la práctica. Por tanto, es importante conocer cuando merece la pena aumentar la complejidad de los modelos antes de aplicarlos. Con este objetivo, la tesis está centrada en determinar hipótesis simplificadoras para la estimación de la densidad, tanto en el caso de los datos lineales como circulares. En este sentido, son dos los objetivos de la tesis: en primer lugar, contrastar el número de modas en el caso de los datos lineales y circulares y, en segundo, en el contexto de datos circulares, determinar si la distribución de la variable aleatoria es simétrica.

A continuación se incluye un resumen con los distintos temas tratados a lo largo de la tesis, así como las principales aportaciones realizadas en cada capítulo de la misma.

Capítulo 1: Introducción. En este capítulo se presentan los distintos conceptos que se abordan a lo largo de la tesis, se introducen los distintos conjuntos de datos y se ponen de relieve las principales contribuciones realizadas.

En primer lugar, se introducen las distintas técnicas no paramétricas que permiten

determinar el número de modas. El concepto de moda, para una variable aleatoria continua (tanto lineal como circular), se define como el valor (o valores) en el cual la función de densidad presenta un máximo relativo. Si la función de densidad (o su distribución asociada) presenta una única moda, se dirá que es unimodal, y si presenta más de una se dirá que es multimodad (bimodal cuando aparezcan dos, trimodal cuando tenga tres, etc.). La identificación del número de modas, en el caso lineal, es un problema que se puede encontrar en numerosos campos aplicados, como la geología, la neurología, la economía, la ecología o la astronomía. Algunos ejemplos se podrían encontrar en el estudio de porcentaje de silicio en los meteoritos de condritas (Good y Gaskins, 1980), el análisis de las neuronas de macacos cuando realizan una actividad que requiere atención (Mitchell et al., 2007), la distribución de los ingresos por hogar en el Reino Unido (Marron y Schmitz, 1992), el estudio del tamaño corporal de los peces en peligro de extinción (Olden et al., 2007) o el análisis de la velocidad a la que las galaxias se alejan de la nuestra (Roeder, 1990). En todos estos problemas identificar el número de modas es un problema importante de por sí o como paso previo para la aplicación de otros procedimientos.

Para determinar el número de modas, una primera idea podría ser realizar un ajuste paramétrico usando una mixtura de distribuciones (en McLachlan y Peel, 2000, se realiza una revisión de esta temática), si bien, la estructura subyacente de los datos puede ser realmente compleja dando lugar a un mal ajuste cuando se utilizan estos modelos paramétricos. Es, por este motivo, que en esta tesis se toma un punto de vista no paramétrico. En particular, para estimar la función de densidad se utilizará la estimación tipo núcleo, la cual se define del siguiente modo:

$$\hat{f}_h(x) = \frac{1}{n}\sum_{i=1}^{n} K_h\left(x - X_i\right),$$

donde K_h es el núcleo reescalado, esto es, una función de densidad unimodal y simétrica centrada en el cero y con parámetro de ventana h. Un ejemplo de núcleo sería la función de densidad Gaussiana centrada en el cero y con desviación típica h. La ventana h juega un papel fundamental a la hora de estimar el número de modas con la estimación tipo núcleo ya que, en general, parámetros de ventana "grandes" darán lugar a estimaciones con menos modas. Una solución exploratoria simple, para determinar el número de modas, sería analizar la cantidad de máximos relativos en la estimación tipo núcleo para diversos valores de h. De hecho, esto es lo que hacen algunas de las herramientas gráficas que existen en la literatura estadística. El problema de este método es que, en general, no permite proporcionar una respuesta formal acerca del número de modas. Es, por este motivo, que en esta tesis se considera una aproximación por contrastes de hipótesis para intentar determinar el número de modas. En particular, dada una variable aleatoria con j modas, este problema fue

formulado en la literatura estadística a través del siguiente contraste:

$$H_0 : j \leq k \quad \text{contra} \quad H_a : j > k,$$

donde k es el número de modas a ser contrastado. Los distintos test que permiten realizar este contraste son revisados en el Capítulo 2 donde, además, se realiza una nueva propuesta.

En segundo lugar, se proporciona una introducción al tema de los datos circulares. La necesidad de la estadística circular para variables unidimensionales aparece cuando se debe tener en cuenta la periodicidad que presentan los datos. Algunos ejemplos de datos circulares aparecen cuando el objetivo es modelar orientaciones o fenómenos periódicos, siendo, estos ejemplos, frecuentes en muchos campos aplicados. En particular, relacionados con las orientaciones se pueden encontrar los siguientes casos: la orientación de la hormiga roja europea en reacción a distintos estímulos (Jander, 1957); la orientación en el vuelo de las palomas cuando vuelven a su hogar (Schmidt-Koenig, 1963); la dirección del viento en Gorleston (Reino Unido) en 1968 (Fisher, 1995, Ch. 5); o la dirección de las olas en el mar Adriático (Jona-Lasinio et al., 2012; Lagona et al., 2015). Mientras que relacionados con los fenómenos periódicos se pueden encontrar los siguientes ejemplos: el número de muertes de soldados (a lo largo de cada año) durante la guerra de Crimea (originalmente introducido por Nightingale en 1858; se puede ver en Brasseur, 2005); o los tiempos de congelación y descongelación (a lo largo del día) en los glaciares del Monte Alvear y Vinciguerra en Ushuaia, Argentina (Oliveira et al., 2013). Teniendo en cuenta la periodicidad que presentan estos datos, para proporcionar su caracterización se deben tomar dos decisiones: la dirección inicial y el sentido de rotación, pero los resultados no pueden depender de estas elecciones. Es por este motivo que los datos circulares requieren de un tratamiento especial donde incluso algunos conceptos básicos, como la media o la función de densidad, deben ser apropiadamente definidos. En este capítulo, también se introducen algunas de las principales familias paramétricas de distribuciones circulares: la cardioid, la von Mises y las distribuciones normal y Cauchy enrolladas. Estos cuatro modelos circulares (simétricos y unimodales) están caracterizados, aparte de por el parámetro de localización, por el parámetro de concentración, donde valores "grandes" de este parámetro serán un indicativo de que la distribución está "muy" concentrada alrededor del cero. Teniendo en cuenta este último parámetro, será necesario redefinir la estimación tipo núcleo, donde el núcleo pasará a ser una función de densidad circular y el parámetro de ventana es cambiado por el parámetro de concentración. Estos cambios motivan la necesidad de adaptar las distintas técnicas presentadas en el Capítulo 2 al caso de querer contrastar el número de modas en este contexto.

También dentro del campo de los datos circulares, el segundo problema que se va

a tratar es el de determinar si la variable aleatoria es simétrica. En el caso del círculo, la simetría no está definida de forma única debido a su compacidad y las isometrías producidas por reflexión y rotación. La simetría circular que se estudia a lo largo de la tesis hace referencia a la simetría reflexiva la cual es equivalente a la simetría que se da en la recta, es decir, se pretenderá determinar si la función de densidad circular f verifica que $f(\theta + \mu) = f(-\theta + \mu)$, donde μ es la dirección central. En este capítulo se realiza una introducción a las distintas propuestas que existen (tanto para datos lineales como circulares) y a cómo se abordará el problema de contrastar simetría circular en el Capítulo 4 siguiendo la metodología de Le Cam introducida en el Apéndice D.

Finalmente, se describen los distintos conjuntos de datos que han sido empleados a lo largo de la tesis para ilustrar las distintas técnicas desarrolladas. El objetivo en los dos primeros conjuntos de datos es el de determinar el número de modas con datos lineales. El primero, haciendo referencia al grosor de los sellos de la colección de Hidalgo de finales del siglo XIX, fue introducido por Wilson (1983) y tiene como objetivo determinar cuantos grupos de sellos distintos se pueden encontrar dentro de esta colección. El segundo, dentro del campo de la malaria, contiene la cantidad de anticuerpos que producen distintos individuos contra los antígenos de la malaria, y en él se pretende identificar grupos seropositivos en distintas poblaciones. En el tercero, también se busca contrastar el número de modas, pero, en este caso, en el caso circular. Este conjunto de datos contiene la fecha y la localización en la que se produjeron todos los incendios a lo largo de la Tierra entre el 10 de julio de 2002 y el 9 de julio de 2012 y tiene como objetivo determinar si hay una temporada de incendios o más de una para tener un mayor conocimiento de dónde los humanos están alterando la temporalidad de los incendios. El cuarto conjunto de datos contiene el ángulo con el que se producen las roturas en la parte cementada del hueso tras realizar un implante de cadera y tiene como objetivo el de determinar si los datos son reflexivamente simétricos alrededor de una dirección central desconocida.

Capítulo 2: Contrastes de multimodalidad para datos lineales. En la literatura estadística se pueden encontrar diversas propuestas para tratar de determinar el número de modas. Desde un punto de vista no paramétrico, este capítulo está centrado en la revisión de los distintos test que permiten contrastar si la distribución es unimodal, siendo algunos de ellos adaptables al caso general en el que se quiere contrastar si la distribución es k–modal (con $k > 1$). Las propuestas existentes se pueden dividir en dos grupos: la ventana crítica y el exceso de masa.

La ventana crítica para k modas, introducida por Silverman (1981), se define como el parámetro ventana más pequeño para el cual la estimación tipo núcleo tiene k modas. Silverman (1981) emplea esta ventana como estadístico de contraste, rechazando

la hipótesis nula cuando esta ventana es muy "grande", ya que eso significa que hay que sobresuavizar la estimación tipo núcleo para obtener una estructura k–modal. Para el caso de contrastar unimodalidad, el calibrado de este estadístico de contraste es proporcionado por Hall y York (2001), cuando se conoce el soporte donde se encuentran las modas y este está acotado. La ventana crítica también ha sido empleada por Fisher y Marron (2001) para construir un estadístico del tipo Cramér–von Mises.

La idea que motivo el estadístico de exceso de masa, introducido por Müller y Sawitzki (1991), para contrastar k modas es medir la diferencia, en masa de probabilidad, entre asumir que la distribución posee $(k+1)$ o k modas. Valores "grandes" de este estadístico serán un indicativo de que la distribución subyacente posee al menos una moda más, indicando que la hipótesis nula es falsa. La primera propuesta, que se introduce en este bloque de test, es la de Hartigan y Hartigan (1985) que, aunque no utilice el exceso de masa, es presentada en esta parte ya que su estadístico (conocido como *dip*) es exactamente igual a la mitad del valor del estadístico de exceso de masa en el caso unimodal, siendo la ventaja del exceso de masa que se pueda adaptar al caso general de contrastar k modas. Además, tanto Hartigan y Hartigan (1985) como Müller y Sawitzki (1991) proponen la misma forma de calibrar sus estadísticos de contraste. Finalmente, para el caso en el que se quiere contrastar unimodalidad, Cheng y Hall (1998) realizan una propuesta que está asintóticamente bien calibrada.

El comportamiento de todas estas alternativas, en distintos escenarios, es comparado en un extenso estudio de simulación. En este se muestra que ninguno de los test presenta un funcionamiento satisfactorio en la práctica. Es, por este motivo, que se diseña un nuevo test combinando ambos enfoques: el uso de la ventana crítica y el estadístico de exceso de masa. Esta propuesta, que está asintóticamente bien calibrada, se compara con los métodos existentes, mostrando un mejor comportamiento en la práctica, especialmente en el caso de contrastar k–modalidad (cuando $k > 1$).

La nueva técnica para contrastar el número de modas se ilustra con dos ejemplos. El primero, en el campo de la filatelia, se trata de una muestra que puede ser considerada como un ejemplo clásico para determinar el número de modas. Los resultados obtenidos con esta muestra, que contiene el grosor de distintos sellos de la colección de Hidalgo de 1872, son discutidos en el contexto histórico proporcionado por Izenman y Sommer (1988). El segundo ejemplo mostrado en este capítulo, en el contexto de la erradicación de la malaria, proporciona una nueva forma de detectar poblaciones con al menos un grupo de la población infectado con malaria.

Capítulo 3: Contrastes de multimodalidad para datos circulares. En este capítulo se aborda el problema de contrastar el número de modas en el caso circular. La motivación de este capítulo es la de conocer si se produce una temporada de incendios o más de una en cada región de la tierra.

En primer lugar, dada una región en la Tierra, se puede contrastar la hipótesis nula de unimodalidad, esto es, si se produce una temporada de incendios o más. En este caso, debido a la estructura circular que presentan los datos, es necesario desarrollar nuevas técnicas que permitan resolver este contraste, ya que las técnicas mostradas en el capítulo anterior no deberían ser empleadas al no estar diseñadas para tener en cuenta la naturaleza circular de los datos. En la literatura no paramétrica, solo se puede encontrar una propuesta, la desarrollada por Fisher y Marron (2001), que permite contrastar el número de modas cuando la variable es circular. En este caso, Fisher y Marron (2001) utilizan el estadístico U^2 de Watson (1961) para realizar este contraste. El mal calibrado que presenta este test en la práctica hace que no pueda ser empleado para contrastar unimodalidad y motiva el desarrollo de un nuevo contraste para datos circulares. Para ello, se emplea una versión análoga del estadístico de exceso de masa para el caso circular y su calibrado se realiza adaptando ideas del capítulo anterior. El comportamiento de la nueva propuesta es analizado y comparado con la de Fisher y Marron (2001) en términos de calibrado y potencia en un estudio de simulación, mostrando que este nuevo test sí que puede ser empleado, de forma efectiva, para determinar el número de modas.

Una vez se tiene una propuesta que permite contrastar el número de modas en una región concreta, el objetivo será el de analizar el mapa global. Cuando se estudia en conjunto estos datos aparecen dos nuevas problemáticas, la primera está relacionada con el elevado número de regiones analizadas, ya que el test es aplicado sistemáticamente en cada una ellas. En este contexto, se requiere el uso de la tasa de falso descubrimiento (*False Discovered Rate, FDR*) para controlar los rechazos incorrectos de la hipótesis nula, esto es, la identificación de regiones unimodales como multimodales. En segundo lugar, también se debería tener en cuenta que el patrón temporal de los incendios en una localización puede estar correlacionado espacialmente con las regiones de su alrededor. Utilizando la información del uso de la tierra para reflejar esta relación espacial, en este capítulo se propone una adaptación de la propuesta de Benjamini y Heller (2007) para corregir el *FDR* teniendo en cuenta la dependencia espacial de los datos.

Capítulo 4: Contrastes de simetría para datos circulares. Este capítulo se centra en contrastar otra de las hipótesis simplificadoras más utilizadas en la práctica, la simetría, o de forma más precisa, la simetría reflexiva. Cuando se está analizando una muestra, para obtener una mejor comprensión de la misma, es importante saber si su distribución se comporta de igual forma a la izquierda y a la derecha de un eje central. Además, cuando se trata de determinar el modelo que genera la muestra, el rechazo de esta hipótesis conlleva, normalmente, al uso de modelos más complejos, con más parámetros que sus homólogos simétricos. En la literatura estadística, se pueden encontrar numerosos test que permiten contrastar simetría (especialmente en

el caso lineal) y, a diferencia de lo que pasa con los test de multimodalidad, muchos de ellos presentan un calibrado correcto. Por este motivo, el objetivo es el de tratar de encontrar la propuesta más potente para contrastar simetría. En el caso lineal, distintas propuestas óptimas (en el sentido *maximin*) han sido presentadas en los últimos años en los dos escenarios que aparecen cuando queremos contrastar simetría: cuando el eje de simetría es conocido o cuando es desconocido. En el caso circular, solo se pueden encontrar una pocas propuestas para contrastar simetría y estas son las proporcionadas en Pewsey (2002), Pewsey (2004) y en Ley y Verdebout (2014). Haciendo referencia al caso más general, este es cuando el centro de simetría es desconocido, solo se debería emplear la propuesta de Pewsey (2002) para la que no hay ninguna referencia a la optimalidad del test. Siguiendo la metodología de Le Cam, el objetivo del Capítulo 4 es el de presentar una nueva propuesta para contrastar la hipótesis nula de si la variable aleatoria circular es reflexivamente simétrica alrededor de una dirección central desconocida. En este capítulo, se demuestra que esta propuesta es óptima cuando se contrasta esta hipótesis contra la alternativa de que sigue una distribución `k`–seno–asimétrica (Umbach y Jammalamadaka, 2009). También se prueba que la propuesta de Pewsey (2002) es un caso particular de los test desarrollados en este capítulo. Una vez se muestran los resultados asintóticos de los test propuestos, se estudia su comportamiento (en términos de calibrado y potencia), en distintos escenarios, en un estudio de simulación y se compara con el resto de propuestas que permiten contrastar simetría circular. Finalmente, los test desarrollados son aplicados en el análisis de una muestra procedente del estudio de las roturas que se producen en la parte cementada del fémur, tras realizar un implante de cadera.

Apéndice A: Modelos usados en los estudios de simulación. En este apéndice, se describen los distintos modelos lineales y circulares empleados a lo largo de la tesis, utilizados tanto para ilustrar distintos conceptos a lo largo de la misma como para realizar los estudios de simulación en las Secciones 2.2, 3.3 y 4.3

Apéndice B: Algunos resultados teóricos. Este apéndice muestra en detalle las demostraciones realizadas para obtener distintos resultados teóricos mostrados a lo largo de la tesis. En primer lugar, se proporcionan las pruebas necesarias para obtener que el test, proporcionado en el Capítulo 2, para contrastar el número de modas está bien calibrado asintóticamente. En segundo lugar, se proporcionan las pruebas que permiten obtener la optimalidad del test de simetría y las distribuciones de su estadístico de contraste bajo la nula y bajo las alternativas `k`–seno–asimétricas.

Apéndice C: Software: paquete multimode. Con el objetivo de hacer accesible a la comunidad científica los contrastes de multimodalidad para datos lineales y, de esta forma, permitir su uso en problemas aplicados, se ha desarrollado un paquete para el software estadístico R (R Core Team, 2017). En este apéndice se describen y

se muestran distintos ejemplos de cómo emplear las funcionalidades integradas en el paquete **multimode**. En este paquete se han implementado todos los test presentados en el Capítulo 2 y algunas de las herramientas gráficas que permiten explorar el número de modas. Además, también se recogen todas las aproximaciones numéricas realizadas para obtener los distintos estadísticos de contraste (ventana crítica y exceso de masa), tanto en el paquete **multimode** como en el estudio de simulación realizado en el Capítulo 2.

Apéndice D: Introducción a la teoría de Le Cam. En este apéndice se recoge una breve introdución a la metodología de Le Cam, con el fin de introducir la notación y de definir los distintos conceptos necesarios para desarrollar los test óptimos para contrastar simetría en el Capítulo 4.

Bibliography

Abe, T., Kubota, Y., Shimatani, K., Aakala, T., and Kuuluvainen, T. (2012). Circular distributions of fallen logs as an indicator of forest disturbance regimes. *Ecological Indicators*, **18**, 559–566.

Abe, T., and Pewsey, A. (2011). Sine–skewed circular distributions. *Statistical Papers*, **52**, 683–707.

Ahmad, I. A., and Li, Q. (1997). Testing symmetry of an unknown density function by kernel method. *Journal of Nonparametric Statistics*, **7**, 279–293.

Ameijeiras-Alonso, J., Crujeiras, R. M., and Rodríguez-Casal, A. (2016). Mode testing, critical bandwidth and excess mass. *arXiv preprint arXiv:1609.05188*. Submitted.

Ameijeiras-Alonso, J., Crujeiras, R. M., and Rodríguez-Casal, A. (2017a). multimode: An R package for mode assessment. Manuscript under preparation.

Ameijeiras-Alonso, J., Crujeiras, R. M., Rodríguez-Casal, A., Benali, A., and Pereira, J. M. (2017b). Fire seasonality identification with multimodality tests. Manuscript under preparation.

Ameijeiras-Alonso, J., Ley, C., Pewsey, A., and Verdebout, T. (2017c). Simple optimal tests for circular reflective symmetry about an unknown central direction. *arXiv preprint arXiv:1707.09272*. Submitted.

Azzalini, A., and Bowman, A. W. (1990). A look at some data on the old faithful geyser. *Applied Statistics*, **39**, 357–365.

Azzalini, A., and Capitanio, A. (2003). Distributions generated by perturbation of symmetry with emphasis on a multivariate skew–t distribution. *Journal of the Royal Statistical Society. Series B*, **65**, 367–389.

Basford, K. E., McLachlan, G. J., and York, M. G. (1997). Modelling the distribution of stamp paper thickness via finite normal mixtures: The 1872 hidalgo stamp issue of mexico revisited. *Journal of Applied Statistics*, **24**, 169–180.

Bechtel, Y. C., Bonaiti-Pellie, C., Poisson, N., Magnette, J., and Bechtel, P. R. (1993). A population and family study n-acetyltransferase using caffeine urinary metabolites. *Clinical Pharmacology & Therapeutics*, **54**, 134–141.

Benali, A., Mota, B., Carvalhais, N., Oom, D., Miller, L. M., Campagnolo, M. L., and Pereira, J. (2017). Bimodal fire regimes unveil a global-scale anthropogenic fingerprint. *Global Ecology and Biogeography*.

Benjamini, Y., and Heller, R. (2007). False discovery rates for spatial signals. *Journal of the American Statistical Association*, **102**, 1272–1281.

Benjamini, Y., and Hochberg, Y. (1997). Multiple hypotheses testing with weights. *Scandinavian Journal of Statistics*, **24**, 407–418.

Benjamini, Y., Krieger, A. M., and Yekutieli, D. (2006). Adaptive linear step–up procedures that control the false discovery rate. *Biometrika*, **93**, 491–507.

Brasseur, L. (2005). Florence nightingale's visual rhetoric in the rose diagrams. *Technical Communication Quarterly*, **14**, 161–182.

Cabilio, P., and Masaro, J. (1996). A simple test of symmetry about an unknown median. *Canadian Journal of Statistics*, **24**, 349–361.

Cassart, D., Hallin, M., and Paindaveine, D. (2008). Optimal detection of fechner-asymmetry. *Journal of Statistical Planning and Inference*, **138**, 2499–2525.

Chan, C., Iata, H., Yaviong, J., Kalkoa, M., Yamar, S., Taleo, G., Isozumi, R., Fukui, M., Aoyama, F., Pomer, A., et al. (2017). Surveillance for malaria outbreak on malaria-eliminating islands in tafea province, vanuatu after tropical cyclone pam in 2015. *Epidemiology and Infection*, **145**, 41.

Chaudhuri, P., and Marron, J. S. (1999). Sizer for exploration of structures in curves. *Journal of the American Statistical Association*, **94**, 807–823.

Cheng, M. Y., and Hall, P. (1998). Calibrating the excess mass and dip tests of modality. *Journal of the Royal Statistical Society. Series B*, **60**, 579–589.

Cook, J., Reid, H., Iavro, J., Kuwahata, M., Taleo, G., Clements, A., McCarthy, J., Vallely, A., and Drakeley, C. (2010). Using serological measures to monitor changes in malaria transmission in vanuatu. *Malaria Journal*, **9**, 169.

Corran, P., Coleman, P., Riley, E., and Drakeley, C. (2007). Serology: a robust indicator of malaria transmission intensity? *Trends in Parasitology*, **23**, 575–582.

Crawford, S. L. (1994). An application of the laplace method to finite mixture distributions. *Journal of the American Statistical Association*, **89**, 259–267.

Cressie, N. (1993). *Statistics for Spatial Data*. John Wiley & Sons, New York.

Drakeley, C., Corran, P., Coleman, P., Tongren, J., McDonald, S., Carneiro, I., Malima, R., Lusingu, J., Manjurano, A., Nkya, W., et al. (2005). Estimating medium-and long-term trends in malaria transmission by using serological markers of malaria exposure. *Proceedings of the National Academy of Sciences of the United States of America*, **102**, 5108–5113.

Efron, B., and Tibshirani, R. J. (1994). *An Introduction to the Bootstrap*. Chapman and Hall, United States of America.

Ferreira, J. T. S., and Steel, M. F. J. (2006). A constructive representation of univariate skewed distributions. *Journal of the American Statistical Association*, **101**, 823–829.

Fisher, N. I. (1995). *Statistical Analysis of Circular Data*. Cambridge University Press, Cambridge, U.K.

Fisher, N. I., and Marron, J. S. (2001). Mode testing via the excess mass estimate. *Biometrika*, **88**, 419–517.

Giglio, L., Descloitres, J., Justice, C. O., and Kaufman, Y. J. (2003). An enhanced contextual fire detection algorithm for modis. *Remote Sensing of Environment*, **87**, 273–282.

Good, I. J., and Gaskins, R. A. (1980). Density estimation and bump-hunting by the penalized likelihood method exemplified by scattering and meteorite data. *Journal of the American Statistical Association*, **75**, 42–56.

Hall, P., and York, M. (2001). On the calibration of silverman's test for multimodality. *Statistica Sinica*, **11**, 515–536.

Härdle, W. (2012). *Smoothing techniques: with implementation in S*. Springer Science & Business Media, New York.

Hartigan, J. A., and Hartigan, P. M. (1985). The dip test of unimodality. *Journal of the American Statistical Association*, **86**, 738–746.

Huckemann, S., Kim, K.-R., Munk, A., Rehfeldt, F., Sommerfeld, M., Weickert, J., and Wollnik, C. (2016). The circular sizer, inferred persistence of shape parameters and application to early stem cell differentiation. *Bernoulli*, **22**, 2113–2142.

Izenman, A. J., and Sommer, C. J. (1988). Philatelic mixtures and multimodal densities. *Journal of the American Statistical Association*, **83**, 941–953.

Jammalamadaka, S. R., and Sengupta, A. (2001). *Topics in Circular Statistics*. World Scientific.

Jander, R. (1957). Die optische richtungsorientierung der roten waldameise (formica ruea l.). *Zeitschrift für vergleichende Physiologie*, **40**, 162–238.

Jeffreys, H. (1946). An invariant form for the prior probability in estimation problems. In *Proceedings of the Royal Society of London a: mathematical, physical and engineering sciences*, vol. 186, (pp. 453–461). The Royal Society.

Johnson, N. L., Kotz, S., and Balakrishnan, N. (1995). *Continuous Univariate Distributions*, vol. 1 and 2. Wiley Series in Probability and Statistics, New York.

Jona-Lasinio, G., Gelfand, A., and Jona-Lasinio, M. (2012). Spatial analysis of wave direction data using wrapped gaussian processes. *Annals of Applied Statistics*, (pp. 1478–1498).

Jones, M. C., and Pewsey, A. (2012). Inverse batschelet distributions for circular data. *Biometrics*, **68**, 183–193.

Jupp, P. E., Regoli, G., and Azzalini, A. (2016). A general setting for symmetric distributions and their relationship to general distributions. *Journal of Multivariate Analysis*, **148**, 107–119.

Jupp, P. E., and Spurr, B. (1983). Sobolev tests for symmetry of directional data. *Annals of Statistics*, **11**, 1225–1231.

Kato, S., and Jones, M. C. (2012). A family of distributions on the circle with links to, and applications arising from, möbius transformation. *Journal of the American Statistical Association*, **105**, 249–262.

Kato, S., and Jones, M. C. (2015). A tractable and interpretable four-parameter family of unimodal distributions on the circle. *Biometrika*, **102**, 181–190.

Korontzi, S., McCarty, J., Loboda, T., Kumar, S., and Justice, C. (2006). Global distribution of agricultural fires in croplands from 3 years of moderate resolution imaging spectroradiometer (modis) data. *Global Biogeochemical Cycles*, **20**.

Koudou, A. E., and Ley, C. (2014). Efficiency combined with simplicity: new testing procedures for generalized inverse gaussian models. *Test*, **23**, 708–724.

Kreiss, J. (1987). On adaptive estimation in stationary ARMA processes. *Annals of Statistics*, **15**, 112–133.

Lagona, F., Picone, M., Maruotti, A., and Cosoli, S. (2015). A hidden markov approach to the analysis of space–time environmental data with linear and circular components. *Stochastic Environmental Research and Risk Assessment*, **29**, 397–409.

Le Cam, L. (1960). Locally asymptotically normal families of distributions. *University California Publication Statistics*, **3**, 27–98.

Le Cam, L. (1986). *Asymptotic Methods in Statistical Decision Theory*. Springer–Verlag, New York.

Le Page, Y., Oom, D., Silva, J., Jönsson, P., and Pereira, J. (2010). Seasonality of vegetation fires as modified by human action: observing the deviation from eco-climatic fire regimes. *Global Ecology and Biogeography*, **19**, 575–588.

Leff, B., Ramankutty, N., and Foley, J. A. (2004). Geographic distribution of major crops across the world. *Global Biogeochemical Cycles*, **18**.

Ley, C., and Paindaveine, D. (2009). Le cam optimal tests for symmetry against ferreira and steel's general skewed distributions. *Journal of Nonparametric Statistics*, **21**, 943–967.

Ley, C., and Verdebout, T. (2014). Simple optimal tests for circular reflective symmetry about a specified median direction. *Statistica Sinica*, **24**, 1319–1339.

Ley, C., and Verdebout, T. (2017). *Modern Directional Statistics*. CRC Press, Boca Ratón, Florida.

Maechler, M. (2015). *diptest: Hartigan's Dip Test Statistic for Unimodality - Corrected*. R package version 0.75-7.
URL `http://CRAN.R-project.org/package=diptest`

Magi, B., Rabin, S., Shevliakova, E., and Pacala, S. (2012). Separating agricultural and non-agricultural fire seasonality at regional scales. *Biogeosciences*, **9**, 3003–3012.

Mammen, E., Marron, J. S., and Fisher, N. I. (1992). Some asymptotics for multimodality tests based on kernel density estimates. *Probability Theory and Related Fields*, **91**, 115–132.

Mann, K. A., Gupta, S., Race, A., Miller, M. A., and Cleary, R. J. (2003). Application of circular statistics in the study of crack distribution around cemented femoral components. *Journal of Biomechanics*, **36**, 1231–1234.

Mardia, K. V. (1972). *Statistics of Directional Data*. Academic Press, London.

Mardia, K. V., and Jupp, P. E. (2000). *Directional Statistics*. Wiley, Chichester.

Marron, J. S., and Schmitz, H. P. (1992). Simultaneous density estimation of several income distributions. *Econometric Theory*, **8**, 476–488.

McLachlan, G., and Peel, D. (2000). *Finite Mixture Models*. John Wiley & Sons, United States of America.

McWilliams, T. P. (1990). A distribution-free test for symmetry based on a runs statistic. *Journal of the American Statistical Association*, **85**, 1130–1133.

Minnotte, M. C., Marchette, D. J., and Wegman, E. J. (1998). The bumpy road to the mode forest. *Journal of Computational and Graphical Statistics*, **7**, 239–251.

Minnotte, M. C., and Scott, D. W. (1993). The mode tree: A tool for visualization of nonparametric density features. *Journal of Computational and Graphical Statistics*, **2**, 51–68.

Mitchell, J. F., Sundberg, K. A., and Reynolds, J. H. (2007). Differential attention-dependent response modulation across cell classes in macaque visual area v4. *Neuron*, **55**, 131–141.

Modarres, R., and Gastwirth, J. L. (1996). A modified runs test for symmetry. *Statistics & Probability Letters*, **31**, 107–112.

Modarres, R., and Gastwirth, J. L. (1998). Hybrid test for the hypothesis of symmetry. *Journal of Applied Statistics*, **25**, 777–783.

Müller, D. W., and Sawitzki, G. (1991). Excess mass estimates and tests for multimodality. *Annals of Statistics*, **13**, 70–84.

NASA Visible Earth (2003). Fires and smoke in Siberia, from Jacques Descloitres, MODISRapid Response Team, NASA/GSFC. `https://visibleearth.nasa.gov/view.php?id=67409`. [Online; accessed April 21, 2017].

NASA Visible Earth (2004). Fires and smoke in Siberia, from Jacques Jeff Schmaltz, MODIS Rapid Response Team, NASA/GSFC. `https://visibleearth.nasa.gov/view.php?id=69947`. [Online; accessed April 21, 2017].

Olden, J. D., Hogan, Z. S., and Zanden, M. (2007). Small fish, big fish, red fish, blue fish: size-biased extinction risk of the world's freshwater and marine fishes. *Global Ecology and Biogeography*, **16**, 694–701.

Oliveira, M. (2014). *Nonparametric Circular Methods for Density and Regression*. Ph.D. thesis, Universidade de Santiago de Compostela.

Oliveira, M., Crujeiras, R. M., and Rodríguez-Casal, A. (2012). A plug-in rule for bandwidth selection in circular density estimation. *Computational Statistics & Data Analysis*, **56**, 3898–3908.

Oliveira, M., Crujeiras, R. M., and Rodríguez-Casal, A. (2013). Nonparametric circular methods for exploring environmental data. *Environmental and Ecological Statistics*, **20**, 1–17.

Oom, D., and Pereira, J. M. C. (2013). Exploratory spatial data analysis of global modis active fire data. *International Journal of Applied Earth Observation and Geoinformation*, **21**, 326–340.

OpenStreetMap contributors (2017). Planet maps retrieved from `https://planet.osm.org` . `https://www.openstreetmap.org`. [Online; accessed April 14, 2017].

Pérez, I. A., Sánchez, M. L., García, M. A., and Pardo, N. (2012). Analysis of CO_2 daily cycle in the low atmosphere at a rural site. *Science of the Total Environment*, **431**, 286–292.

Pewsey, A. (2002). Testing circular symmetry. *Canadian Journal of Statistics*, **30**, 591–600.

Pewsey, A. (2004). Testing for circular reflective symmetry about a known median axis. *Journal of Applied Statistics*, **31**, 575–585.

Postman, M., Huchra, J., and Geller, M. (1986). Probes of large-scale structure in the corona borealis region. *The Astronomical Journal*, **92**, 1238–1247.

R Core Team (2017). *R: A Language and Environment for Statistical Computing*. R Foundation for Statistical Computing, Vienna, Austria.
URL `https://www.R-project.org/`

Richardson, S., and Green, P. J. (1997). On bayesian analysis of mixtures with an unknown number of components (with discussion). *Journal of the Royal Statistical Society: series B (statistical methodology)*, **59**, 731–792.

Roeder, K. (1990). Density estimation with confidence sets exemplified by superclusters and voids in the galaxies. *Journal of the American Statistical Association*, **85**, 617–624.

Romano, J. P. (1988). On weak convergence and optimality of kernel density estimates of the mode. *Annals of Statistics*, **16**, 629–647.

Romano, J. P., et al. (1989). Bootstrap and randomization tests of some nonparametric hypotheses. *Annals of Statistics*, **17**, 141–159.

Salgado-Ugarte, I. H., Shimizu, M., and Taniuchi, T. (1998). Nonparametric assessment of multimodality for univariate data. *Stata Technical Bulletin*, **7**, 27–35.

Schach, S. (1969). Nonparametric symmetry tests for circular distributions. *Biometrika*, **56**, 571–577.

Schmidt-Koenig, K. (1963). On the role of the loft, the distance and site of release in pigeon homing (the "cross-loft experiment"). *The Biological Bulletin*, **125**, 154–164.

Scott, D. W. (2015). *Multivariate density estimation: theory, practice, and visualization*. John Wiley & Sons, Hoboken, New Jersey.

Sepúlveda, N., Ameijeiras-Alonso, J., Cistjakovs, M., van den Hoogen, L., Crujeiras, R. M., Rodríguez-Casal, A., Zakeri, S., Murovska, M., Paulino, C. D., and Drakeley, C. (2017). Statistical methods for the analysis of seropositivity in malaria elimination and eradication settings. Submitted.

Sepúlveda, N., Stresman, G., White, M. T., and Drakeley, C. J. (2015). Current mathematical models for analyzing anti-malarial antibody data with an eye to malaria elimination and eradication. *Journal of Immunology Research*, **2015**.

Silverman, B. W. (1981). Using kernel density estimates to investigate multimodality. *Journal of the Royal Statistical Society. Series B*, **43**, 97–99.

Umbach, D., and Jammalamadaka, S. R. (2009). Building asymmetry into circular distributions. *Statistics & Probability Letters*, **79**, 659–663.

van der Vaart, A. (2002). The statistical work of Lucien Le Cam. *Annals of Statistics*, **30**, 631–682.

Vounatsou, P., Smith, T., and Smith, A. (1998). Bayesian analysis of two-component mixture distributions applied to estimating malaria attributable fractions. *Applied Statistics*, **47**, 575–587.

Wand, M. P., and Jones, M. C. (1995). *Kernel Smoothing*. Chapman and Hall, Great Britain.

Watson, G. S. (1961). Goodness–of–fit tests on a circle. *Biometrika*, **48**, 109–114.

Weisberg, S. (2005). *Applied linear regression*, vol. 528. John Wiley & Sons, New York.

Wikimedia Commons (2004a). Comparison of Plasmodium Lactate Dehydrogenase malaria antibodies, from user: Michael Makler. `https://commons.wikimedia.org/wiki/File:PLDH_Malaria_Antibodies.jpg`. [Online; accessed April 21, 2017].

Wikimedia Commons (2004b). Map of Iran, originally derived from the public domain maps of the CIA World Factbook. `https://commons.wikimedia.org/wiki/File:Iran_map.png`. [Online; accessed April 21, 2017].

Wikimedia Commons (2009a). Crown CA watermark on the back of a Zululand stamp, scanned by user: Stan Shebs. `https://commons.wikimedia.org/wiki/File:Watermark_Crown_CA.jpg`. [Online; accessed April 21, 2017].

Wikimedia Commons (2009b). Mexico 12c stamp of 1872 with image of Miguel Hidalgo, scanned August 2009 by user: Ecphora. `https://commons.wikimedia.org/wiki/File:Mexico_1872.jpg`. [Online; accessed April 21, 2017].

Wilson, I. G. (1983). Add a new dimension to your philately. *The American Philatelist*, **97**, 342–349.

Zakeri, S., van den Hoogen, L. L., Mehrizi, A. A., Karimi, F., Raeisi, A., and Drakeley, C. (2016). Anti-malarial seroprevalence assessment during an elimination programme in chabahar district, south-eastern iran. *Malaria Journal*, **15**, 382.

USC
UNIVERSIDADE
DE SANTIAGO
DE COMPOSTELA

USC
UNIVERSIDADE
DE SANTIAGO
DE COMPOSTELA

USC
UNIVERSIDADE
DE SANTIAGO
DE COMPOSTELA